Modulation of the BH3/BCL-x_L Protein-Protein Interactions Using Peptidomimetic Approaches

Peiyu Zhang

Submitted in accordance with the requirements for the degree of
Doctor of Philosophy

The University of Leeds

School of Chemistry

Mar 2023

Intellectual Property and Publication Statements

The candidate confirms that the work submitted is his own, except where work has formed part of jointly-authored publications has been included. The contribution of the candidate and the other authors to this work has been explicitly indicated below. The candidate confirms that appropriate credit has been given within the thesis where reference has been made to the work of others.

Some of the work in 1.4 formed the basis of a review article published in March 2021: 'Peptide-based inhibitors of protein–protein interactions: biophysical, structural and cellular consequences of introducing a constraint', Hongshuang Wang; Robert S. Dawber; Peiyu Zhang; Martin Walko; Andrew J. Wilson and Xiaohui Wang, *Chem. Sci.*, **2021**, 12, 5977-5993. The contributions of the authors were as follows: X. W. and A. J. W. conceived the scope and focus of the review. The selection of material was made by H. W., R. S. D. and P. Z. (the candidate) who wrote the manuscript with contributions from all authors. M. W., A. J. W. and X. W. edited the manuscript into its final form.

The work reported in Chapter 2 formed the basis for a research article published in Mar 2023: 'Maleimide constrained BAD BH3 domain peptides as BCL-x_L inhibitors: A versatile approach to rapidly identify sites compatible with peptide constraining', Peiyu Zhang, Martin Walko, and Andrew J. Wilson., *Bioorg. Med. Chem. Lett.*, **2023**, 87, 129260. The contributions of the authors were as follows: AJW, PZ (the candidate) and MW conceived and designed the study. PZ performed synthesis and biophysical analyses. PZ and MW performed modelling. PZ and MW performed BCL-x_L expression. The manuscript was written by PZ and edited into its final form by MW and AJW.

The work reported in Chapter 3 formed the basis for a research article published in Jan 2023: Rational design of Harakiri (HRK)-derived constrained peptides as BCL-x_L inhibitors. Peiyu Zhang, Martin Walko, and Andrew J. Wilson. *Chem. Commun.*, **2023**, 59, 1697-1700; The contributions of the authors were as follows: PZ (the candidate) performed syntheses, biophysical and proteolysis experiments; PZ and MW carried out BCL-x_L protein preparation; PZ, MW and AJW wrote and edited the manuscript.

Acknowledgements

First of all, I would like to thank my main supervisor Prof Andy Wilson, who has provided endless help and guidance during my PhD project. In particular, I feel deeply grateful to Andy for accepting me into his group, and supervising me in the past three years and a half; every time I made more progress after his encouragement and guidance. I also would like to extend my gratitude to my second supervisor, Dr Mike Webb, who has provided essential training for using equipment in the biolab and useful discussions about protein expressions.

I also want to thank Dr Martin Walko, who has been training and helping me since my first day in the lab. He has always been patient when I was struggling with science and has never said no to me when I asked very naïve questions. I wouldn't have been able to complete my project in time without his help. I also would like to say a huge thanks to people who have put great efforts in the key characterisation work for this research. I would like to thank Dr Jeanine Williams for her immense help with HPLC experiments. I haven't stopped bothering her with my large amount of HPLC samples and also troubles with the prep-HPLCs. I also want to say thanks to Dr Stuart Warriner and Dr Nasir Khan, who have provided valuable help and support for high-resolution mass spectroscopy and circular dichroism spectroscopy, respectively.

I owe a debt of gratitude to all old and current group members in the Wilson group. I would like to say a huge thanks to Amanda and Anastasija, who have provided timely help for my research regarding protein preparation. I also want to thank Mike for his help with any difficult synthetic problems I had; and I want to thank Diana for useful discussions about proteolysis and NMR. Special thanks to Kris; the happiness you brought and the teamwork you showed helped me a lot when I was kicking off my PhD. I also want to thank Emma, Rob, Suz, Martin, Eleanor, Yue, for every sentence on each lovely card and every funny moment we spent together off campus. A huge thank you goes to Drs Yong Xu and Qi Meng, who are like a big brother and a big sister to me and have taken thoughtful care of me and borne with me in many cases.

Thank you to my girlfriend Ziyao, who has been understanding the difficulties for communication due to time difference and distance. Thank you to my parents, your support and love always motivated me to try my best during my study. I would appreciate the experience I had and time I spent with the lovely people in the beautiful city, Leeds: **求学四载，三生有幸，**经**此一别，后会有期！**

Abstract

Protein-protein interactions (PPIs) play essential roles in regulating cellular processes, thus emerging as an important class of targets for drug discovery. The B cell CLL/lymphoma-2 (BCL-2) family of proteins control the intrinsic (or mitochondrial) apoptotic pathway, and can be divided into two major classes: pro-apoptotic members and pro-survival members. In cancer cells, the overexpression of pro-survival proteins can block pro-apoptotic signalling by sequestering the BH3-only proteins (pro-apoptotic), thus allowing cancer to grow and spread. Selective inhibition of BCL-x_L, a pro-survival member, is of great interest due to its functional roles in solid tumours and drug resistance. Using peptides as inhibitors of PPIs serves as a promising approach because of their larger sizes and intrinsic conformations mimicking native binding domains. However, peptides that have native helical structures do not readily adopt bioactive shapes when taken out of the corresponding parent proteins. The main aim of this project was to design potent and selective inhibitors of BCL-x_L using peptidomimetic approaches. The generated hits were proposed to serve as starting points for development of therapeutics for treatment of BCL-x_L-overexpressed cancer. To do this, two main methods, peptide constraining and coiled-coil grafting, were used with assistance of computational tools.

Peptide constraining is one of the notable methods for generating stabilised helices. Strategies and consequences of constraining are described in chapter 1 (published in *Chem. Sci.*). Two BH3 ligands, BAD and HRK, were chose as starting points for the design of peptidomimetics targeting BCL-x_L. Chapter 2 describes efforts to constrain the BAD BH3 domain (published in *Bioorganic Med. Chem. Lett.*). CD spectroscopy and MD simulations revealed that the loss of potency after introducing a constraint might be due to disruption of the orientation of key hot-spot residues and a reduced helicity of the bound-state ligand or complex.

Efforts to construct HRK-derived constrained peptides led to more promising outcomes as described in chapter 3 (also published in *Chem. Commun.*). A combination of computational modelling and a maleimide-staple scan led to a constrained peptide, HRKS4, with slightly improved potency, enhanced helicity in comparison to the linear precursor, and improved proteolytic stability. Further sequence truncation alongside hybridisation led to shorter peptides with significantly improved potency. The corresponding constrained peptide, HRKS4H, had slightly reduced potency; but more importantly, was observed to have improved selectivity.

Finally, the well-fined coiled coil, CC-Di, was selected for grafting hot-spot residues from BH3 ligands, in order to develop coiled-coil-templated inhibitors targeting the BCL-x_L. Using computational tools, suitable grafting sites in the sequence were successfully identified. Several designed peptides showed weak potency in the FA competition assays. Further studies will focus on the improvement of potency and investigation of selectivity.

Table of contents

List of tables

List of figures

Abbreviation

6-HB	6-helical bundle
ADC	antibody-drug conjugate
Ahx	aminohexanoic acid
Aib	aminoisobutyric acid
AML	acute myelocytic leukemia
AUC	analytical ultracentrifugation
BAD	BCL-2 agonist of cell death
BAK	BCL-2 antagonist/killer
BAlaS	BUDE Alanine Scan
BAX	BCL-2-associated X
BCL-2	B cell CLL/lymphoma-2
BCL9	B-cell CLL/lymphoma 9
BCL-x_L	B cell lymphoma extra-large
BH	BCL-2 homology
BID	BH3-interacting domain death agonist
BIM	BCL-2-interacting mediator of cell death
Bph	4,4′-bis(bromomethyl)biphenyl
BUDE	Bristol University Docking Engine
CD	circular dichroism
CHR	C-terminal heptad repeat
CuAAC	Cu(I)-catalyzed azide–alkyne cycloaddition
DAR	drug-to-antibody ratio
DBM	dibromomaleimide
DCA	dichloroacetone
DHA	dehydroalanine

DIC	*N*,*N*'-diisopropylcarbodiimide
DIPEA	*N*,*N*-diisopropylethylamine
DLBCL	diffuse large B-cell lymphoma
DMF	dimethylformamide
DODT	3,6-dioxa-1,8-octanedithiol
DOX	doxorubicin
DP5	death protein 5
DTC	dithiocarbamate
FA	fluorescence anisotropy
FAM	5,6-carboxy fluorescein
Fmoc	fluorenylmethyloxycarbonyl
GBM	glioblastoma
GK	glucokinase
GKA	glucokinase activator
HCTU	*O*-(1*H*-6-Chlorobenzotriazole-1-yl)-1,1,3,3-tetramethyluronium hexafluorophosphate
HOBt	hydroxybenzotriazole
HR	heptad repeat
HRK	Harakiri
IEDDA	inverse electron demand Diels-Alder reaction
MCL-1	myeloid cell leukemia-1
MD	molecular dynamics
MEF	mouse embryonic fibroblasts
MOMP	mitochondrial outer membrane permeabilization
MTT	3-(4,5-dimethylthiazol-2-yl)-2,5-diphenyltetrazolium bromide
MULE	MCL-1 ubiquitin ligase E3

NGF	nerve growth factor
NHR	N-terminal repeat
Nle	norleucine
NOXA	Phorbol-12-myristate-13-acetate-induced protein 1
OPA	ortho-phthalaldehyde
Orn	ornithine
Oxyma	ethyl cyanohydroxyiminoacetate
p53	tumour protein 53
p73	tumour protein 73
PEG	polyethylene glycol
PPI	protein-protein interaction
PROTAC	Proteolysis targeting chimera
PS	phosphatidyl serine
PTM	post-translational modification
PUMA	p53-upregulated modulator of apoptosis
RCM	ring-closing metathesis
RuAAC	Ru(II)-catalyzed azide–alkyne cycloaddition
SAR	structure-activity relationship
SPR	surface plasmon resonance
T-ALL	T-cell acute lymphoblastic leukemia
TCEP	tris(2-carbonxyethyl)phosphine
TFA	trifluoroacetic acid
TIPS	triisopropyl silane
VHL	Von Hippel–Lindau tumor suppressor

Table of amino acid

Amino acid	Three letter code	Single letter code
Alanine	Ala	A
Arginine	Arg	R
Asparagine	Asn	N
Aspartic acid	Asp	D
Cysteine	Cys	C
Glutamic acid	Glu	E
Glutamine	Gln	Q
Glycine	Gly	G
Histidine	His	H
Isoleucine	Ile	I
Leucine	Leu	L
Lysine	Lys	K
Methionine	Met	M
Phenylalanine	Phe	F
Proline	Pro	P
Serine	Ser	S
Threonine	Thr	T
Tryptophan	Trp	W
Tyrosine	Tyr	Y
Valine	Val	V

Chapter 1 Introduction

1.1 Protein-protein interactions

1.1.1 Protein-protein interactions and hot-spot residues

Protein-protein interactions (PPIs) play an essential role in many biological functions.[1] The human interactome is estimated to span over 600,000 PPIs.[2] In addition, PPIs offer opportunities for therapeutic interventions in a large number of diseases; modulation of key PPIs involved in different diseases, e.g., cancer, Alzheimer's disease and viral infections, has been considered as a promising approach to discover potent therapeutics.[3] Unfortunately, PPIs are difficult to target, due to their lack of clear features and well-defined pockets for small-molecule binding; they are considered less suitable for *de novo* drug design or *in silico* drug screening.[4]

In traditional small-molecule drug discovery, a small molecule ligand binds to a well-defined protein pocket which is usually composed of a few amino acid residues, e.g. an enzyme with an active site for a substrate (usually described as a "lock and key" model, Figure 1-1 (a)).[1] In contrast, the binding interfaces of PPIs are often flat, continuous or discontinuous, and show various topographies that require contact across an area larger than 800 Å, usually 1200-2000 Å.[5,6] Inhibiting this class of interactions using small molecules remains a difficult challenge mainly because of their small molecular weight and shape that is unsuitable for binding to a large protein interface; therefore a larger ligand is usually required, and is analogous to a "hand holding an object" manner (Figure 1-1 (b)).

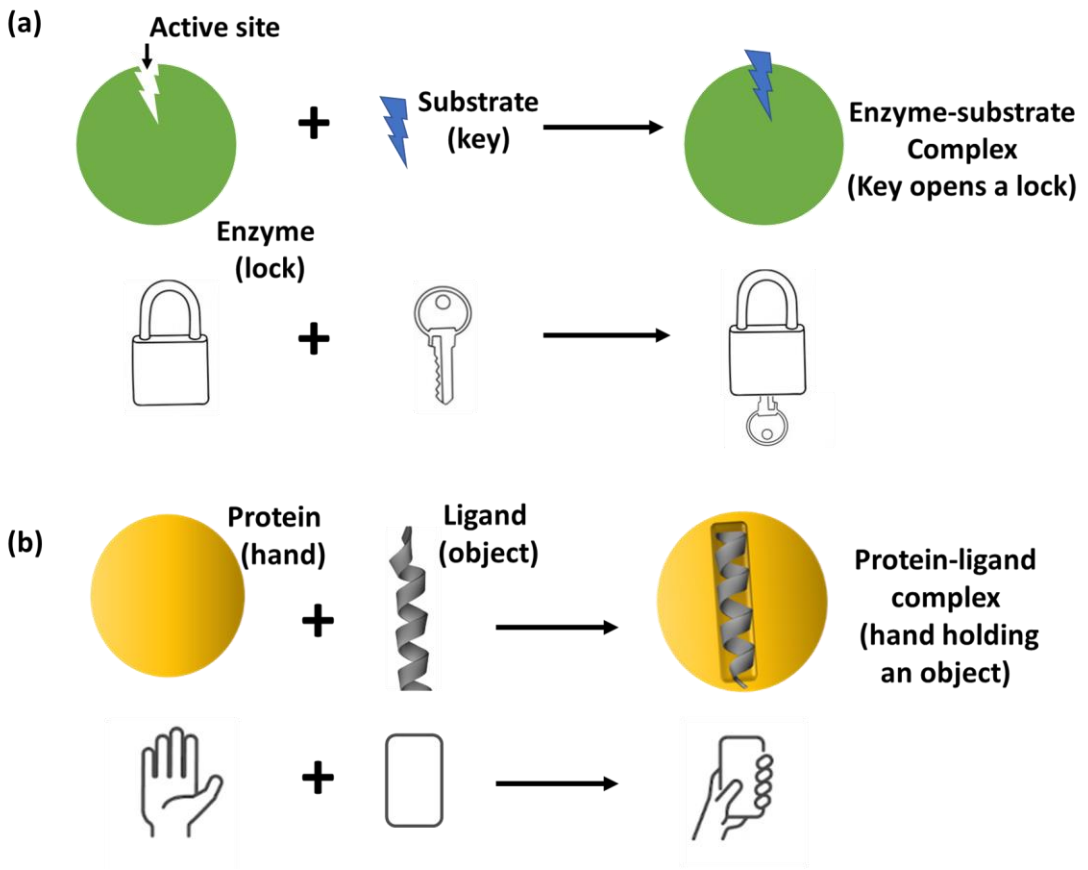

Figure 1-1 Comparison between binding features of pockets for small molecules and PPIs;. (a) a “lock and key” model for small-molecule binding; (b) a “hand holding an object” model for PPIs

The concept of “hot-spots” was initially introduced by Clackson and Wells.[7] During their study of the binding energy in the PPI complex between human growth hormone (hGH) and its first bound receptor (hGHbp), only a few residues showed a significant contribution to the binding energy for formation of the hGH/hGHbp complex. When replacing each of them with alanine, the binding free energy exhibited a significant decrease. Therefore, these residues were identified as hot-spots for the PPI. Since then, alanine scanning has become a useful procedure to detect hot-spots, and applied to a wide range of PPIs.[6] However, experimental alanine scanning methodology involves a time-consuming and costly procedure, thus computational identification of hot-spots has become an attractive alternative (Figure 1-2). Here, the methodological studies are not discussed in detail; versatile algorithms and models have been previously reviewed.[8–10]

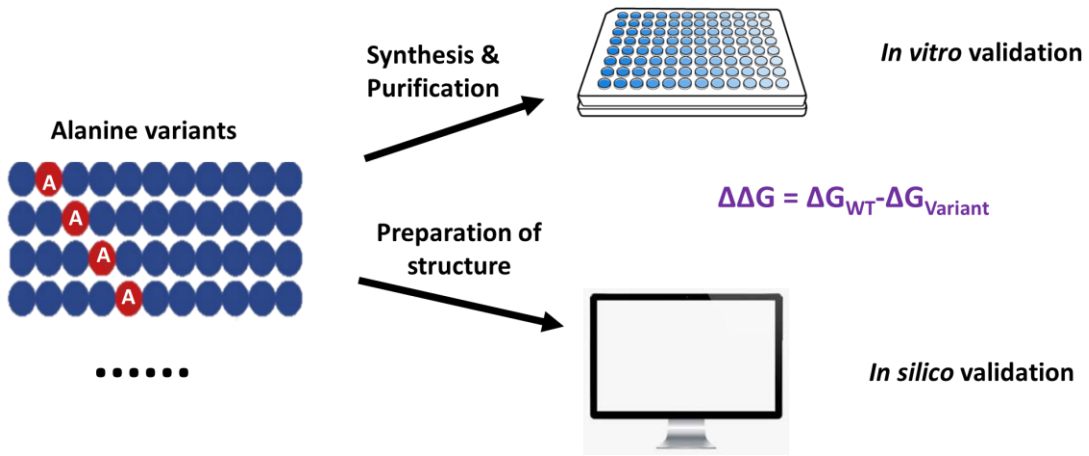

Figure 1-2 Alanine scanning to identify hot-spot residues.

1.1.2 Helix-mediated PPIs

The most common secondary structures are the α-helix and the β-sheet. PPI complexes are often mediated by several different classes of structural elements, among which α-helices are the most common class of motif[10]. An α-helix has a right-handed spiral conformation. The typical one turn α-helix consists of 3.6 amino-acid residues, with backbone dihedral angles of Φ=-60°, ψ=-45°, and Ω=180° (Ω =0° for proline) (Figure 1-3 (a)).[11] The α-helical structure repeats itself every 5.4 Å (a pitch) along the helix axis; and each C=O (*i*) and N-H (*i*+4) group form a hydrogen bond, stabilising the main chain (Figure 1-3 (b)). Therefore, in an α-helical region, a given amino-acid residue at the *i* position is located on the same face as the *i*+4 or *i*+7 residues (Figure 1-3 (c)).[11] This structural characteristic determines the molecular functional pattern, providing a starting point for designing diverse molecules as helix-mediated PPI inhibitors.

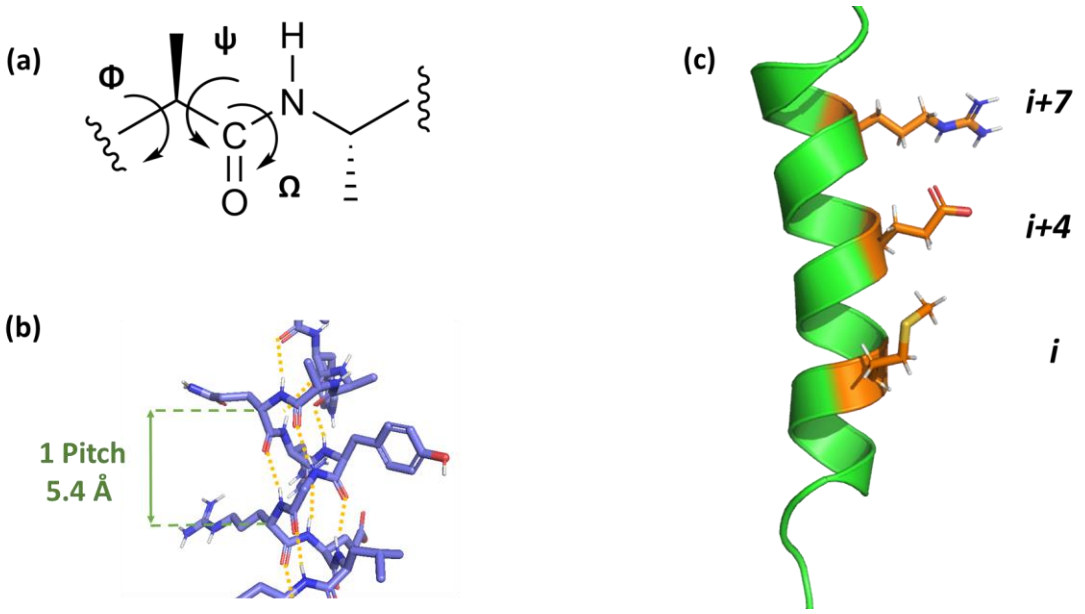

Figure 1-3 Structural features of an α-helix; a) torsion angles in α-helical peptides; b) hydrogen bonds (yellow) formed between i and i+4 residues; c) i and i+4/7 residues are located on the same face.

Different helix-mediated PPIs, e.g., tumour protein 53 (p53)/hDM2,[12] BCL-2 family[13] and HIV-1 gp41 fusion core,[14] showed various architectures. The simplest interacting model mediated by helices is the coiled-coil.[15] Coiled coils consist of two or more α-helices, which interact with another helix to form supercoiled assemblies.[16] The formation of coiled-coils is mediated by the so-called “knobs-into-holes” (KIH) model, in which stretches of side-chains from one helix insert into a binding area formed by adjacent helice(s).[17] The most common type of sequence in coiled-coils is the heptad repeat (HR), in which hydrophobic (***h***) and polar (***p***) residues appear repeatedly as ***hpphppp***, often denoted ***abcdefg*** (Figure 1-4). At appropriate spacing between the *i* and *i*+4 positions, hydrophobic ***a*** and ***d*** residues, located on the same face of a helix, can give rise to an amphipathic structure.

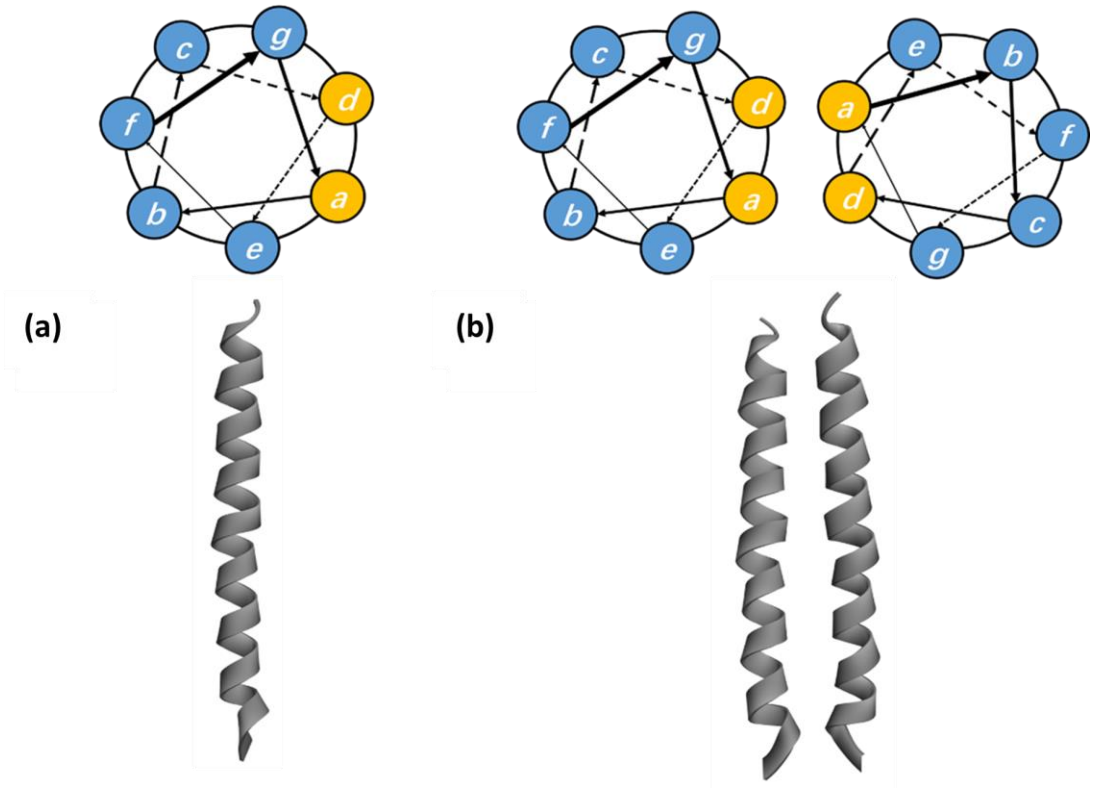

Figure 1-4 Single α-helices and coiled coils; (a) The helical wheel and structure of a single α-helix (PDB code: 1CE9); (b) The helical wheel and structure of a dimeric coiled-coil (PDB code: 5IIV) (*a* and *d* positions are shown in yellow, which are usually hydrophobic residues; other positions are shown in blue).

The HIV-1 gp41 fusion core (also referred to as 6-helical bundle, 6-HB) is a more complex protein-protein interaction driven by formation of a hexameric coiled coil assembly.[18,19] In the structure of HIV-1 6-HB, three N-terminal heptad repeat (NHR) domains form a trimeric core, with three C-terminal heptad repeat (CHR) domains binding in an anti-parallel manner.[20] 6-HBs in other analogous viruses share structural similarities, e.g., MERS-CoV,[21] EBOLA virus,[22] and SARS-CoV-2 (Figure 1-5).

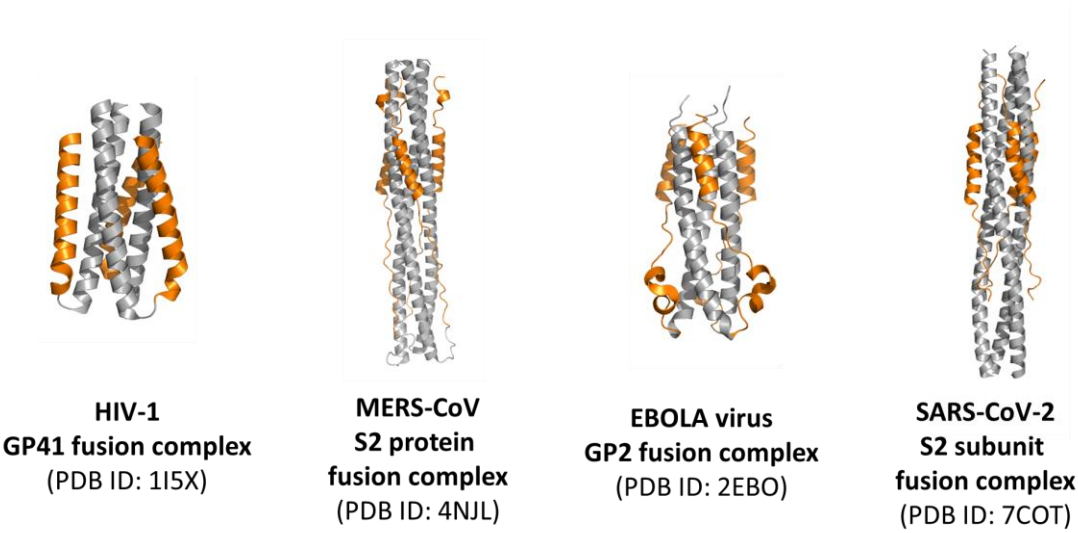

Figure 1-5 Crystal structures of 6-helical bundles (6-HBs) in different viruses [20–22] (NHRs are shown in grey and CHRs are shown in orange).

In addition to the helical coiled interactions, other interactions have remarkably different features. A different type is the mode in which a monomeric helical ligand binds to a globular protein.[23–25] For instance, *h*DM2 binds to a short helical region of the tumour suppressor p53 (Figure 1-6(a)); therefore, short helical peptides derived from the p53 helical region act as inhibitors against p53/*h*DM2.[26] In this interaction, three hydrophobic hot-spot residues insert into a cleft formed on the interacting face of *h*DM2. PPIs of BCL-2 family proteins usually involve the interactions between a helical segment, which contains 4 hydrophobic hot-spot residues (h1-h4), and a globular protein that contains a hydrophobic cleft (Figure 1-6 (b)).

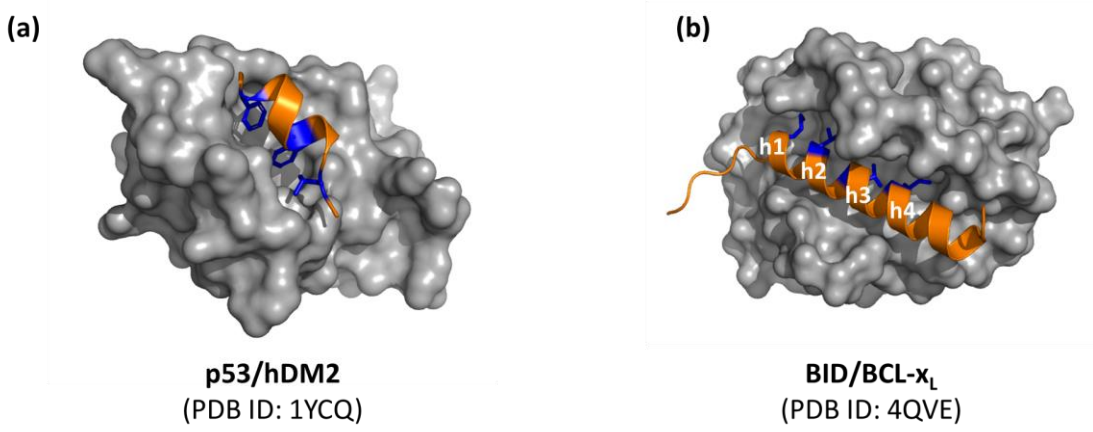

Figure 1-6 Representative PPI structures for p53/hDM2 and BCL-2 family proteins (a) structure of p53/hDM2 (PDB ID:1YCQ);[27] (b) structure of BID/BCL-x_L (PDB ID:4QVE)[28] (*h*DM2 and BCL-x_L are shown in grey; p53 and BID are shown in orange with hot-spot residues shown in blue).

1.2 BCL-2 family

1.2.1 Intrinsic apoptosis pathway

The mitochondrial pathway (intrinsic pathway) of apoptosis (programmed cell death) plays an essential role in normal eukaryotic cell development, organismal homeostasis and immunity.[29,30] This pathway is controlled by the B cell CLL/lymphoma-2 (BCL-2) family of proteins, which can be divided into two functional classes: pro-survival (anti-apoptotic) and pro-death(pro-apoptotic) (Figure 1-7).[31] In addition, pro-apoptotic members consist of two subfamilies: BH3 only pro-apoptotic sensitizers and effectors.[32]

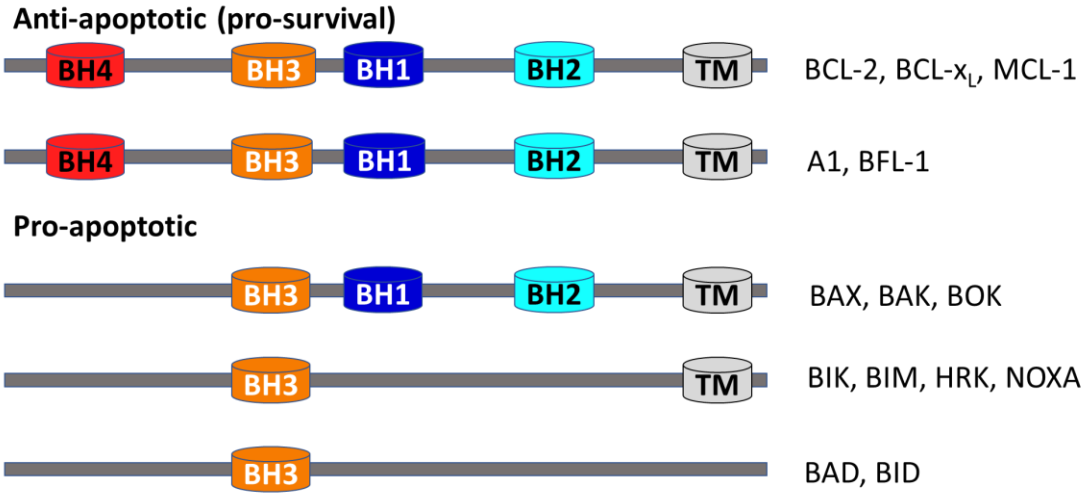

Figure 1-7 BCL-2 family proteins containing one or more BH domains : pro-survival and pro-apoptotic effector proteins consist of four BH domains (BH1-4) and transmembrane domain (TM) while BH3-only proteins only have BH3 domains with or without TM domains.

Most cells express a variety of BCL-2 proteins; regulation of their interactions determines cellular fate i.e. to survive or to commit to apoptosis. The BCL-2 family includes almost 20 members, each of which comprise one or more BCL-2 homology (BH) domains, BH1-BH4. To initiate apoptosis, cellular stress, such as viral infection, DNA damage, Endoplasmic Reticulum (ER) stress or growth factor deprivation, causes transcriptional and posttranscriptional upregulation of the BH3-only proteins, which contain only the BH3 domain, such as BCL-2-interacting mediator of cell death (BIM), BH3-interacting domain death agonist (BID) and p53-upregulated modulator of apoptosis (PUMA). These BH3-only proteins are initiators or activators of apoptosis, and they can be sequestered by pro-survival proteins, which consist of four BCL-2 homology (BH) domains

(BH1-4) (Figure 1-7). BCL-2, B cell lymphoma extra-large (BCL-x_L) and myeloid cell leukemia-1 (MCL-1) are major members of the pro-survival subfamily.[33] BH3-only proteins bind to different pro-survival or effector proteins with various binding affinities.[34,35] When these pro-survival proteins are saturated by BH3 only proteins, excess BH3 only proteins can act as direct or indirect activators of the pro-apoptotic members BCL-2-associated X protein (BAX) and/or BCL-2 antagonist/killer (BAK), resulting in their conformational changes and mitochondrial outer membrane permeabilization (MOMP). The resulting release of cytochrome c and other pro-apoptotic proteins initiates the formation of the apoptosome and the activation of a proteolytic cascade that ensures the cells' demise (Figure 1-8).[34]

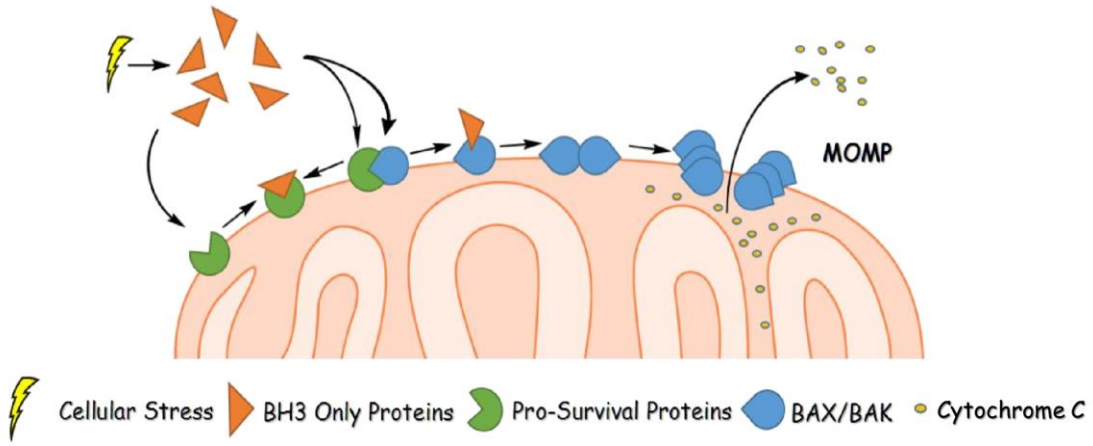

Figure 1-8 The mitochondrial apoptosis pathway.

Resistance to apoptosis is an important hallmark of cancer.[36] In cancer cells, the upregulation of pro-survival BCL-2 family proteins, for example, BCL-2, BCL-x_L and MCL-1, can block pro-apoptotic signalling, thus preventing cancer cells from removal. Based on this paradigm, a significant number of inhibitors of pro-survival members of the BCL-2 family, termed BH3 mimetics, have been developed, including peptides and small molecules.[5,37,38] BH3-mimetics can inhibit pro-survival proteins and free the BH3 only proteins that are binding to those pro-survival proteins. Recently, the US FDA approved the BCL-2 inhibitor venetoclax (ABT-199) for the treatment of chronic lymphocytic leukaemia. Agents targeting other pro-survival proteins, such as MCL-1 and BCL-x_L, are also undergoing clinical evaluation.[39,40]

1.2.2 BCL-2 family proteins and BCL-x_L

Regulation of the intrinsic apoptotic pathway by the BCL-2 family proteins is essential for normal embryonic development and control of cancer progression.[34,41] The name of the family is based on the member, BCL-2, which shows abnormal expression in B-cell lymphomas.[42,43] BCL-2 family proteins consist of two functional classes: pro-survival (anti-apoptotic) and pro-death(pro-apoptotic).[31] Pro-apoptotic members consist of two subfamilies: BH3 only pro-apoptotic sensitizers (only containing BH3 domains) and effectors.[32]

The gene *bcl-2* was the first oncogene discovered that inhibits cell death by blocking programmed cell death, rather than promoting cell growth. [43–45] Other functions, e.g. autophagy,[46] metabolism,[47] and neuronal activities,[48] also involve the engagement of BCL-x_L.[49] Animal studies (knockout studies) have shown the important roles of BCL-2 family proteins in cell death and embryonic development.[50,51] Individual knockout of BH3-only proteins, e.g. BID or BAD, didn't abolish cell apoptosis induced by DNA damage.[52] On the contrary, deletion of individual pro-survival members may result in various phenotypes. It was shown that deletion of either MCL-1 or BCL-x_L cause embryonic death at different stages[50,51] Deletion of BCL-2 doesn't lead to lethality but does cause immune side effects and kidney diseases.[53,54] Unlike BCL-2, BCL-x_L is fundamental for maintaining platelet circulation.[55,56] Deletion of BAK can rescue the loss of platelets caused by deletion of BCL-x_L [55,56]

1.2.3 Structural features of BCL-x_L and its recognition mode

Although BCL-2 was the first member discovered in the BCL-2 family, the first extensive structural data were disclosed based on its analogue, BCL-x_L.[57] *apo*-BCL-x_L is composed of eight helices (α1- α8) (Figure 1-9 (a)). BCL-x_L has all BH1-4 domains in its structure. The BH1 domain is located on α4 and α5 while the BH2 domain is located on α7 and α8; the BH3 domain is only located on α2 while the BH4 is only located on α1. Notably, the BH1-BH3 domains create a large hydrophobic cleft (Figure 1-9 (b)), involving α2, α3, α4, α5 and α8, which provides binding sites for native BH3-only proteins and also provides a template for designing small molecule inhibitors.

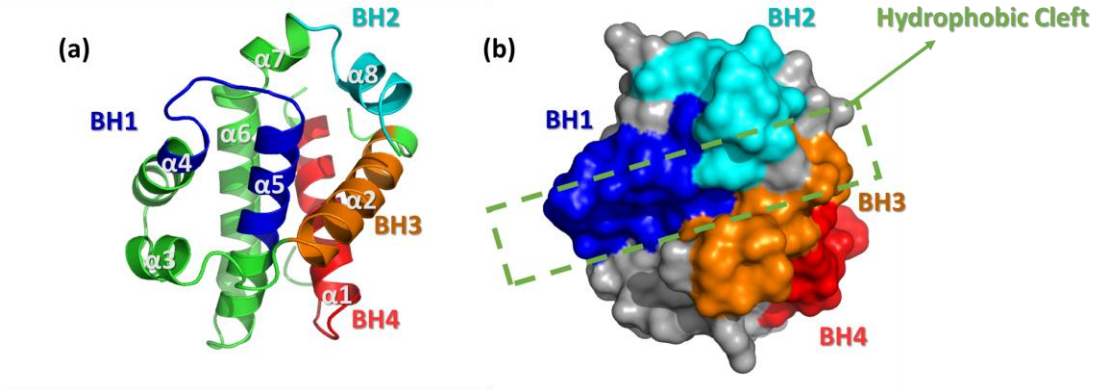

Figure 1-9 Structure features of *apo*-BCL-x_L (PDB ID: 1MAZ). (a) location of BH1-4 domains and α1-8 helices; (b) the hydrophobic cleft for BH3 ligands binding comprising BH1-3 domains.

BCL-x_L is known to bind to multiple BCL-2 family members, e.g. BAX, BAK and many BH3-only members.[34,41,58,59] Early structural studies on BAK/BAX or BH3 only proteins verified that the BH3 domain in each member is the key part participating in the interaction with the BCL-x_L. [60] The BH3 domain is usually a short helical region containing four hydrophobic residues, referred to as h1-h4, and a highly conserved aspartic acid residue, which usually interacts with an arginine on the multiple-domain BCL-2 protein. In addition, residues at h1+1 and h3+1(Asp-1) are usually alanine or glycine, which have small-sized side chain (Table 1-1). In a structural study using NMR, the 16-mer BAK peptide has a helical conformation in the complex with BCL-x_L.[60] The helical peptide embeds into the hydrophobic cleft of BCL-x_L, with all h1-h4 residues on one face and project into the cleft (Figure 1-10 (a)). Similar interaction modes were found in other complexes of BCL-x_L with various BH3-only peptides, including BIM, BID, PUMA and BAD. In each case, four hydrophobic residues at h1-h4 positions insert into the hydrophobic cleft and the conserved Asp interacts with Arg139 in BCL-x_L, forming a charge-reinforced hydrogen bond. However, a slight difference was also found in different BH3/BCL-x_L interactions. For instance, the fifth hydrophobic residue Phe125 in BAD shows π-π interaction with Tyr195 in BCL-x_L (Figure 1-10 (b)), whilst a His residue at h2-1 in BID exhibits pi-pi interaction with Phe105 in BCL-x_L (Figure 1-10(c));[28] neither of the interactions is observed in other complexes.

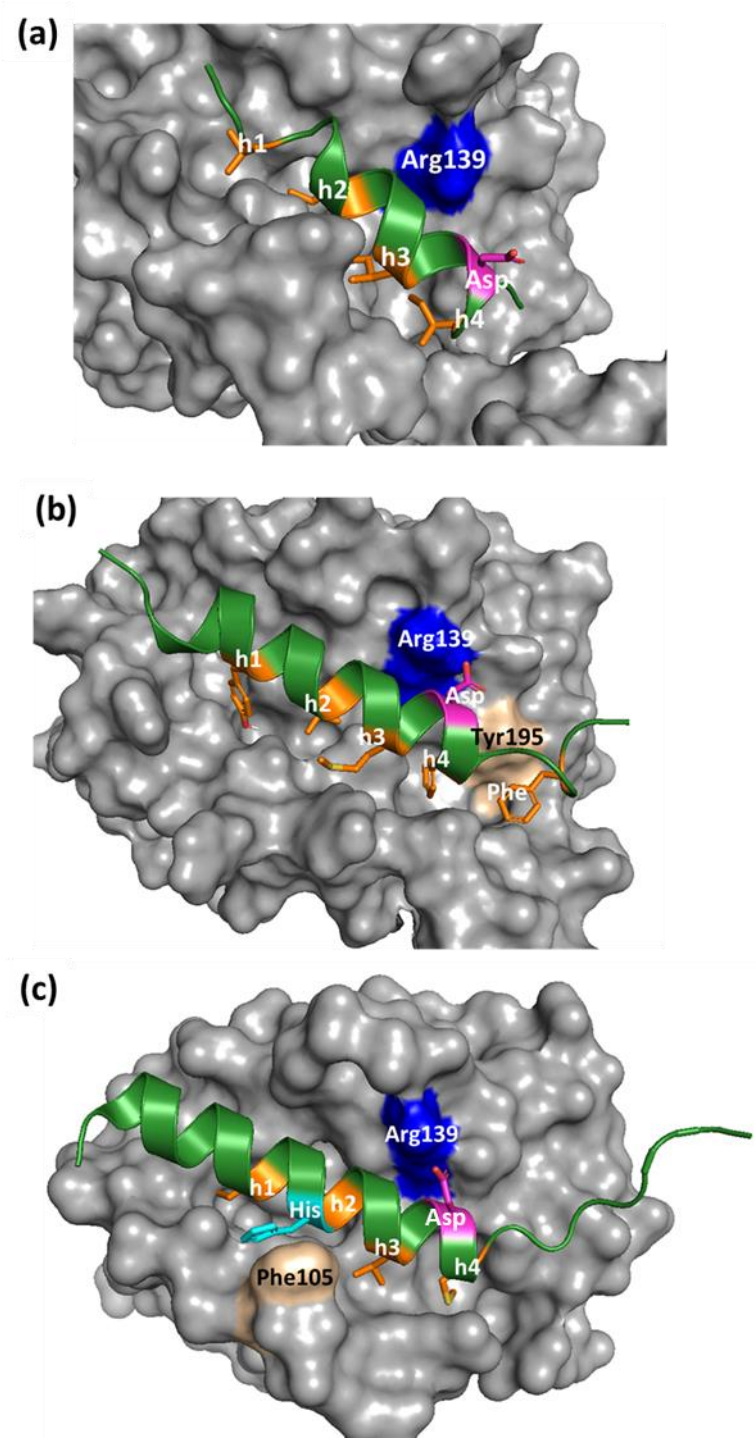

Figure 1-10 Structures for complexes between BCL-x_L and different native BH3 ligands (a) structure of BAK/BCL-x_L (PDB ID: 1BXL); (b)structure of BAD/BCL-x_L (PDB ID: 1G5J); (c) Structure of BID/BCL-x_L (PDB ID: 4QVE)

1.2.4 Native ligands and small molecule inhibitors of BCL-x_L

BCL-x_L can interact with various BH3 only proteins to inhibit apoptosis. A number of BH3-only peptide sequences show binding to the BCL-x_L, including BIM, BID, PUMA, BAD, BMF, HRK and BIK.[52]

Wang and co-workers chose BH3 sequences with comparable lengths and tested their binding affinity (K_d) for different pro-survival proteins.[35] In SPR assays, BIM and PUMA showed low nanomolar K_ds (<5 nM), whilst BMF and HRK showed slightly weaker binding, with K_d of 8.3 and 11 nM, respectively. BID and BIK showed medium binding in the assays, with 48 and 102 nM, respectively (Table 2-1).

Other BH3-like proteins also bind to BCL-x_L, e.g. Beclin-1,[58,61] translationally controlled tumour protein (TCTP),[62] and SOUL.[59] Beclin-1 is a key regulator of autophagy, which contains a BH3-like domain. The weaker affinity of Beclin-1 peptide may arise from the polar residue Thr at the h3 position. [58] Similarly, the TCTP peptide lacking the conserved h1 residue also binds to BCL-x_L with low affinity. [62] The SOUL peptide showed even weaker binding to BCL-x_L, potentially due to its Asp residue at the h3 position and also a basic Lys residue instead of the highly conserved Asp residue in other BH3 peptides.[59] Another sequence from p73TAD binds to BCL-x_L with weak affinity however it lacks BH3 sequence homology (Table 1-1).[59]

Table 1-1 Native peptide ligands of BCL-x_L

Ligand	Sequence[a] *h1 h2 h3 h4*	K_d or IC_{50}[b]	Specificity	Ref
BIM_{79-104}	DMRPEIW AQE RR G E NAYYARR	0.65 nM (K_d SPR)	Non-specific	35
$PUMA_{130-155}$	EEQWARE GAQ RR A D NAQYERR	2.2 nM (K_d SPR)	Non-specific	35
$BMF_{128-151}$	HRAEVQ ARK QC A Q HRLHTQ	8.3 nM (K_d SPR)	BCL-2, BCL-x_L, BCL-w	35
$BAD_{103-128}$	NLWAAQR GRE RR S E VDSFKKG	0.27 nM (K_d SPR)	BCL-2, BCL-x_L, BCL-w	35
BIK_{51-75}	MEGSDA ALR AC G E DVSLRAP	102 nM (K_d SPR)	BCL-x_L, BCL-w	35
HRK_{26-51}	RSSAAQL AAR KA G E HQRTMWR	11 nM (K_d SPR)	Non-specific	35
BID_{79-104}	QEDIIRN ARH AQ G S DRSIPPG	48 nM (K_d SPR)	Non-specific	35
BAK_{72-87}	GQ GRQ AI G D NR	4 nM (K_d FA)	Non-specific	63
$Beclin\text{-}1_{104-131}$	GTMEN SRR KV G L DIMSGQT	1.4 μM (K_d FA)	Not clear	61
$TCTP_{11-31}$	DEMFS IYK RE A G CLEV	12 μM (K_d ITC)	Not clear	62
$SOUL_{147-172}$	SAQKNQEQ---- ----LLT ASI RE G V DEK	~40 μM	Not clear	59
$P73TAD_{10-25}$	DGGGTTFEHLWSSLEPD	ND	Not clear	64

[a]h1-4 positions are highlighted in red and the positions for conserved Asp are highlighted in blue; [b]Values cannot be compared directly due to different conditions in different studies.

Since ABT-737 was discovered as the first small molecule inhibitor of BCL-2 and BCL-x_L, further studies led to discovery of ABT-263 (Navitoclax,Table 1-2).[37] ABT-263 is an orally bioactive small molecule inhibitor against BCL-2, BCL-w and BCL-x_L. However, the potential thrombocytopenia, which derives from the reduction of platelets caused by BCL-x_L inhibition, limits its clinical use.[65–67] Optimisation led to a BCL-2 selective inhibitor, ABT-199 (Venetoclax), which was approved by the FDA in 2016 for treatment of restrictive types of chronic lymophoblastic leukemia (CLL) and acute myeloid leukemia (AML).[68] BCL-x_L-specific inhibitors have also been developed. For example, WEHI-539 was discovered as the first selective small molecule inhibitor of BCL-x_L.[69] A more potent compound, A1155463, was discovered based on WEHI-539.[70] Targeting BCL-x_L using proteolysis-targeting chimera (PROTAC) showed potency in BCL-x_L-dependent cancer cells but less toxicity than ABT-263 as lack of E3 ligases in platelets and low doses needed for targeted protein degradation.[71]

Table 1-2 Representative small molecule ligands for BCL-x_L

Compound	Structure	K_i, K_d or EC_{50} (BCL-x_L)	Specificity	Ref
ABT-373	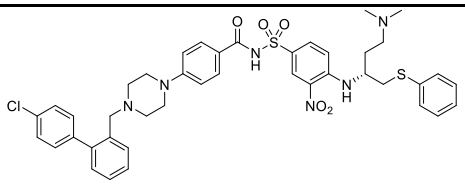	<0.5 (K_i)	BCL-x_L, BCL-2, BCL-W	37
ABT-263 (Navitoclax)	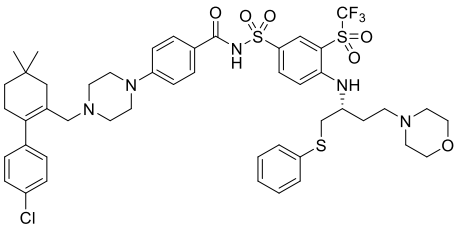	<0.5 (K_i)	BCL-x_L, BCL-2, BCL-W	37

ABT-199 (Venetoclax)	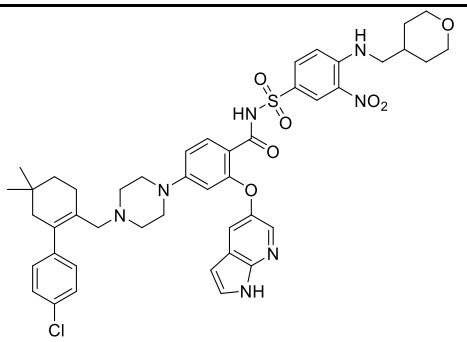	48nM (K_i)	BCL-2	69
WEHI-539	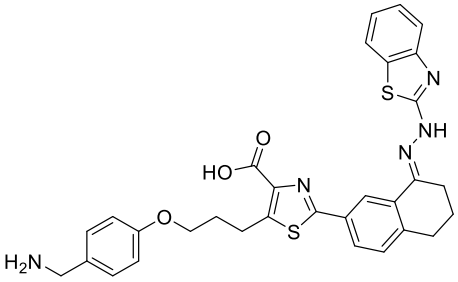	0.6 nM (K_d)	BCL-x_L	69
A1155463	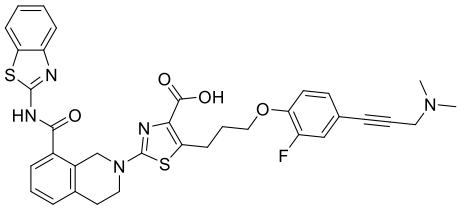	<0.01 nM (K_i)	BCL-x_L	70
DT2216	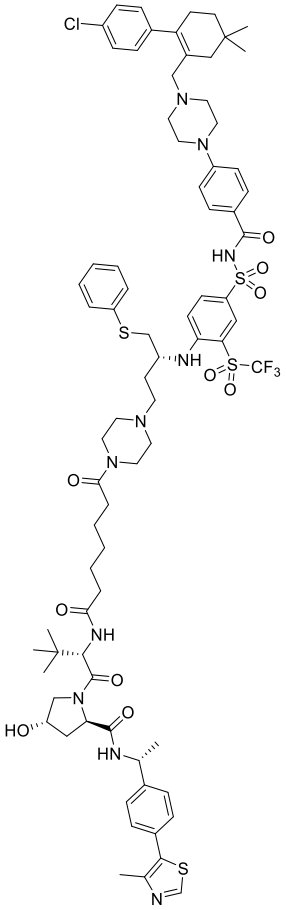	0.052 μM (EC_{50})	BCL-x_L	71

1.2.5 Conformational diversity of BCL-x_L upon binding

Superposition of *apo*-BCL-x_L and BH3-bound BCL-x_L provides insights on conformational changes occurred due to binding. The α3 region moves away from the BH3 ligand and becomes disordered and less helical upon binding whilst the α4 helix moves towards the BH3 ligand, resulting in a longer and wider hydrophobic cleft for the BH3 ligand to embed (Figure 1-11). For example, when PUMA BH3 binds to the BCL-x_L, the α2- α3 corner becomes highly disordered (Figure 1-11(c)).[72]

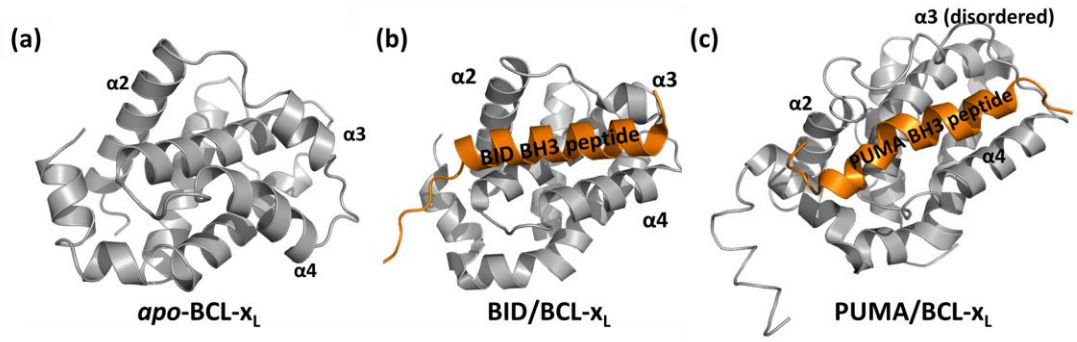

Figure 1-11 Unbound and BH3-bound BCL-x_L structures; (a) structure of *apo*-BCL-x_L (PDB ID: 1MAZ); (b) Structure of BID/BCL-x_L (PDB ID: 4QVE); (c) structure of PUMA/BCL-x_L (PDB ID: 2M04).

Extensive structural studies were carried out on the small molecules, e.g. ABT-373 and WEHI-539, with BCL-x_L. Taken together, all complexes between the compounds and BCL-x_L show similar features, with the ligand binding to the top of the cleft where the h2-h4 residues usually bind. In contrast to peptide-bound BCL-x_L, the ABT-373-bound protein has a more helical α3 (Figure 1-12 (a)), whilst WEHI-539-bound BCL-x_L bears a moved α2-α3 corner that is less disordered than the BH3-bound counterparts (Figure 1-12 (b)). In a structure of a ternary complex of VHL/PROTAC/BCL-x_L, BCL-x_L also has shifted α2-α3 corner (Figure 1-12 (c)).[73] It has not been clear whether the ability to disturb the α2-α3 corner is relevant to selectivity of BCL-x_L inhibition.

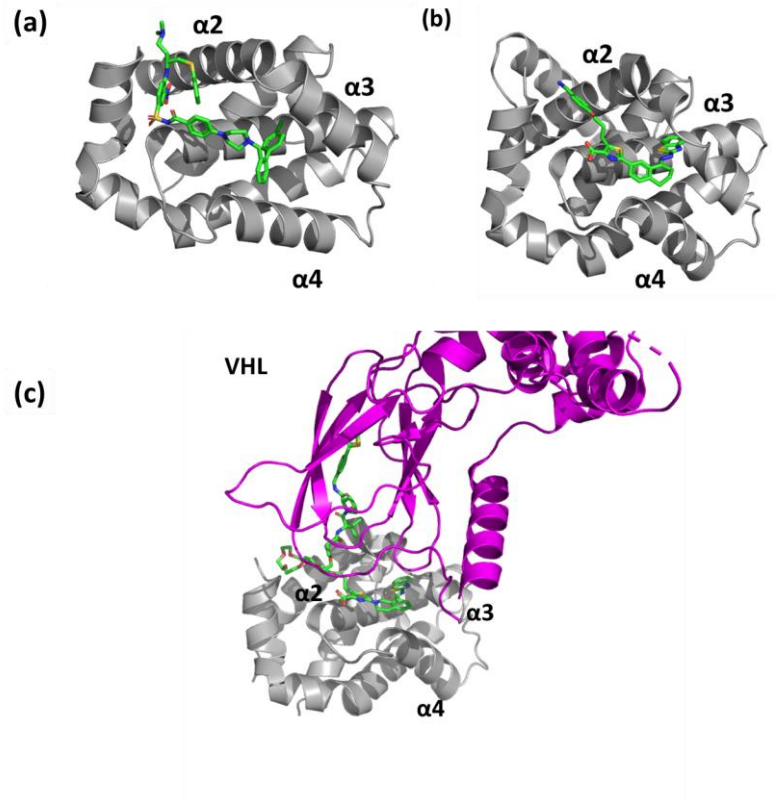

Figure 1-12 Small-molecule-bound BCL-x_L structures; (a) structure of the complex of ABT-373 with BCL-x_L (PDB ID: 2YXK); (b) structure of the complex of WEHI-539 with BCL-x_L (PDB ID: 3ZLR) (c) structure of the ternary complex of PROTAC6, BCL-x_L and VHL (PDB ID: 6ZHC).

In addition, BCL-x_L is a unique pro-survival protein that can directly bind to cytosolic p53, which is promoted by tetramerization of p53,[72] and also p73,[64] both in noncanonical modes. Structural studies revealed that the p73-TAD peptide interacts with a different site of BCL-x_L in a different orientation from that of other BH3 peptides, involving contacts with BH1, BH3 and BH4 domains (Figure 1-13 (a)); [64] p53 doesn't bind to the traditional hydrophobic cleft for BH3-only proteins, but an acidic region involving α1, the loop between α3 and α4, and the loop between α5 and α6 (Figure 1-13 (b)). PUMA and BAD also showed an ability to block the p53/BCL-x_L interactions through an allosteric mechanism.[72,74]

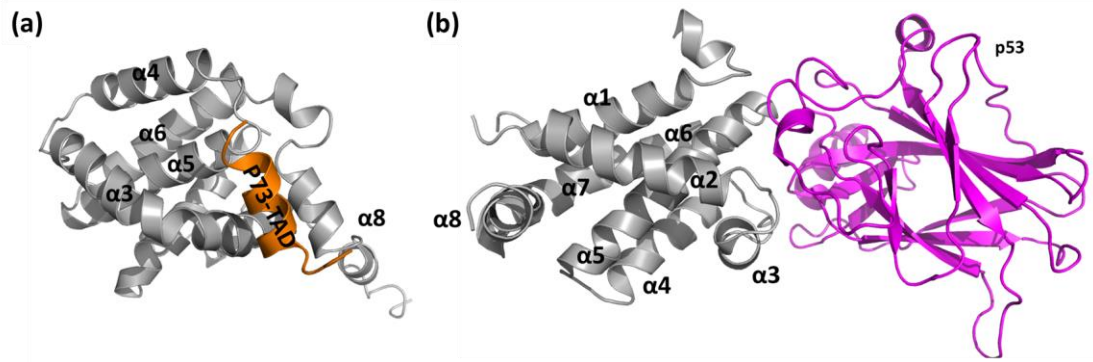

Figure 1-13 (a) structure of the complex of P73-TAD with BCL-x_L (PDB ID: 6IJQ); (b) structure of the complex between p53 and BCL-x_L (PDB ID: 2MEJ).

1.3 Chemical toolbox to make constrained peptides

Utilising peptides as modulators of PPIs has emerged as a promising strategy, given their larger sizes and intrinsic conformations mimicking native binding domains.[75] Peptides have many advantages to serve as highly potent and biocompatible drug candidates, but possess also limitations that hamper their applications in the clinic, e.g. low oral absorption, poor membrane permeability and rapid clearance.[76–80] One of the problems for peptides that have intrinsic helical structures, is the high tendency to lose their bioactive shape when taken out of their natural parent proteins, therefore developing an efficient chemical toolbox to stabilise the helical conformation of peptides could result in improved pharmacodynamic properties.[81,82] Constraining a peptide into a preorganised helical conformation can promote the binding between a peptide and its target protein, facilitating modulation of helix-mediated PPIs.[77,83,84] Many chemical biologists are enriching the arsenal of synthetic linkages that can reinforce the α-helical conformation of peptides, commonly referred to as “constraining” or “stapling”. Peptide constraining techniques have many advantages, e.g. they can increase the α-helical propensity, facilitate ligand-target binding, enhance cellular uptake and improve metabolic stability.[77,84–86]

The earliest reported investigation of cross-linking between peptide side-chains was intramolecular lactamisation developed by Madison and co-workers[34]. They created a lactam linkage by replacing the natural salt bridge with a covalent amide bond between Lys and Asp residues. In the last few decades, a blooming chemical library of stapled peptides has been established, e.g.

hydrocarbon bridges,[87] triazoles,[88] thioether,[89] and others,[83] some of which will be discussed in the rest of this chapter.

1.3.1 Hydrocarbon peptide stapling

1.3.1.1 Hydrocarbon stapling using α,α-disubstituted amino acids

Importantly, one of the most notable methods in this field is hydrocarbon stapling, which was firstly developed by Verdine and colleagues,[87] to create intramolecular side-chain to side-chain cross-linkages using two α,α-disubstituted amino acids with one methyl group and one hydrocarbon side chain containing a terminal olefin handle of variable length. This work was inspired by Grubbs' pioneering work in which they cross-linked peptide sidechains using *O*-allyl serine variants *via* ring-closing metathesis (RCM).[90] Verdine and co-workers further incorporated the α,α-disubstituted non-natural amino acids into the BID BH3 domain to synthesise hydrocarbon stapled bioactive peptides, laying a solid foundation for application of hydrocarbon stapled peptides to other PPIs which were considered as undruggable targets.[91] Nowadays, hydrocarbon stapling has become the most widely used method to stabilize α-helical segments as useful modulators or inhibitors of helix-mediated PPIs.[92] The most notable advantages of hydrocarbon stapled peptides are improved proteolytic stability and enhanced cell penetration, promoting their use as probes of intracellular targets.[77]

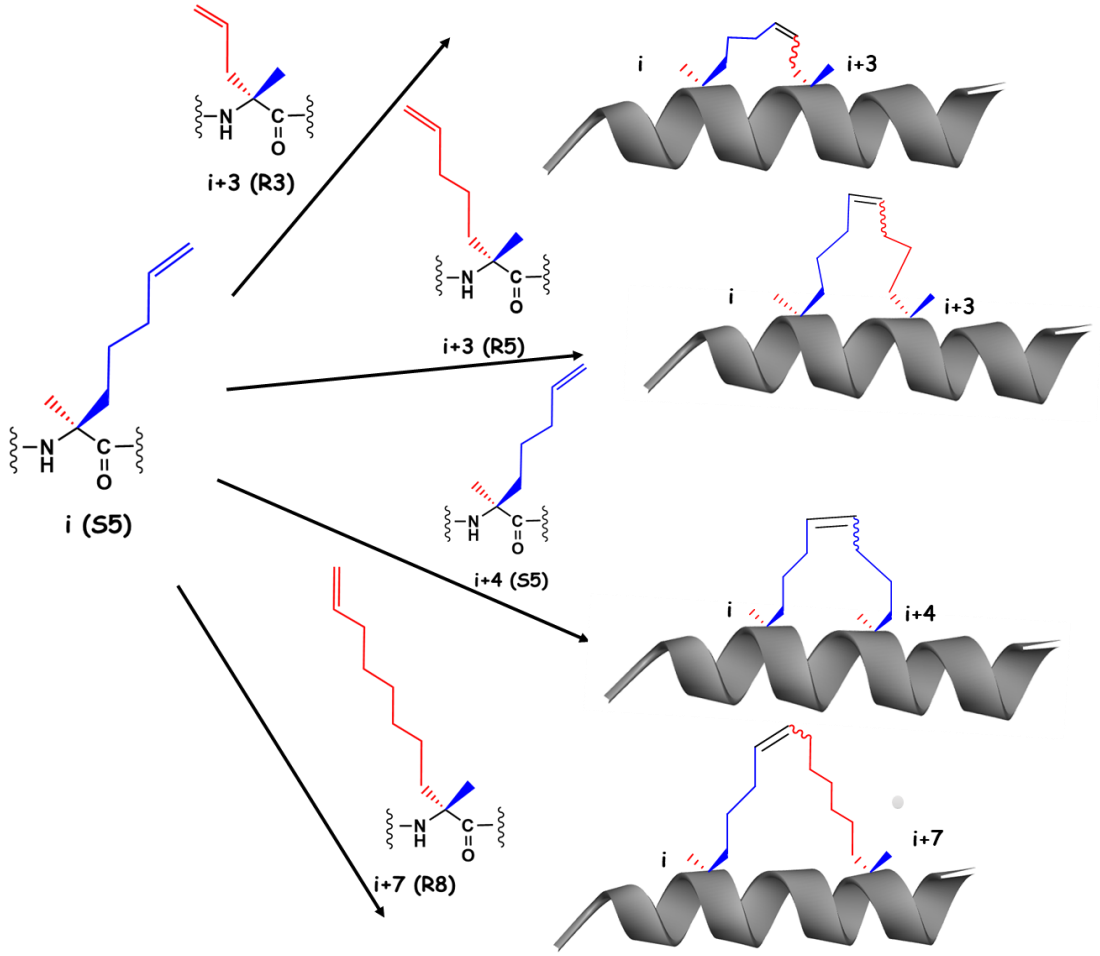

Figure 1-14 α,α-disubstituted non-natural amino acids pairs for different stapling positions[93–95]

Various lengths of olefinic side chains of α,α-disubstituted non-natural amino acids provide opportunities to create staples of different lengths at different positions. These non-natural amino acids are usually presented as Sn or Rn, where S or R denotes the absolute configuration and n denotes the number of carbon atoms in the hydrocarbon side chain. Positions *i*, *i*+3 and *i*, *i*+4 in a helical peptide are located on the same face of a helix one turn from each other and are most commonly used to introduce a staple. For stapling at *i*, *i*+3 positions, an eight-atom or six-atom hydrocarbon linkage can be created, through R5/S5[96] or R3/S5[94] pairs, respectively (Figure 1-14). So far, *i*, *i*+4 stapling is the most widely used method, which involves two S5 building blocks to afford a hydrocarbon bridge. The reduction of helix stabilisation as well as cellular uptake, as a result of replacement of an S5/S5 pair with an R5/R5 pair,

has been reported.[93] Although the stereochemical difference of an R5 pair was found to result in loss of helix stabilisation in left-handed helices of $_{L}$-peptides, the R5 pair was reported to be used in the synthesis of *i*, *i*+4 stapled $_{D}$-peptides which comprise right-handed helices.[97] Positions *i*, *i*+7 usually span two turns of a helix and are also located on the same surface of a helical peptide, thus they are another popular pair of stapling sites. To achieve *i*, *i*+7 hydrocarbon stapling, R8/S5 are the most commonly used building blocks, creating a hydrocarbon linkage containing 11 carbon atoms.[92]

Walensky and co-workers reported that the incorporation of double staples exhibited a synergistic effect on bioactivity and proteolytic stability of hydrocarbon stapled peptides (Figure 1-15 (a)).[98] Moreover, Verdine and co-workers reported a unique bicyclic form of double stapled peptides, termed "stitched peptides", with two contiguous staples sharing one common bridging site (Figure 1-15 (b)).[99] In this strategy, a bis-alkenyl non-natural amino acid, termed B5, was used. B5 has two 5-atom alkenyl side chains, each contributing to one hydrocarbon staple different from the other. Through this method, *i*, *i*+4+4 or *i*, *i*+4+7 staples can be inserted into a peptide.

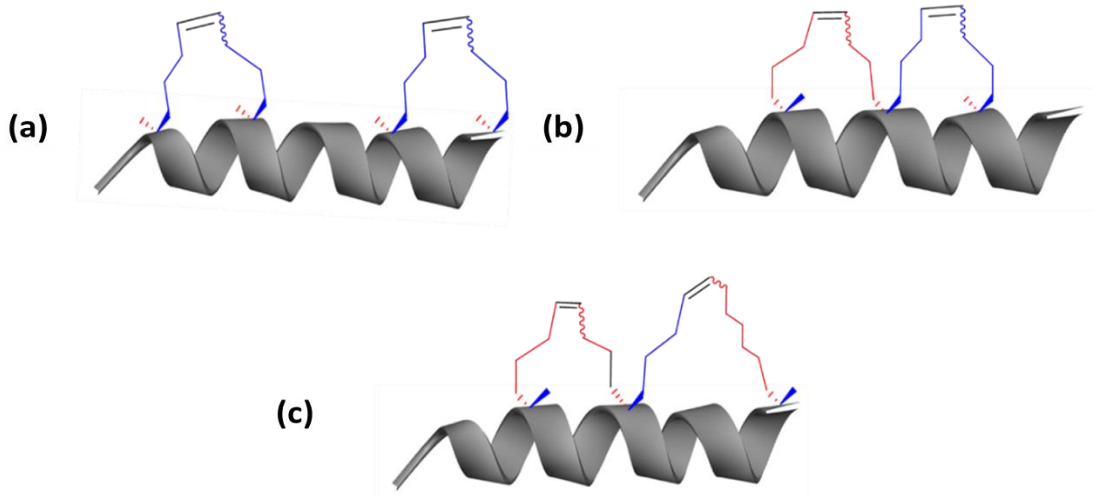

Figure 1-15 Double hydrocarbon stapling methods Double *i*, *i*+4 stapled peptide;[98] (b) i, i+4+4 stitched peptide;[99] (c) *i*, *i*+4+7 stitched peptide.[99]

1.3.1.2 Hydrocarbon stapling using monosubstituted amino acids

In general, incorporation of the α, α-disubstituted non-natural amino acids can be challenging due to steric hindrance arising from the co-existence of the α-methyl group and the α-alkenyl group.[100] Therefore, monosubstituted alkenyl amino acids provide an alternative strategy to assemble hydrocarbon stapled peptides. The Wilson group reported the incorporation of *(S)*-alkenylglycine into

a BID BH3 peptide to synthesise the corresponding stapled peptides, and compared them to a peptide stapled using conventional α, α-disubstituted amino acids (Figure 1-16).[101] The monosubstituted stapled BID showed not only similar inhibitory activity in a fluorescence anisotropy assay against the BCL-x_L/BAK PPI, but also comparably improved helicity and proteolytic stability, demonstrating an efficient approach to simplify synthesis of hydrocarbon stapled peptides.

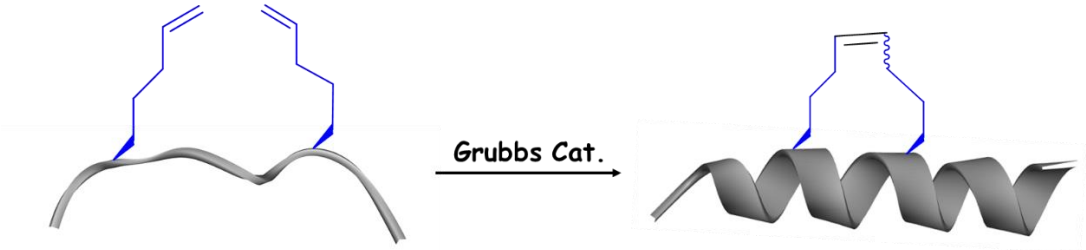

Figure 1-16 Schematic diagram of monosubstituted hydrocarbon stapling. [101]

1.3.1.3 Hydrocarbon stapling using naturally mimicking non-natural amino acids

Synthesising a hydrocarbon stapled peptide requires the replacement of two original residues. To avoid the loss of interaction with targets, the stapling sites are typically located at a non-interacting surface (also known as the solvent-exposed surface).[102] While creating a stapled peptide, maintaining intrinsic properties of naturally occurring residues could prevent the reduction of interaction between peptide and target. Moore and co-workers reported γ-methylated disubstituted amino acids based on S5 as both building blocks for staples and mimics of isoleucine and leucine (Figure 1-17 (a)).[103] The resulting stapled peptide using the *(S)*-γ-methylated amino acid showed higher binding affinity in comparison to the S5 stapled counterpart in the Estrogen Receptor/Coactivator PPI.

Recently, Hu and co-workers developed a novel class of α,α-disubstituted non-natural amino acids with replacement of the α-methyl group with the original side chain (Figure 1-17(b)).[104] These amino acids can be used for *i*, *i*+3/4 stapling and also contain protecting groups for standard Fmoc-based solid phase peptide synthesis.

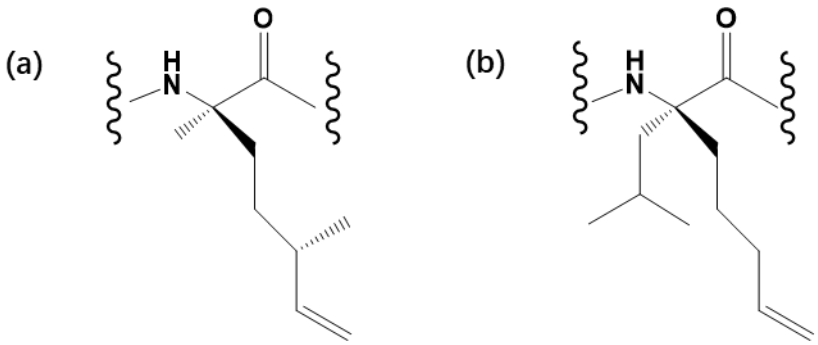

Figure 1-17 Structures of Non-natural amino acids for mimicking native amino acid residues (a) non-natural amino acid with γ-methylated hydrocarbon side chain;[103] (b) non-natural amino acid containing alkenyl side chain derived from leucine.[104]

1.3.2 Click chemistry in peptide stapling

The concept of a "click" reaction was initially introduced by Sharpless, to synthesise a triazole linkage from an azido group and an alkynyl group under Cu(I) catalysis in an aqueous environment (Cu(I)-catalysed azide–alkyne cycloaddition, (CuAAC)).[105] The concept of "click" reactions has since been vastly broadened. The "Click" reaction can denote a variety of conjugation reactions that occur with high yield, under biologically compatible conditions and produce limited byproducts, and has been extensively reviewed by Tang *et al*.[106] The type of click reactions that are related to azide-alkyne cycloaddition, will be discussed in this section, because they have emerged as a class of widely used approaches in peptide modifications, particularly in peptide stapling.

One approach to synthesise stapled peptides by CuAAC is to incorporate two non-natural amino acids, of which one has an azido side chain and the other has an alkyne side chain, into a linear peptide sequence at appropriate positions and perform the cross-linking reaction (Figure 1-18). In practice, Wang and co-workers designed a series of peptides targeting the PPI between β-catenin and B-cell CLL/lymphoma 9 (BCL9).[88] The 24-residue helical segment in BCL9 was selected and was incorporated with the complementary azido and alkynyl amino acids at specific *i*, *i*+4 positions. They systematically investigated the lengths of cross-linking as well as the stapling positions that would have influence on the α-helicities and binding affinities of the resulting peptides. They also utilised the click reaction to create double stapled peptides that showed better α-helicity and metabolic stability.

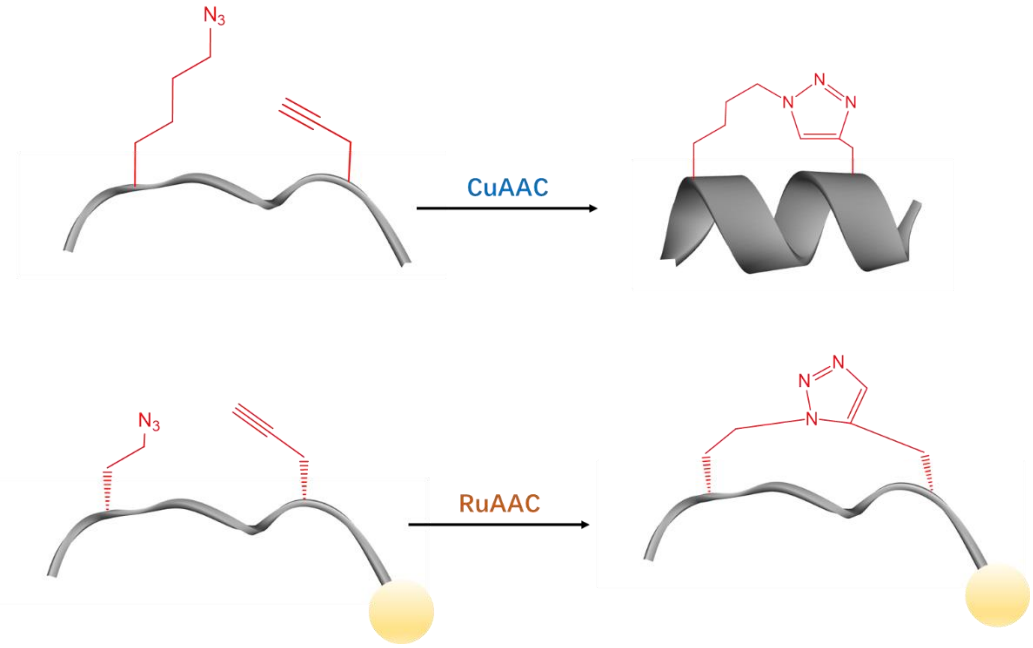

Figure 1-18 CuAAC and RuAAC form different triazole bridges between peptide side chains. [88, 107]

Kormar and co-workers' work provides an alternative solid-phase synthetic route to triazole stapled peptides (Figure 1-18).[107] Normally aqueous CuAAC combines azides and terminal alkynes to exclusively afford 1,4-disubstituted 1,2,3-triazoles.[108] In contrast, Kormar's method using a ruthenium(II)-based catalyst (RuAAC) creates a 1,5-disubstituted 1,2,3-triazole. However, the difference between these two triazole bridges results in divergence of biological activities.[109]

While a single click reaction can link two complementary functionalised residues to form a staple, a bis-triazole staple is accessible using a diyne cross-linker that reacts with two residues bearing azido sidechains. Bong and co-workers applied double click reaction to a 21-residue segment from the GCN leucine zipper.[110] They incorporated a pair of azidoalanine residues at *i*, *i*+4 positions for the formation of staples with several diyne linkers. Spring and co-workers developed an *i*, *i*+7 double click stapling methodology, that allows for various functional groups to be attached on the stapling bridges (Figure 1-19),[111] and utilised the stapled peptide-conjugates in a cellular study. They afterwards explored the application of double-click *i*, *i*+4/7 stapled peptides as well as their corresponding functionalised conjugates, either helical[112] or non-helical,[113] in targeting PPIs.

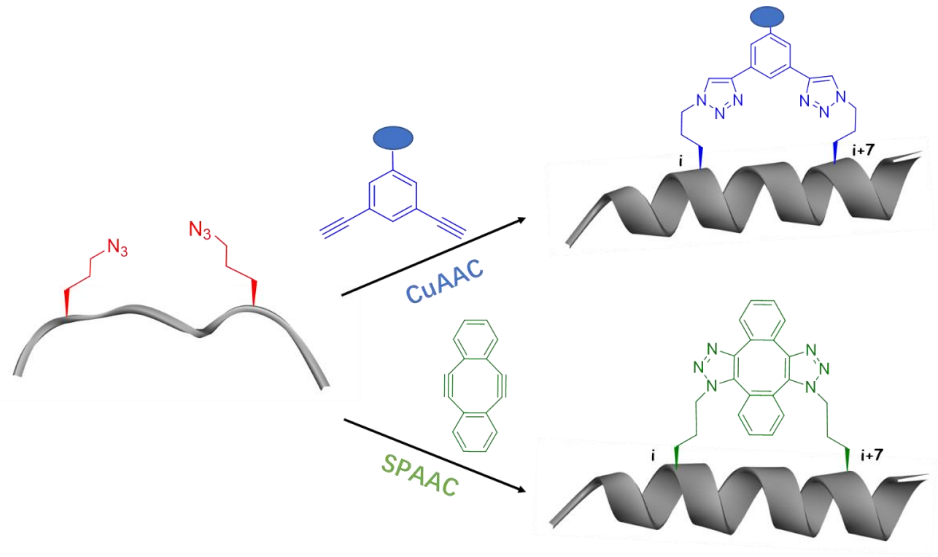

Figure 1-19 Comparison of i, i+7 stapling via CuAAC and SPAAC double-click methods (the blue spheres denote functionalities). [111, 114]

Although CuAAC plays an important role in the peptide constraining repertoire, the residual copper may have significant influence on interpretation of biological analyses due to the cytotoxicity of Cu(I).[106] To overcome the barriers caused by copper, Bertozzi and co-workers replaced the alkyne with a strained cyclooctyne.[115] Because this class of click reactions are driven by the strain in the alkyne rings, they are referred to as "Strain-promoted azide-alkyne cycloaddition" (SPAAC) reactions. Spring and co-workers developed a new copper-free double-click constraining method based on SPAAC (Figure 1-19).[116] The constraining was carried out on a p53-derived peptide in cell culture. Several *in situ* constrained peptides showed inhibitory activities against the p53/hDM2 interaction. This method allows scientists to screen constrained peptides without further purifications after constraining. More recently, they optimised the cyclooctadiyne-derived linker with water-soluble tertiary and/or quaternary ammonium groups.[114] In addition, the post-macrocyclization modification was successfully achieved *via* substituted crosslinkers.[117]

1.3.3 Cysteine-based peptide constraining

Cysteine can serve as an efficient handle to install staples due to its unique properties as a naturally occurring amino acid. The reasons why cysteine becomes an ideal stapling site are as follows: 1) high accessibility of incorporation into a peptide or protein through solid-phase peptide synthesis or engineered coding *E-coli* expression machinery; 2) easy and selective modification because of the high nucleophilicity of the thiolate group; 3) stapling

can be achieved through many reactions that use biocompatible conditions and cheap reagents; 4) spatial versatility of staples provided by other cysteine analogues (e.g. $_{D}$-cysteine and homocysteine).

Dawson and co-workers developed a thioether constraining technique via inserting an α-bromoacetyl ornithine residue (Orn) that can react on-resin with free cysteine after deprotection of the orthogonal protecting group (Figure 1-20 (a)).[89] Li and co-workers reported a novel constraining reaction between a free cysteine and a free lysine on a peptide in PBS buffer, involving an *ortho*-phthalaldehyde (OPA) molecule as a covalent linking mediator (OPA-guided cyclization, Figure 1-20 (b)).[118] At the same time, Perrin and co-workers utilised substituted OPAs as fluorescent linkers; they have named this constraining reaction as “Fluorescent Isoindole Crosslink (FIICk) chemistry”.[119]

Cysteine is a chemical precursor of dehydroalanine (DHA) which is a useful starting point for different post-translational modifications (PTMs).[120] Lu and co-workers started from cysteine and lysine to create stapled peptides as hDM2/hDMX inhibitors.[121] In their procedure, they firstly converted the cysteine to DHA, then formed the dithiocarbamate (DTC) linkage via a thiocarbonyl group with the lysine. However, the stapling cysteine loses its stereogenic center during the DHA formation (Figure 1-20 (c)). Li and co-workers developed a photo-induced thiol-yne constraining strategy with the assistance of a photoinitiator (Figure 1-20 (d)).[122] Recently, the same group reported a new stapling strategy involving alkylation of one cysteine and one methionine with a dihalogenated small-molecule linker.[123] The resultant stapled peptide has applicable potential in peptide-based ligand induced protein labelling (Figure 1-21).

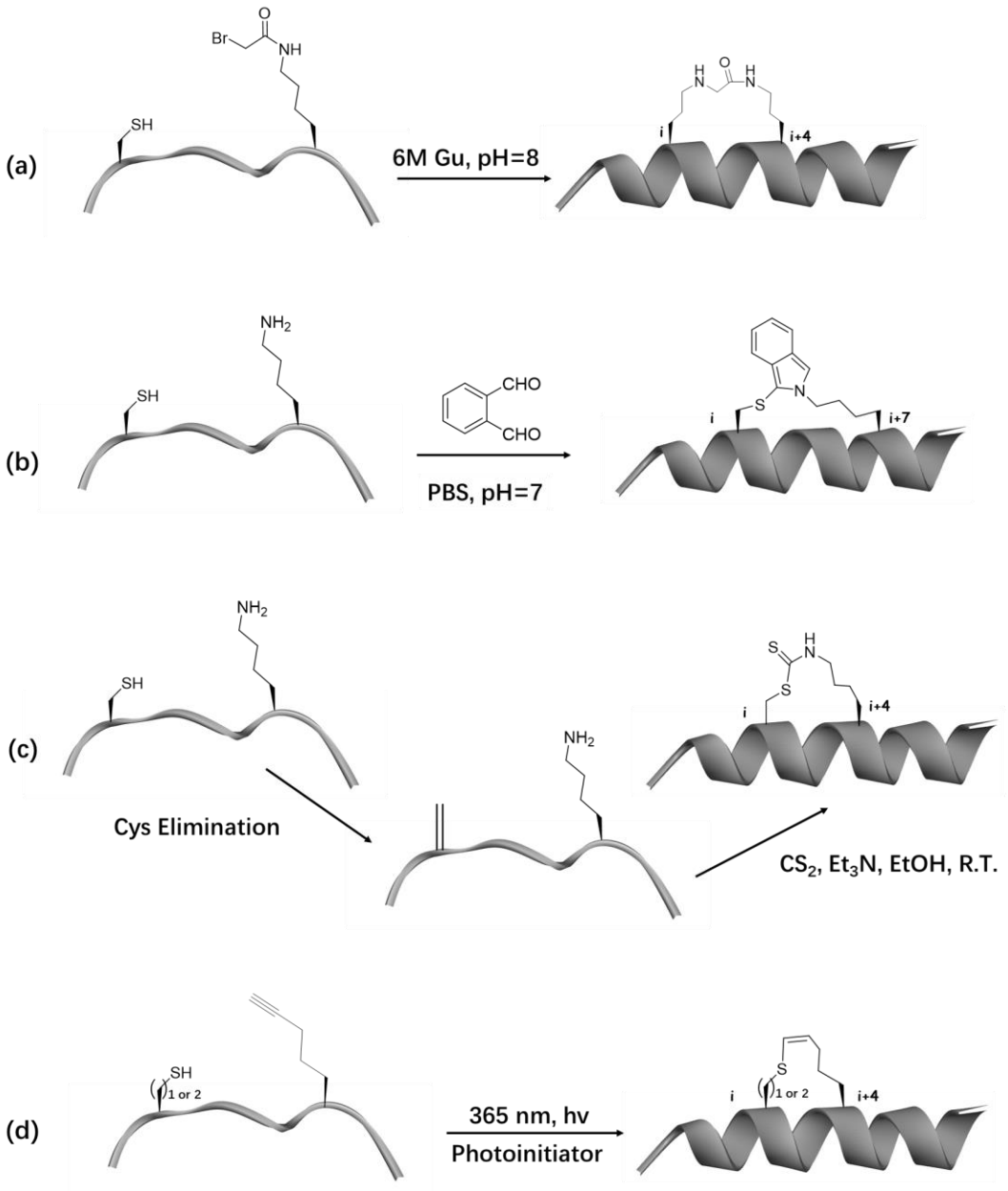

Figure 1-20 Single-cysteine-based peptide constraining methods; (a) Thioehther stapling method developed by Dawson; [89] (b) OPA-guided stapling; [118,119] (c) Photo-induced intermolecular thiol-yne stapling;[122] (d) DTC stapling via thiocarbamate.[121]

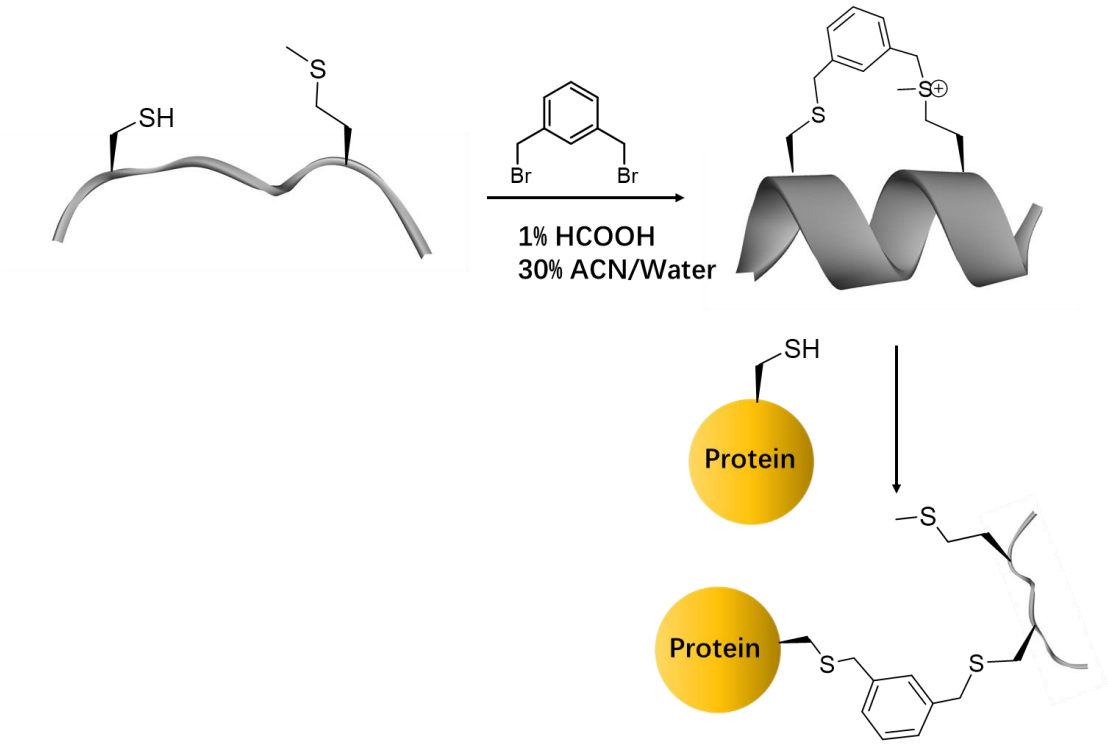

Figure 1-21 Methionine-based peptide stapling and protein labelling.[123]

Placing two cysteines into a peptide sequence as stapling handles has been widely studied with a variety of chemical linkers. In general, the stapling reactions for bis-cysteine-containing peptides are usually achieved by *S*-alkylation or *S*-arylation with bis-electrophilic spacers. The nucleophilic substitution reactions are often carried out in aqueous solution using pre-treatment with tris(2-carbonxyethyl)phosphine (TCEP) as a reducing reagent. Avoidance of disulfide-bond formation, and the assistance of water-soluble organic solvents (e.g. acetonitrile, DMSO and DMF), are usually necessary.[124]

Typically, bis-cysteine staples are formed between two thiolate groups of unprotected cysteine and a bifunctional small-molecule linker. Dihalogenated spacers have been widely used and studied as thiol-reactive reagents. The Woolley group reported photo-switchable bis-cysteine stapled peptides containing a photosensitive azobenzene linker located at *i*, *i*+7 positions with light-dependent tunability between the *cis*- and *trans*- conformation.[125] The Lin group utilised optimal rigid bisarylmethylene bromides to achieve *i*, *i*+7 stapling.[126,127] In this staple, a pair of L- or D-cysteines or the hybrid combination could be selected as building blocks to match the spatial distance between two ends of the linkers.

In order to synthesise *i*, *i*+4 bis-cysteine stapled peptides, many commercially available dibromo-linkers have been screened in various templates.[128]

Pentelute and co-workers developed a class of perfluoroaryl linkers for *i*, *i*+4 stapling.[129] Although the resulting stapled peptides showed an abnormal circular dichroism (CD) spectrum probably due to the C_6F_4 linker, they exhibited improved binding to the C-terminal domain of an HIV-1 capsid assembly polyprotein, enhanced cellular uptake and better metabolic stability. In addition, *i*, *i*+3 bis-cysteine stapled peptides are also accessible by many linkers which are commonly used in *i*, *i*+4 spacing.[130] More recently, Wang and co-workers developed a novel class of dinitroimidazole-based cross-linkers in peptide stapling involving a pair of cysteines or lysines at *i*, *i*+2/4/6 positions.[131]

The rapid and quantitative conversion and biocompatible condition for bis-alkylation of cysteines provide opportunities for screening constrained peptides without further purification.[132] Kritzer and co-workers described a diversity-oriented stapling method to generate cell-permeable autophagy inducers. In this study, $_L$- or $_D$- cysteines were introduced into a 10-mer Beclin-1 sequence, followed by constrained with various dibromo-linkers to generate diverse peptides and tested in cell-based assays. A constrained peptide was observed to have retained cell-permeability and autophagy inducing activity in comparison to the conjugate containing the cell-penetrating motif.

Similar to the double-click stapling, post-macrocyclization modification is a special advantage of the bis-cysteine stapling techniques using spacers with sites accessible for further modifications.[83,86] Smith and colleagues introduced a tetrazine into an unprotected peptide between two cysteines located at various positions (Table 1-3).[133] An inverse electron demand Diels-Alder reaction (IEDDA) was then used to conjugate other functional probes with the stapled peptides.

The Wilson group reported a novel *i*, *i*+4 bis-cysteine or bis-homocysteine stapling method using dibromomaleimide.[134] The formed staples significantly improved α-helicities of the precursors, with the added benefit of being reversibly removed by excess glutathione. Moreover, an alkynyl handle onto the maleimide bridge as installed via a Mitsunobu reaction, was shown to facilitate further modification via CuAAC click chemistry (Table 1-3).

Conjugations are not easily achieved on aliphatic cross linkers due to their lack of reactive sites. The Dawson group reported a new bis-cysteine stapling strategy using dichloroacetone (DCA), facilitating further modification via an oxime ligation (Table 1-3).[135] What's more, they expanded the scope of this acetone-crosslinking technique to generation of N-terminus to side-chain macrocyclic peptides.

Table 1-3 A summary of representative post-macrocyclization modification methods for bis-Cys peptide constraining.

Constraint	Linker	Conjugate	Ref
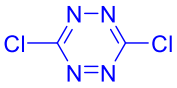	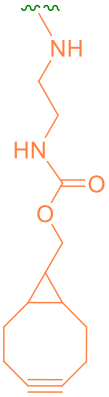	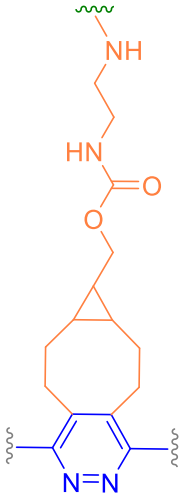	133
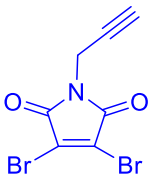		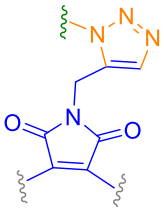	136
		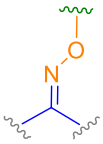	135

1.3.4 Other stapling methods

Horne and co-workers reported the synthesis of stapled peptides via an oxime cross-linkage (Figure 1-22 (a)).[137] They created the oxime staple, affording a *Z*- and *E*- mixture, between an isostere of Orn or Lys bearing an aminooxy group and Ser-acylated side chain that can be oxidised to an aldehyde under mild conditions in solution. Based on this methodology, they showed that the presence of protein (receptor) can induce conformational changes of disordered peptide ligands and affect crosslinking reaction yield and rate.[138]

Apart from the oxime stapling, the blooming C-H activation toolkit has also triggered a wave of applications in creating new constrained peptide architectures. Lavilla and co-workers reported a stapling strategy between Phe/Tyr and Trp via a selective Pd-catalysed C-H arylation, which is suitable to create an *i*, *i*+3/4 linkage (Figure 1-22 (b)).[139] They have also successfully achieved cross-linking between two peptides as well as a bicyclic peptide. Albericio and co-workers then described a new stapling approach through a C(sp^3)-H activation (Figure 1-22 (c)).[140] This method showed ideal tolerance for different sequences and accessibility for both *i*, *i*+3 and *i*, *i*+4 positions. Moreover, they expanded the methodological scope of this strategy to solid-phase chemistry. Moellering and co-workers recently reported an unprecedented stapled structure using a Diels-Alder cycloaddition (Figure 1-22 (d)).[141] They described the synthesis of *i*, *i*+4 as well as *i*, *i*+7 stapled peptides using this method.

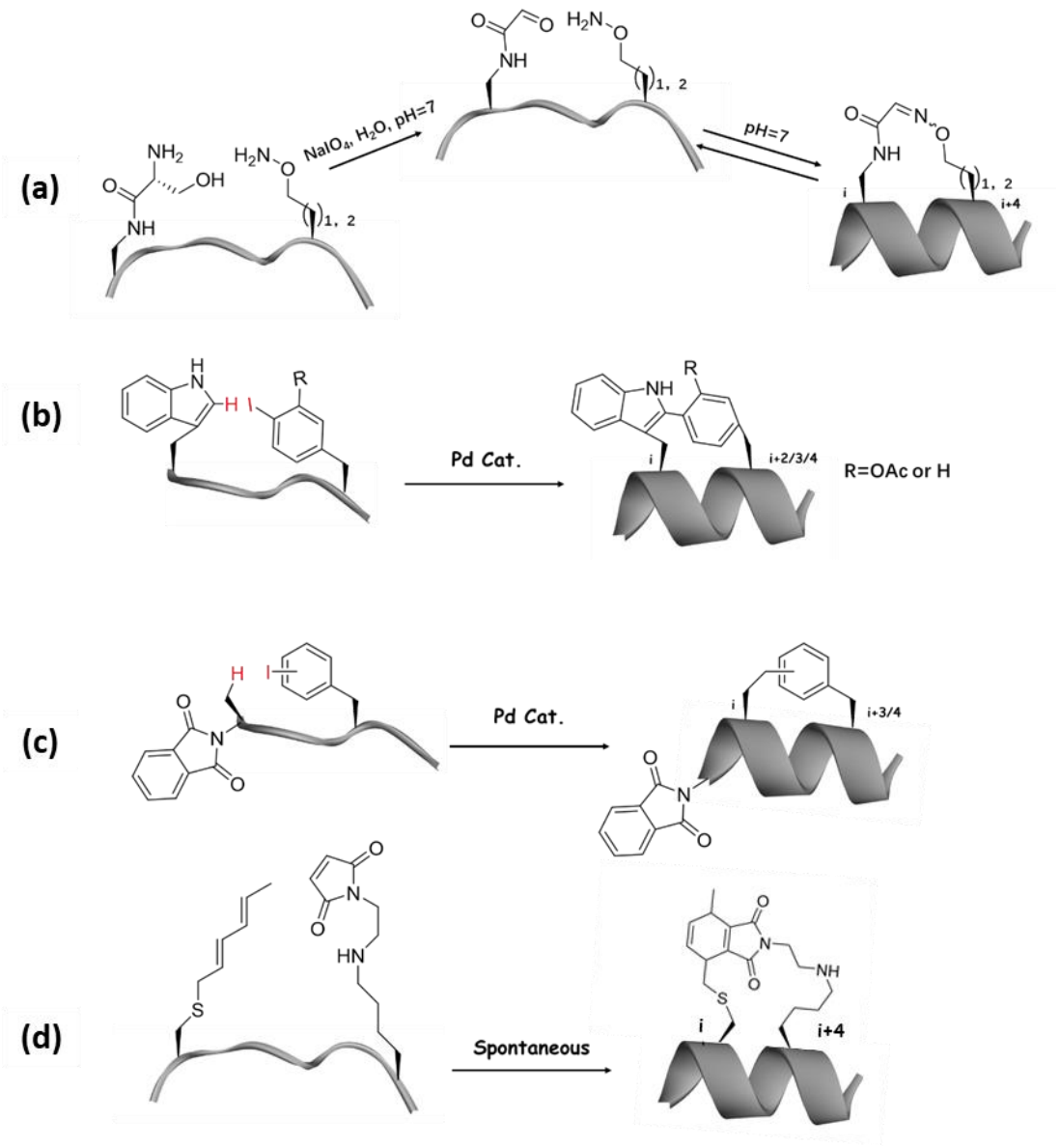

Figure 1-22 Other peptide constraining methods (a) Reversible oxime stapling;[137] (b) C(sp2)-H activation peptide stapling;[139] (c) C(sp3)-H activation peptide stapling;[140] (d) Peptide stapling via Diels-Alder reaction.[141]

1.4 An introduction of cysteine crosslinking using maleimide-based linkers

Maleimide-derived linkers have been widely used in protein modification and bioconjugation since the Baker 2010 study.[142] In this study, the group showed the power of using *N*-Methylbromomaleimide for efficient cysteine crosslinking and protein modification, which was shown to be reversible under treatment with TCEP, when the maleimide moiety is monosubstituted; and irreversible when the maleimide moiety is disubstituted (Figure 1-23(a)).[142] In the same study, bromomaleimide and dibromomaleimide (DBM) were also reported to be used for bis-cysteine crosslinking (Figure 1-23 (b)). Further functionalities, e.g. fluorescent label or PEG, could be installed through a dehydrative cyclisation using dibromomaleic anhydride[142] or a Mitsunobu reaction.[143] Dibromomaleimide can also be used as a starting material to generate dithiophenolmaleimide, which is more reactive for crosslinking and more tolerant to reducing reagents.[143]

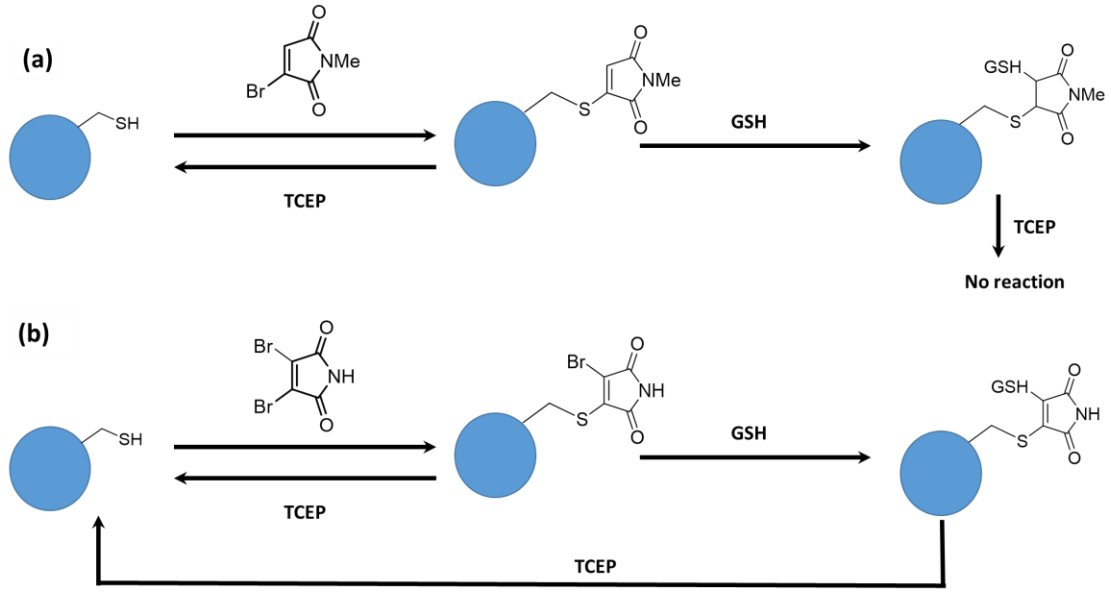

Figure 1-23 Maleimide-based linkers for protein modification; (a) protein modification using N-methylbromomaleimide; (b) protein modification using dibromomaleimide.[136]

Thereafter, maleimides have been widely used to generate antibody-drug conjugates (ADCs). Caddick and co-workers developed an acid-cleavable linker for generation of ADCs.[143] The payload can be released under lysosomal pH. Cyclisation and hydrolysis of substituted maleic acid/anhydride have also been used to develop drug delivery systems with acid-cleavable or charge reversal functions.[144] The Caddick group thereafter applied maleimide-based

linkers to generate ADCs from trastuzumab and doxorubicin (DOX), with controlled drug-to-antibody ratio (DAR) (Figure 1-24).[145] Lyon *et al.* described self-hydrolysing maleimides for generation of stable ADCs.[145] The maleimide containing an adjacent amino group can undergo hydrolysis rapidly under neutral pH.

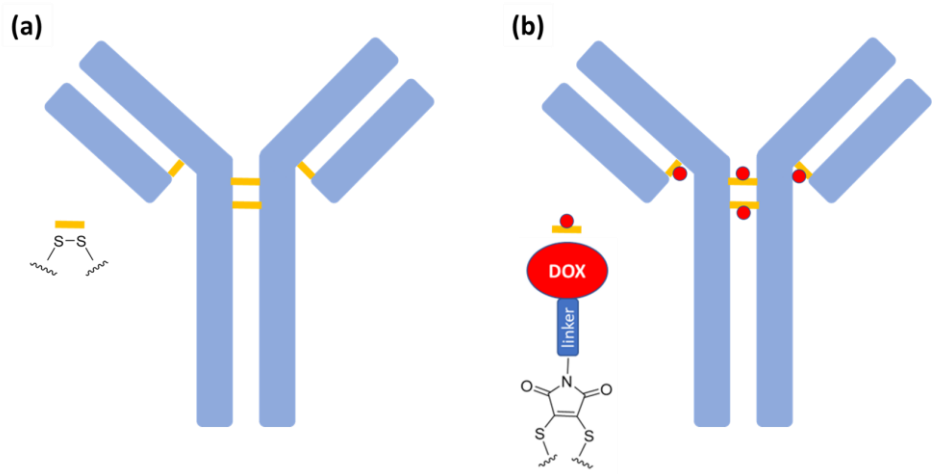

Figure 1-24 Dibromomaleimide linkers to generate ADCs (a) antibodies without further chemical modification; (b) ADC generated by dibromomaleimide linker and DOX.[145]

Baker and co-workers described a method using monosubstitued maleimides to irreversibly crosslink a pair of cysteines via [2+2] photocyclisation in peptides (Figure 1-25 (a)).[146] The Wilson group firstly used dibromomaleimide for peptide constraining.[136] Using BID and RNase S peptides as models, dibromomaleimide (DBM) was used to generate constrained peptides at *i*, *i*+4 positions (Figure 1-25 (b)). The constraint can be removed using excess reducing reagents. The DBM constrained peptides showed enhanced helicity, retained bioactivity and improved proteolytical stability. Additional functionalities could be added using an alkyne modified dibromomaleimide and further alkyne-azide cycloaddition.

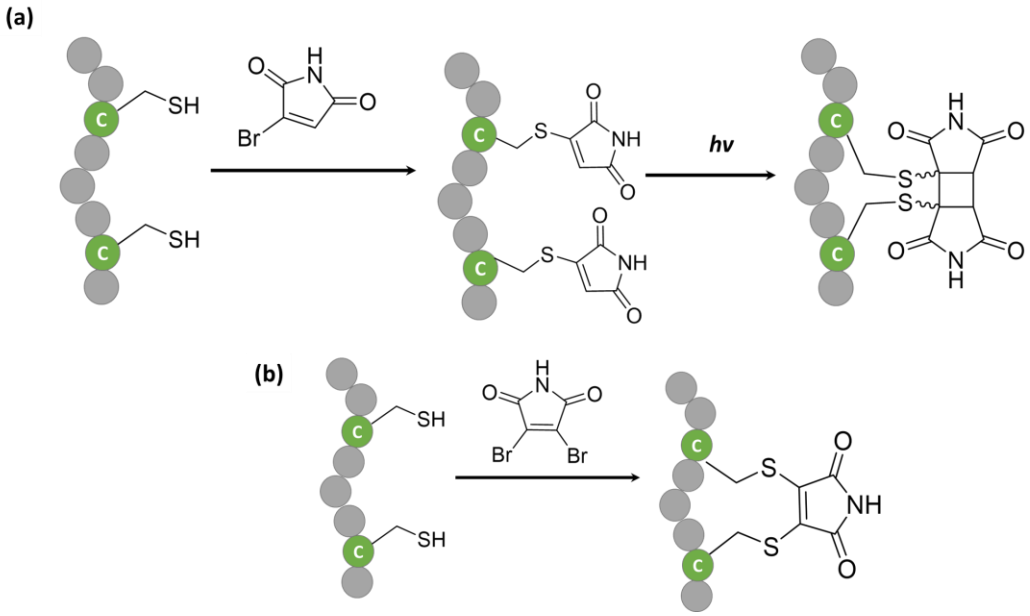

Figure 1-25 Maleimide-based molecules for peptide cyclisation; (a) [2+2] photocyclization of bromomaleimide-modified peptides; [146] (b) peptide cyclisation using dibromomaleimide.[136]

1.5 Importance of peptide binding mechanisms and influence of introducing a constraint

Pre-organisation of a peptide by introducing a constraint has been shown to improve binding affinity towards the target in a large number of examples.[77,147] This effect is usually attributed to increased concentration of the bioactive conformer arising from limited conformational freedom, thus reducing the entropic cost for binding and resulting in favourable interaction with its target.[148] This binding process is usually referred to as a conformational selection model (Figure 1-26 (a)).[148] In contrast, accumulated studies demonstrate binding processes are more complex in other cases, which are usually described as a "bind and fold" or an "induced fit" mechanism (Figure 1-26 (b)).[148–150] In these cases, the target protein is able to recognise various conformers and undergo a conformational change during binding and the ligand adopts the bound conformation upon binding.[149,150] Addition of a constraint onto a peptide is expected to restrict conformational flexibility and limit existence of conformers that potentially bind to the target. As a result, the constrained peptide is expected to bind and unbind to the target with a lower rate (k_{on} and k_{off}); and lose the enthalpy contribution associated with folding, e.g. contributions from backbone and side chain hydrogen-bonding, in comparison to the unconstrained peptide. These opposing entropic and enthalpic outcomes,

referred to as enthalpy-entropy compensation, are likely to lead to little or negative impact on affinity of constrained peptides.[147,149,150]

Enthalpy-entropy compensation has been observed in previous studies.[63,151,152] In a study on constrained peptides as BCL-x_L and MCL-1 inhibitors, the Wilson group found that introduction of a constraint led to increased helicity; however no enhancement of potency was observed and some constrained peptides lost potency.[63] From crystal structures, the constraints did not show steric clashes with the target; and the constrained peptides adopted a similar bound conformation compared to that of the wild-type. Further surface plasmon resonance (SPR) assays disclosed that the constrained peptides had slower binding rates (k_{on}) and similar unbinding rate (k_{off}) in comparison to the wild-type; whilst Van't Hoff analyses of direct fluorescent anisotropy binding assays revealed that the decreased entropy, which is favourable for the binding, was compensated by an increased enthalpy, thus resulting in an overall unfavourable influence on the binding free energy. Similar observations were reported in other studies, e.g. H3/ASF1[152] and eIF4E/eIF4G[153] interactions.

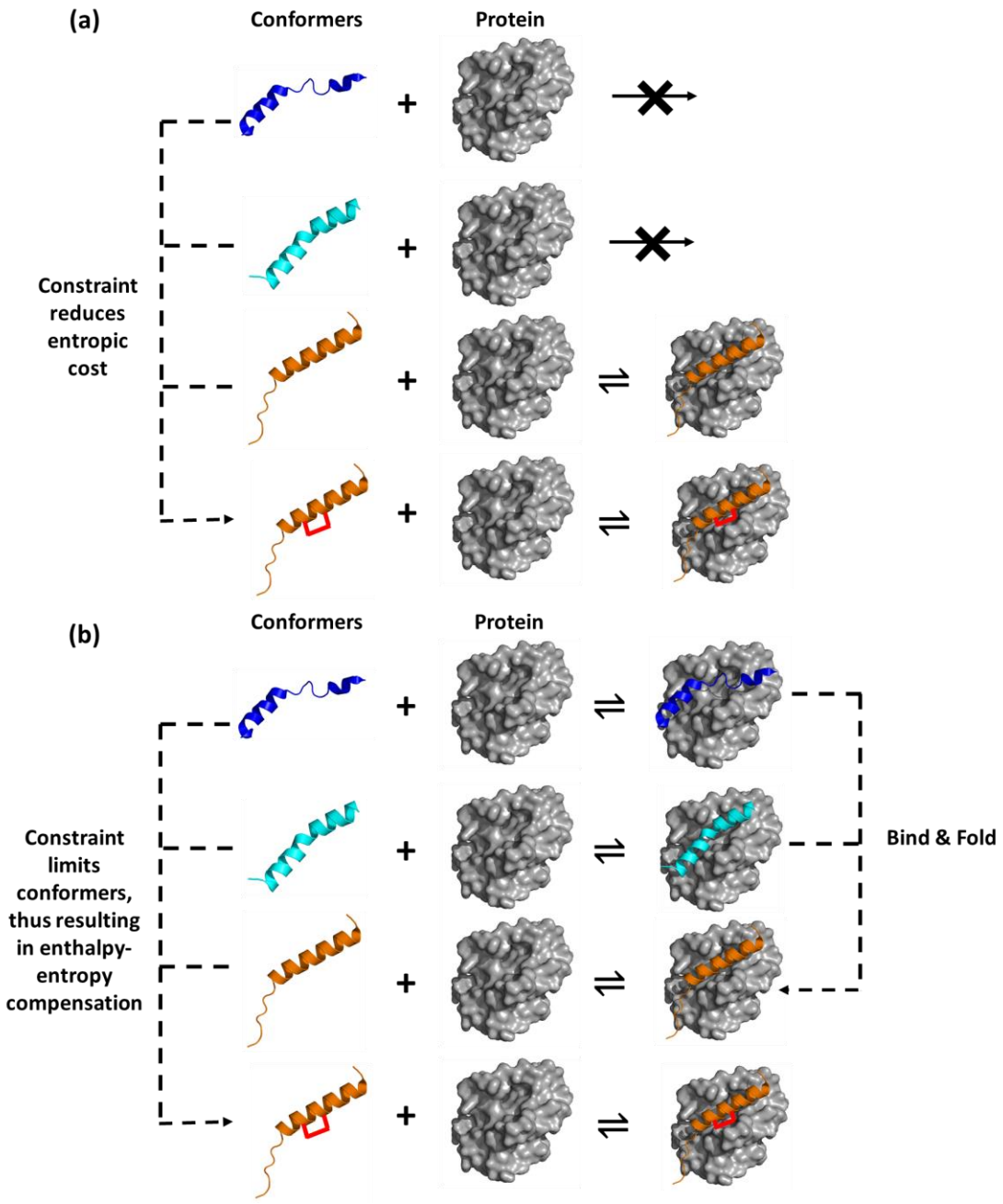

Figure 1-26 The influence of introducing a constraint on peptides; (a) constraining a peptide limits its potential conformers, thus (a) favouring peptide-ligand binding for a conformational selection mechanism; (b) resulting in loss of enthalpy upon backbone folding although reduced entropy from pre-organization in a "bind and fold" recognition mode (enthalpy-entropy compensation).

1.6 Applications of constrained peptides in modulation of BCL-2 family PPIs

Peptides are considered a class of candidate molecules for traditionally undruggable targets because of their intermediate molecular sizes and fully or partially retained binding affinities in comparison to native proteins.[77] The development of peptide stapling technologies has allowed scientists to synthesise conformationally stabilised peptides, which often have improved binding affinities arising from the pre-organisation towards a bioactive conformation, as well as more optimal biophysical properties, e.g. enhanced cellular penetration and proteolytic stability. Up to date, a variety of stapled peptides have been created based on versatile templates, e.g. hormones, antimicrobial peptides, and PPI inhibitors, for a broad range of biomedical applications, which have been reviewed previously.[77,154] In the following section, stapled peptides which serve as PPI inhibitors towards the BCL-2 family will be discussed.

BCL-2 family proteins include a number of proteins which are involved in cell survival and death processes.[34,41] Walensky *et al*. firstly introduced hydrocarbon stapling to a peptide from the BID BH3 domain.[91] Compared with the wild-type BID peptide, one of the stapled peptides, BID-1 ($SAHB_A$) showed high α-helicity, improved binding affinity, strong *in vivo* activity against human leukemia in mouse models, longer half-life and significant cell-permeability. Inspired by this pioneering work, numerous studies have been reported applying various stapling methods to different BCL-2 family proteins.

1.6.1 BID-derived constrained peptides

Walensky *et al*. reported the first hydrocarbon stapled BID BH3 peptide $SAHB_A$.[91] Thereafter, the same group described a stapled peptide BID $SAHB_A$, truncated from both the N-terminal and C-terminal by one residue according to $SAHB_A$ that can not only interact with BCL-x_L, but also bind to and activate BAX directly *in vivo*.[91] The Wilson group replaced the hydrocarbon staple formed by α, α-disubstituted amino acids with the one formed using monosubstituted alkenyl amino acids.[155] The stapled BID BH3 peptide, BID-MM, built using monosubstituted amino acids (Figure 1-27 (a)), showed comparable binding affinity in a BCL-x_L/BAK competition assay and proteolytic stability to its

counterpart (Table 1-4), $SAHB_A$, which incorporated α, α-disubstituted amino acids. Thereafter, the group described that the increased α-helical helicity does not enhance the inhibitory activity of constrained peptides against PPIs involving an induced fit mechanism.[63] Furthermore, Green and co-workers demonstrated that the same hydrocarbon stapled BID peptide $SAHB_A$ can trigger the conformational changes of BAK via a "hit and run" mechanism, thus activating the further homodimerization that is required for MOMP; the co-crystal structure of the constrained peptide, $SAHB_A$ with BAK was reported (Figure 1-27 (b)).[156] Recently, the Wilson group developed a novel dibromomaleimide crosslinker for cysteine-based peptide stapling, and applied it to the BID BH3 domain.[136] The dibromomaleimide-stapled peptides with two cysteines (STA-BID-Cys) or two homocysteines (STA-BID-hCys) both exhibited increased binding affinities in a BID/MCL-1 competition FA assay (Table 1-4), and improved proteolytic stabilities as demonstrated by trypsin proteolysis.

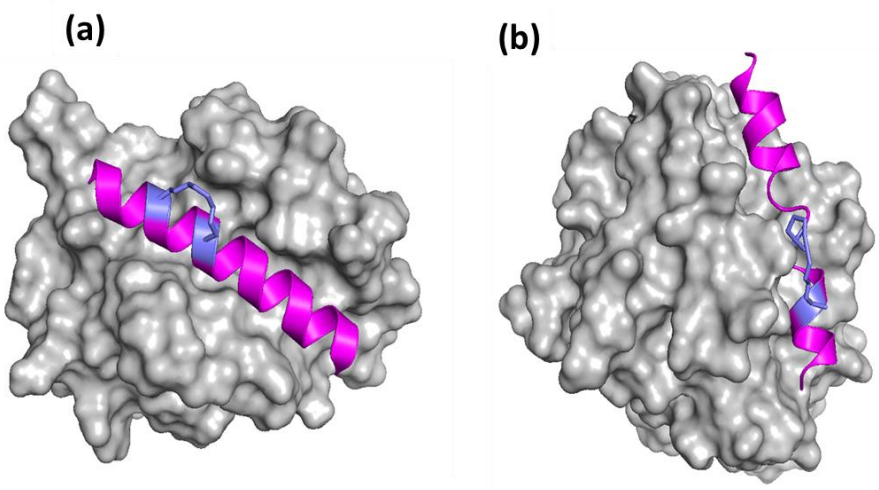

Figure 1-27 Two crystal structures for complexes between hydrocarbon stapled peptides and their targets (a) Crystal structure of the complex between BID-MM and MCL-1. (PDB ID: 5C3F); [63] (b) Crystal structure of the complex between $SAHB_A$ and BAK (PDB ID: 2M5B). [156]

Table 1-4 A summary of BID-derived constrained peptides.

Peptide	Sequence[a]	k_d or IC_{50} (Target/ testing method)[b]	Ref
BID BH3	EDIIRNIARHLAQVGDSZDRSIW	ND	
$SAHB_A$	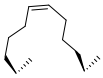 EDIIRNIARHLA*VGD*ZDRSIW	38.8 nM (BCL-2/FA)	91
BID $SAHB_A$	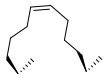 DIIRNIARHLA*VGD*ZDRSI	230 nM (BCL-x_L/FA)	91
BID-MM	 EDIIRNIARHLA*VGD*ZDRSIW	620 nM (BCL-x_L/FA)	155
STA-BID-Cys	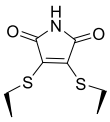 EDIIRNIARHLA*C*VGD*C*ZDRSIW	16.6 μM (BCL-x_L/FA); 19.4 μM (MCL-1/FA)	136
STA-BID-hCys	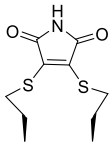 EDIIRNIAwRHLA*C*VGD*C*ZDRSIW	4.2 μM (BCL-x_L/FA); 9.5 μM (MCL-1/FA)	136

[a]Z denotes nor-Leucine; Asterisk denotes non-natural amino acids participating in formation of hydrocarbon staples; italic C denotes homocysteine; [b]ND: not determined; k_d values are shown in red and IC_{50} values are shown in blue; FA: fluorescent anisotropy.

1.6.2 BIM-derived constrained peptides

BIM is a BH3-only member of the BCL-2 family that can bind to many anti-apoptotic proteins, e.g. BCL-2, BCL-w, BCL-x_L, BFL1 and MCL1, and directly activate the effectors like BAK and BAX (Figure 1-28).[34,41,157] The Walensky group identified the interaction between the BAX protein and the BIM BH3 domain using a hydrocarbon stapled peptide.[158] Thereafter, the same group investigated the *in vivo* anticancer activity of a BIM BH3-derived stapled peptide, termed BIM $SAHB_A$.[159] The stapled peptide was found to bind to different anti-apoptotic proteins with increased affinities, e.g. BCL-x_L, MCL-1, BCL-w, and BFL-1, while the replacement of Arg153 with Asp resulted in significant loss of affinity (BIM $SAHB_A$ R153D, Table 1-3). In the *in vivo* study, BIM $SAHB_A$ selectively restored the death pathway in *Bim*-deficient immune cells, and exhibited significant anticancer activity in a human acute myelocytic leukemia (AML) xenograft model.

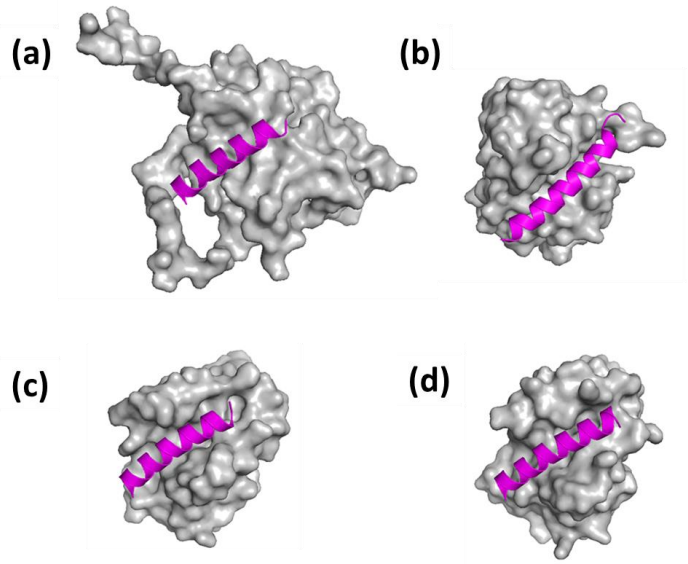

Figure 1-28 Representative structures for complexes between BIM and its BCL-2 family receptor proteins; Crystal structure of the complex between BIM and BAX (PDB ID: 2K7W);[158] (b) Crystal structure of the complex between BIM and BCL-2 (PDB ID: 4B4S);[160] (c) Crystal structure of the complex between BIM and BCL-x_L (PDB code: 4QVF);[28] (d) Crystal structure of the complex between BIM and MCL-1 (PDB code: 2PQK).[161]

Interestingly, Okamoto *et al.* reported an unexpected result when they used a similar BIM-derived hydrocarbon stapled peptide, BimSAHB (Figure 1-29), to investigate binding affinities for anti-apoptotic members of the BCL-2 family and cellular uptake.[162] They found that the stapled peptide showed reduced binding affinities to several anti-apoptotic proteins and no significant cell-permeability

or cellular apoptotic activity in mouse embryonic fibroblasts (MEF) cells. In response to these unusual results, the Walensky group suggested that this stapled peptide was not considered as a strong candidate for cellular studies due to its poor biophysical properties, e.g. low α-helical propensity, weak binding affinity and overall negative charge.[163] The Walensky group later revealed that BIM SAHB$_A$, with improved α-helicity and positive net charge, showed significant cytotoxicity and caspase 3/7 activation in living cells.[164] These studies have demonstrated the importance of biophysical properties of stapled peptides in biomedical applications.

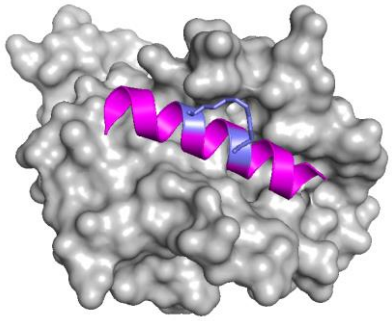

Figure 1-29 Crystal structure of the complex between BimSAHB and BCL-x$_L$. (PDB code:2YQ6).[162]

Repression of BIM was found to be associated with T-cell acute lymphoblastic leukemia (T-ALL) by Reynolds *et al*.[165] They utilised the stapled peptide BIM SAHB$_A$ to restore BIM activity in a zebrafish model. Recently, LaBelle and co-workers found that BIM SAHB$_A$ can efficiently decrease the viability of diffuse large B-cell lymphoma (DLBCL) cell lines but not the MCL-1 deficient MEF cells, demonstrating that the stapled peptide acts as a potent MCL-1 inhibitor.[109] The Keating Group synthesised a library of hydrocarbon stapled peptides from a BIM-derived peptide MS1, among which several exhibited low nanomolar binding affinity for MCL-1.[166] The most advanced stapled peptide incorporating aminoisobutyric acid (Aib) and Norleucine showed specifically improved binding affinity to MCL-1 and low nanomolar depolarisation activity of mitochondrial membranes. Later they reported a set of hydrocarbon stapled peptides, e.g. SAH-MS1-18, with enhanced α-helicity, cell-permeability and selectivity for inhibition of MCL-1-dependent cancer cells (Figure 1-30, Table 1-5).[167]

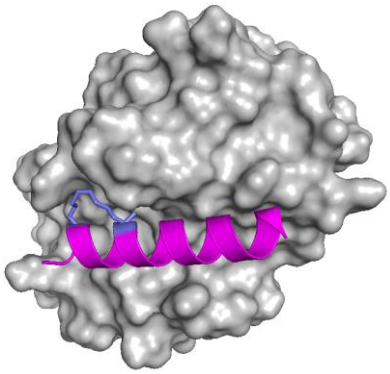

Figure 1-30 Crystal structure of the complex between MCL-1 and SAH-MS1-18. (PDB code: 5W5F).[167]

In addition to hydrocarbon stapled BIM peptides, Spring and co-workers developed functionalised stapled BIM peptides using a two-component CuAAC reaction.[168] Compared with ABT-373, a small molecule inhibitor of BCL-2 and BCL-x_L,[169] a BIM-derived stapled peptide (peptide 19, Table 1-5) was found to have comparable bioactivity but different mechanisms for apoptosis of platelets.

Table 1-5 A summary of BIM-derived constrained peptides.

Peptide	Sequence[a]	k_d or IC_{50} (Target/ testing method)[b]	Ref
BIM BH3	IWIAQELRRIGDEFNAYYARR	ND	
BIM SAHB$_A$	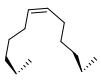 IWIAQELR*IGD*FNAYYARR	3.2 nM (BCL-x_L/FA);	159
		2.7 nM (BCL-w/FA);	
		10.7 nM (MCL-1/FA);	
		1.4 nM (BFL-1/FA);	
BIM SAHB$_A$ R153D	 IWIAQELD*IGD*FNAYYARR	>400 nM (BCL-x_L/FA);	159
		>400 nM (BCL-w/FA);	
		33 nM (MCL-1/FA);	
		>400 nM (BFL-1/FA);	
BimSAHB	 EIWIAQELR*IGD*FNAYYA	460 nM (BCL-2/SPR);	162
		300 nM (BCL-x_L/SPR);	
		370 nM (BCL-w/SPR);	

		3.4 nM (MCL-1/SPR)	
MS1	RPEIWMTQGLRRLGDEINAYYAR	>5000 nM (BCL-2, BCL-x_L BCL-w, MCL-1/FA)	166
M3d	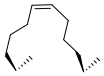 IWZXQGBRRLGDEI*AYY*RR	25 nM (MCL-1/FA)	166
SAH-MS1-18	 IWZ*QEL*RLGDEINAEYAR	74 nM (MCL-1/FA)	167
Peptide 19	 IWIAQELR#IGD#FNAYYARR	ND	169

[a] Z denotes nor-Leucine; Asterisk denotes non-natural amino acids participating in formation of hydrocarbon staples; X denotes aminoisobutyric acid; hash denotes azidoalanine residue for triazole staples; [b]ND: not determined; k_d values are shown in red and IC_{50} values are shown in blue; FA: fluorescent anisotropy; SPR: surface plasmon resonance; the values cannot be compared directly as different conditions were used in different studies.

1.6.3 Constrained peptides based on the MCL-1 BH3 domain

Myeloid cell leukemia 1 (MCL-1) protein has been reported to be particularly associated with drug resistance in human cancer.[170] The Walensky group reported that the MCL-1 BH3 helix can inhibit MCL-1 itself efficiently and selectively.[171] They synthesised a library of hydrocarbon stapled peptides derived from BH3 domains of different BCL-2 family members, among which only MCL-1 SAHB$_A$ showed no significant binding affinities for other anti-apoptotic proteins but low nanomolar affinity for MCL-1. Interestingly, a single point mutation V220F eliminated the MCL-1 selectivity (Table 1-6). The MCL-1 BH3 stapled helix MCL-1 SAHB$_D$ induced caspase-dependent apoptosis in living cells. Furthermore, according to a structural study, the stapled peptide was found to gain additional interaction with MCL-1 via the hydrophobic hydrocarbon staple (Figure 1-31),[171] which was also supported by molecular dynamics simulations.[172]

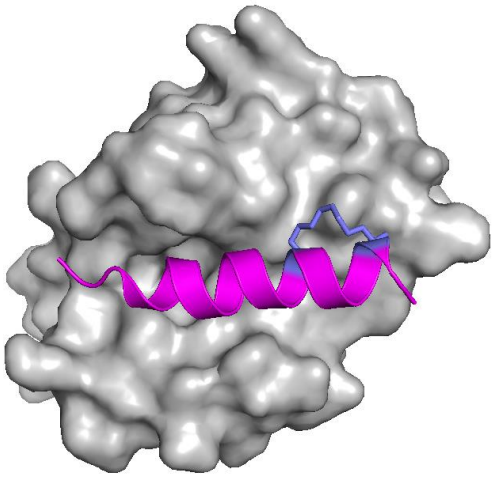

Figure 1-31 Crystal structure of the MCL-1 SAHB$_D$ and MCL-1 complex. (PDB code: 3MK8). [171]

Table 1-6 A summary of MCL-1-BH3-derived constrained peptides.

Peptide	Sequence[a]	k_d (Target/ testing method)[b]	Ref
MCL-1 BH3	KALETLRRVGDGVQRNHETAF	245 nM (MCL-1/FA)	171
MCL-1 $SAHB_A$	 KALETLR*VGD*VQRNHETAF	43 nM (MCL-1/FA);	171
MCL-1 $SAHB_A$ V220F	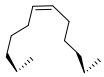 KALETLR*VGD*FQRNHETAF	89 nM (BCL-x_L/FA); 191 nM (BCL-w/FA);	171
MCL-1 $SAHB_D$	 KALETLRRVGDGV*RNH*TAF	10 nM (MCL-1/FA);	171

[a] Asterisk denotes non-natural amino acids participating in formation of hydrocarbon staples; [b]k_d values are shown in red; FA: fluorescent anisotropy.

1.6.4 BAD-derived constrained peptides

Bcl-2 agonist of cell death (BAD) protein is a BH3-only protein that not only interacts with anti-apoptotic members in the BCL-2 family, but also regulates insulin secretion by phosphorylation of Ser155.[173] Danial *et al*. described that a hydrocarbon stapled phospho-BAD peptide can selectively activate glucokinase (GK) and restore insulin secretion in pancreatic β-cells induced by glucose.[174] Thereafter, Szlyk *et al*. reported that the mechanism of insulin secretion activation by stapled phospho-BAD is different from that of other allosteric activators due to interaction with a new region in GK, suggesting that stapled peptides can act as glucokinase activators (GKAs).[175]

To investigate the binding to BCL-x_L and cytotoxicity of short BAD-derived peptides in cells, Fairlie and co-workers described a set of lactam-stapled

peptides truncated from the wild-type BAD peptide.[176] A triple constrained short peptide (Peptide 12) showed 4-fold weaker binding affinity than that of the wild-type peptide (Table 1-7). Peptide 16 which incorporated four hydrophobic non-natural amino acids, including norleucine (Nle), hydrophobic 1-naphthylalanine (1Nal), aminoisobutyric acid (Aib) and 3,4-dichlorophenylalanine (F(Cl2)), showed 2-fold higher activity in an MTT (3-(4,5-dimethylthiazol-2-yl)-2,5-diphenyltetrazolium bromide) assay compared to the wild-type BAD, although it exhibited 134-fold weaker *in vitro* binding affinity for BCL-x_L, indicating that the enhanced activity of the short stapled peptide in the cells results from the improvement of cellular uptake.

Table 1-7 A summary of BAD-derived constrained peptides.

Peptide	Sequence[a]	IC_{50} (Target/ testing method)[b]	Ref
BAD BH3	NLWAAQRYGRELRRMSDEFVDSFKK	53 nM (BCL-x_L/FA);	176
Peptide 12	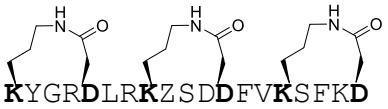	252 nM (BCL-x_L/FA);	176
Peptide 16	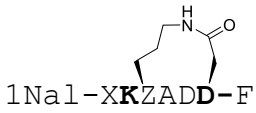	5.8 μM (BCL-x_L/FA);	176

[a]X denotes aminoisobutyric acid; 1-Nal denotes 1-naphthylalanine; F(Cl2) denotes 3,4-dichloro-phenylalanine; [b]IC_{50} values are shown in blue; FA: fluorescent anisotropy

1.6.5 NOXA-derived constrained peptides

The Walensky group reported a hydrocarbon stapled peptide, termed NOXA-1 (NOXA SAHB$_B$), derived from the NOXA (Phorbol-12-myristate-13-acetate-induced protein 1) BH3 domain. This peptide showed high and specific binding affinity for MCL-1, with K_d~110 nM, and sensitised the apoptotic response of Jurkat cells to death receptors, such as TRAIL and FasL.[171] Based on a previous study of p53 stapled peptides, Lin and co-workers applied the 4,4′-bis(bromomethyl)biphenyl (Bph)-mediated (Bph)-mediated stapling to a NOXA BH3 peptide.[126] A set of NOXA peptides with incorporation of $_L$- or $_D$- cysteines were synthesised and further stapled with the (Bph)-crosslinker (Figure 1-32 (a), Table 1-8). Surprisingly, all the stapled peptides showed improved binding affinity and also retained selectivity for MCL-1. The decreasing net charge and *N*-methylation of alanines at the N-terminus resulted in improvement of cellular uptake (Peptide 8, Table 1-8Table 1-8). Furthermore, the stapled peptides exhibited enhanced proteolytic stabilities in chymotrypsin, trypsin and mouse serum. Thereafter, the same group reported several rigid or flexible crosslinkers.[177] Interestingly, the flexible stapled peptides (Noxa-6) showed better inhibitory activities than the rigidly stapled peptides (Noxa-3) in a FA competition assay. Additionally, the stapled peptides with relatively hydrophobic and flexible crosslinkers exhibited more significant cell-permeabilities. More recently, Walensky and co-workers incorporated an acrylamide as a covalent crosslinking warhead into stapled NOXA peptides, which can react with BFL-1 Cys55. The resulting peptides selectively and covalently inhibited BFL-1 and showed improved inhibitory activity against BFL-1 in melanoma cells.[178] The same group later revealed the crystal structure of the covalent inhibitor with BFL-1 (based on NOXA SAHB$_A$ C25S, Table 1-8), suggesting that BFL-1 is the only member that has a surface-exposed cysteine in the BCL-2 family and an additional hydrophobic contact can be exploited for affinity, in this case involving the $_D$-nipecotic acid and a hydrophobic cavity proximal to Cys55.[179]

Table 1-8 A summary of NOXA-derived constrained peptides.

Peptide	Sequence[a]	k_d or IC_{50} (Target/ testing method)[b]	Ref
NOXA BH3	LEVESATQLRRFGDKLNFRQKL	ND	171
NOXA SAHB$_B$	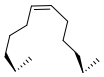 LEVES*TQL*RFGDKLNFRQKL	110 nM (MCL-1/FA);	171
Peptide 2	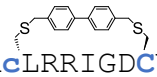 AAcLRRIGDCVNLRQKLLN	54 nM (MCL-1/FA);	126
Peptide 8	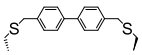 A_mA_mcLRRIGDCVNLRQKLLN	22 nM (MCL-1/FA);	126
Noxa-3	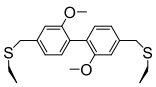 AACLRRIGDCVNLRQKLLN	183 nM (MCL-1/FA);	177
Noxa-6	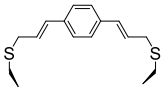 AACLRRIGDCVNLRQKLLN	49 nM (MCL-1/FA);	177
NOXA SAHB$_A$ C25S	 AELEVESATQLR*FGD*LNFRQKLL	46.6 nM (BFL-1/BLI)	179

[a] Asterisk denotes non-natural amino acids participating in formation of hydrocarbon staples; c denotes D-cysteine; A_m denotes *N*-methylated alanine; [b]k_d values are shown in red; IC_{50} values are shown in blue; FA: fluorescent anisotropy; BLI: Biolayer Interferometry; the values cannot be compared directly as different conditions were used in different studies.

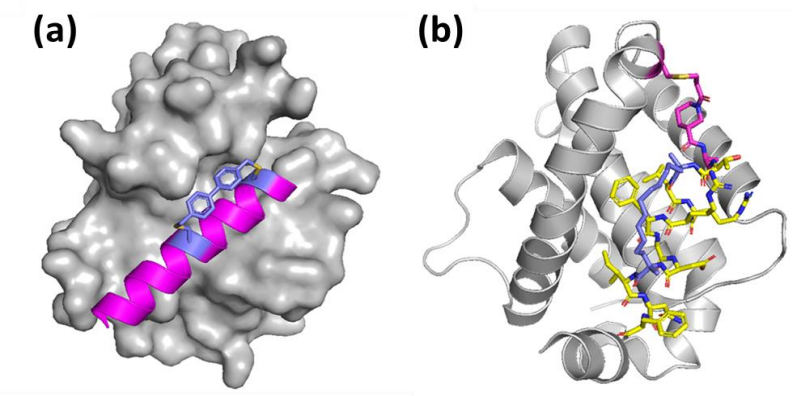

Figure 1-32 Crystal structures of the constrained peptides with MCL-1 or BFL-1. (a) Crystal structure of the complex between MCL-1 and a stapled peptide with the (Bph)-crosslinker (PDB ID: 4G35);[126] (b) Crystal structure of BFL-1 and its covalent complex with a stapled peptide (PDB ID: 5WHH, peptide in yellow, constraint in blue and covalent warhead in magenta).[179]

1.7 Coiled-coils

1.7.1 An introduction

The coiled coil is one of the most common structural motifs in native proteins, which is estimated to occur in 10% of all eukaryotic proteins.[180,181] Crick initially proposed that the packing in coiled coils is in a “knobs in holes” manner,[182] which means that α-helices wrap together and form coiled coils with an angle of 20° away from a perfectly parallel orientation and with side chain residues from one helix filling the gaps generated by clusters of side chains on the other helix (Figure 1-33 (a) and (b)). Left-handed coiled coils exhibit a seven-residue periodicity where seven amino acids span two turns of helices, because of the distortion from 3.6 residues per turn to 3.5 residues during the formation of this motif.[17] In coiled coils, this seven-residue repeat is typically termed a heptad repeat, denoted $(abcdefg)_n$, and illustrated as helical wheels from a top view (Figure 1-33 (c)).

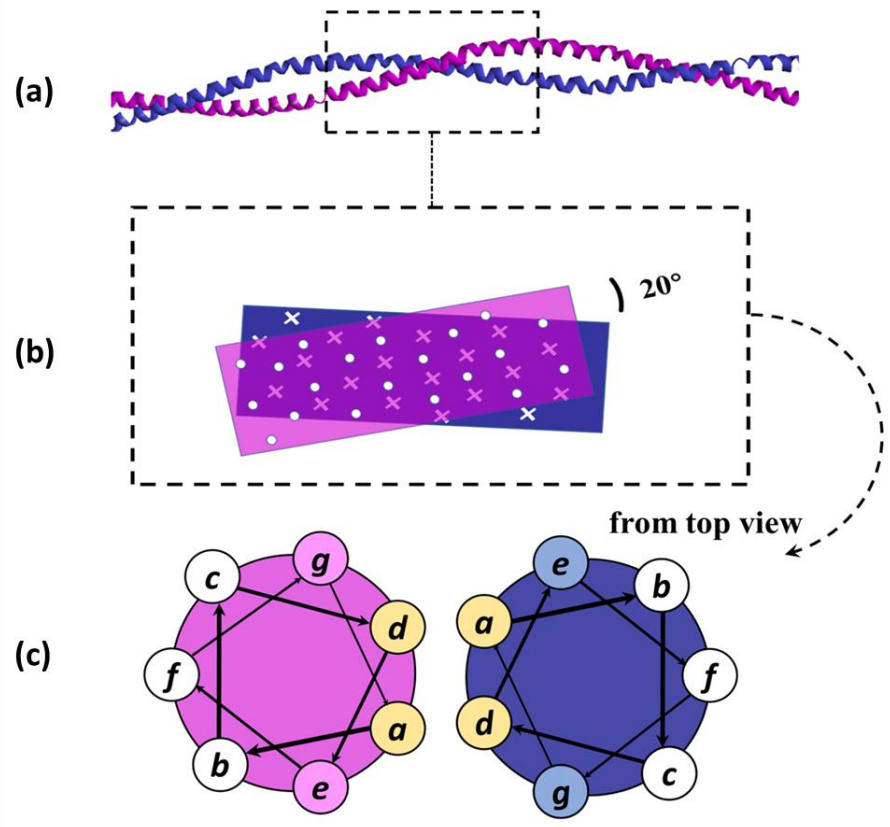

Figure 1-33 Coiled coils and helical wheels; (a) Crystal structure of a representative coiled coil (PDB code 1C1G), illustrating how two helices (purple and blue) wrap around one another; (b) A schematic diagram of "knobs in holes" packing with 20° away from parallel orientation (knobs (x) filling the holes (·)); (c) Helical wheel representation of a parallel dimeric coiled coil from top view (*a*, *d* positions are in yellow, which are usually hydrophobic; *e*, *g* positions are shown in magenta or blue, which usually form interchain salt-bridges; *b*, *c* and f positions are shown in white, which are exposed to solvents and flexible for modification).

Coiled coils are a class of useful building blocks in construction of different self-assemblies.[183] For instance, coiled coils can assemble into cages with different shapes,[184], nanotubes[185] and α-helical barrels.[186] In addition, coiled coils can undergo conformational changes triggered by many environmental factors, e.g. temperature,[187] pH,[188] and oxidation[189]. The diversity of coiled coils architectures and the tunability of coiled coils conformation open a new avenue for a broad range of biological applications.[15,190–193] In the following part, the *de novo* design principles of oligomeric coiled coils consisting of two to four helices, and their applications for the modulation of PPIs will be discussed.

1.7.2 *De novo* design of coiled-coil assemblies

The diversity of coiled coils architectures provides opportunities to understand the principles to modulate their folding and specificity. Generally, the residues at positions *a* and *d* are hydrophobic, promoting tight contact via the hydrophobic effect and van der Waals interactions.[193,194] Secondly, the residues at positions *e* and *g* are usually charged, providing interhelical or intrahelical electrostatic forces to stabilise the structures of coiled coils. The positions *b, c* and *f* are considered relatively flexible. However, they were found to provide additional benefits for coiled coils stability or inserting sites of residues that are essential for biological functions.[195–197]

1.7.2.1 residues *a* and *d*

The hydrophobic and steric nature of *a* and *d* residues play important roles in oligomerization of coiled coils.[193] The leucine zipper structure of the yeast transcriptional activator GCN4, sometimes termed GCN4-p1 facilitates its homodimerization.[198] Alber and co-workers systemically investigated the influence of positions *a* and *d* on the oligomeric states of GCN4 variants (Table 1-9).[199] Briefly, isoleucine at *a* and leucine at *d* favour a homodimer; isoleucine at both *a* and *d* favour a homotrimer; leucine at *a* and isoleucine at *d* favour a homotetramer; leucine at both *a* and *d* favour a homotrimer; valine at *a* and leucine at *d* favour a homotrimer while the inverse arrangement leads to a mixture of dimer and trimer. Inspired by this seminal work, Woolfson and co-workers described a series of *de novo* designed peptides that form different oligomers.[200] They found that the incorporation of asparagine at position *a* favours the dimer while asparagine at position *d* favours the trimer. Thereafter, the same group described that central locations of asparagine retained the specificity of oligomerization while weakening the thermal stability of coiled coils. On the contrary, the locating asparagine near the termini led to increasing stability but undermined specificity (Table 1-9).[201]

Table 1-9 A summary of sequences that form parallel homooligomeric coiled coils

Peptide	Sequence[α]	Oligomeric state	Ref
	e gabcdef gabcdef gabcdef gabcdef gabcd		
GCN4	RMKQLED KVEELLS KNYHLEN EVARLKK LVGER	Homodimer	199
GCN-pIL	RIKQLED KIEELLS KIYHLEN EIARLKK LIGEL	Homodimer	200
GCN-pII	RIKQIED KIEEILS KIYHIEN EIARIKK LIGEI	Homotrimer	200
GCN-pLI	RLKQIED KLEEILS KLYHIEN ELARIKK LLGEI	Homotetramer	200
GCN-pVL	RVKQLED KVEELLS KVYHLEN EVARLKK LVGEL	Mixture[b]	200
CC-pIL	G EIAALKQ EIAALKK EIAALKW EIAALKQ GYY	Homodimer	201
CC-Tri-N13	G EIAAIKQ EIAANKK EIAAIKW EIAAIKQ GYG	Homotrimer	201
CC-Tet	G ELAAIKQ ELAAIKK ELAAIKW ELAAIKQ GAG	Homotetramer	201

[α]*a* and *d* residues are highlighted in bold and orange. [b]Mixture of dimer and trimer.

1.7.2.2 Residues *e* and *g*

In coiled coils, positions *e* and *g* are usually occupied by charged residues, e.g. lysine and glutamic acid.[193] The pairing pattern determines the preference for the formation of homo- or heterooligomeric coiled coils. Kim and co-workers designed two peptides, ACID-p1 and BASE-p1, by replacing all *e* and *g* residues with glutamic acid or lysine in a peptide derived from GCN4, respectively.[202] The resulting peptides were found to form a heterodimer rather than a homodimer, which has been described as a “velcro”-like model (Figure 1-34 (a) and (b)). Similarly, Chaiken and co-workers designed two 35-mer peptides, E/E35 and K/K35, containing only glutamic acid or lysine at positions *e* and *g*, respectively.[203] These two peptides were found to form a heterodimer at neutral pH (Figure 1-34 (c)).

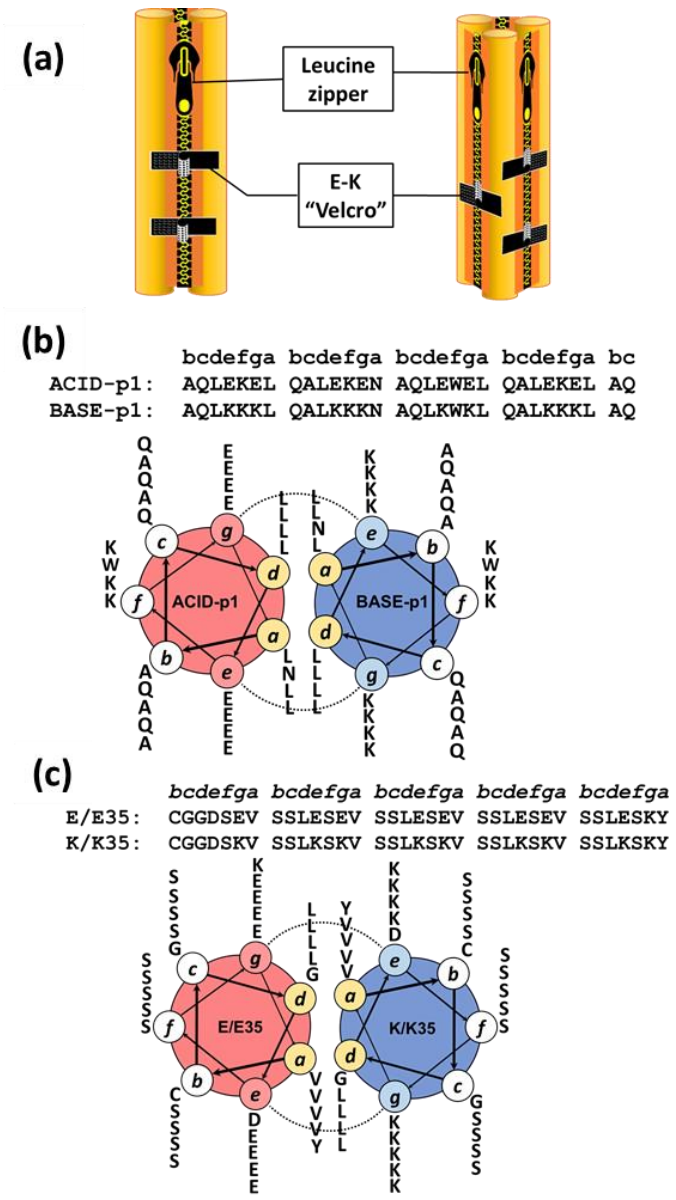

Figure 1-34 "Zipper" and "Velcro" models and heterodimers; (a) A schematic diagram of "Zipper" and "Velcro" models in dimeric or trimeric coiled coils; (b) Helical wheel representation of ACID-p1/BASE-p1 heterodimer from top view;[202] (c) Helical wheel representation of E/E35/K/K35 heterodimer from top view.[203]

In addition to the specificity of oligomeric states, residues *e* and *g* also play important roles in selecting the orientation of dimeric coiled coils. Hodges and co-workers designed a set of disulfide-crosslinked dimeric coiled coils.[204] The peptides have leucine or alanine at positions *a* and *d*. Different combinations of glutamic acid and lysine at positions *e* and *g* were used to control whether parallel or anti-parallel orientation would be favoured (Figure 1-35).

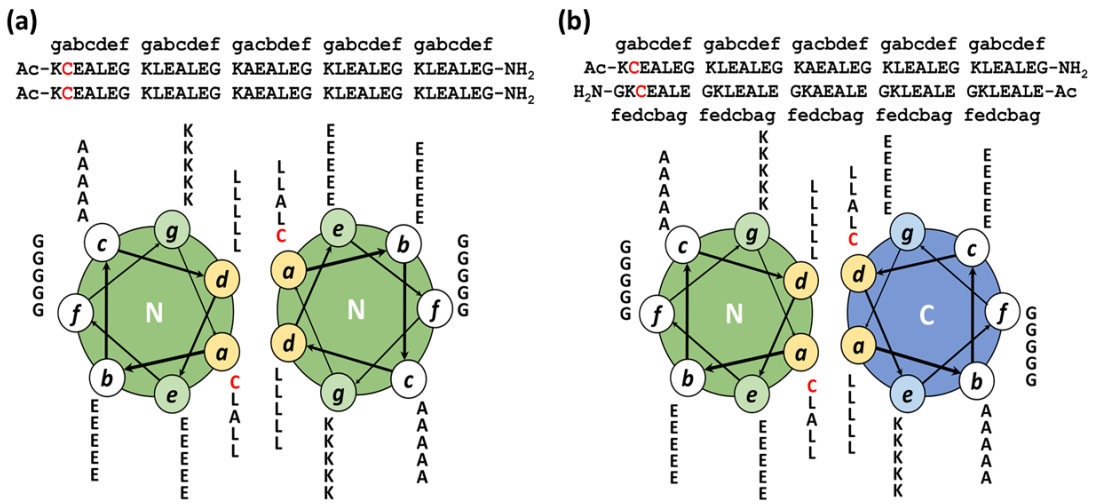

Figure 1-35 Disulfide-bond crosslinked parallel and antiparallel dimeric coiled coils; (a) Disulfide-bond crosslinked parallel dimeric coiled coil;[204] (b) Disulfide-bond crosslinked antiparallel dimeric coiled coil[204] (cysteines forming the interchain disulfide-bonds are highlighted in red).

The E-K “Velcro”-like effect plays an essential role in the formation of triple stranded coiled coils. Alber and co-workers designed a A-B-C type heterotrimeric coiled coil mediated by isoleucines at both positions *a* and *d*, and specific interchain E-K pairing at positions *e* and *g* (Figure 1-36 (a)).[205] The Tanaka group previously described a *de novo* design peptide IZ, which can form a homotrimeric coiled coil, driven by both the *a*, *d* isoleucine zipper and *e*, g E-K “Velcro”.[206] Inspired by Alber’s work, the Tanaka group designed a heterotrimeric coiled coil combining the tryptophan-alanine-alanine steric matching from *a* residues and *e*, *g* interchain E-K “Velcro”(Figure 1-36 (b)).[207]

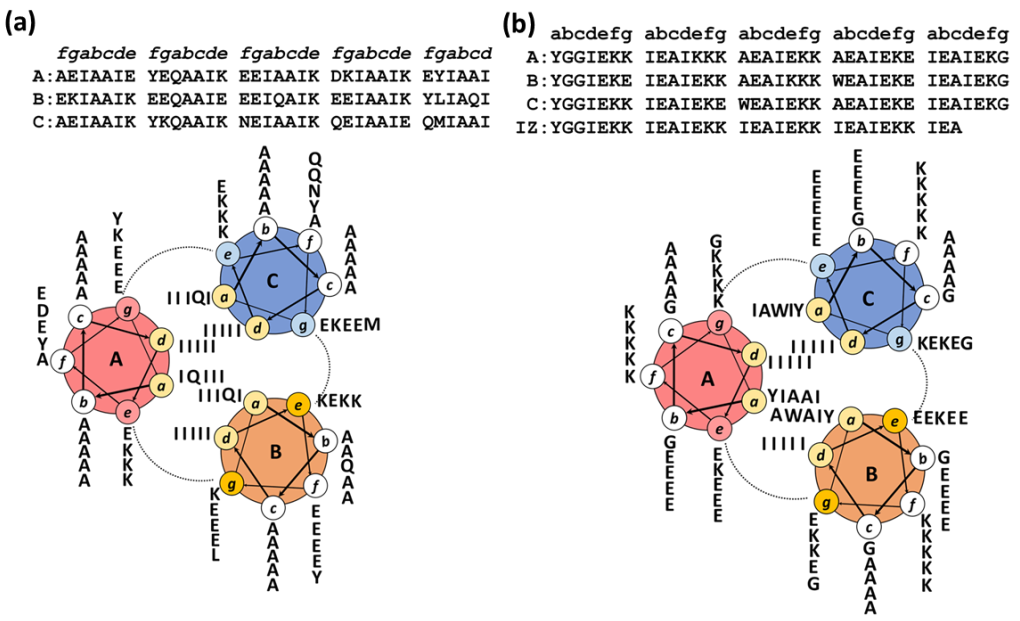

Figure 1-36 ABC-type heterotrimers; Helical wheel representation of ABC-type heterotrimer reported by Alber;[205] (b) Helical wheel representation of ABC-type heterotrimer reported by Tanaka.[207]

1.7.2.3 Residues *b, c* and *f*

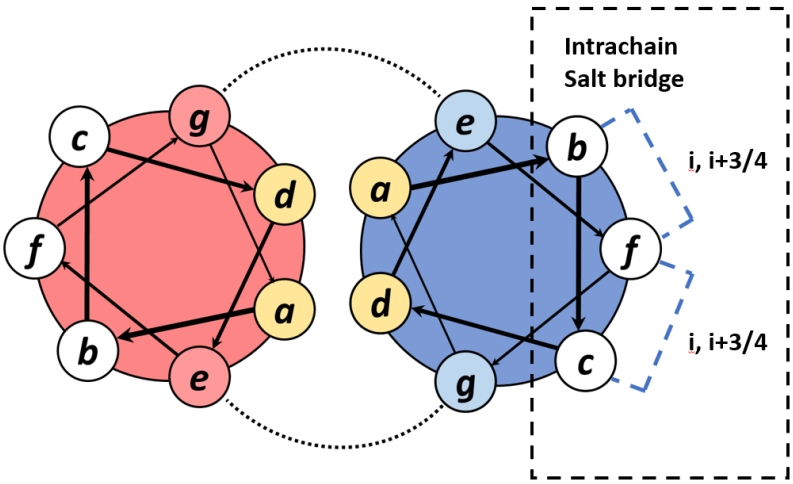

Figure 1-37 A schematic diagram of insertion of intrachain i, i+3/4 salt bridges at positions *b*, *c* and *f* in coiled coils.

The specificity and stability of coiled coils can not only be affected by *a*, *b*, *e*, *g* residues, but also residues at positions b, c and f.[193,208] Dahiyat et al. reported that replacement of *b*, *c*, *f* residues with glutamic acid, aspartic acid, lysine,

arginine and alanine, to incorporate intramolecular hydrogen bonds, salt bridges, or promote α-helical propensity, resulted in increased stability of GCN4-derived homodimeric coiled coils (Figure 1-37,Table 1-10).[209] Interestingly, the insertion of alanine to all positions *b*, *c* and *f* led to a conversion of the oligomeric state from dimerization to tetramerization, while increasing the thermal stability. Keating and co-workers also reported that intrachain *i*, *i*+3/4 salt-bridges can tighten the binding between a single strand and its partner during the formation of coiled coils.[210] Recently, Jerala and co-workers found that the α-helical propensity and thermal stability of dimeric coiled coils can be dramatically improved by incorporating intrachain *i*, *i*+3/4 salt-bridges by E/K or E/R pairs at positions *b*, *c* and *f* without changing the specificity of oligomerisation.[196]

Table 1-10 Peptides with *b*, *c*, *f* variations based on GCN4[209]

Peptide	Sequence[α]	Tm (°C)	Oligomeric state
	gabcdef gabcdef gabcdef gabcdef gabcd		
GCN4	RMKQLED KVEELLS KNYHLEN EVARLKK LVGER	57	2
GCN4-A	RMEKLED KVRELLR KNRRLEE EVRRLKE LVGER	71	2
GCN4-B	RMEKLEQ KVKELLR KNERLEE EVERLKQ LVGER	72	2
GCN4-C	RMARLEA KVAALLA KNRRLER EVARLKA LVGER	69	2
GCN4-D	RMRELEE KVRRLLR KNEDLER EVARLKA LVGER	71	2
GCN4-E	RMNTLER KVAKLLS KNANLEH EVNTLKQ LVGER	15	2
GCN4-F	RMAALEA KVAALLA KNAALEA EVAALKA LVGER	73	4

[α]Original residues *b, c* and *f* are shown in blue, the changed residues are shown in red.

1.7.3 Coiled-coil-based strategies to modulate protein-protein interactions

Highly stable *de novo* designed coiled coils serve as useful tools to stabilise α-helical structures, thus enriching the arsenal to construct modulators of α-helix-mediated PPIs.[197] Compared with constrained peptides, this new class of methods provides unique advantages, e.g. simplicity of synthesis, tunability of structures and less risk of unnecessary interactions from staples. [197] Two rational ways to create coiled-coil-based PPI modulators will be discussed in this part, including grafting and fusing strategies (Figure 1-38).

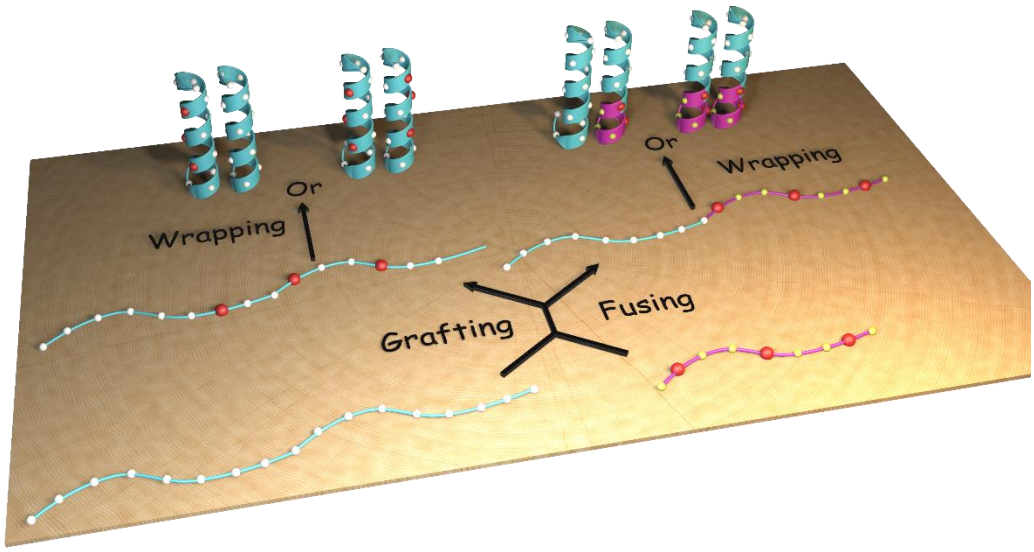

Figure 1-38 A schematic diagram of grafting and fusing strategies to create coiled coil-based PPI modulators (coiled coil templates are shown in cyan and residues in the templates are shown as white spheres; bioactive peptide segments are shown in magenta; hot-spot residues are shown as red spheres (big) and other residues are shown as yellow spheres in bioactive peptides (small)).

1.7.3.1 Coiled coils as scaffolds: grafting hot-spots

Oakley and co-workers reported a proof-of-concept study that a coiled coil can be utilised as a scaffold to graft key residues involving in PPIs.[211] According to a previous structural study, protein kinase N is an antiparallel heterodimeric coiled coil. The PKN/RhoA interaction involves two contacting interfaces, contact 1 and 2.[212] To clarify the mechanism of this PPI, the Oakley group introduced 15 key residues from contact 1 or 2 interfaces of PKN, respectively, into an anti-parallel coiled coil derived from seryl tRNA synthetase (SRS-ACC). As a result, the contact 2-derived coiled coil, HPC2, showed binding affinity for RhoA similar to the corresponding domain in PKN, while the contact 1-derived

HPC1 exhibited no significant interaction with RhoA, suggesting that the contact 2 is solely pivotal for the PKN/RhoA interaction (Figure 1-39).

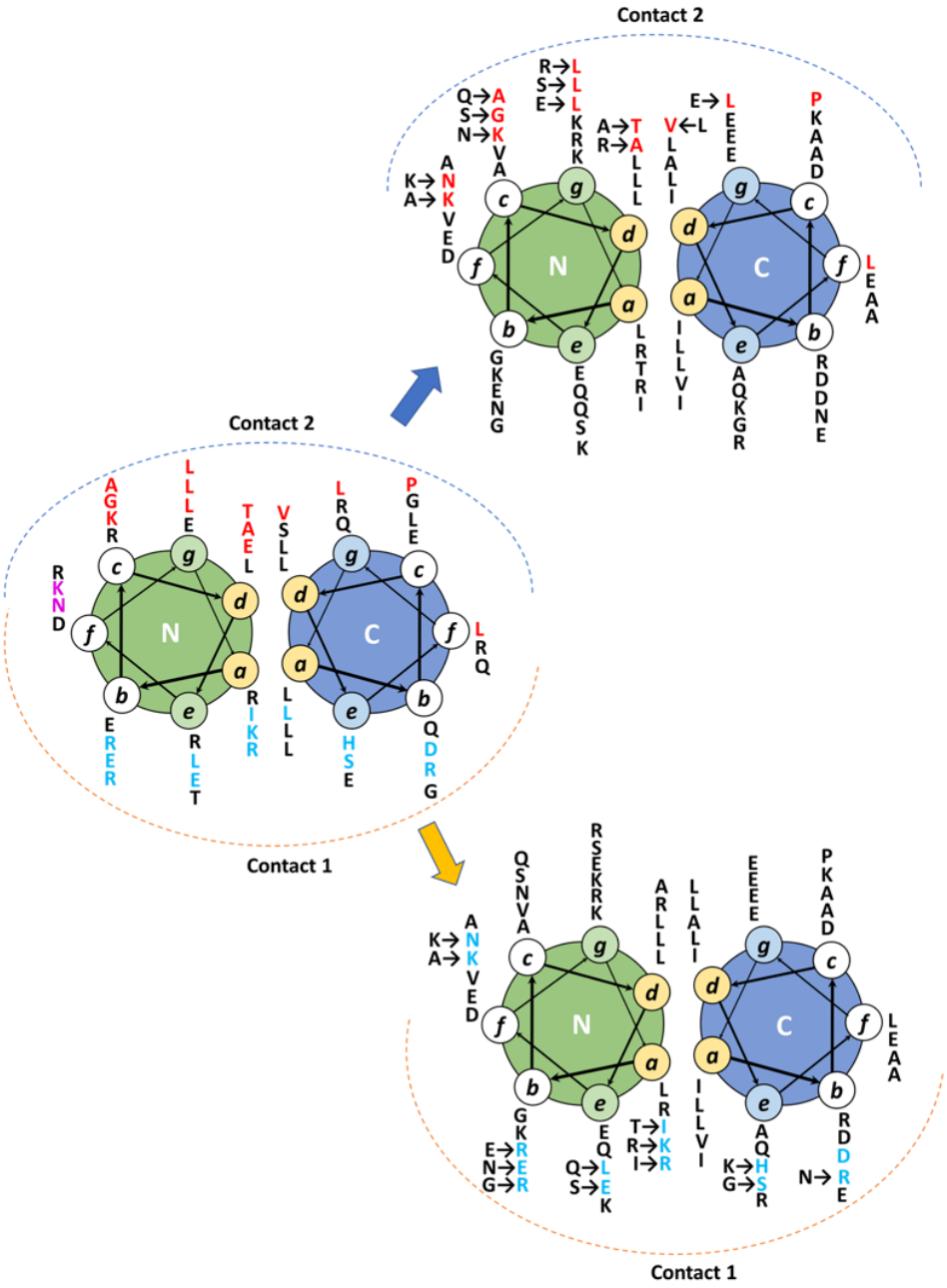

Figure 1-39 Grafting hot-spots in contact 1 or 2 involved in PKN/RhoA PPI on SRS-ACC antiparallel heterodimeric coiled coil [211] (hot-spots in contact 1 are highlighted in cyan; hot-spots in contact 2 are highlighted in red; hot-spots involved in both contacts are highlighted in purple).

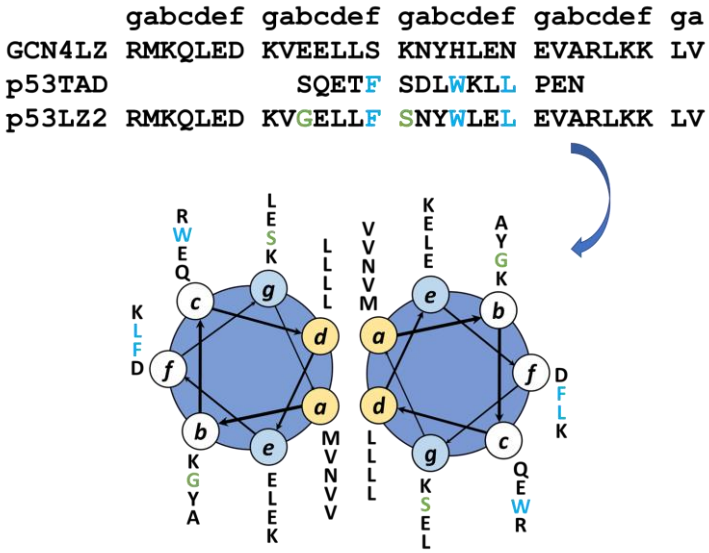

Figure 1-40 Grafting hot-spots of the p53TAD peptide involved in p53-hDM2/hDMX PPI on GCN4 homodimeric coiled coil [213] (hot-spots in the p53-hDM2/hDMX PPI were highlighted in cyan; additional mutations of the GCN4LZ based on the sequence of p53TAD were highlighted in green).

Lee *et al.* utilised a homodimeric coiled coil derived from the GCN4 sequence as a scaffold to graft hot-spots in a p53-derived peptide p53TAD, involved in its interactions with hDM2 and hDMX.[213] The most advanced coiled coil, p53LZ2, showed high binding affinities for both hDM2 and hDMX, with values of 18 and 80 nM, respectively (Figure 1-40). Moreover, the variant conjugated with a cell-penetrating peptide TAT, TAT-P53LZ2, showed significant anticancer activity on the HCT 166 xenograft model.

Recently, Fletcher *et al.* developed a set of homo- and heterodimeric coiled coils that can disrupt the MCL-1/NOXA B PPI.[197] After being identified using virtual alanine scanning, the hot-spots were grafted on a *de novo* designed homodimeric coiled coil, CC-Di, with different numbers of hot-spots. As expected, the coiled coil with more grafted hot-spots showed stronger binding as evidenced by lower IC_{50} in an MCL-1/BID competition fluorescent anisotropy assay. Surprisingly, the homodimers showed specificity of MCL-1 inhibition in the presence of other proteins, e.g. BCL-x_L and hDM2. Additionally, heterodimers were also designed using the E-K "Velcro" principle, with the hot-spots on only one of the coils. Interestingly, grafting the hot-spots on the acidic or basic strand resulted in different selectivity, suggesting non-specific electrostatic interactions could be involved in the binding (Figure 1-41).

	fgabcde	fgabcde	fgabcde	fgabcde	fgab
NOXA B:	PADLKDE	CAQLRRI	GDKVNLR	QKLLNM	
CC-Di:	GEIAALK	QEIAALK	KENAALK	QEIAALK	QGYG
CC-Di_S:	GEIAALK	QEILRLI	GDNVALK	QEIAALK	QGYG
CC-Di_E1:	GEILALK	QEILRLI	GDNVALK	QEILNLK	QGYG
CC-Di_E2:	GKILALE	QEILRLI	GDNVNLK	QEILNLK	QGYG
CC-Di-A:	GEIAALE	QEIAALE	KENAALE	QEIAALE	QGYG
CC-Di-A_S:	GEIAALE	QEILRLI	GDNVALE	QEIAALE	QGYG
CC-Di-B:	GKIAALK	QKIAALK	KKNAALK	QKIAALK	QGYG
CC-Di-A_S:	GKIAALK	QKILRLI	GDNVALK	QKIAALK	QGYG

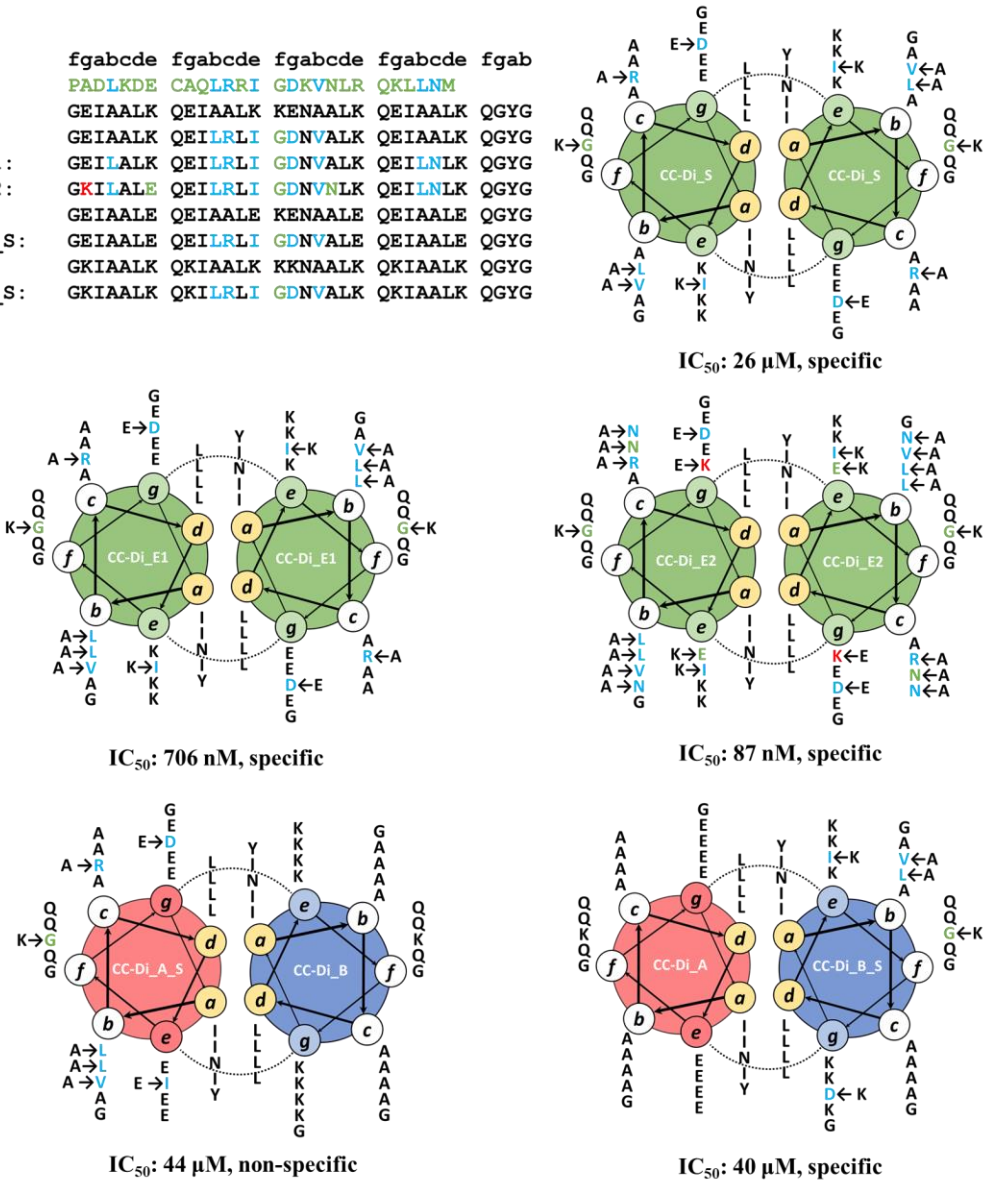

IC_{50}: 26 µM, specific

IC_{50}: 706 nM, specific

IC_{50}: 87 nM, specific

IC_{50}: 44 µM, non-specific

IC_{50}: 40 µM, specific

Figure 1-41 Grafting hot-spots of the NOXA B peptide involved in the NOXA B/MCL-1 PPI on CC-Di dimeric coiled coils set [197] (hot-spots in the NOXA B/MCL-1 PPI are highlighted in cyan; mutations of CC-Di based on the sequence of NOXA B are highlighted in green); additional residues are highlighted in red).

1.7.3.2 Coiled coils as templates: fusing with bioactive domains

In addition to the grafting strategy, coiled coils can be fused with a segment with an original α-helical bioactive conformation, to induce and stabilise the conformation essential for bioactivity. HIV-1 6-HB is a coiled coil complex formed by three NHR domains and three CHR domains.[22] The approval of the CHR-derived (C-peptide) fusion inhibitor enfuvirtide offers an alternative option for the regular antiretroviral treatment of HIV-1. However, the rapidly increasing drug resistance to C-peptide fusion inhibitors hampers their clinical applications.[214] Therefore, developing NHR-derived (N-peptide) fusion inhibitors emerged as a promising approach to overcome the drug resistance caused by C-peptides. However, native N-peptides are not bioactive due to their high tendency towards aggregation, which precludes the formation of the trimer required for the binding of C-peptides.[215] Bianchi *et al.* reported a fusing strategy to reinforce the N-trimers.[216] They first truncated the native N36 sequence to generate short N-peptides, followed by fusion with the previously reported homotrimer-forming sequence IZ. Surprisingly, the chimeric peptide IZN17 and IZN23 showed low nanomolar inhibitory activities against HIV-1 fusion, with IC_{50} = 1.3 and 2.3 nM, respectively. Moreover, N-capped cysteine pairs were incorporated for the formation of interchain disulfide-bridges. The covalent crosslinked coiled coil $(CCIZN17)_3$ exhibited 30-fold lower IC_{50} than IZN17 (Table 1-11). Crosslinking coiled coils with stable crosslinkers dramatically improves the stability of coiled coils.[217] Liu and co-workers reported a novel crosslinking method using an isopeptide-tether (Figure 1-42). The group first developed *de novo* designed peptides 3HR and 4HR, which can form a homotrimeric coiled coil with high stability.[218] By fusing 3HR or 4HR with an NHR-derived peptide, N23, and incorporating isopeptide-bridges by an acyl transfer reaction, a set of covalently crosslinked homotrimeric coiled coils were found to exhibit anti-HIV-1 activities similar to enfuvirtide (Table 1-11).

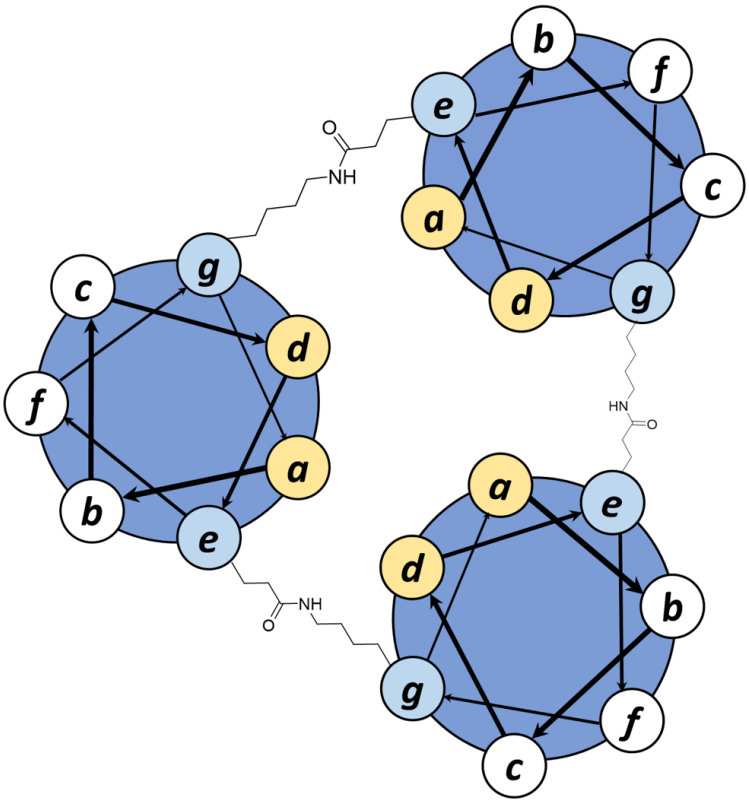

Figure 1-42 A schematic diagram of isopeptide-bond tethered trimeric coiled coil. [218]

Thereafter, based on the native N36 sequence, the same group mutated appropriate residues at *a* and *d* positions to isoleucine which favours trimeric coiled coil formation, incorporated intrachain *i*, *i*+3/4 salt-bridges at positions *b, c* and *f* and replaced the interchain *e*, *g* salt-bridges with covalent isopeptide-bridges (Figure 1-42, Table 1-11).[219] The resulting coiled coil $(N36MEK2)_3$ showed improved anti-HIV-1 activity in comparison to enfuvirtide, as well as extremely enhanced metabolic stability in proteinase K solution, liver homogenate, kidney homogenate and rat plasma. These results demonstrate that variation of native sequences is another rational way for *de novo* design of coiled coil PPI inhibitors.

Table 1-11. A summary of coiled-coil-based N-peptide fusion inhibitors against HIV-1

Peptide	Sequence[α]	IC_{50} (nM)	Ref
	bcdefgabcdefgabcdefgabcdefgabcdefgab		
N36	SGIVQQQNNLLRAIEAQQHLLQLTVWGIKQLQARIL	920	219
N23	IEAQQHLLQLTVWGIKQLQARIL	>5000	218
N17	LLQLTVWGIKQLQARIL	N.D.	216
IZ	IKKEIEAIKKEQEAIKKKIEAIEK	N/A	216
IZN17	IKKEIEAIKKEQEAIKKKIEAIEKLLQLTVWGIKQLQARIL	1.26	216
$(CCIZN17)_3$	CCGGIKKEIEAIKKEQEAIKKKIEAIEKLLQLTVWGIKQLQARIL	0.04	216
4HR	WRIQQIEQKIHHIEQRIQQIEQRIQQIEQ	N/A	218
3HR	WRIQQIEQKIHHIEQRIQQIEQ	N/A	218
$(4HRN23)_3$	WRIQQIEQKIHHIEQRIQQIEQRIQQIEQIEAQQHLLQLTVWGIKQLQARIL	11.6	218
$(3HRN23)_3$	WRIQQIEQKIHHIEQRIQQIEQIEAQQHLLQLTVWGIKQLQARIL	10.2	218
$(N36MEK2)_3$	SEIVKKINNIERAIEAQQKLLQLTVWGIKQLQARIL	27.1	219

[α]The residues participating in the formation of interchain covalent crosslinker are highlighted in red; residues *a* and *d* are highlighted in bold; residues for interchain crosslinking are shown in red; N23 segment are shown in blue and N17 segment are shown in green; additional variations in $(N36MEK2)_3$ are highlighted in orange.

1.8 Overall aims

Discovery of inhibitors and further understanding of the BH3/BCL-x_L PPIs would pave the way to develop new modulators as probes or therapeutics. To this end, I envisaged that constrained peptides and coiled coils would be ideal approaches for discovery of efficient peptidomimetic inhibitors targeting the BH3/BCL-x_L PPIs. The Wilson group recently introduced stapled and coiled-coil peptides that inhibit helix mediated PPIs (e.g. MCL-1 and BCL-x_L inhibitors) and are amenable to solid phase synthesis.[136,197] The mono-substituted hydrocarbon staple and dibromomaleimide-staple were introduced into the BID peptide, which is a non-selective inhibitor of pro-survival BCL-2 family

proteins.[155,136] More recently, coiled coils based on NOXA-B, which can selectively inhibit MCL-1, reported.[197]

In this work, the BAD/BCL-x_L and HRK/BCL-x_L PPIs were chosen as targets. The main goal was to develop constrained peptides and coiled coils based on the BAD and HRK BH3 domains with improved binding and selectivity towards BCL-x_L. I planned to explore both monosubstituted hydrocarbon stapling and dibromomaleimide constraining approaches. In the long-term, I also planned to explore the current peptide constraining techniques e.g. developing irreversible constraining methods based on dibromomaleimide. Secondly, coiled-coils based on the BAD and HRK peptides were planned to be investigated. I planned carry out computational modelling for peptide design; and I planned to perform biophysical evaluation, e.g. fluorescent anisotropy (FA) for screening potency, and circular dichroism (CD) for investigation of secondary structures. The expected outcome of this work was the successful identification of selective peptide-based BCL-x_L inhibitors. Accordingly, I planned to generate crystal structures for the complexes of the compounds with the BCL-x_L protein, and also optimise the peptides by adding cell-penetrating functionalities for further cell-based studies.

Chapter 2 Inhibition of the BAD/BCL-x_L interaction using constrained peptides

2.1 The introduction to BAD and chapter aims

The BAD protein is a BH3-only protein that binds to several anti-apoptotic proteins, including BCL-2, BCL-W and BCL-x_L, rather than pro-apoptotic effector proteins, e.g. BAK or BAX.[220] Similar to other BH3-only proteins, such as NOXA, BIK, BMF and HRK, single deletion of BAD has little effect on normal development in mice models, although deletion of BIM shows a lethal effect.[221–224]

BAD has dual functions in both apoptotic and anti-apoptotic processes, which are regulated by posttranslational modification (PTM).[174] The pro-apoptotic function of BAD can be inhibited through phosphorylation mediated by several kinases, e.g. Akt, in response to growth factors.[220,225] As a result of phosphorylation, phospho-BAD can be recognised and inactivated by 14-3-3 proteins, suppressing the interaction with anti-apoptotic proteins.[226] Moreover, BAD BH3 phosphorylation also contributes to the regulation of glucokinase activity.[174,227]

In this chapter, the aim was to use the BAD BH3 domain as a starting point to construct constrained peptides using dibromomaleimide, for inhibition of the BAD/BCL-x_L interaction. Virtual alanine scan would be used to predict hot-spot residues in the sequence. The peptides would be characterised by FA and CD and MD simulations would be used to investigate the difference of the bound and unbound states of peptides.

2.2 Virtual alanine scanning to determine hot-spot residues

Hot-spot residues are a subset of key residues that contribute to the affinity within PPIs, for which, the variation to alanine causes a significant calculated decrease of binding free energy (ΔΔG>1 kcal/mol or 4.2 kJ/mol).[228,229] Alanine scanning is a commonly used method to identify hot-spot residues (amino acids with contribution > 4.2 kJ/mol to the binding free energy) at a protein-protein interface.[7,229] A virtual alanine scan can be quicker and lower-cost in comparison to experimental approaches.[230] In order to inform the design of peptidomimetics based on the BAD BH3 domain, I first selected the human *h*BAD/BCL-x_L structure (PDB ID: 1G5J)[230] and performed a virtual alanine scan using the BUDE[231] Alanine Scan (BAlaS). [232] BAlaS is a efficient and versatile approach for rapid analysis of PPIs and allows scientist to use different types of input files.[232] Previously the Wilson group compared virtual alanine scanning results using six different computational tools with experimental results.[233] The data showed that BAlaS had above-average accuracy in comparison to others. For using BAlaS, the input files can be uploaded to the BAlaS webserver for modelling and users don't need to install extra softwares. Therefore, it is a convenient and user-friendly tool to rapidly predict hot-spot residues in PPIs.

To identify potential hot-spot resides in the *h*BAD BH3 sequence, BAlaS was employed. As a result, several residues were identified as potential hot-spot residues in the BAD/BCL-x_L interaction, including Leu104, Tyr110, Leu114, Arg115, Phe121 and Phe125 (Figure 2-1 (a)). Notably, two aromatic residues, Phe121 and Phe125, were predicted to exhibit a significant increase in binding free energy after replacement with alanine (18 kJ/mol and 13.2 kJ/mol respectively), highlighting an important contribution for these two residues for interaction with BCL-x_L. For comparison, a crystal structure of the complex between *z*BAD and an anti-apoptotic analogue of BCL-x_L from zebra fish, NRZ (*z*BAD/NRZ, PDB ID:6FBX), was subjected to BAlaS.[230] In the complex with NRZ, the *z*BAD peptide was identified to have Tyr95, Leu99, Arg100 and Phe106 as hot-spot residues associated with BCL-x_L recognition (Figure 2-1 (b)).

The observed residue locations are consistent with the typical h1, h2, h3, and h4 hydrophobic residue constellations in other BH3-only proteins, although M117 (h3) showed ΔΔG<4.2 kJ/mol, indicating it is not identified as a hot-spot residue. The similarity of the virtual alanine scanning results using *z*BAD/NRZ provided additional confidence in informing the design of BAD-derived

peptidomimetics. In detail: Tyr95, Leu99, Arg100 and Phe106 were identified as hot-spot residues together with three more residues including Lys93, Lys94 and Gln110.

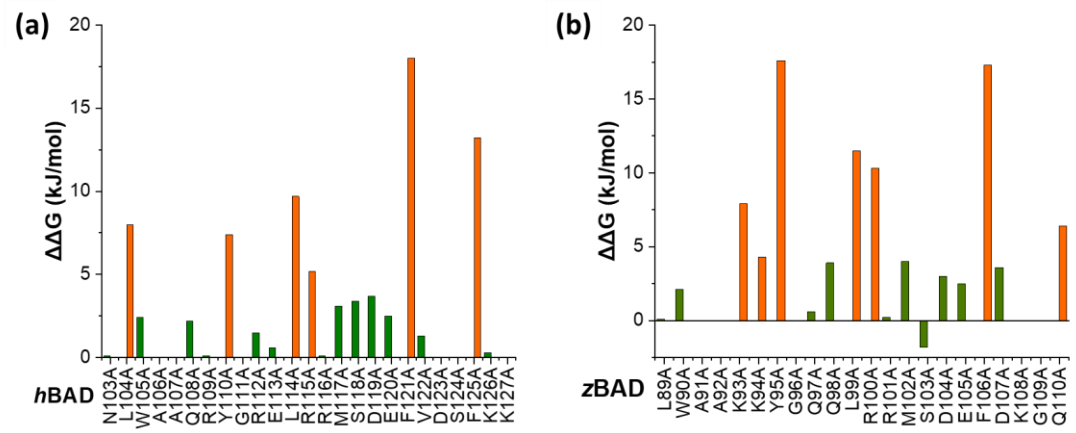

Figure 2-1 Virtual alanine scanning results using BAlaS: (a) results for *h*BAD/BCL-x_L (PDB ID: 1G5J); (b) results for *z*BAD/NRZ (PDB ID: 6FBX) (the predicted hot-spot residues are shown in orange and other residues are shown in green).

To clarify the conformational orientation and detailed interactions involving the identified hot-spot residues, I inspected the *h*BAD/BCL-x_L structure, confirming that the five hydrophobic hot-spot residues, Leu104, Tyr110, Leu114, Phe121 and Phe125, are grafted on the same face of the α-helix and insert into the hydrophobic cleft of the BCL-x_L (Figure 2-2 (a)). The aromatic residues, Phe121 and Phe125 of BAD, interact with Phe97 and Tyr195 of BCL-x_L via π-π interactions, respectively. Notably, the conserved Asp119 forms a charge reinforced hydrogen-bond with Arg139 of BCL-x_L. Similarly, in the interaction between the BAD and NRZ, Tyr95, Leu99, Phe106 sit on the same face of the α-helix and embed into the hydrophobic cleft of NRZ; Asp104 forms a charge reinforced hydrogen-bond with Arg90 of NRZ (Figure 2-2 (b)); the role of Gln110 as a hot-spot residue is less clear, however Arg100 is engaged in charge reinforced hydrogen-bonding interaction with Glu79 and Asp83 simultaneously. In addition, the two lysine residues, Lys93 and Lys94 were also identified as hot-spot residues, which interact with acidic residues in NRZ in terms of the crystal structure. (Figure 2-2 (b)).

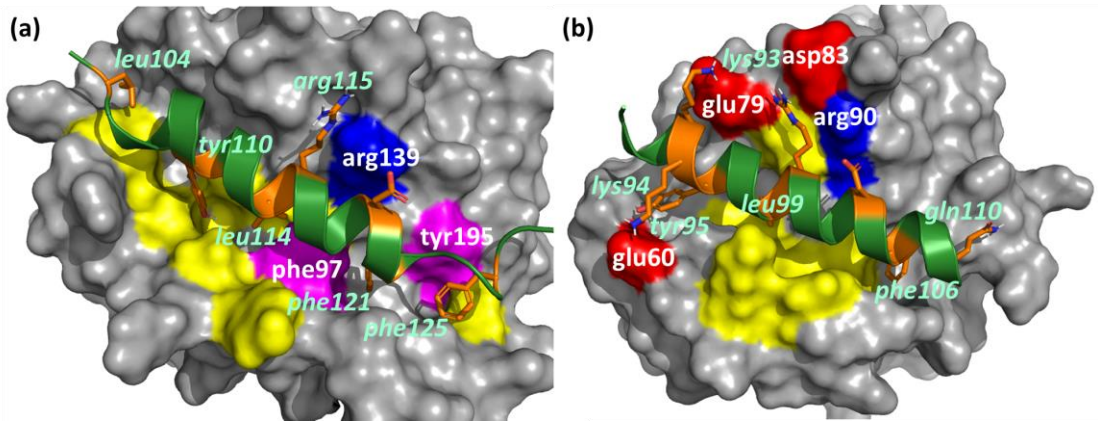

Figure 2-2 Ligand-receptor interactions for BAD BH3 peptides and the receptors; (a) ligand-receptor interactions in *h*BAD/BCL-x_L structure (PDB ID: 1G5J); (b) ligand-receptor interactions in *z*BAD/NRZ structure (PDB ID: 6FBX) (hot-spot residues in the BAD peptides are coloured orange with light green labels; residues involved in recognition of BAD in BCL-x_L or NRZ are labelled in white and coloured: yellow for hydrophobic, blue for simultaneous electrostatic interaction and hydrogen-bond, purple for π-π interaction and red for electrostatic interaction).

2.3 Dibromomaleimide constraint scan

2.3.1 Direct titration FA assays

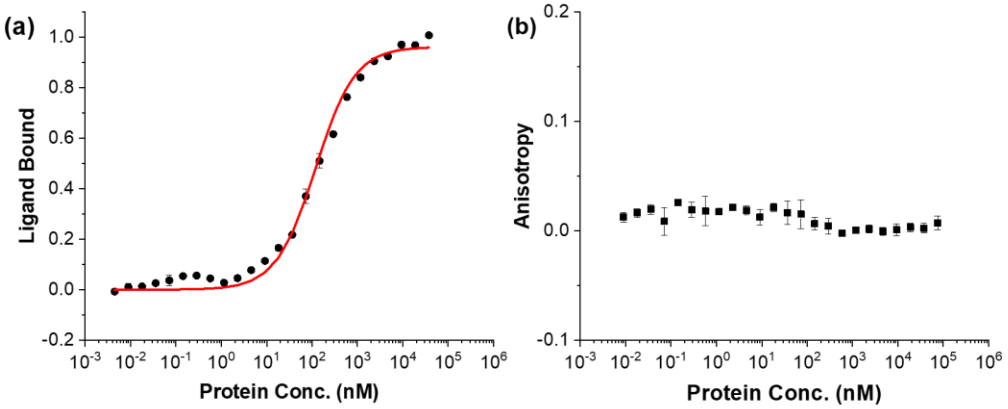

Figure 2-3 Fluorescence anisotropy direct titration results for titration of FAM-Ahx-BAD with the receptors proteins; (a) BCL-x_L;(b) MCL-1 (FAM-Ahx-BAD (50 nM), BCL-x_L (6 nM-125 μM), MCL-1 (5 nM-105 μM), 20 mM Tris, 150 mM NaCl, pH 7.6, 20 °C, all experiments were repeated for three times, error bars show standard deviations).

First of all, a direct fluorescence anisotropy (FA) assay was established for testing the binding affinity of *h*BAD peptides (hereafter referred to as BAD) towards BCL-x_L and also facilitating the development of competition FA assays to screen designed molecules. A 19-mer BAD tracer was used in this study (FAM-Ahx-$BAD_{109-127}$ (FAM-Ahx-RYGRELRRMSDEFVDSFKK-NH_2), here after referred to as FAM-Ahx-BAD) for the direct titration assay. FAM-Ahx-BAD was found to bind to BCL-x_L with a K_d = 119 ± 23 nM (Figure 2-3 (a)).

In addition, I also used MCL-1 to investigate the selectivity of the BAD sequence; FAM-Ahx-BAD failed to exhibit any anisotropy change up to 100 μM of MCL-1 (Figure 2-3 (b)), suggesting that the 19-mer sequence has excellent selectivity and serves as a suitable tracer for assay development and a promising starting point for designing BAD-based peptidomimetic BCL-x_L inhibitors.

2.3.2 Peptide design and competition FA screening

In this section, I applied the fast and efficient peptide constraining method using dibromomaleimide at *i* and *i* + 4 positions[136] to identify suitable sites for generation of constrained peptides based on BAD BH3. To do this, pairs of *i* and *i* + 4 residues in the wild-type $BAD_{109-127}$-BH3 sequence (hereafter referred to as BAD-s) were replaced by cysteines for constraining. To retain the hot-spot residues from the binding interface and minimise the influence arising from the replacement of original residues, cysteines were incorporated to avoid changing the relatively hydrophobic hot-spot residues Leu104, Tyr110, Leu114, Phe121 and Phe125, identified from the virtual alanine scan. All peptides were synthesised using Fmoc-based standard solid-phase peptide synthesis and purified by prep-HPLC for further study (purity>85%).

A dibromomaleimide constraint scan led to 8 bis-cysteine variants (BADL1-L8) based on BAD-s, by incorporating a pair of cysteines at different *i* and *i*+4 positions from the N-terminus to the C-terminus. Thereafter, a maleimide constraint was installed on each peptide using dibromomaleimide as previously described[136] and all resultant peptides were tested in fluorescence anisotropy competition assays. The longer wild-type peptide, $BAD_{103-127}$ (25-mer, hereafter referred to as BAD-wt), gave an IC_{50} = 0.2 ± 0.01 μM, which was more potent than that of the shorter template peptide, BAD-s (3.6 ± 0.2 μM, Figure 2-4 (a)). Several cysteine variants showed comparable IC_{50} values in comparison to BAD-s. However, BADL2, BADL4 and BADL7 showed diminished inhibitory potency (all >50 μM) after incorporation of the cysteines, indicating that those positions are unsuitable to for replacement (Figure 2-5). The loss of inhibitory

potency may be attributed to the replacement of Arg115 which interacts with BCL-x_L or Asp119 which is highly conserved across BH3-only ligands and can interact with Arg139 in BCL-x_L.[234] Loss of inhibitory potency was observed for most maleimide constrained peptides in comparison to either their unconstrained precursors or the wild-type sequence. Notably, two constrained peptides, BADS1 and BADS5, showed similar IC_{50} values to that measured for BAD-s. In competition against the BID/MCL-1 interaction these peptides showed poor inhibitory activity or no significant anisotropy change (Figure 2-4 (b), Table 2-1), demonstrating that the selectivity preference of the parent wild-type sequence is well-retained.

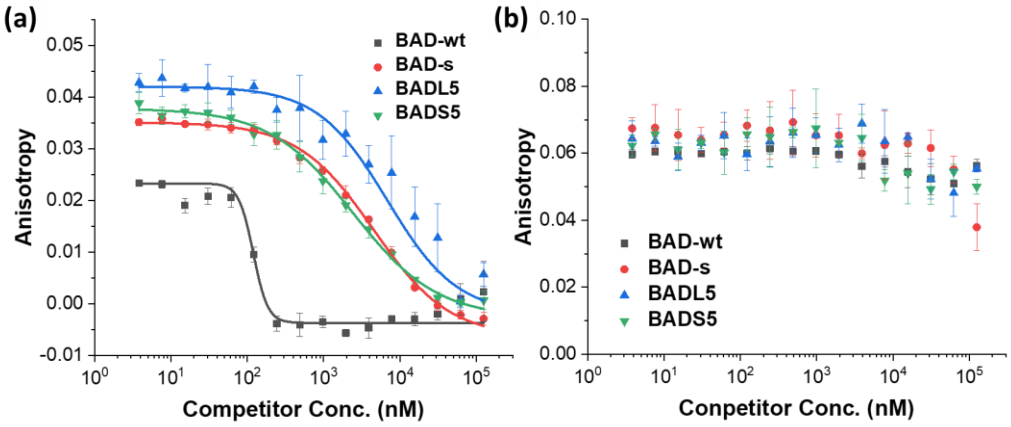

Figure 2-4 Competition FA results for BAD-wt, BAD-s, BADL5 and BADS5; (a) against BCL-x_L (20 mM Tris, 150 mM NaCl, pH 7.6, 200 nM BCL-x_L, 50 nM FAM-Ahx-BAD, 20 °C); (b) against MCL-1 (20 mM Tris, 150 mM NaCl, pH 7.6, 150 nM MCL-1, 25 nM FAM-Ahx-BID, 20 °C) (see sequences in Table 2-1) (error bars show standard deviations observed in triplicate experiments and errors are standard deviations generated in data fitting).

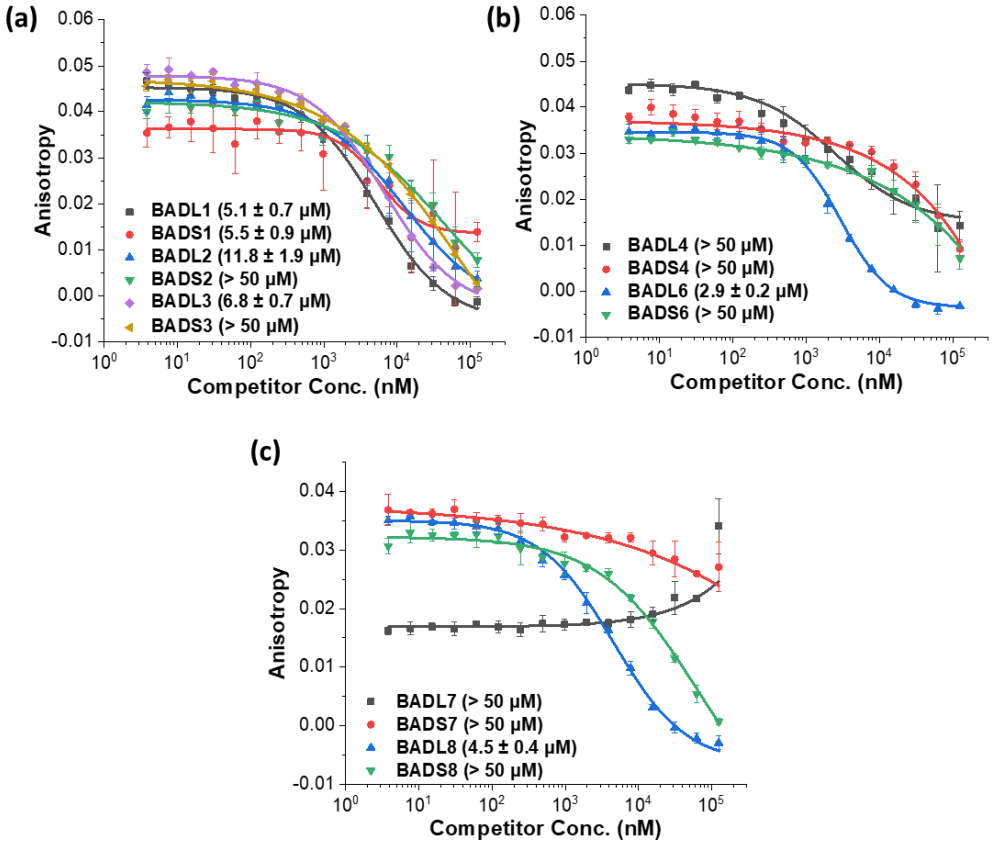

Figure 2-5 Competition FA results for the BAD peptides against BCL-x_L (a) competition FA results for BADL1, BADS1, BADL2, BADS2, BADL3 and BADS3; (b) competition FA results for BADL4, BADS4, BADL6 and BADS6; competition FA results for BADL7, BADS7, BADL8 and BADS8 (20 mM Tris, 150 mM NaCl, pH 7.6, 200 nM BCL-x_L, 50 nM FAM-Ahx-BAD, 20 °C, error bars show standard deviations observed in triplicate experiments and errors are standard deviations generated in data fitting).

2.3.3 Structural analysis using CD

In order to investigate the conformational features of the peptides and the relationship between helicity and potency, CD was used to determine the secondary structures of the peptides, including the linear and constrained. The two wild-type peptides, BAD-wt and BAD-s were observed to adopt a combination of random coil and helical conformation, with helicities of 14% and 10%, respectively (Table 2-1 and Figure 2-6 (a)), which is consistent with a prior report.[176] In most sequences, the installation of the maleimide linker did not significantly improve the observed helicity for each single peptide in solution in comparison to BAD-s or the corresponding cysteine precursors (Figure 2-6). For example, the best constrained candidate, BADS5, was observed to have a helicity of only 10%, whereas it showed an IC_{50} of 2.4 ± 0.2 μM, which is comparable to that of BAD-s. Also, the other peptide with retained binding, BADS1, did not show improvement of helicity after constraining. One constrained peptide, BADS4, showed improved helicity in comparison to the linear precursor (8% to 14%). However, BADS4 did not retain inhibitory potency in the FA competition assay against BAD/BCL-x_L. Taken together, these results indicate that in-solution α-helicity of the BAD peptides are relatively low and do not have strong correlations with potency, indicating that BAD potentially interacts with BCL-x_L through a bind-and-fold mechanism as has been observed for other BCL-2 family interactions.[235,236]

Table 2-1 A summary of FA competition results of the peptides against BCL-x_L

Peptide	Sequence[a]	IC_{50} BAD/BCL-x_L (μM)[b] (Helicities)[c]	
		(L) 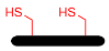	(S) 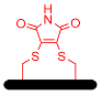
$BAD_{109-127}$	Ac-N**L**WAAQR**Y**GRE**LR**RMSDE**F**VDS**F**KK-NH_2	0.2±0.01 (14%)	
$BAD_{103-127}$	Ac-R**Y**GRE**LR**RMSDE**F**VDS**F**KK-NH_2	3.6±0.2 (10 %)	
BADL1/S1	Ac-**C**Y**G**R**C****LR**RMSDE**F**VDS**F**KK-NH_2	5.1 ± 0.7 (11%)	5.5±0.9 (11%)
BADL2/S2	Ac-R**Y****C**RE**L****C**RMSDE**F**VDS**F**KK-NH_2	>50 (11%)	>50 (10%)
BADL3/S3	Ac-R**Y**G**C**E**LR****C**MSDE**F**VDS**F**KK-NH_2	6.8 ± 0.7 (10%)	> 50 (8%)
BADL4/S4	Ac-R**Y**GRE**L****C**RMS**C**E**F**VDS**F**KK-NH_2	> 50 (8%)	> 50 (14%)
BADL5/S5	Ac-R**Y**GRE**LR****C**MSD**C****F**VDSFKK-NH_2	6.9±0.4 (9%)	2.4±0.2 (10%)
BADL6/S6	Ac-R**Y**GRE**LR**RM**C**DE**F****C**DS**F**KK-NH_2	2.9±0.2 (7%)	> 50 (9%)
BADL7/S7	Ac-R**Y**GRE**LR**RMS**C**E**F**V**C**S**F**KK-NH_2	> 50 (7%)	> 50 (8%)
BADL8/S8	Ac-R**Y**GRE**LR**RMSD**C****F**VD**C****F**KK-NH_2	4.5 ±0.4 (10%)	> 50 (10%)

[a]Hot residues are underlined and shown in bold; incorporated cysteines are highlighted in red; a maleimide constraint was added on the cysteines in each BADSn peptide; [b]20 mM Tris, 150 mM NaCl, pH 7.6, 200 nM BCL-x_L, 50 nM FAM-Ahx-BAD, 20 °C; all experiments were repeated for three times, fitting errors showed in table; [c] [peptide] = 50 μM, 20 mM phosphate, 100 mM NaCl, pH 7.4.

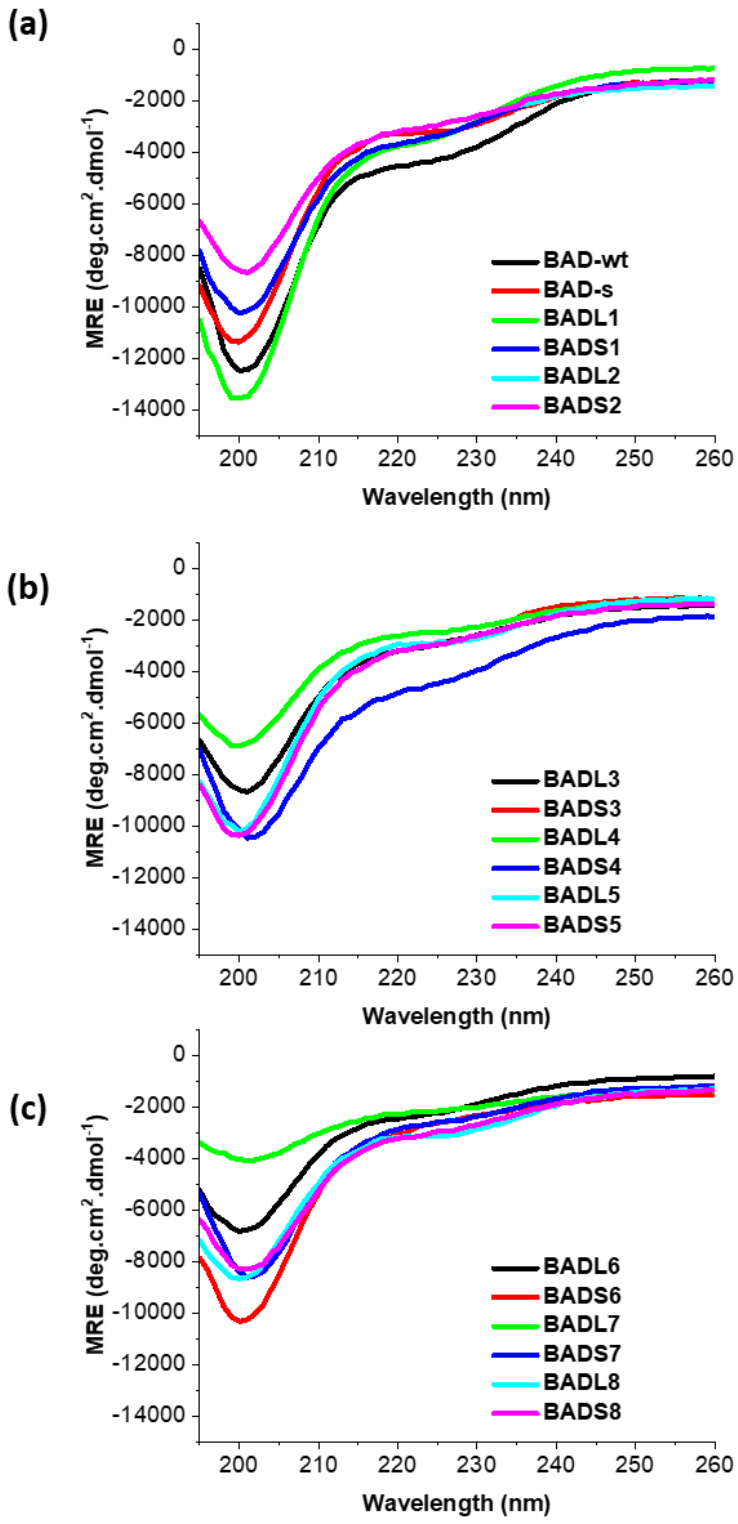

Figure 2-6 CD spectra for the BAD peptides (peptide concentration: 50 μM, 20 mM phosphate, 100 mM NaCl, pH 7.4)

2.3.4 Molecular dynamics simulations

The unusual observation of the relationship between in-solution helicity and potency motivated me to further investigate the impact of introducing a maleimide constraint on the conformation of the peptides in isolation and their complexes with BCL-x_L. To do this, I performed molecular dynamics (MD) simulations using YASARA.[237] First, I modelled structures of complexes between BAD-s or each constrained peptide and BCL-x_L in YASARA and performed energy minimisation. The minimised structures showed that installation of a maleimide constraint does not cause steric clashes in most complexes with the protein, although it did make slight conformational changes or drift of the peptides in several complexes (Figure 2-7 and Figure 2-8). However, clashes in BADS2/BCL-x_L and BADS6/BCL-x_L were observed, suggesting that these positions are not suitable for introducing a maleimide constraint.

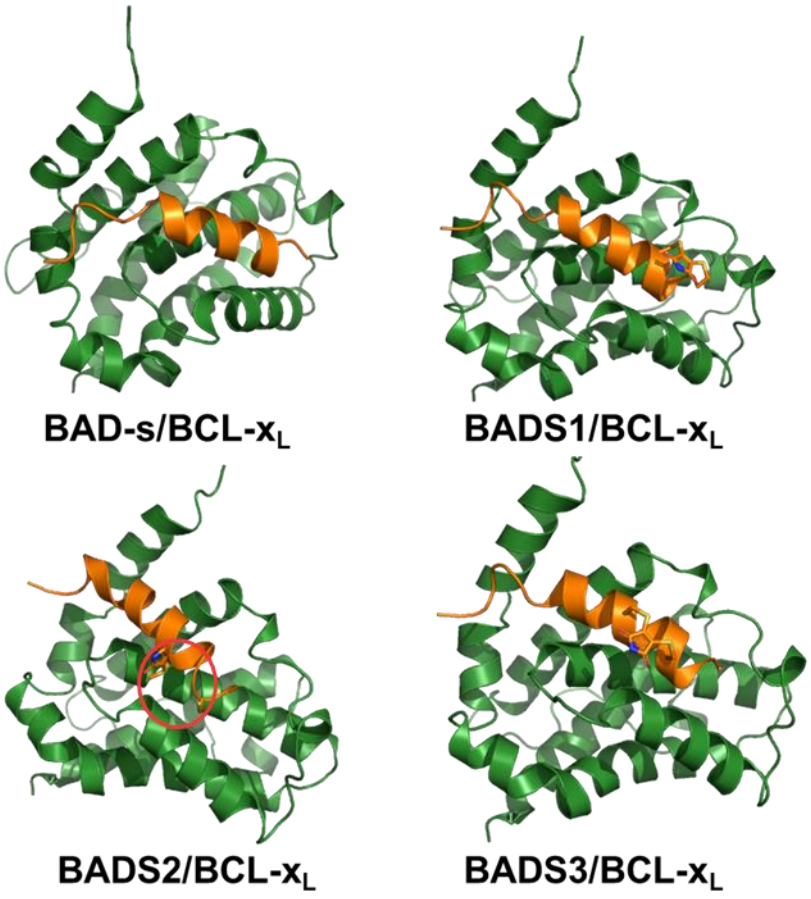

Figure 2-7 Energy-minimised structures of the complexes of BAD-s, BADS1, BADS2, and BADS3 with BCL-x_L (clashes are highlighted in BADS2/BCL-x_L).

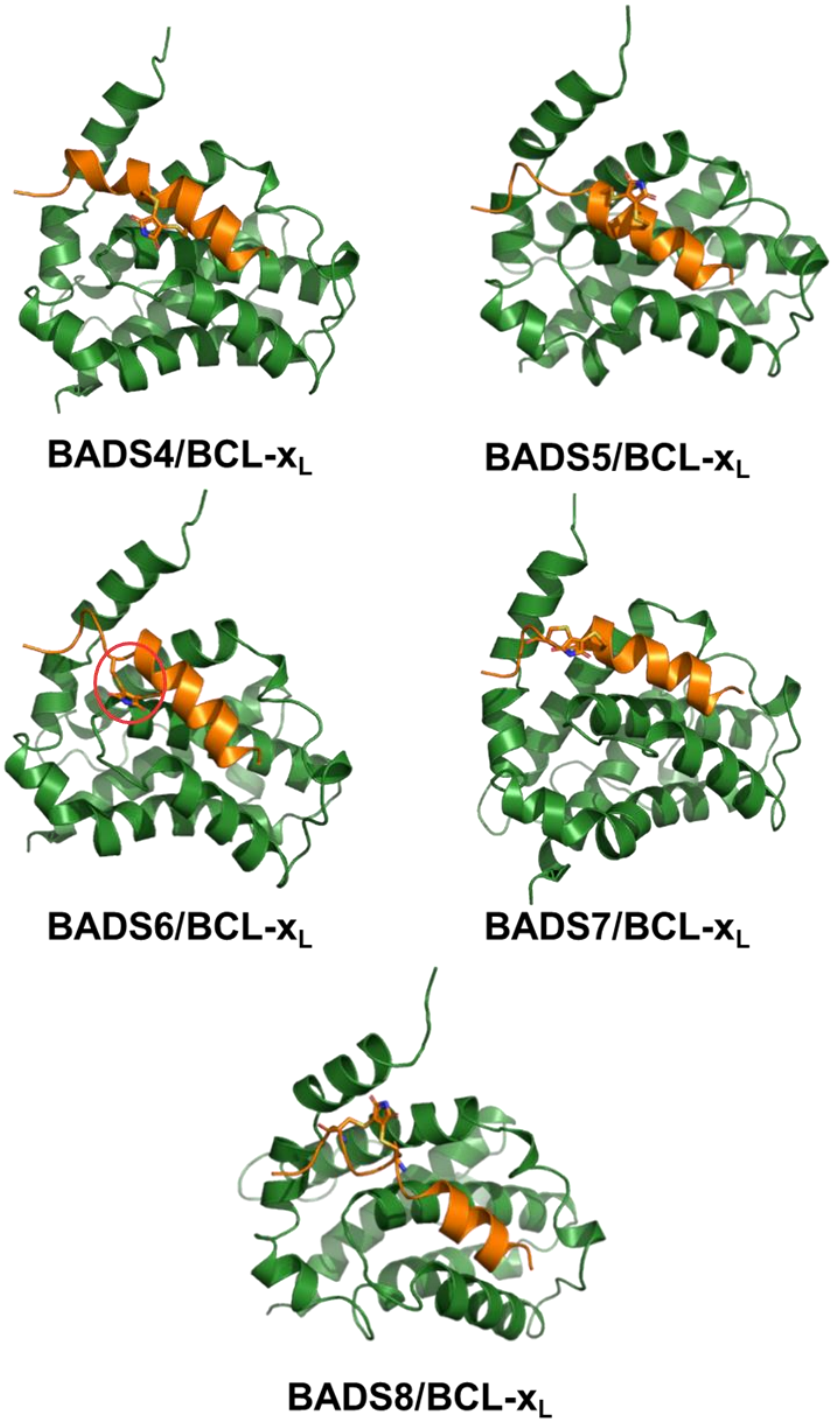

Figure 2-8 Energy-minimised structures of the complexes of BADS4, BADS5, BADS6, BADS7 and BADS8 with BCL-x_L (clashes are highlighted in BADS6/BCL-x_L).

Thereafter, BAD-s, BADL5, BADS5, BADL8 and BADS8 and their complexes with the BCL-x_L were subjected to simulations for >160 ns using the AMBER14 forcefield (Figure 2-17 - 2-26, Table 2-2). To calculate helicity of each peptide, the conformer at 50 ns was chosen as a starting point and helicity from 50 to 160 ns was averaged. In the simulations, the *apo*-peptides showed various helicity. BAD-s was calculated to have an average helicity of 63% in two simulations, whilst BADL5 and BADS5 gave average helicity of 72% and 57%, respectively; BADL8 and BADS8 gave higher helicity, with 71% and 75%. However, these results did not show strong correlation to the observed helicity using CD.

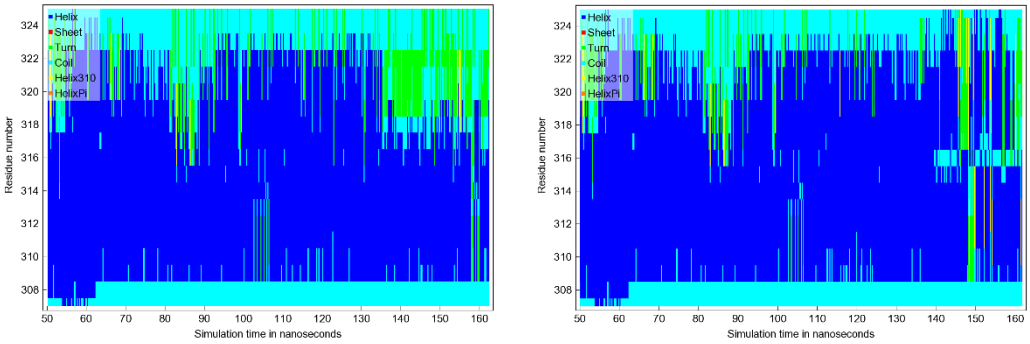

Figure 2-9 Replicate MD simulations for BAD-s

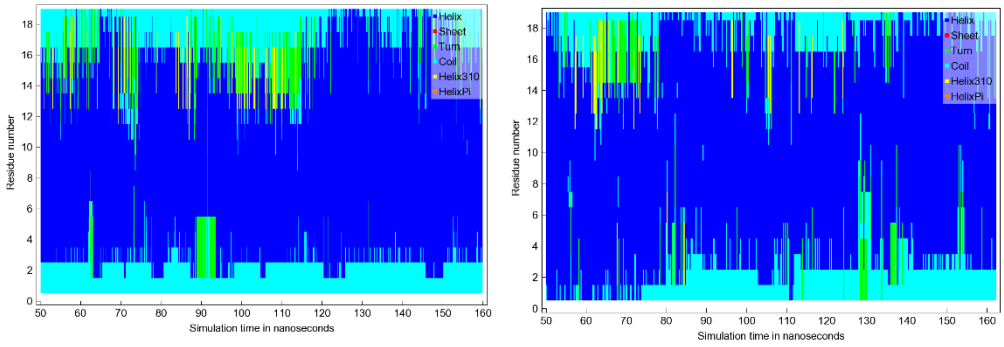

Figure 2-10 Replicate MD simulations for BADL5

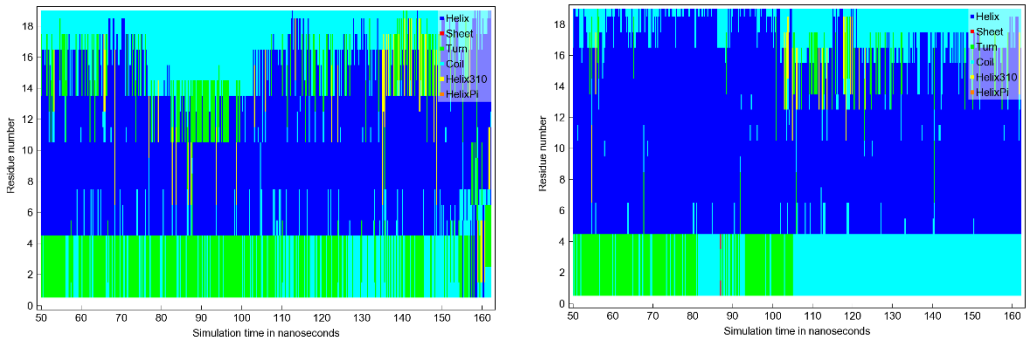

Figure 2-11 Replicate MD simulations for BADS5

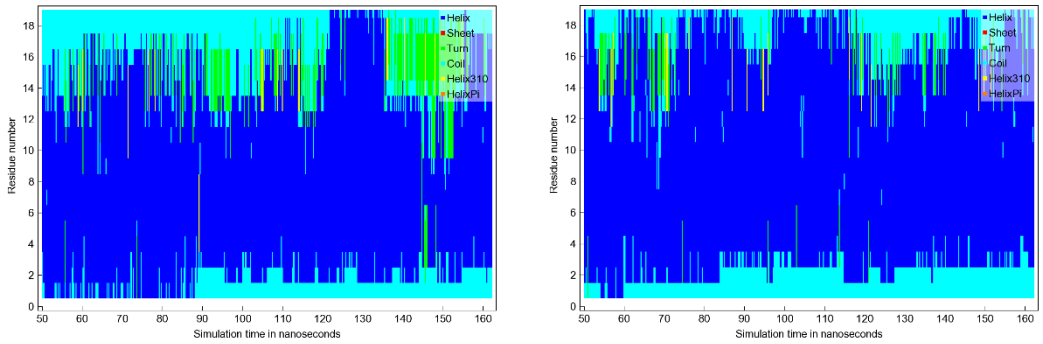

Figure 2-12 Replicate MD simulations for BADL8

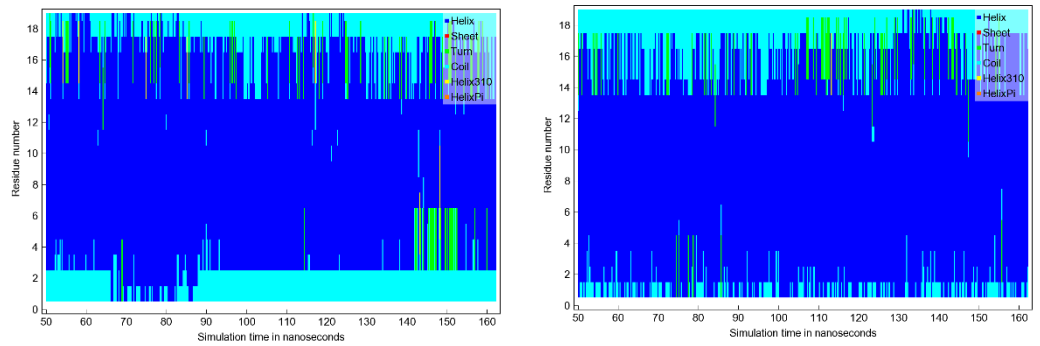

Figure 2-13 Replicate MD simulations for BADS8

In the simulations of the complexes, BAD-s, BADL5, BADS5 and BADL8 were observed to maintain high helicity in the corresponding complexes with BCL-x_L after 120 ns. In general, the peptides exhibited similar or greater helicity in the bound state than in isolation (Table 2-2). BAD-s showed an average helicity of 76% in the complex with BCL-x_L (Figure 2-14), whilst BADL5 and BADS5 showed similarly high helicities of 75% and 81% (Figure 2-15 and Figure 2-16), respectively. However, compared with the other three peptides and its linear precursor BADL8 (79% helicity in bound state), the bound BADS8 showed a lower helicity (62%) (Figure 2-18), suggesting that introducing a maleimide constraint at this position potentially decreases helicity of the peptide in its bound state, which may attribute to the loss of inhibitory potency observed in the competition FA assays.

Table 2-2 A summary of helicities in MD simulations

Peptide	Helicity$_{apo\text{-peptide}}$	Helicity$_{bound\text{-peptide}}$
BAD-s	63%	76%
BADL5	72%	75%
BADS5	57%	81%
BADL8	71%	78%
BADS8	75%	62%

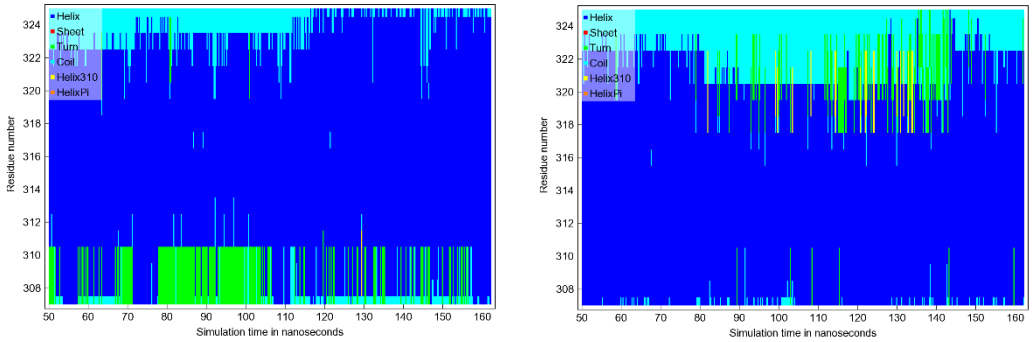

Figure 2-14 Replicate MD simulations for bound BAD-s in BAD-s/BCL-x_L

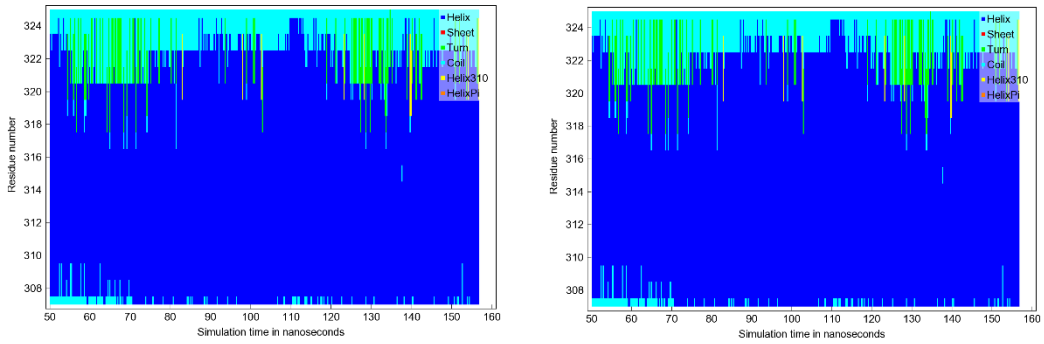

Figure 2-15 Replicate MD simulations for bound BADL5 in BADL5/BCL-x_L

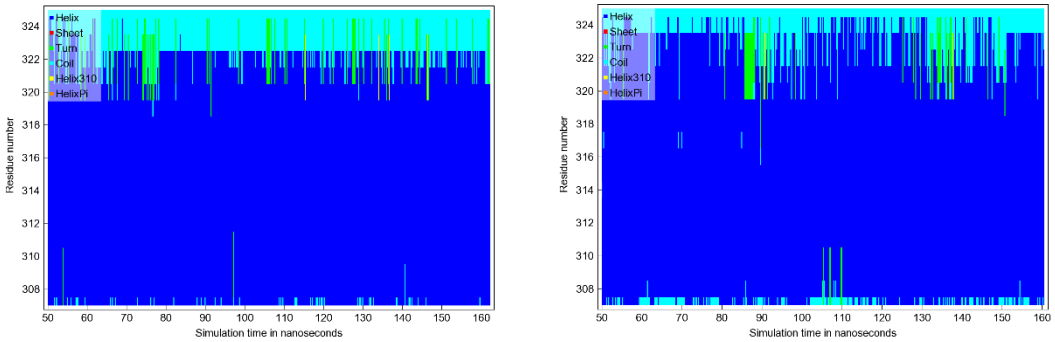

Figure 2-16 Replicate MD simulations for bound BADS5 in BADS5/BCL-x_L

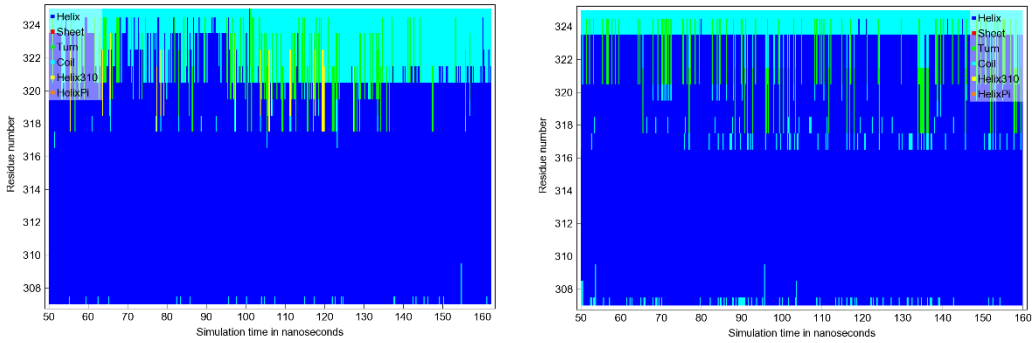

Figure 2-17 Replicate MD simulations for bound BADL8 in BADL8/BCL-x_L

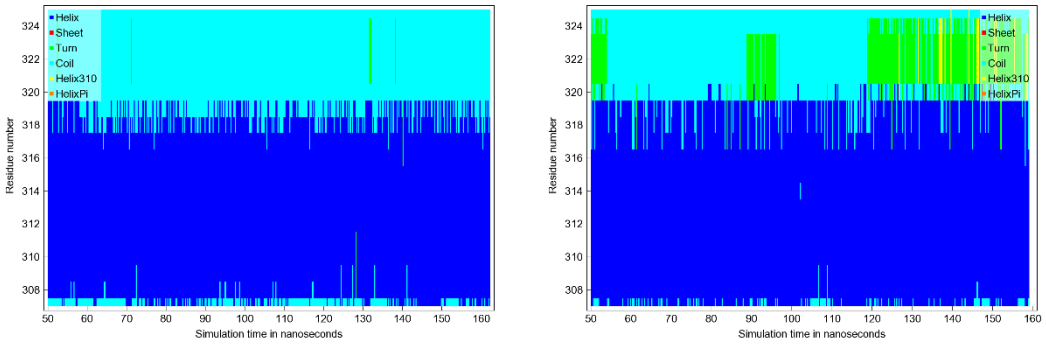

Figure 2-18 Replicate MD simulations for bound BADS8 in BADS8/BCL-x_L

Next, I analysed changes in interactions between the linear/constrained peptides and BCL-x_L using the average structures generated by MD simulations. After 160 ns simulation, BAD-s maintained major interactions observed in the original structure (Figure 2-19). Furthermore, a new hydrogen bonding between Tyr110 in BAD and Ala104 in BCL-x_L was observed (Figure 2-19), indicating the potential for MD to map missing interactions in crystal structures. The key interactions, including the new hydrogen-bonding, between BADL5/BADS5/BADL8 and BCL-x_L were also maintained after the simulations (Figure 2-20, Figure 2-21 and Figure 2-22); however, the important Phe121-Phe97 π-π interaction disappeared in BADS8/BCL-x_L average structure (Figure 2-23). These results suggest that the loss of potency may arise from conformational changes resulting in a loss of helicity of bound peptide in combination with a failure to orient key residues optimally for productive interaction between peptide and protein as a consequence of the constraint.

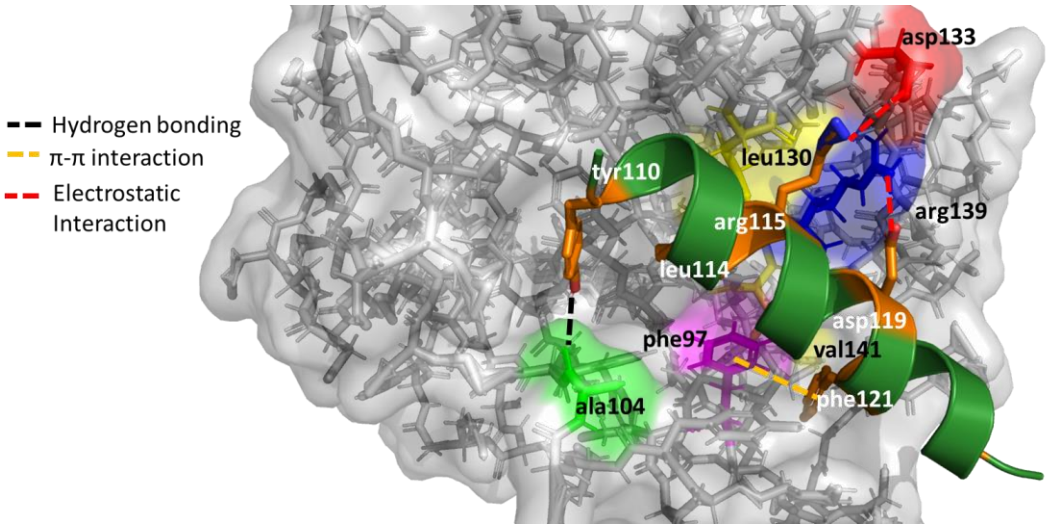

Figure 2-19 Interactions between BAD-s and BCL-x_L after MD simulation (residues in BCL-x_L are highlighted in: green for hydrogen-bond, yellow for hydrophobic contacts, blue for simultaneous electrostatic interaction and hydrogen-bond, purple for π-π interaction and red for electrostatic interaction).

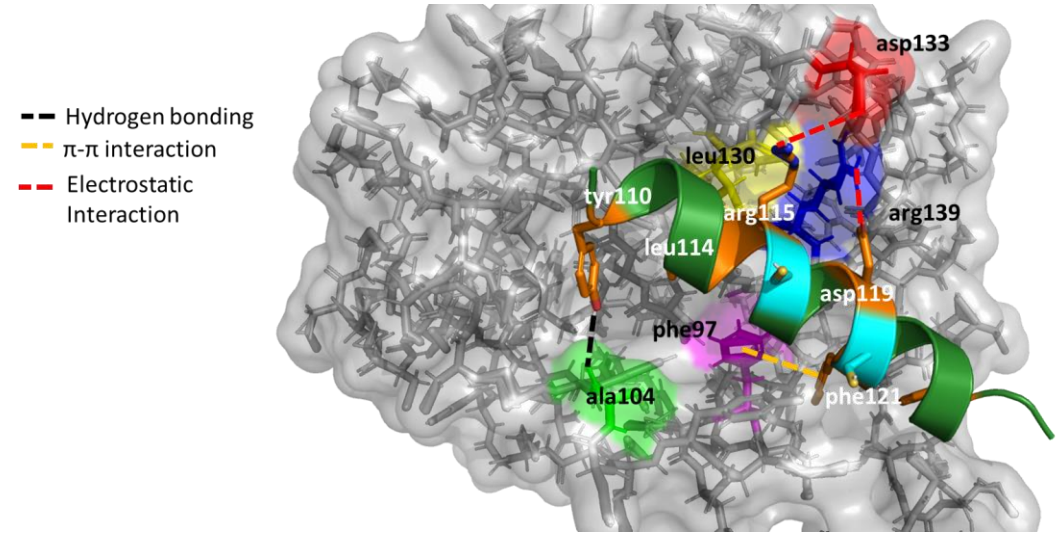

Figure 2-20 Interactions between BADL5 and BCL-x_L after MD simulation (residues in BCL-x_L are highlighted in: green for hydrogen-bond, yellow for hydrophobic contacts, blue for simultaneous electrostatic interaction and hydrogen-bond, purple for π-π interaction and red for electrostatic interaction).

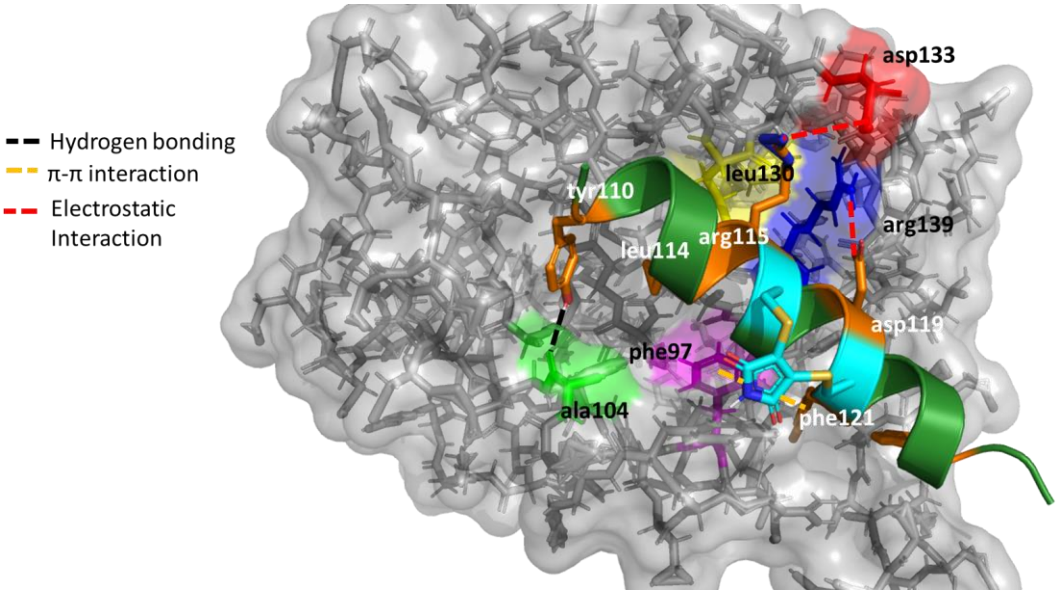

Figure 2-21 Interactions between BADS5 and BCL-x_L after MD simulation (residues in BCL-x_L are highlighted in: green for hydrogen-bond, yellow for hydrophobic contacts, blue for simultaneous electrostatic interaction and hydrogen-bond, purple for π-π interaction and red for electrostatic interaction).

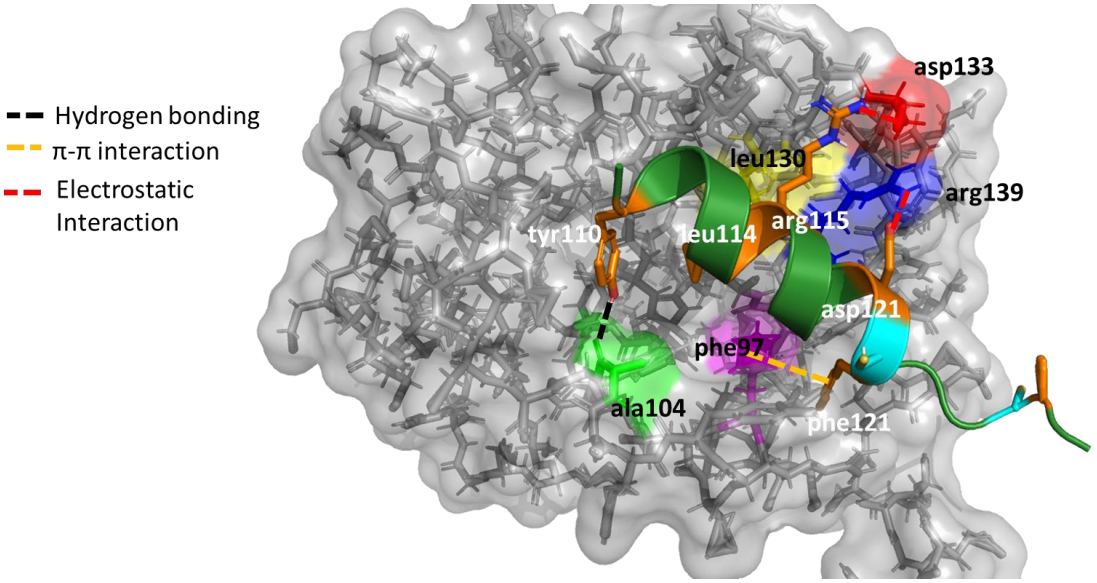

Figure 2-22 Interactions between BADL8 and BCL-x_L after MD simulation (residues in BCL-x_L are highlighted in: green for hydrogen-bond, yellow for hydrophobic contacts, blue for simultaneous electrostatic interaction and hydrogen-bond, purple for π-π interaction and red for electrostatic interaction).

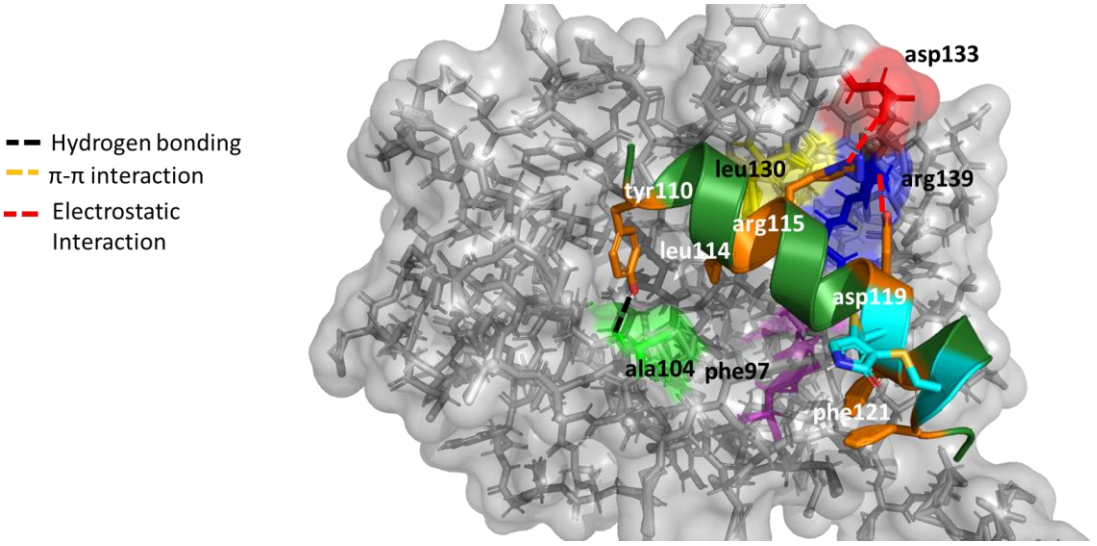

Figure 2-23 Interactions between BADS8 and BCL-x_L after MD simulation (residues in BCL-x_L are highlighted in: green for hydrogen-bond, yellow for hydrophobic contacts, blue for simultaneous electrostatic interaction and hydrogen-bond, purple for π-π interaction and red for electrostatic interaction).

2.4 Conclusions

In this chapter, I chose the BAD BH3 sequence as a starting point and have successfully designed maleimide-constrained peptides as BCL-x_L inhibitors. Using a maleimide-staple scan, I identified suitable sites for incorporation of a maleimide constraint in the wild-type peptide, BAD-s. A number of peptides exhibited diminished inhibitory potency as the bis-cysteine and constrained variants, whilst a number exhibited diminished potency only as the constrained variant. Conformational analyses by CD indicated that α-helicity of the peptides in isolation is unlikely to influence inhibitory potency. These unusual results motivated me to use MD simulations to further investigate the bound states of the complexes between peptide ligands and the protein. These MD simulations suggest that differences in bound-state-helicity between the active and inactive constrained peptides might influence inhibitory potency and that for a number of peptides, constraining modulates the orientation of key side chains such that optimal interaction with BCL-x_L cannot be achieved. These observations highlight the importance of constraint placements in peptide design, and emphasise the complex effects that introducing a constraint can have on potency.[238–240]

2.5 Future work

2.5.1 Irreversible maleimide constraining

Dibromomaleimide is a linker to rapidly crosslink two cysteines in peptides under biocompatible conditions, thus serving as a powerful tool to generate constrained peptides. However, the constraining reaction is reversible, which may result in uninstallation of the maleimide linker in cytosolic reducing environment.[134] The outcome of this on-and-off process is not certain, as the constraint always add more benefits, e.g. improvement of proteolytic stability. Therefore, optimisation to an irreversible linker based on dibromomaleimide may open a new avenue to apply the constrained peptides in cell-based assays. The existence of the double bond in a maleimide ring plays an important role in this reversible process. Hence, conversion of the maleimide to a succinimide may cancel the reversibility of the constraint. To do this, using reducing regents is not ideal as the maleimide constraint itself can also be removed. Therefore, using a monosubstituted maleimide, e.g. bromomaleimide or *N*-methylbromomaleimide may provide possible options to generate irreversible constrained peptides with similar structural preference.

In addition, hydrolysis of the maleimide ring is another option to make the constraint irreversible. For instance, Lyon *et al.* described a class of self-hydrolysing maleimides that can make stabilised and irreversible ADCs (Figure 2-24). [145] The dibromomaleimide linker will be investigated by hydrolysis.

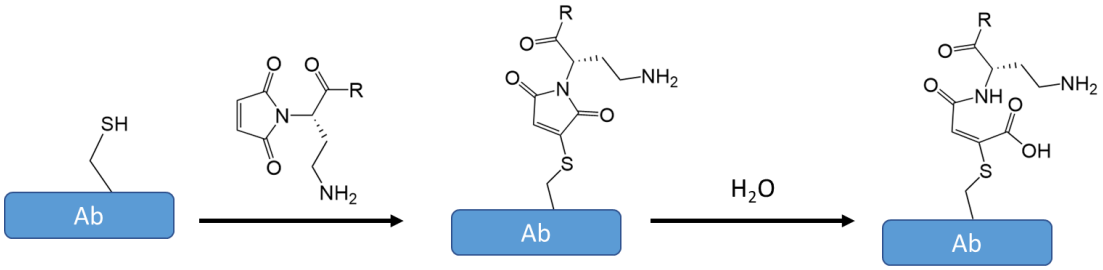

Figure 2-24 Self-hydrolysing maleimide linker for antibody-drug conjugation (Ab: antibody).[145]

2.5.2 Acid-cleavable maleimide constraining

The structural reversibility between maleic acid and maleimide has been used in design of various delivery systems targeting the tumour acidic microenvironment.[144] A large number of peptide conjugates with functionalities adding to a trifunctional constraint have been reported. Caddick and co-workers developed an acid-cleavable linker for generation of ADCs (Figure 2-25).[143] However, an acid-cleavable linker is yet to be developed. To generate an acid-cleavable constrained peptide conjugate, dibromoanhydride can be used to add a constraint, following by a ring-opening reaction using a nucleophile e.g. free amine (Figure 2-26). This type of constrained peptides may pave the way to design new peptide pro-drugs with better cell-permeability but minimised impact on potency.

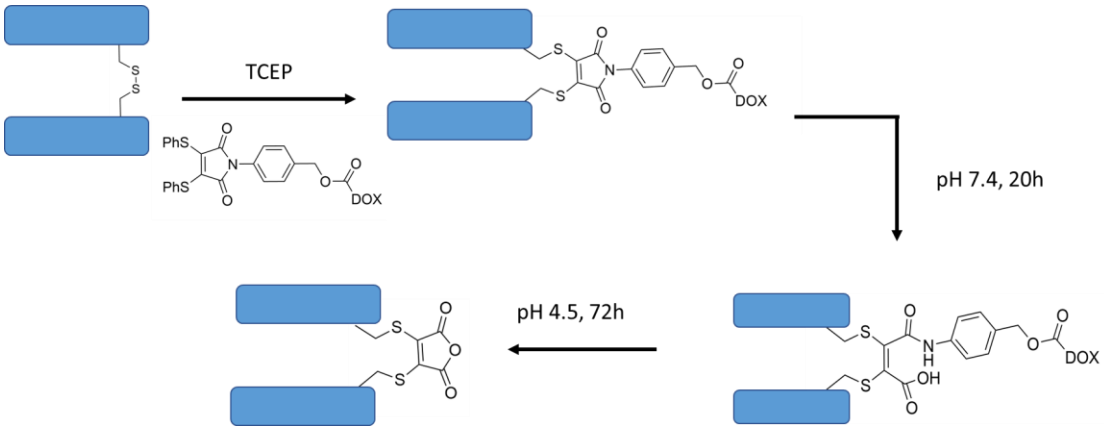

Figure 2-25 Acid-cleavable thiomaleamic acid linker for homogeneous antibody–drug conjugation. [143]

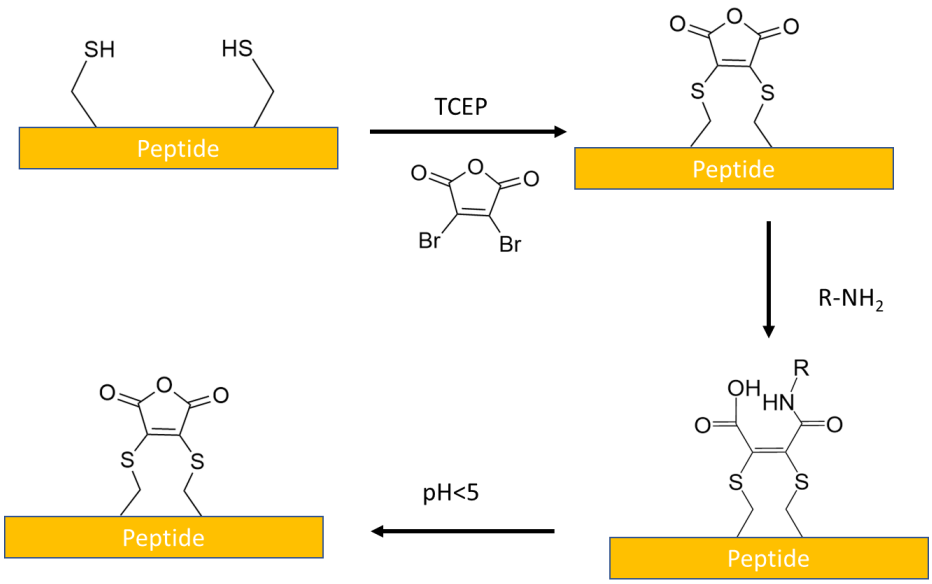

Figure 2-26 Proposed acid-cleavable linker to make constrained peptides.

2.5.3 Structural study

The observations of the BAD peptides in biophysical studies in this chapter are consistent with a bind-and-fold mechanism. Crystallography may provide new structural insights of the interaction between constrained peptides and BCL-x_L in combination with computational analysis.

Chapter 3 Development of HRK-derived constrained peptides as BCL-2 family inhibitors

3.1 A brief introduction of the HRK protein

The Harakiri/death protein 5 (HRK/DP5) protein is a BH3-only member of the BCL-2 family, encoded by the gene *harakiri*, which interacts predominantly with BCL-2 and BCL-x_L.[241] HRK plays a pivotal role in neuronal cell death in response to nerve growth factor (NGF) deprivation.[242] NGF deprivation induces upregulation of BIM and HRK in neonatal sympathetic neurons.[243] HRK also regulates pancreatic β-cell apoptosis, indicating the possibility to prevent loss of β-cells, which is observed in type 1 diabetes, by blocking HRK-mediated apoptosis.[244] Another study showed that HRK is not essential for apoptosis of haematopoietic cells although it was found to be expressed in the central and peripheral nervous system.[245]

3.2 Chapter aims

Previous studies have described constrained peptides based on other BH3 ligands, e.g. BID[101] and BIM.[246] However, HRK-derived constrained peptides have been less explored. HRK was classified as BCL-2 and BCL-x_L selective in prior studies.[241] Herein, clarifying the binding profiles of peptide sequences derived from the HRK BH3 domain and constructing constrained peptides based on the sequence would pave the way to develop new BCL-x_L selective peptidomimetic inhibitors. The main goal of the chapter was to design HRK-derived constrained peptides targeting BCL-x_L and to further identify selective BCL-x_L inhibitors.

3.3 Rational design of HRK-derived constrained peptides as BCL-x_L and MCL-1 inhibitors

3.3.1 *In silico* modelling to identify potential hot-spot residues

To identify the hot-spot residues in the HRK BH3 sequence involved in the interaction with BCL-x_L, I chose BUDE[231] Alanine Scan (BAlaS),[232] a well-established and fast tool, to perform a virtual alanine scan. To carry out a virtual alanine scan, a structure of the complex between a peptide ligand and a protein is required; however, a structure for the HRK/BCL-x_L

interaction has not been reported. I initially chose the structure of HRK with SPPV14 (HRK/SPPV14, PDB ID:6XY4),[247] which is a BCL-2 analogue in sheeppox virus,[248] to perform alanine scanning. To compare the modelling results and facilitate the peptide design, I thereafter chose the structure of BAD/BCL-x_L (PDB ID:1G5J), and also generated a homology model by replacing the BAD from the BAD/BCL-x_L structure with an HRK ligand (Figure 3-1 and Figure 3-2 (a)). The homology structure was repacked in Rosetta to remove small clashes. All three structures were subjected to a virtual alanine scan using the BAlaS webserver (Figure 3-1).

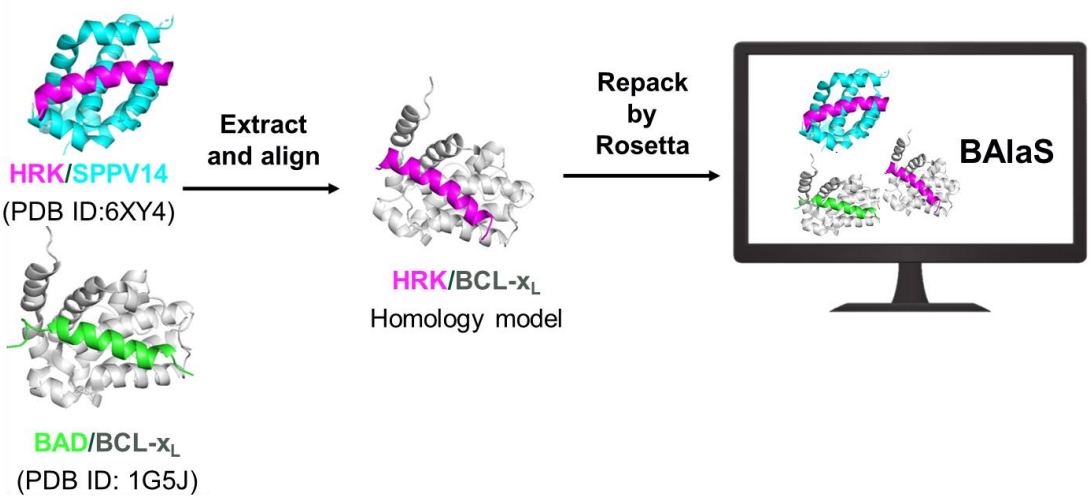

Figure 3-1 Workflow for generation of homology model and virtual alanine scan.

The virtual alanine scanning results showed that the hot-spot residues in the HRK peptide involving interactions with either SPPV14 or BCL-x_L are similar (Figure 3-2 (b)), which provides confidence that there is similarity in recognition modes between SPPV14 and human BCL-2 family proteins. Three leucine residues, Leu37, Leu40 and Leu44, showed decrease of calculated free binding energy ($\Delta\Delta G$>4.2 kJ/mol) in both HRK/SPPV14 and HRK/BCL-x_L PPIs. Lys38 showed $\Delta\Delta G$>4.2 kJ/mol in HRK/BCL-x_L but <4.2 kJ/mol in HRK/SPPV14. Six Residues, including Leu104, Tyr110, Leu114, Arg115, Phe121 and Phe125, were identified as hot-spots in the BAD sequence, which is consistent with the fact that BAD is a stronger ligand for BCL-x_L than HRK.[35] Notably, variation of the two Phe for Ala resulted in significant decrease in binding free energy, with 18 kJ/mol and 13.2 kJ/mol, respectively, suggesting that these two residues play more important roles in the BAD/BCL-x_L interaction.

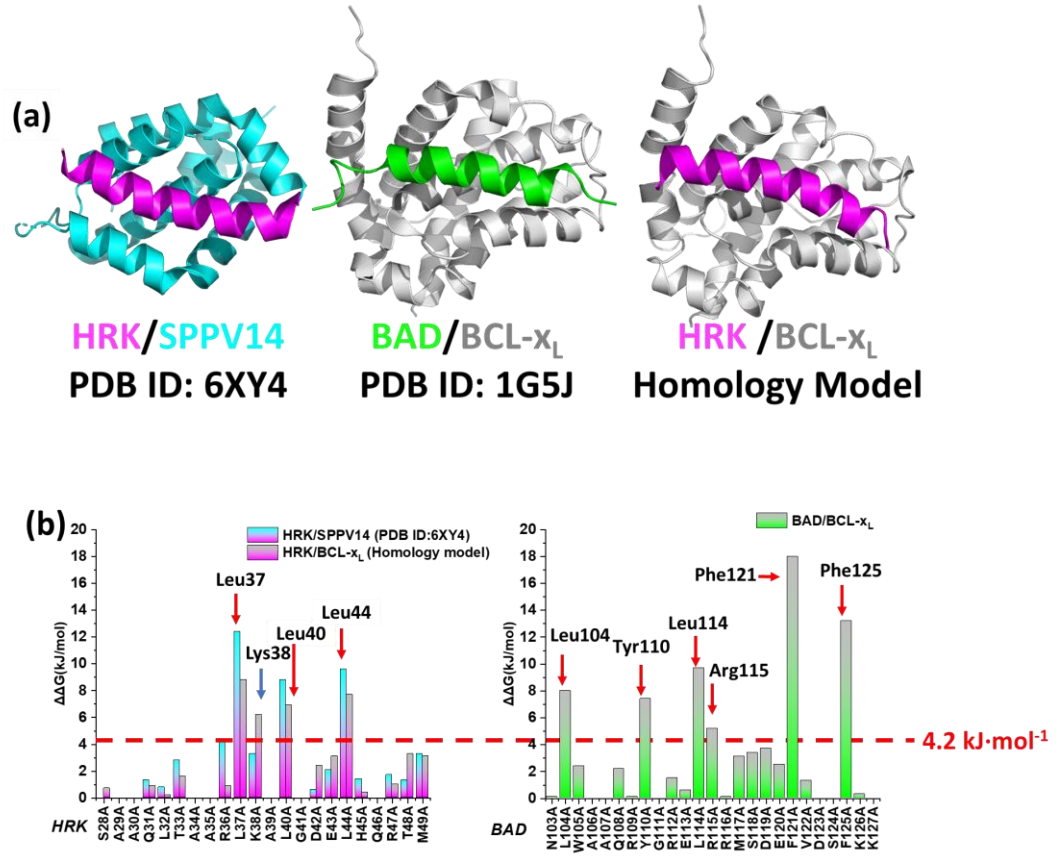

Figure 3-2 Homology modelling and virtual alanine scanning (a) Structures of complexes of HRK/SPPV14 (PDB ID: 6XY4), BAD/BCL-x_L (PDB ID: 1G5J) and HRK/BCL-x_L (homology model); (b) Virtual alanine scanning results for the three structures.

3.3.2 Direct titration FA assays

To establish a fluorescence anisotropy assay for screening, I prepared a tracer peptide, FAM-Ahx-HRK, by adding an aminohexanoic (Ahx) linker and a 5(6)-carboxyfluorescein (FAM) group at the N-terminus of the 23-mer HRK sequence after automated Fmoc-based standard solid-phase peptide synthesis (purity >90% after prep-HPLC purification). In the direct titration experiment, the tracer was observed to bind to the BCL-x_L with an affinity of K_d = 38 (± 6) nM (Figure 3-3). These data indicate the HRK peptide to be a good starting point for design of BCL-x_L inhibitors and suitable to develop competition assays for screening.

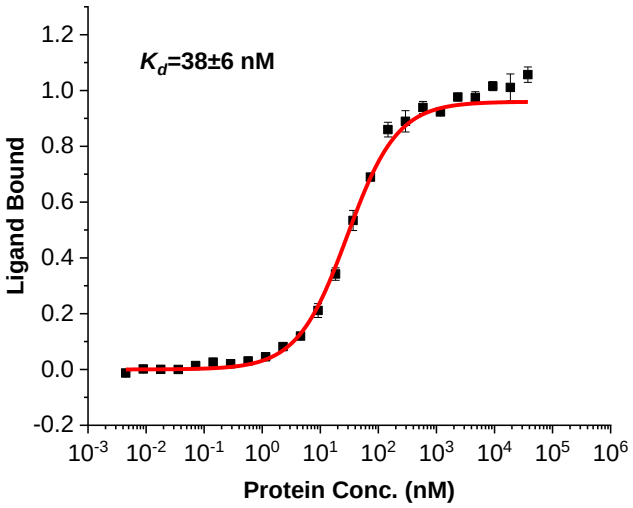

Figure 3-3 Direct titration of FAM-Ahx-HRK with BCL-x_L (FAM-Ahx-HRK (50 nM) BCL-x_L (6 nM-125 μM) 20 mM Tris, 150 mM NaCl, pH 7.6, 20 °C; error bars show standard deviations observed in triplicate experiments and errors are standard deviations generated in data fitting; the tested data agrees with the range in the literature).[249]

3.3.3 Maleimide constraint increases potency

Subsequent to the virtual alanine scan analysis, I designed 10 peptides by inserting a pair of cysteines into the 23-mer peptide sequence, HRK_{28-50} (Ac-SAAQLTAARLKALGDELHQRTMW-NH_2, hereafter referred to as HRK-wt), at *i*, *i*+4 positions. HRKC1-9 peptides were designed by incorporating *i*, *i*+4 cysteines from the N-terminus to C-terminus excluding hot-spot residues (Table 3-1). In addition, peptide HRKS10 was designed by replacing the original D-K salt-bridge with a maleimide-bridge, in order to investigate the influence of replacement of the native salt bridge with a covalent linker. After Fmoc based solid-phase peptide synthesis, the linear peptides were treated with TCEP and each maleimide-constraint was installed using dibromomaleimide. All peptides were purified by prep-HPLC and lyophilised to afford solid peptides for further study (purity >85% after prep-HPLC purification).

Thereafter, the constrained peptides and their linear precursors were tested in competition FA assays with BCL-x_L and FAM-Ahx-HRK. All assays were repeated for three times and HRK-wt was used as a positive control for comparison. As a result, several peptides showed no significant response in the competition assays, e.g., HRKC6, HRKS6, HRKC7, HRKS7, HRKC10 and HRKS10 (Figure 3-4 (b) and (c)), indicating

neither incorporation of a pair of cysteines at these positions nor insertion of a maleimide-staple could sustain interactions with the BCL-x_L. These results may be attributed to changing of the highly conserved XD motif (X is a residue with a small sidechain, e.g. Gly, Ala or Ser, and D (Asp) forms a charged reinforced hydrogen-bond with an arginine residue in the receptor protein) in BH3-only members.[234] In addition, some peptides showed a slight decrease in potency. For instance, HRKC1, HRKS1, HRKC3, HRKC4, HRKC5, HRKS5, HRKC8 and HRKS8 exhibited 1.5-4-fold loss of potency (Figure 3-4 (a), (b) and (c)). Two maleimide-constrained peptides, HRKS3 and HRKS9, showed similar potency in comparison to the wild-type sequence, with IC_{50} = 1.6 (±0.1) and 2.6 (±0.2) μM, respectively. Moreover, HRKS4 showed slightly improved potency in comparison to HRK-wt, whereas the linear peptide, HRKC4, showed decreased potency (Figure 3-4 (d)).

These results demonstrate that incorporation of a maleimide constraint at appropriate sites can add potency, which may arise from the pre-organisation of peptides' secondary structures based on the HRK BH3 sequence.

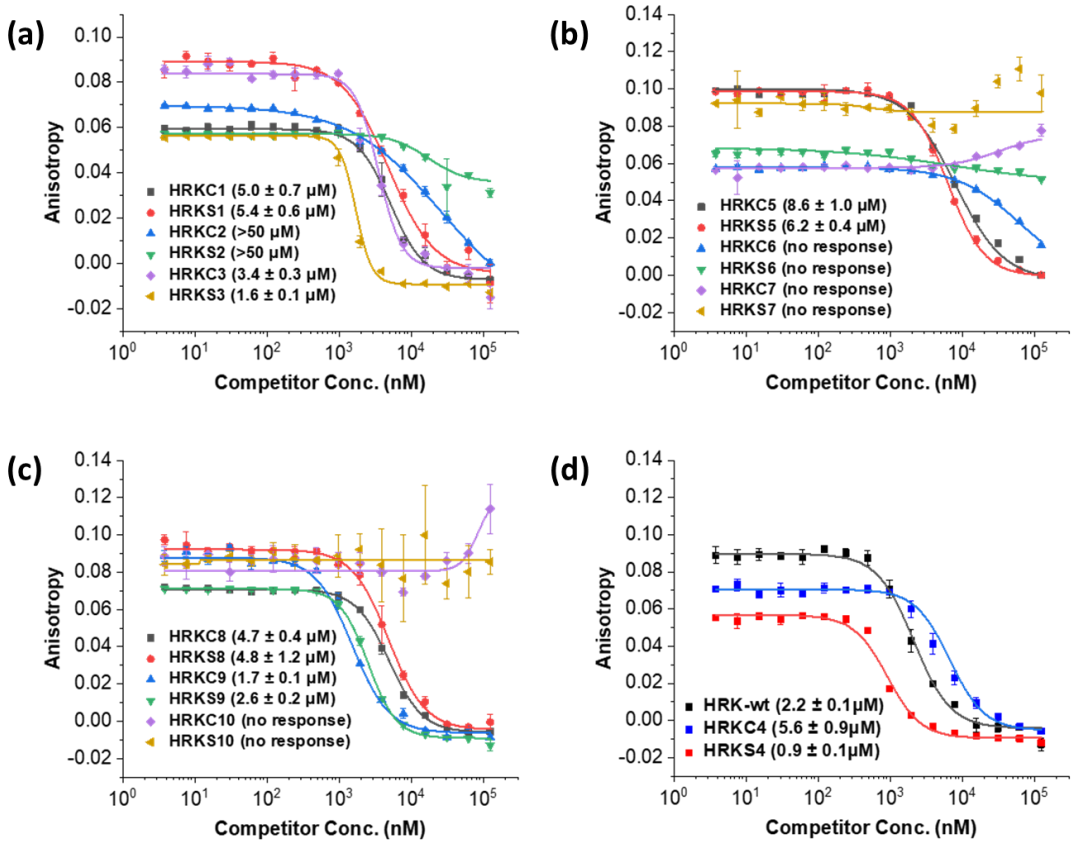

Figure 3-4 FA competition results for the HRK peptides; (a) HRKC/S1, HRKC/S2 and HRKC/S3; (b) HRKC/S5, HRKC/S6, and HRKC/S7; (c) HRKC/S8, HRKC/S9 and HRKC/S10; (d) HRK-wt, HRKC4 and HRKS4 (20 mM Tris, 150 mM NaCl, pH 7.6, 250 nM BCL-x_L, 50 nM tracer, 20 °C; error bars show standard deviations observed in triplicate experiments and errors are standard deviations generated in data fitting).

3.3.4 Structural analysis of the constrained peptides

Additionally, I investigated the secondary structural preference of the peptides using CD. I tested HRK-wt, HRKC1-10 and HRKS1-10 in phosphate buffer using CD. It was found that the maleimide constraint did not significantly change the conformational preference of most peptides in solution. For example, HRKS6 was observed to have a helicity of 32% whilst HRKC6 gave a helicity of 29% (Figure 3-5 (b)). Other peptides, like HRKC/S2, HRKC/S3, HRKC/S7, HRKC/S8, and HRKC/S9, gave similar observations (Figure 3-5 (a), (b) and (c)). Decrease of helicity was observed in HRKC/S5 and HRKC/S10, suggesting that the constraint is not favourable for helicity at these positions. Notably, HRKS1 and HRKS4 conferred observable enhancement of helicity after dibromomaleimide

constraining, with 26% to 35, and 14% to 25%, respectively (Figure 3-5 (a)(d)). Taken FA competition results together, HRKS4 also showed improved potency after maleimide stapling (Table 3-1), suggesting the pre-organisation by the maleimide constraint might reduce the entropic cost for binding or stabilise the conformation of bound state.[63] The loss in helicity of the unconstrained variant – HRKC4 – in comparison to the wild-type sequence is consistent with variation of two Ala for two Cys residues and the concomitant loss in inhibitory potency supports a role for preorganisation in HRKS4. Although HRKS1 exhibited improved helicity in solution, it did not show improved potency. This might arise because the maleimide constraint was placed away from the cluster of hot-spot residues in the sequence. These data demonstrate that maleimide peptide constraining is a promising approach to generate BCL-x_L inhibitors based on the HRK and the placement of the *i*, *i*+4 maleimide constraint is important for improved bioactivity and helicity in solution.

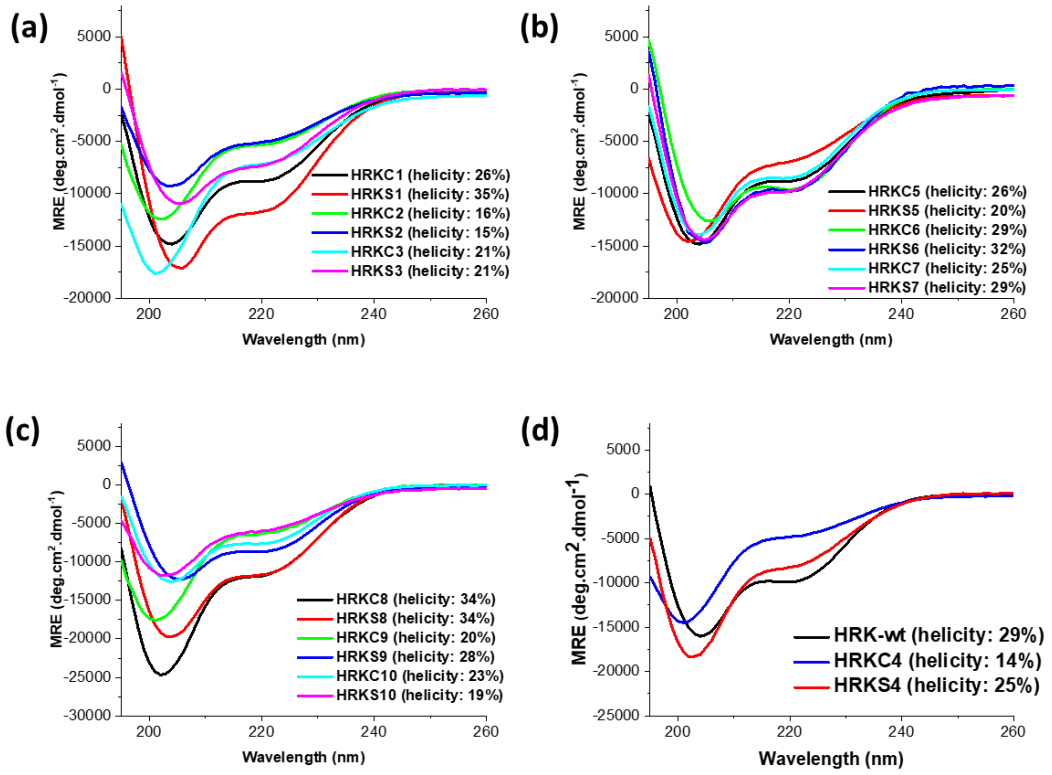

Figure 3-5 CD spectra for the HRK peptides; (a)HRKC/S1, HRKC/S2 and HRKC/S3; (b) HRKC/S5, HRKC/S6 and HRKC/S7; (c) HRKC/S8, HRKC/S9 and HRKC/S10; (d) HRK-wt, HRKC4 and HRKS4 (peptide concentration: 50 µM, 20 mM phosphate, 100 mM NaCl, pH 7.4).

Table 3-1 A summary of FA competition results and helicity of the peptides.

Peptide	Sequence[a]	IC_{50} HRK/BCL-x_L (μM)[b]	Helicity [c]
HRK-wt (HRK_{28-50})	SAAQLTAAR**LK**A**L**GDE**L**HQRTMW	2.2 ± 0.1	29%
HRKC1	SCAQLCAAR**LK**A**L**GDE**L**HQRTMW	5.0 ± 0.7	26%
HRKS1	S**C**AQL**C**AAR**LK**A**L**GDE**L**HQRTMW	5.4 ± 0.6	35%
HRKC2	SACQLTCAR**LK**A**L**GDE**L**HQRTMW	>50	16%
HRKS2	SA**C**QLT**C**AR**LK**A**L**GDE**L**HQRTMW	>50	15%
HRKC3	SAACLTACR**LK**A**L**GDE**L**HQRTMW	3.4 ± 0.3	21%
HRKS3	SAA**C**LTA**C**R**LK**A**L**GDE**L**HQRTMW	1.6 ± 0.1	21%
HRKC4	SAAQLTACR**LK**C**L**GDE**L**HQRTMW	5.6 ± 0.9	14%
HRKS4	SAAQLTA**C**R**LK**C**L**GDE**L**HQRTMW	0.9 ± 0.1	25%
HRKC5	SAAQLTAAR**LK**C**L**GDC**L**HQRTMW	8.6 ± 1.0	26%
HRKS5	SAAQLTAAR**LK**C**L**GD**C**LHQRTMW	6.2 ± 0.4	20%
HRKC6	SAAQLTAAR**LK**A**L**CDE**L**CQRTMW	No response	29%
HRKS6	SAAQLTAAR**LK**A**L**C**C**DE**L**C**C**QRTMW	No response	32%
HRKC7	SAAQLTAAR**LK**A**L**GCE**L**HCRTMW	No response	25%
HRKS7	SAAQLTAAR**LK**A**L**G**C**E**L**H**C**RTMW	No response	29%
HRKC8	SAAQLTAAR**LK**A**L**GDC**L**HQCTMW	4.7 ± 0.4	34%
HRKS8	SAAQLTAAR**LK**A**L**GD**C**LHQ**C**TMW	4.8 ± 1.2	34%
HRKC9	SAAQLTAAR**LK**A**L**GDE**L**CQRTCW	1.7 ± 0.1	20%
HRKS9	SAAQLTAAR**LK**A**L**GDE**L**C**C**QRT**C**W	2.6 ± 0.2	28%
HRKC10	SAAQLTAAR**L**CA**L**GCE**L**HQRTMW	No response	23%
HRKS10	SAAQLTAAR**L**C**C**A**L**G**C**E**L**HQRTMW	No response	19%

[a]Hot-spot residues are highlighted in bold; the incorporated cysteines are underlined, constrained cysteines are highlighted in red; all peptides are acetylated at the N-terminus and C-terminally amidated; [b]conditions: 20 mM Tris, 150 mM NaCl, pH 7.6, 50 nM tracer, 250 nM BCL-x_L; all experiments were repeated for three times; error numbers are standard deviations generated in data fitting [c]conditions: 20 mM phosphate, 100 mM NaCl, pH=7.2.

3.3.5 Proteolytic studies

Next, I tested the proteolytic stability of the maleimide-constrained peptide, HRKS4 using alpha-chymotrypsin and trypsin, respectively, and compared it with its linear precursor, HRKC4, and also HRK-wt (Figure 3-6). As a result, similar effects were observed in both assays. The constrained peptide, HRKS4, was observed to have half-lives of 53.5 min (α-chymotrypsin, Figure 3-6 (a)(b)) and 5.8 min (trypsin, Figure 3-6 (c)(d)), respectively, of which each is approximately twice as long as that of HRK-wt or HRKC4. These data show that incorporation of a maleimide constraint can enhance the proteolytic stability of the HRK BH3 peptide sequence.

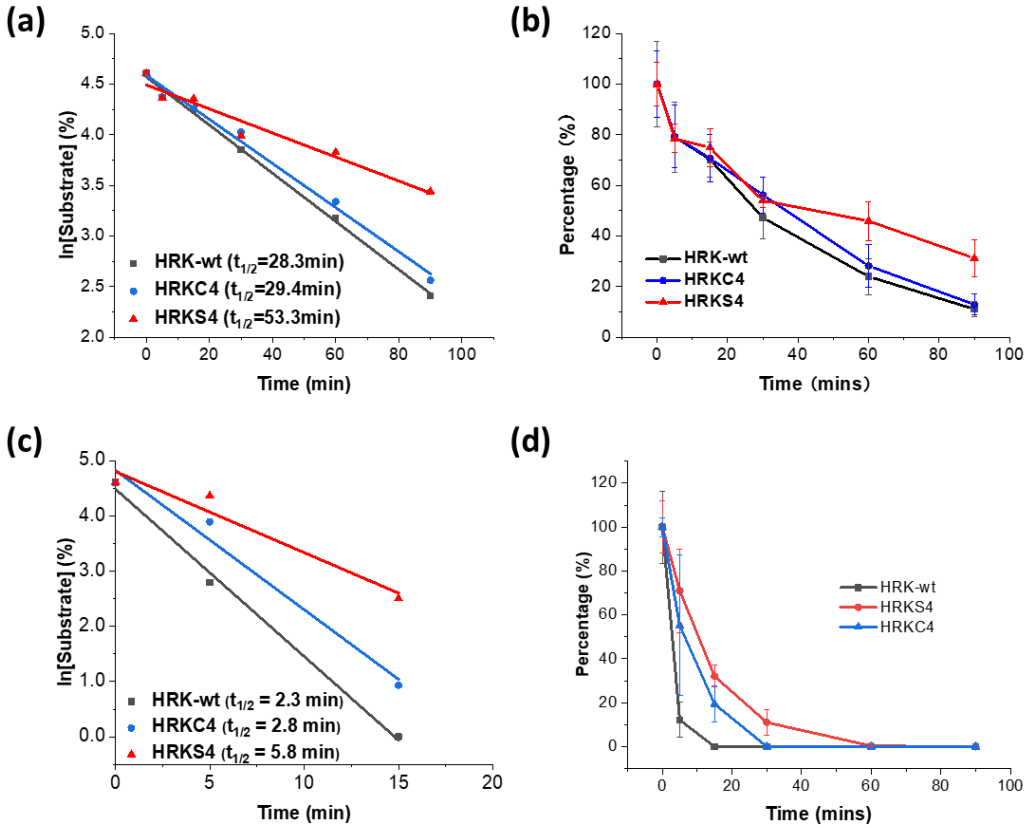

Figure 3-6 Proteolysis of HRK-wt, HRKC4 and HRKS4 using (a) (b) α-chromotrypsin (c) (d) trypsin (buffer condition: 20 mM Tris, 150 mM NaCl, pH 7.6; enzyme:peptide=1:25000); (all experiments were repeated for three times and error bars show standard deviations).

3.3.6 Attempts to generate bicyclic peptides based on the HRK BH3 sequence

In the first series of HRK constrained peptides, HRKS3 and HRKS4 showed similar-to-better potency in comparison to the wild-type, and also shared a constraining site for maleimide installation (Table 3-2). Therefore, I planned to expand the constraining area in the peptide sequence in two ways: 1) using a longer linker, 4,4'-bis(bromomethyl)-1,1'-biphenyl, to connect the two cysteine at i, i+8 positions; 2) or generating a bicyclic peptide by crosslinking three cysteines using a trifunctional linker, 1,3,5-Tris(bromomethyl)benzene. As a result, the cysteine variants, HRKBPh34 and HRKBC34, were found to have maintained or decreased potency, with 2.7± 0.1, or 16.2 ± 5.2μM, respectively (Figure 3-7, Table 3-2). Unfortunately, cyclisation of these peptides resulted in significant loss of potency, demonstrating that a direct combination of contiguous constraining sites may not be beneficial to potency, which may arise from the different conformation caused by pre-organisation (this section supports section 3.4.5.4 in Chapter 3).

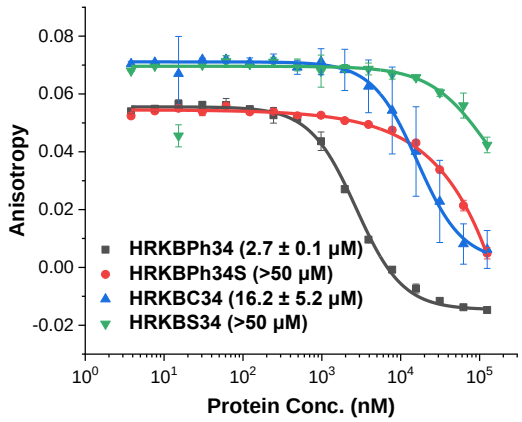

Figure 3-7 Competition FA results of HRKBPh34, HRKBPh34S, HRKBC34 and HRKBS34 (20 mM Tris, 150 mM NaCl, pH 7.6, 250 nM BCL-x_L, 50 nM tracer, 20 °C, error bars show standard deviations observed in triplicate experiments and errors are standard deviations generated in data fitting)

Table 3-2 A summary of FA competition results for the peptides derived from HRKS3 and HRKS4.

Peptide	Sequence[a]	IC_{50} HRK/BCL-x_L (μM)[b]
HRK-wt (HRK_{28-50})	SAAQLTAAR**LK**A**L**GDE**L**HQRTMW	2.2 ± 0.1
HRKC3	SAACLTACR**LK**A**L**GDE**L**HQRTMW	3.4 ± 0.3
HRKS3	 SAA**C**LTA**C**R**LK**A**L**GDE**L**HQRTMW	1.6 ± 0.1
HRKC4	SAAQLTACR**LK**C**L**GDE**L**HQRTMW	5.6 ± 0.9
HRKS4	 SAAQLTA**C**R**LK**C**L**GDE**L**HQRTMW	0.9 ± 0.1
HRKBPh34	SAACLTAAR**LK**C**L**GDE**L**HQRTMW	2.7 ± 0.1
	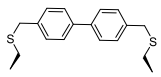 SAA**C**LTAAR**LK**C**L**GDE**L**HQRTMW	>50
HRKBC34	SAACLTACR**LK**C**L**GDE**L**HQRTMW	16.2 ± 5.2
HRKBS34	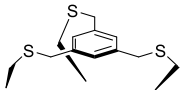 SAA**C**LTA**C**R**LK**C**L**GDE**L**HQRTMW	>50

[a]Hot-spot residues are highlighted in bold; the incorporated cysteines are underlined; the maleimide constraint crosslinking two cysteines is highlighted in red; the biphenyl constraint crosslinking two cysteines is highlighted in green; the trimethylphenyl linker crosslinking three cysteines is highlighted in pink; all peptides are N-terminally acetylated and C-terminally amidated; [b] conditions: 20 mM Tris, 150 mM NaCl, pH 7.6, 50 nM tracer, 250 nM BCL-x_L; all experiments were repeated for three times and errors are standard deviations generated in data fitting.

3.3.7 A comparison study: influence of constraint types on potency

3.3.7.1 Regarding the synthesis of Fmoc-mS5-OH

Hydrocarbon peptide stapling at *i*, *i*+4 positions using disubstituted alkenyl amino acid Fmoc-(*S*)-2-(4-pentenyl)alanine (Fmoc-S5-OH, **1**, Figure 3-8) has been widely studied.[101] Previously the Wilson group developed a new hydrocarbon stapling method using a monosubstituted alkenyl amino acid, Fmoc-(*S*)-2-(4-pentenyl)glycine (Fmoc-mS_5-OH, **2**, Figure 3-8), by which the acquired stapled peptides showed similar biophysical and biological properties in comparison to their disubstituted-amino-acid-derived counterpart.[101] In this part, the initial aim was to efficiently synthesise the monosubstituted alkenyl amino acid suitable for peptide synthesis and further peptide stapling. To this end, I planned to utilise and compare different routes to complete the synthesis of this non-natural amino acid in high yield and high enantiomeric purity.

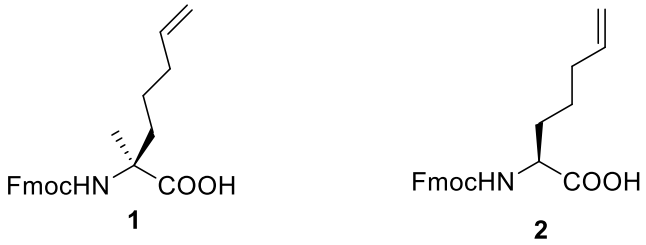

Figure 3-8 Structures of Fmoc-S5-OH (1) and Fmoc-mS5-OH (2).

To synthesise Fmoc-mS_5-OH, I firstly prepared the BPB based ligand **6** starting from L-proline *via* the synthetic route as previously reported7 In these two synthetic routes, the benzylproline **3** or fluorobenzylproline **4** generated from proline were not suitable for flash chromatography because of the free carboxylic group, which gave less pure products *via* precipitation and filtration although the calculated yields for the first step were high.

After formation of the ligands **6** or **7**, the nickel complexes **8** or **9** were synthesised as previously described7, 15 (Scheme 7-1). With the nickel complexes **7** or **8** in hand, the alkylation with 5-bromopent-1-ene was found to be successful. Thereafter, the alkylated complex **10** or **11** was disassociated by acidolysis, affording the free amino acid **12**. The crude compound was purified

using ion exchange chromatography, followed by addition of Fmoc-protecting group, giving the final product Fmoc-mS_5-OH **2**.

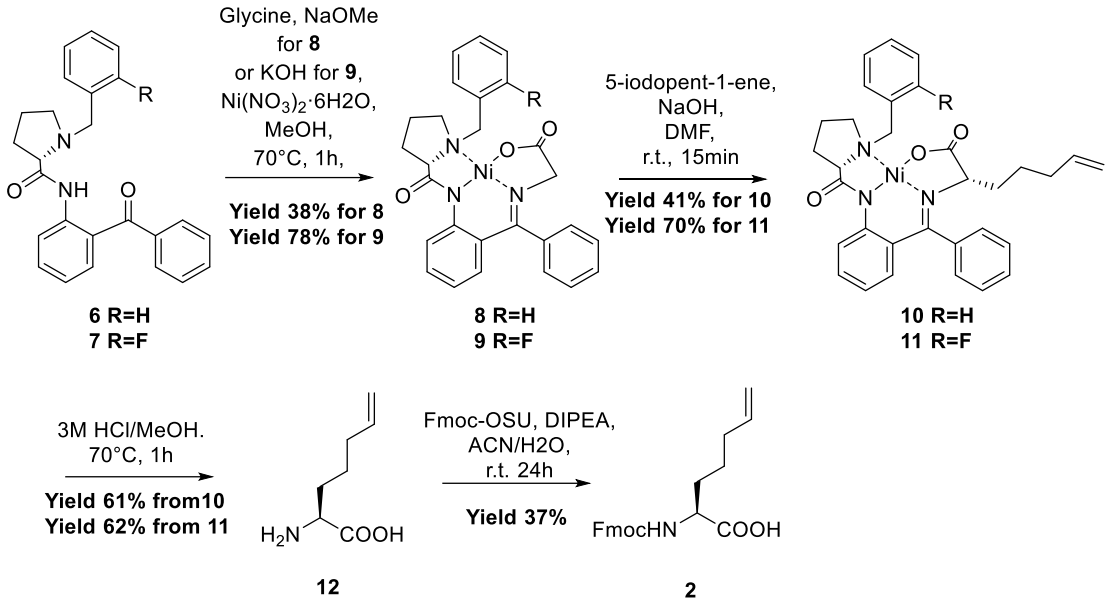

Scheme 3-1 Synthetic route of Fmoc-mS5-OH from ligand 6 or 7.

I also used the method based on (1*R*,2*R*,5*R*)-hydroxypinan-3-one to synthesise the amino acid **2** (Scheme 7-2). The desired amino acid was synthesised in four steps. Briefly, (1*R*,2*R*,5*R*)-hydroxypinan-3-one was used to synthesise Schiff base **13** which was alkylated using Lithium diisopropylamide (LDA) and 5-bromopent-1-ene or 5-iodopent-1-ene. It was found that the alkylation of the Schiff base using 5-iodopent-1-ene gave better yield than using 5-bromopent-1-ene. The alkylated Schiff base **20** was then hydrolysed using citric acid, followed by deprotection of *O*tBu using TFA and Fmoc *N*-protection, affording the desired amino acid **2** with a total yield of 30%.

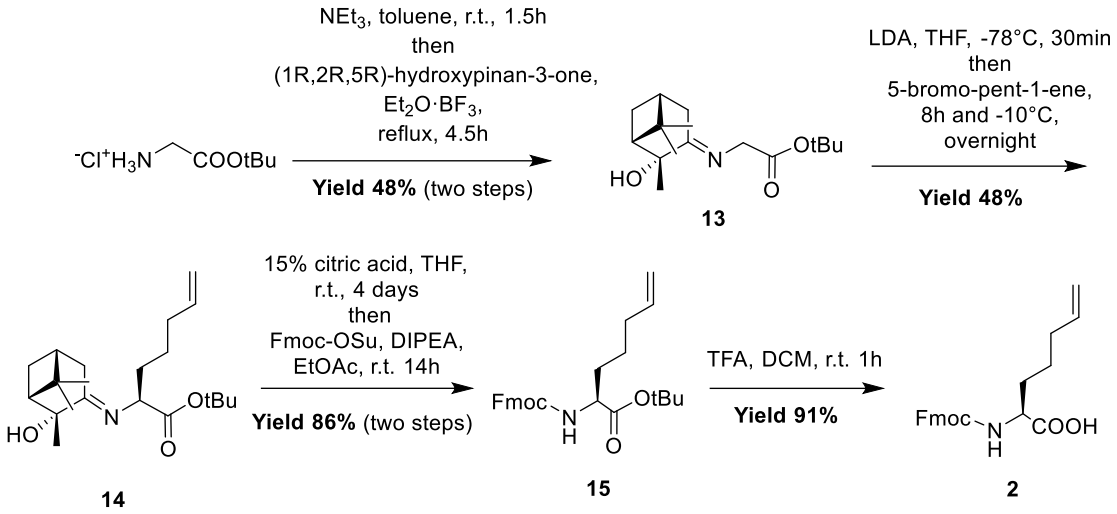

Scheme 3-2 The synthetic route of Fmoc-mS5-OH using (1R,2R,5R)-hydroxypinan-3-one

The enantiomeric purities of Fmoc-mS$_5$-OH derived from different synthetic routes were determined using a chiral HPLC. The (*R*)-configured control was synthesised based on the BPB route but using D-proline as a starting material. And the mixture of this product and Fmoc-mS5-OH final product made using the pinanone-based route were mixed and subjected to chiral HPLC analysis (Figure 3-12). Two main separate peaks were observed, indicating the racemates can be separated using the chiral HPLC. I found that the *ee* value of amino acid **2** synthesised using (*S*)-BPB-based method was 85% (Figure 3-9, Table 3-3). Unfortunately, the (*S*)-FBPB-based route gave much worse *ee* value, which was only 63% (Figure 3-10, Table 3-3). This might arise from unsuccessful alkylation or poor separation of the diastereomers. Using (1*R*,2*R*,5*R*)-hydroxypinan-3-one as an auxiliary gave the best *ee* value, 98% (Figure 3-11, Table 3-3), and higher optical activity than that of the (*S*)-BPB-derived product, suggesting a more convenient method with higher yield and better stereoselectivity. Therefore, the synthetic route based on (1*R*,2*R*,5*R*)-hydroxypinan-3-one was selected to produce the amino acid **2** for hydrocarbon stapled peptides assembly in this study.

Table 3-3 Chiral HPLC analysis and optical rotation of Fmoc-mS5-OH from different synthetic routes and Fmoc-mR5-OH

Compound	Ligand	$[\alpha]_D^{25}$(CHCl$_3$, c = 1)$^{\alpha}$	ee%$^{\beta}$
Fmoc-mS$_5$-OH	(*S*)-BPB	+3.5	85
Fmoc-mS$_5$-OH	(*S*)-FBPB	ND	63
Fmoc-mS$_5$-OH	(1*R*,2*R*,5*R*)-hydroxypinan-3-one	+5.1	97

$^{\alpha}$ND: not determined; $^{\beta}$see chiral HPLC traces.

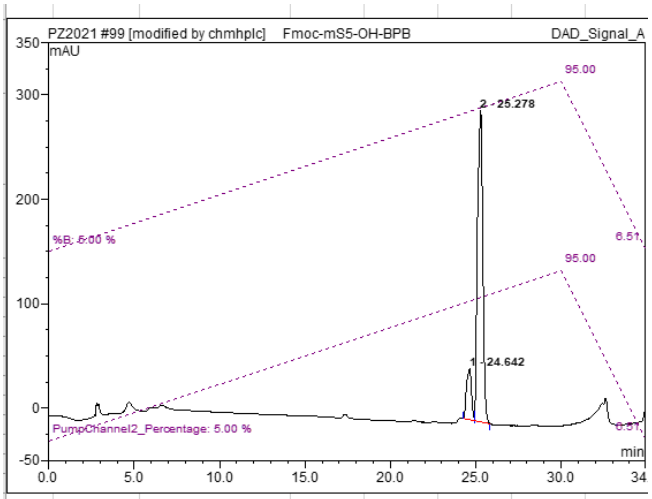

No.	Ret.Time min	Peak Name	Height mAU	Area mAU*min	Rel.Area %	Amount	Type
1	24.64	n.a.	49.026	16.138	13.09	n.a.	BM *
2	25.28	n.a.	298.096	107.176	86.91	n.a.	MB*
Total:			347.122	123.314	100.00	0.000	

Figure 3-9 Chiral HPLC trace for Fmoc-mS5-OH synthesised by the BPB-based route

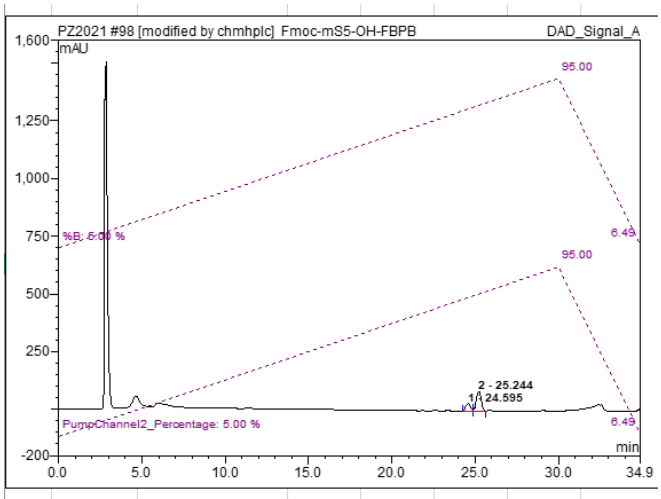

No.	Ret.Time	Peak Name	Height	Area	Rel.Area	Amount	Type
	min		mAU	mAU*min	%		
1	24.59	n.a.	31.271	10.555	27.02	n.a.	BM
2	25.24	n.a.	85.127	28.503	72.98	n.a.	MB
Total:			116.398	39.058	100.00	0.000	

Figure 3-10 Chiral HPLC trace for Fmoc-mS5-OH synthesised by the FBPB-based route

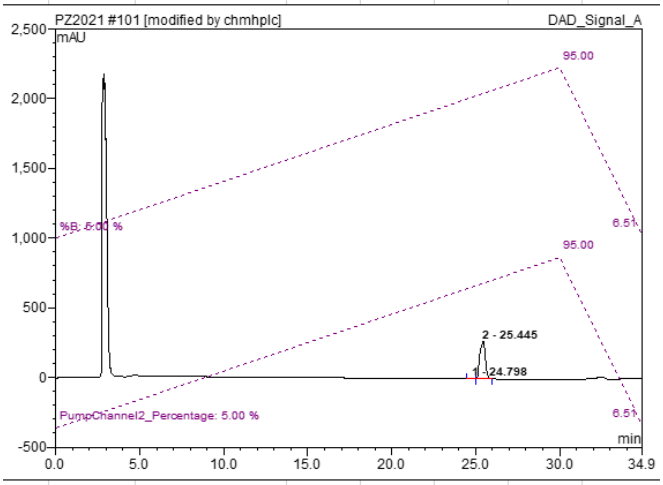

No.	Ret.Time	Peak Name	Height	Area	Rel.Area	Amount	Type
	min		mAU	mAU*min	%		
1	24.80	n.a.	5.234	1.692	1.64	n.a.	BMB*
2	25.45	n.a.	271.031	101.305	98.36	n.a.	BMB
Total:			276.265	102.997	100.00	0.000	

Figure 3-11 Chiral HPLC trace for Fmoc-mS5-OH synthesised using (1R,2R,5R)-hydroxypinan-3-one

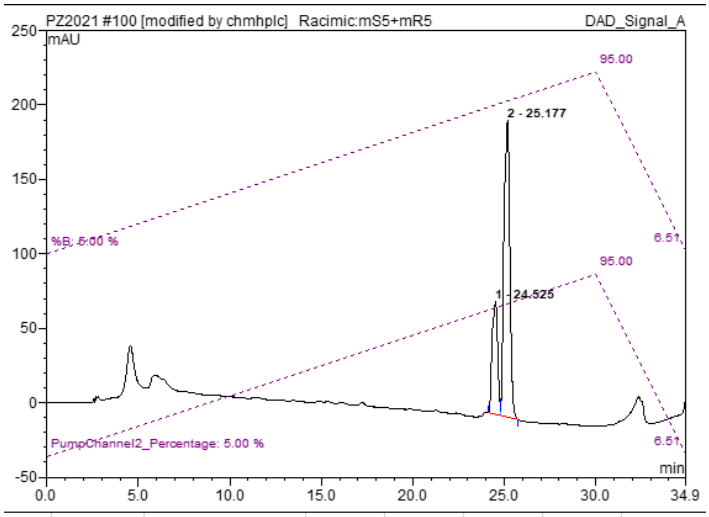

No.	Ret.Time min	Peak Name	Height mAU	Area mAU*min	Rel.Area %	Amount	Type
1	24.53	n.a.	75.779	26.483	26.33	n.a.	BM
2	25.18	n.a.	199.197	74.093	73.67	n.a.	MB
Total:			274.975	100.575	100.00	0.000	

Figure 3-12 HPLC trace for mixture of Fmoc-mS5-OH synthesised by pinanone-based route with the product synthesised from D-Proline using BPB-based method

3.3.7.2 FA competition assays

So far, various synthetic linkages have been developed, e.g. lactam bridges, hydrocarbon bridges, triazoles and xylene, amongst which hydrocarbon stapling has been widely used for its significant effects on improvements of helicity, proteolytic stability and cell-permeability.[81, 240, 250] Based on the constraining using dibromomaleimide, the Wilson group previously studied the influence of different combinations of cysteine and homocysteine on *i*, *i*+4 maleimide stapling and found that the *i* (Cys), *i*+4 (hCys) is optimal to improve helicity in solution.[251] In this study, I selected different combinations of cysteine/homocysteine or a pair of D-configured cysteines for maleimide constraint and different types of constraints[132] to replace the original constraint in HRKS4, and tested the resultant variants in FA assays for comparison. For hydrocarbon stapling, a monosubstituted alkenyl amino acid, 2-(4'-pentenyl)glycine,[101,238] was used for peptide synthesis instead of the commonly used disubstituted building block, 2-(4'-pentenyl)alanine.[100] The Wilson group previously demonstrated that this monosubstituted non-native amino acid can be used as an alternative building peptide assembly (for synthesis see: section 3.3.7.1). Herein, a pair of 2-(4'-pentenyl)glycine (mS5) were used to replace the cysteines in HRKC4 and further crosslinked using a ring-

closing metathesis (RCM) reaction. All peptides were synthesised using standard Fmoc-based chemistry and purified using prep-HPLC for further study (purity > 90%). Both linear and constrained variants were tested in the FA assays.

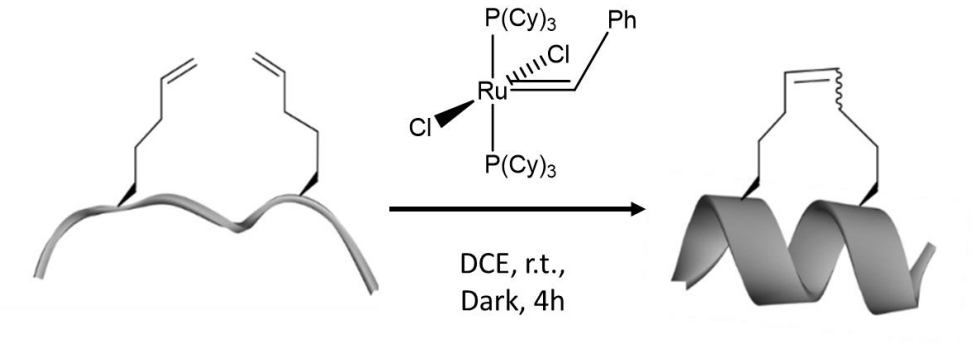

Figure 3-13 Synthesis of hydrocarbon stapled peptides containing mS5 residues via an RCM reaction.

As a result, neither the xylene nor hydrocarbon stapled peptides showed enhanced potency in comparison to the maleimide constrained peptide, HRKS4 (Table 3-4). Using the optimal combination of Cys/hCys, HRKS4-ChC showed tolerated potency, with an IC_{50} of 0.8 (±0.1) μM. Using a pair of homocysteines instead of a pair of cysteines gave an IC_{50} of 1.9 (±0.2) μM, which is similar to that observed with hydrocarbon stapling. However, using the maleimide constrained peptide, HRKS4-DCys, with the constraint generated from a pair of $_D$-cysteines, showed dramatically decreased potency, indicating the important role of the absolute configuration of anchoring residues for stapling. Combining the results together, the peptides containing relatively rigid constraints (HRKS4, HRKS4-ChC, HRKS4-xylene) showed slightly stronger potency than the constrained peptides with relatively flexible constraints (HRKS4-hCys, HRKS4-hydrocarbon), suggesting that installation of a relatively rigid constraint at the identified position is more favourable for BCL-x_L binding.

In summary, compared with other constraints, the maleimide constraint showed similar-to-better ability to improve the potency of the HRK-based peptides towards BCL-x_L.

Table 3-4 FA results of HRKS4 variants with different staples[a]

SAAQLTA**X_1**R**LK**X_2**L**GDE**L**HQRTMW**

Peptide	Staple	X_1	X_2	IC_{50} HRK/BCL-x_L (μM)[b]
HRK-wt	None	Ala	Ala	2.2 ± 0.1
HRKC4	None	Cys	Cys	5.6 ± 0.9
HRKS4	Maleimide	Cys	Cys	0.9 ± 0.1
HRKS4-xylene	*m*-Xylene	Cys	Cys	1.2 ± 0.1
HRKC4-DCys	None	D-Cys	D-Cys	21.4 ± 2.7
HRKS4-DCys	Maleimide	D-Cys	D-Cys	16.5 ± 1.4
HRKC4-ChC	None	Cys	hCys	2.9 ± 0.1
HRKS4-ChC	Maleimide	Cys	hCys	0.8 ± 0.1
HRKC4-hCys	None	hCys	hCys	2.6 ± 0.3
HRKS4-hCys	Maleimide	hCys	hCys	1.9 ± 0.2
HRKL4-hydrocarbon	Unstapled	mS5	mS5	1.8 ± 0.3
HRKS4-hydrocarbon	hydrocarbon	mS5	mS5	1.7 ± 0.1

[a]Hot-spot residues are highlighted in bold; all peptides are N-terminal acetylated and C-terminal amidated; the residues participating in the formation of constraints are referred to as X_1 and X_2, and highlighted in red; mS5 denotes 2-(4'-pentenyl)-glycine; [b] conditions: 20 mM Tris, 150 mM NaCl, pH 7.6, 50 nM tracer, 250 nM BCL-x_L.

3.3.8 Inhibition of MCL-1 using HRK-derived peptides

The anti-apoptotic BCL-2 member, Myeloid cell leukaemia-1 (MCL-1),[252] is overexpressed in a number of cancers and provides a mechanism for drug resistance in response to BCL-2 inhibition.[253] Prior studies classified the HRK BH3 domain as BCL-x_L selective.[254,255] To assess the selectivity of HRK constrained peptides I thus tested the selectivity using MCL-1 and an appropriate MCL-1 binding BH3 ligand –MCL-1 ubiquitin ligase E3 (MULE). Surprisingly, the 23-mer HRK tracer was found to have a K_d of 66 (±3) nM, which is comparable with that of the 23-mer MULE tracer (57 (±9) μM) (Figure 3-14 (a) (b)) whereas the MULE tracer didn't show significant binding for the BCL-x_L in the direct titration assay (Figure 3-14 (c)). These results showed that the 23-mer HRK sequence had a comparable K_d to the equally long sequence derived from the MULE BH3 domain.

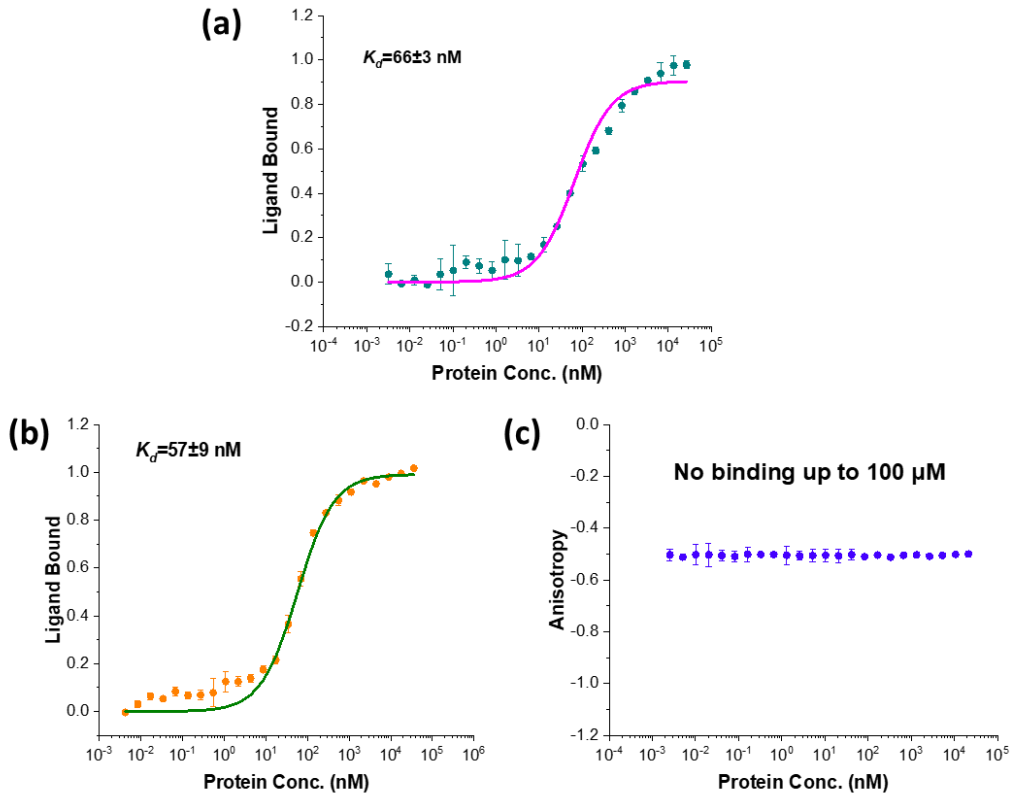

Figure 3-14 Direct FA titration results for HRK and MULE tracers; (a) Direct titration of FAM-Ahx-HRK with MCL-1 (FAM-Ahx-HRK (50 nM) MCL-1 (6 nM-125 μM) 20mM Tris, 150 mM NaCl, pH 7.6, 20 °C; (b) Direct titration of FAM-Ahx-MULE with MCL-1 (FAM-Ahx-MULE (50nM) MCL-1 (6 nM-125 μM) 20 mM Tris, 150 mM NaCl, pH 7.6, 20 °C); (c) Direct titration of FAM-Ahx-MULE with BCL-x_L (FAM-Ahx-MULE (50 nM) BCL-x_L (6 nM-125 μM) 20 mM Tris, 150 mM NaCl, pH 7.6, 20 °C).

Next, I tested the potency of HRK-wt, HRKC4 and HRKS4 against MCL-1 using either the HRK tracer or the MULE tracer in the FA assays (Figure 3-15). The further competition FA assays showed that HRK-based peptides were able to displace different tracers from MCL-1 and that the maleimide constraint plays a positive role in enhancing the potency for the inhibition of the BCL-x_L and MCL-1. HRK-wt showed an IC_{50} of 2.7 (±0.3) μM against HRK/MCL-1 whereas it showed an IC_{50} of 28.4 (±1.9) μM, which is 1.5-fold weaker than that of MULE-wt against MULE/MCL-1. Although the cysteine variant, HRKC4, showed reduced potency for both HRK/MCL-1 (3.9 (±0.2 μM)) and MULE-MCL-1 (>30 μM), the maleimide constraint was shown to improve the potency for inhibition of both interactions. Compared with HRK-wt, HRKS4 showed maintained potency against HRK/MCL-1 (2.0 (±0.2 μM)); but also enhanced potency against MULE/MCL-1 (14.3 (±1.1 μM)), which is comparable to that of MULE-wt (11.4 (±1.7 μM)).

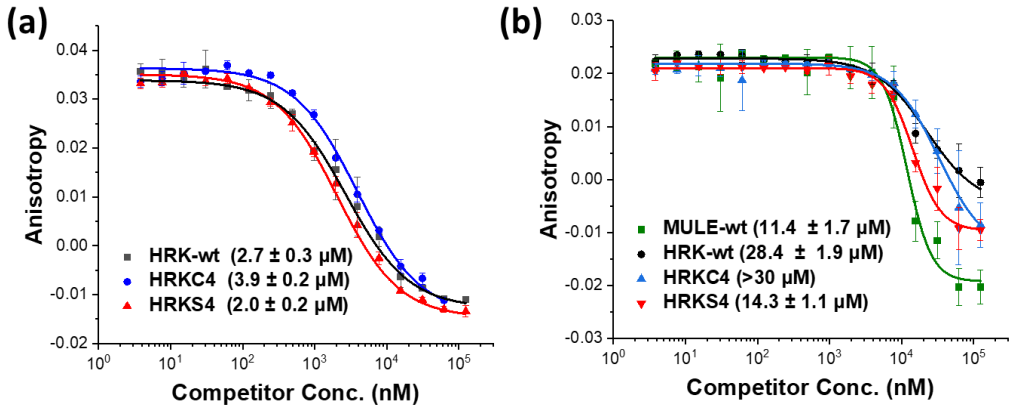

Figure 3-15 Competition FA results for MULE-wt, HRK-wt, HRKC4 and HRKS4 using (a) the HRK tracer (20 mM Tris, 150 mM NaCl, pH 7.6, 250 nM BCL-x_L, 50 nM FAM-Ahx-HRK); (b) the MULE tracer (20 mM Tris, 150 mM NaCl, pH 7.6, 200 nM MCL-1, 50 nM FAM-Ahx-MULE.

3.4 Sequence truncation and hybridisation to generate more selective BCL-x_L peptidomimetic inhibitors.

3.4.1 *In silico* modelling and peptide design

In order to inform peptide design to improve selectivity for BCL-x_L over MCL-1, a number of structures of complexes between BH3 peptides and BCL-x_L or MCL-1 were selected and subjected to BAlaS, including the BID/BCL-x_L (PDB ID: 4QVE), BID/MCL-1 (PDB ID: 2KBW), NOXAB/MCL-1 (PDB ID: 2JM6), MULE/MCL-1 (PDB ID: 2KBW), and Beclin-1/BCL-x_L (PDB ID:2PON). In addition, a homology model of HRK/MCL-1 was generated by replacing the BID BH3 ligand in BID/MCL-1 (PDN ID: 5C6H) with the HRK peptide. The additional BAlaS analyses indicated that C-terminal residues play more important roles in the interactions between BH3 ligands and MCL-1, whereas they showed less important roles in the interactions with BCL-x_L (Table 3-5).

Table 3-5 A summary of BAlaS analyses of the PPIs.

Peptide	Sequence[a]
	h1 h2 h3 h4
BID (with BCL-x_L)	ESQEDIIRNIARHLAQVGDSMDRSIPPG
BID (with MCL-1)	ESQEDIIRNIARHLAQVGDSMDRSIPPGLV
HRK (with BCL-x_L)	SAAQLTAARLKALGDELHQRTMW
HRK (with MCL-1)	SAAQLTAARLKALGDELHQRTMW
BAD (with BCL-x_L)	NLWAAQRYGRELRRMSDEFVDSFKK
MULE (with MCL-1)	PGVMTQEVGQLLQDMGDDVYQQYRS
NOXAB (with MCL-1)	PADLKDECAQLRRIGDKVNLRQKLLNM
Beclin-1(with BCL-x_L)	GTMENLSRRLKVTGDLFDIMS

[a]Hot-spot residues are highlighted in red (with BCL-x_L) and blue (with MCL-1); all conserved h1-4 residues and the conserved Asp residue are underlined.

For instance, in BID/BCL-x_L interaction, only residue Asp98 at h4+1 position was identified as a hot spot among the residues close to the C-terminus; whilst three residues, including Arg99 (h4+2), Ile101 (h4+4), and Leu105 (h4+8) were

identified as hot-spot residues at the C-terminus involved in the interaction of BID/MCL-1 (Figure 3-16 (a)). Similarly, using the homology models of HRK/BCL-x_L and HRK/MCL-1, Met49 at h4+5 position was predicted to be a hot-spot residue in HRK/MCL-1 although it was not predicted to have a significant decrease in ΔΔG in HRK/BCL-x_L. Additionally, Thr48 (h4+4) was calculated to have a negative ΔΔG in the HRK/BCL-x_L model generated from BID/MCL-1 (PDB ID:2KBW, Figure 3-16 (b)), suggesting a negative role of this polar Thr residue in the interaction.

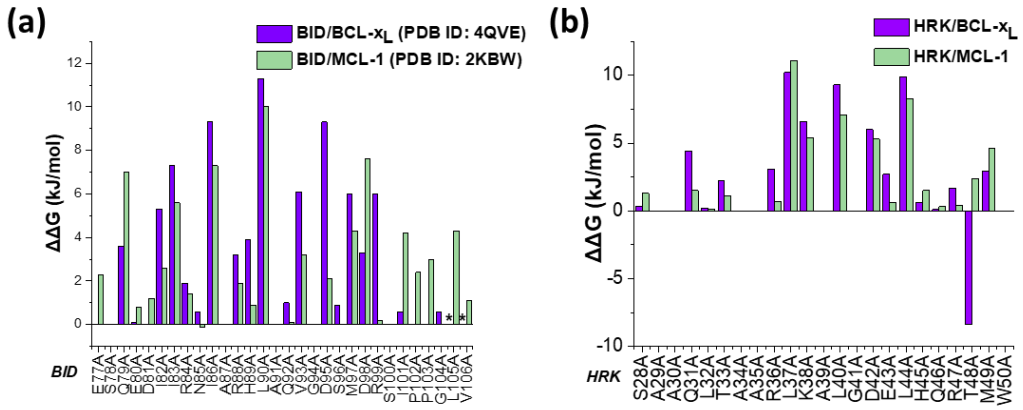

Figure 3-16 BAlaS modelling results for additional structures and homology models (a) BID/BCL-x_L (PDB ID:4QVE) and BID/MCL-1 (PDB ID: 2KBW); (b) HRK/BCL-x_L and HRK/MCL-1 (homology models).

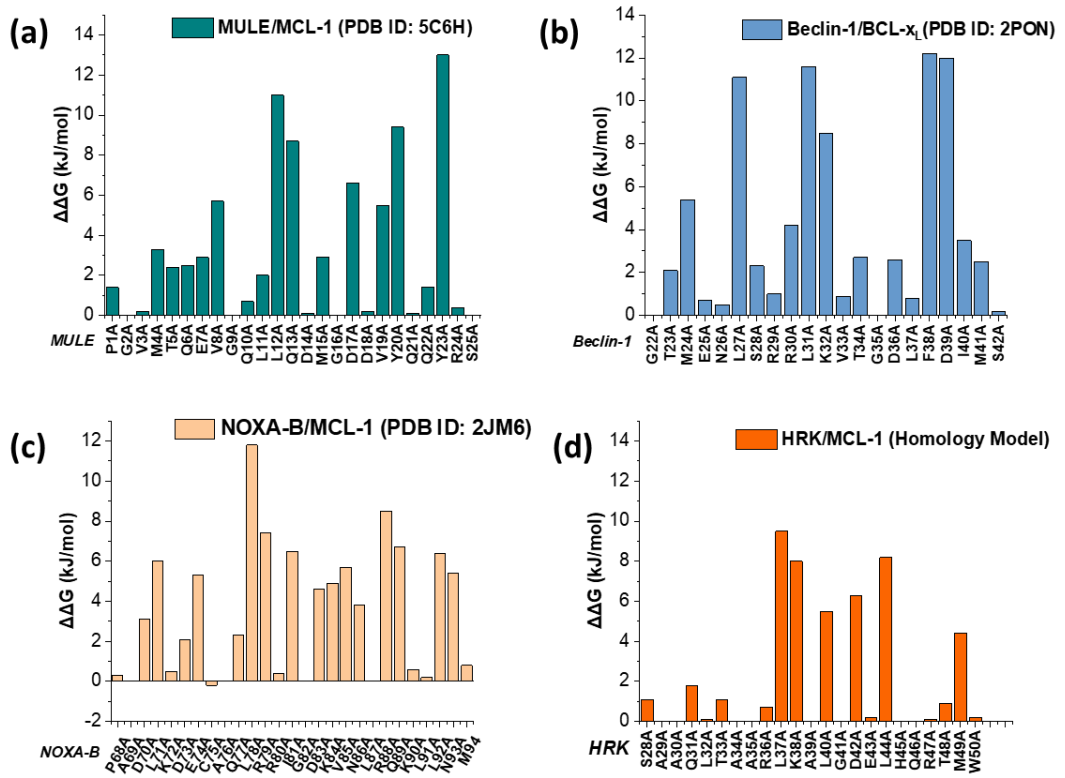

Figure 3-17 BAlaS modelling results for additional structures and a homology model (a) MULE/MCL-1 (PDB ID:5C6H); (b) Beclin-1/BCL-x_L (PDB ID: 2PON); (c) NOXA-B/MCL-1 (PDB ID:2JM6); (d) HRK/MCL-1 (homology model generated from MULE/MCL-1 (PDB ID:5C6H)).

BAlaS analyses using other structures gave similar results. Tyr20 (h4+1) and Tyr23 (h4+4) were identified as hot spot residues in MULE/MCL-1(PDB ID:5C6H, Figure 3-17 (a)). In Beclin-1, Leu2y at the h1 position was identified as a hot spot residue for interacting with BCL-x_L whilst the The24 at the h3 position was not (Figure 3-17 (b)); the C-terminal region of this peptide was shorter than others. In NOXA-B, several residues close to the C-terminus were predicted to have significant ΔΔG, including Arg88 (h4+3), Gln89 (h4+4), Leu92 (h4+7) and Asn93 (h4+8) (Figure 3-17 (c)). An additional HRK/MCL-1 model, generated from HRK and MULE/MCL-1 (PDB ID:5C6H), further verified the positive role of Met49 (h4+5) in this interaction (Figure 3-17 (d)).

3.4.2 FA competition assays for the short peptides

In terms of the BAlaS analyses, a series of C-terminal residues in BH3 ligands were identified as being productive for binding to MCL-1 but not BCL-x_L. Previous studies also demonstrated that a shorter (21-mer) HRK sequence exhibits selectivity for BCL-x_L although weaker potency than

other BH3-only sequences.[255] Therefore, I created a shorter (19-mer) peptide, termed HRK-s. This shorter peptide indeed showed reduced potency against BCL-x_L (21.7 ±7.7 μM) but improved selectivity (Figure 3-19). BH3-only sequences typically contain 4 important hydrophobic residues that are usually hot-spots, denoted as h1, h2, h3 and h4.[239,250] By comparing the sequences of BAD-wt and HRK-wt, I found that each sequence has three hot-spots among the four important hydrophobic positions (Table 3-6). In BAD-wt, h1-Tyr, h2-Leu and h4-Phe identify as hot spots whereas h3-Met was not identified by the virtual alanine scan. In the HRK-wt sequence, h1-Thr was not identified as a hot-spot residue whereas h2-Leu, h3-Leu and h4-Leu were. A further BH3 ligand, Beclin-1-wt, gave similar insight (Table 3-6). An FA direct titration assay was performed for validation of the Beclin-1/BCL-x_L interaction (Figure 3-18); a weaker binding was observed, which may arise from the polar h3-Thr residue (also h3-Thr was not identified as a hot-spot residue, Table 3-6, Figure 3-17 (b)). I hypothesised that replacing HRK-wt residues with hot-spots from other BH3 ligands might add additional potency. Therefore, I synthesised HRK-1 and HRK-4, which alternatively contains h1Y and h1L, respectively. Furthermore, I introduced one or two phenylalanine residues, which are hot-spot residues of BAD-wt, into the short HRK sequences, generating HRK-2, HRK-3, HRK-5 and HRK-hybrid. Thereafter, I tested the designed shorter peptides using FA competition assays.

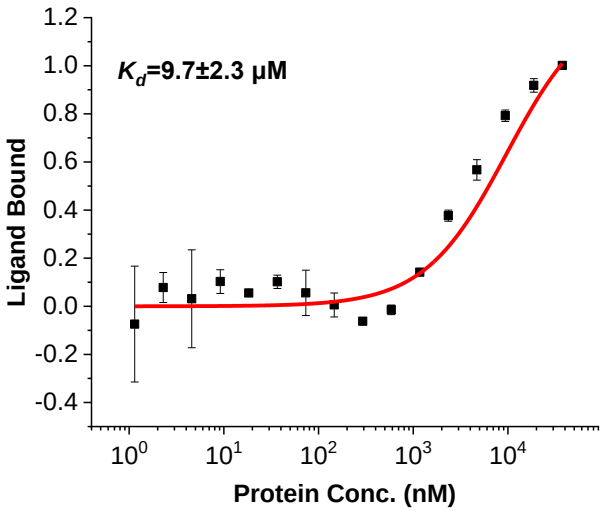

Figure 3-18 Direct FA titration of FAM-Ahx-Beclin-1 with BCL-x_L (FAM-Ahx-Beclin-1 (150 nM) BCL-x_L (6 nM-125 μM) 25 mM Tris, 150 mM NaCl, pH 7.4, 20 °C, error bars show errors observed in triplicate experiments and error numbers are standard deviations generated in data fitting).

Surprisingly, introducing one more hydrophobic hot-spot residue at the h1 position significantly improved the potency of shorter sequences (Table 3-6). 1.6-fold improvement was observed by replacing the polar h1-Thr residue with tyrosine; whilst a 14.5-fold improvement was observed after change of h1-Thr to h1-Leu (Figure 3-21 (a)). However, the Thr-to-Leu variation did not give retained selectivity (Figure 3-21, Table 3-6). Further variation using phenylalanine led to HRK-2, HRK-3, HRK-5 and HRK-hybrid. All peptides showed restored potency in comparison to HRK-wt, except HRK-3, for which the data could not be fitted. These results demonstrate that mapping and adding the missing hot-spot residues at the conserved h1-h4 positions may be beneficial to the inhibitory potency of BH3-only peptides; and suggest transposition of key hot-spot residues from other BH3 sequences may improve selectivity.

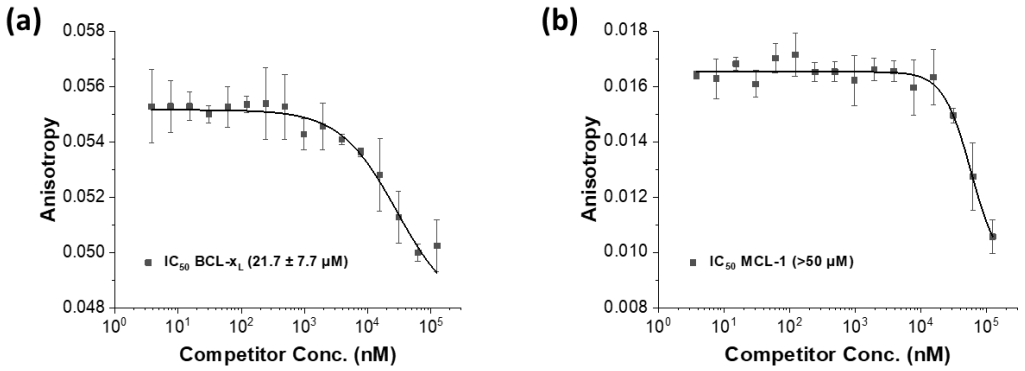

Figure 3-19 Competition FA results of HRK-s (a) for inhibition of HRK/BCL-x_L (20 mM Tris, 150 mM NaCl, pH 7.6, 250 nM BCL-x_L, 50 nM tracer, 20 °C); (b) for inhibition of HRK/MCL-1 (20 mM Tris, 150 mM NaCl, pH 7.6, 200 nM MCL-1, 50 nM tracer, 20 °C, error bars show errors observed in triplicate experiments and error numbers are standard deviations generated in data fitting).

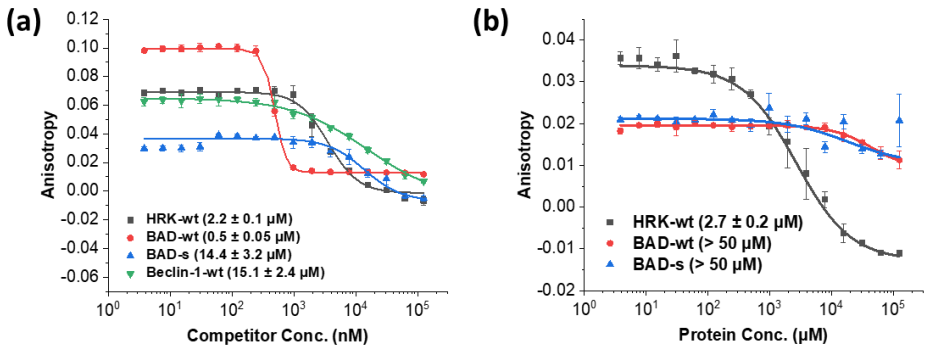

Figure 3-20 Competition FA results for BAD-wt, BAD-s, Beclin-1-wt, HRK-wt, and HRK-s for inhibition of (a) HRK/BCL-x_L (20 mM Tris, 150 mM NaCl, pH 7.6, 250 nM BCL-x_L, 50 nM tracer, 20 °C); (b) HRK/MCL-1 (20 mM Tris, 150 mM NaCl, pH 7.6, 200 nM MCL-1, 50 nM tracer, 20 °C, error bars show errors observed in triplicate experiments and error numbers are standard deviations generated in data fitting).

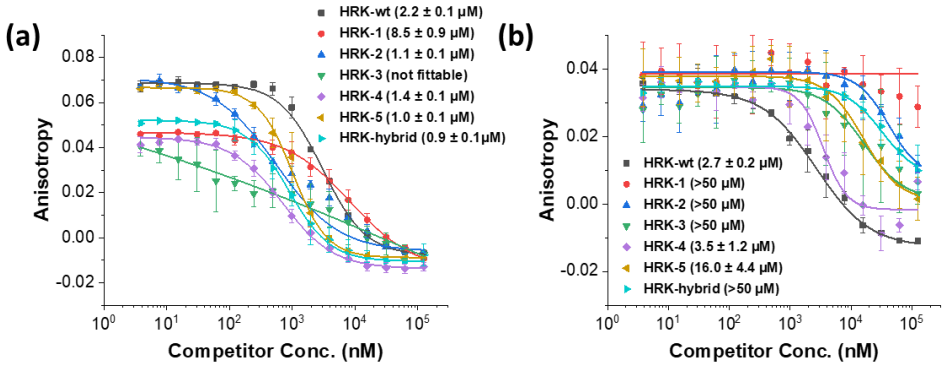

Figure 3-21 Competition FA results for HRK-1, HRK-2, HRK-3, HRK-4, and HRK-5, HRK-hybrid for inhibition of (a) HRK/BCL-x_L (20 mM Tris, 150 mM NaCl, pH 7.6, 250 nM BCL-x_L, 50 nM tracer, 20 °C); (b) HRK/MCL-1 (20 mM Tris, 150 mM NaCl, pH 7.6, 200 nM MCL-1, 50 nM tracer, 20 °C, error bars show errors observed in triplicate experiments and error numbers are standard deviations generated in data fitting).

Table 3-6 FA results for the short HRK-based peptides

Peptide	**Sequence**[a] *h1 h2 h3 h4*	IC_{50} HRK/BCL-x_L (μM)[b]	IC_{50} HRK/MCL-1 (μM)[c]	Selectivity index (IC_{50} ratio MCL-1:BCL-x_L)[d]
BAD-wt	N**L**WAAQR**Y**GRE**LR**R**M**SDE**F**VDS**F**KK	0.5 ± 0.05	>50	>96.1
BAD-s	R**Y**GRE**LR**R**M**SDE**F**VDS**F**KK	14.4 ± 3.2	>50	>3.4
Beclin-1-wt	T**M**EN**L**SRR**LK**V**T**GDL**F**DIMS	15.1 ± 2.4	ND	NA
HRK-wt	SAAQL**T**AAR**LK**A**L**GDE**L**HQRTMW	2.2 ± 0.1	2.7 ± 0.2	1.2
HRK-s	SAAQL**T**AAR**LK**A**L**GDE**L**HQ	21.7 ± 7.7	>50	>2.3
HRK-1	SAAQL**Y**AAR**LK**A**L**GDE**L**HQ	8.5 ± 0.9	>50	>5.8
HRK-2	SAAQL**Y**AAR**LK**A**L**GDE**F**HQ	1.1 ± 0.1	>50	>45.4
HRK-3	SAAQL**Y**AAR**LK**A**Z**GDE**F**HQ	NF	>50	NA
HRK-4	SAAQL**L**AAR**LK**A**L**GDE**L**HQ	1.4 ± 0.1	3.5 ± 1.2	2.5
HRK-5	SAAQL**L**AAR**LK**A**F**GDE**F**HQ	1.0 ± 0.1	16.0 ± 4.4	16.0
HRK-hybrid	SAAQL**Y**AAR**LK**A**F**GDE**F**HQ	0.9 ± 0.1	>50	>55.5

[a]Hot-spot residues are highlighted in bold; the conserved h1-h4 positions and incorporated cysteines are underlined; the maleimide constraint crosslinking two cysteines is highlighted in red; all peptides are N-terminally acetylated and C-terminally amidated; Z denotes norleucine; [b] NF: the original data could not be fitted; conditions: 20 mM Tris, 150 mM NaCl, pH 7.6, 50 nM tracer, 250 nM BCL-x_L; [c] ND: not determined; [d] NA: not applicable; all experiments were repeated for three times and error numbers are standard deviations generated in data fitting.

3.4.3 The influence of introducing a constraint on potency

From the FA competition assays for short HRK peptides, HRK-hybrid was identified as the optimal hit with high potency and selectivity. I then made a constrained peptide, HRKS4H, by transposing the identified constraint position of HRKS4 into HRK-hybrid and adding the constraint using dibromomaleimide. However, a 20-fold loss of potency resulted from the replacement of original residues with cysteines (Figure 3-22 (a)). Surprisingly, improved potency was observed after dibromomaleimide constraining, although not fully restored in comparison to HRK-hybrid. Moreover, a good selectivity was retained (Figure 3-22, Table 3-7), indicating the maleimide constraint to have a potency-enhancement effect and minimal influence on selectivity.

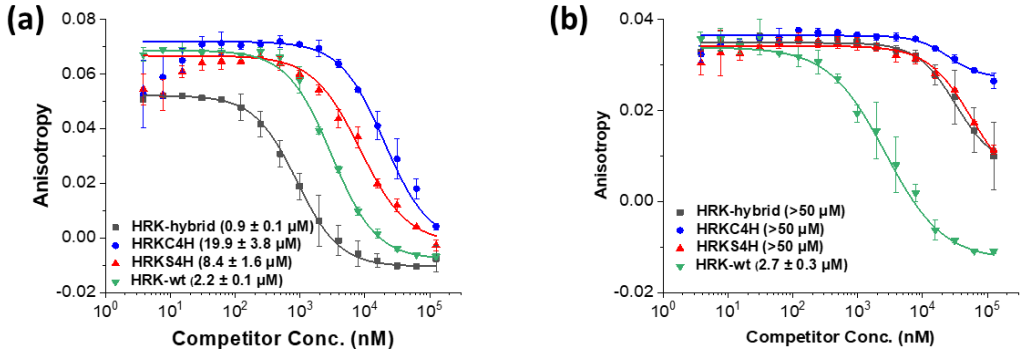

Figure 3-22 Competition FA results of HRK-wt, HRK-hybrid, HRKC4H and HRKS4H (a) for inhibition of HRK/BCL-x_L (20 mM Tris, 150 mM NaCl, pH 7.6, 250 nM BCL-x_L, 50 nM tracer, 20 °C); (b) for inhibition of HRK/MCL-1 (20 mM Tris, 150 mM NaCl, pH 7.6, 200 nM MCL-1, 50 nM tracer, 20 °C, error bars show errors observed in triplicate experiments and error numbers are standard deviations generated in data fitting).

Table 3-7 Summary of FA results for the shorter HRK-based peptides

Peptide	Sequence[a] *h1 h2 h3 h4*	IC_{50} HRK/BCL-x_L (μM)[b]	IC_{50} HRK/MCL-1 (μM)[c]	IC_{50} ratio MCL-1:BCL-x_L
HRK-wt	SAAQLTAARLKALGDELHQRTMW	2.2 ± 0.1	2.7 ± 0.2	1.2
HRK-hybrid	SAAQLYAARLKAFGDEFHQ	0.9 ± 0.1	>50	>55.5
HRKC4H	SAAQLYACRLKCFGDEFHQ	19.9 ± 3.8	>50	>2.5
HRKS4H	SAAQLYACRLKCFGDEFHQ	8.4 ± 1.6	>50	>5.9

[a]Hot-spot residues are highlighted in bold; the conserved h1-h4 positions and incorporated cysteines are underlined; the maleimide constraint crosslinking two cysteines is highlighted in red; all peptides are N-terminal acetylated and C-terminal amidated; Z denotes norleucine; [b] conditions: 20 mM Tris, 150 mM NaCl, pH 7.6, 50 nM tracer, 250 nM BCL-x_L; [c]conditions: 20 mM Tris, 150 mM NaCl, pH 7.6, 50 nM tracer, 200 nM MCL-1

3.4.4 Conclusions

In summary, using a combination of homology modelling and virtual alanine scanning, I have successfully identified the potential hot-spot residues involving in the HRK/BCL-x_L interaction. Next, I described the first constrained peptides based on the HRK-BH3 sequence; I showed that dibromomaleimide constraining scan serves as a powerful tool for rapid identification of optimal *i*, *i*+4 constraining sites. The optimal constrained peptide, HRKS4, was observed to have improved potency, enhanced helicity in comparison to the unconstrained precursor, and increased proteolytic stability. Compared with other techniques for peptide constraining, e.g. hydrocarbon and xylyl), I showed that the maleimide linker acts as an alternative constraint to construct constrained peptides with optimal potency in inhibition of HRK/BCL-x_L. The first series of HRK-peptides were observed to inhibit MCL-1 with similar potency to BCL-x_L. The poor selectivity of these peptides motivated me to further investigate more PPIs using homology modelling and virtual alanine scanning. Additional BAlaS results inspired peptide truncation and residue transposition from other BH3 ligands. Several short 19-mer peptides were identified to have good selectivity for BCL-x_L over MCL-1. HRK-hybrid, the most potent and selective candidate in this series, was selected to construct cysteine variant and constrained peptide using dibromomaleimide. The maleimide constrained peptide, HRKS4H, showed partially restored potency and well-maintained selectivity for HRK/BCL-x_L over HRK/MCL-1. These results highlight that a rational approach to peptide design can identify truncated constrained peptides and that the constraint can potentiate selectivity.

3.4.5 Future work

3.4.5.1 Constructing constrained peptides hybridisation and dibromomaleimide constraining

In this chapter, two series of peptides were designed, synthesised and characterised, including the long 23-mer peptides and the short 19-mer peptides. Sequence hybridisation was found to have a positive role in adding potency in the short sequences. However, the positive impact of sequence hybridisation on long 23-mer sequences has not been studied. In future studies, I would make 23-mer HRK peptides by combining dibromomaleimide constraining and residue transposition, in order to optimise both potency and selectivity for the long HRK sequence.

3.4.5.2 Crystallography for the HRK/BCL-x_L and HRK/MCL-1 structures

So far, the structures of HRK with human BCL-2 family members have been less well-studied. In this chapter I have shown that HRK BH3 sequences are potent binders for BCL-x_L. Solving a crystal structure between HRK and BCL-x_L would be helpful to understand the recognition mode of the PPI. In future studies, I would screen crystallising conditions for HRK/BCL-x_L and HRK/MCL-1 and further solve crystal structures for the complexes.

3.4.5.3 Screening peptide-small-molecule hybrids using dynamic ligand exchange

The short HRK-s sequence was shown to have improved selectivity but reduced potency. The Wilson group described a general method to rapidly screen peptide-small-molecule conjugates as PPI inhibitors using dynamic arylhydrazone exchange and fluorescent anisotropy.[256] In the future, I would apply this method on the HRK short sequence, in order to discover hybrid molecules with enhanced potency and selectivity.

3.4.5.4 Sulfonium-tethered bicyclic prodrug peptides

I have shown that bicyclic peptides would not have retained potency towards BCL-x_L. Bicyclic peptides could have more advantageous properties like enhanced proteolytic stability and cell-permeability.[257,99] Li and co-workers reported a peptide stapling method which involves cysteine (*i*) and methionine (*i*+4).[258] The generated sulfonium bridge could be attacked by other nucleophiles, thus could be applied for protein labelling. Herein, a bicyclic peptide with prodrug-like property could be generated using methionine instead of one cysteine among the three in the peptide HRKBC4 (see section 3.3.6), and the trifunctional linker (Figure 3-23). The peptide is expected to have high proteolytic stability, better cell-permeability and less off-target effect due to no direct inhibition for BCL-x_L. The average concentration of glutathione in cancer cells is higher and can cause dissociation of maleimide constraints.[134] In cellular assays, the bicyclic peptide is expected to restore the bioactive conformation in reducing cytosolic environment, thus inhibiting anti-apoptotic proteins and promoting further apoptosis.

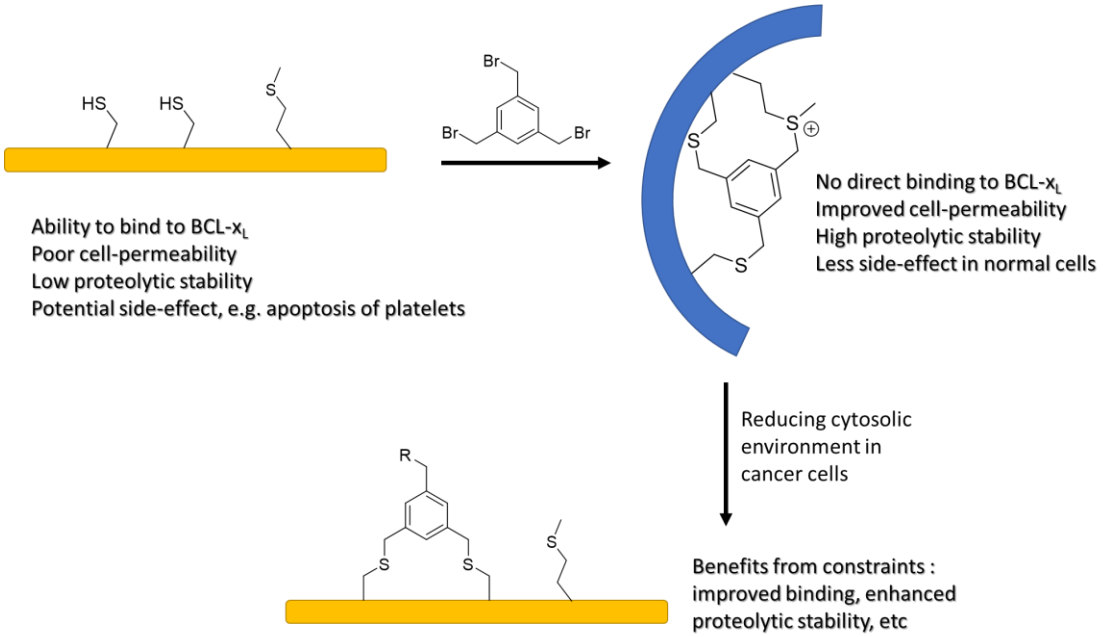

Figure 3-23 Proposed sulfonium-tethered bicyclic peptides with pro-drug-like properties (R=reducing reagent).

3.4.5.5 Cell-based studies

As mentioned above, I would like to know how the peptides behave in cellular assays and if the peptides would have effect on apoptosis of platelets. Subsequent studies would focus on testing the peptides on cells.

Chapter 4 Coiled coils to disrupt the BAD/BCL-x_L interaction

4.1 Chapter Aims

In previous studies, coiled coils were developed for binding to *h*DM2[213] and MCL-1.[197] Grafting hot-spot residues of a native ligand onto a well-defined coiled-coil template shows promise for developing PPI inhibitors; coiled coils could be used to recognise multiple targets given the availability of two or more recognition faces to induce event-driven pharmacology, e.g. PROTAC.[193] Briefly, the typical repeat sequences spanning 7 residues are termed heptad repeat (HR), denoted $(abcdefg)_n$. Residues at *a* and *d* positions are usually hydrophobic and play important roles in switching the oligomeric states of coiled coils: a-Ile and d-Leu lead to dimers; *a*, *d*-Ile lead to trimers; *a*-Leu and *d*-Ile lead to tetramers (see section 1.6.1 for the introduction of coiled coils).[193]

So far, coiled coils targeting other BCL-2 family members, e.g. BCL-x_L, have not been described. The main aim of this chapter was to apply coiled-coil templates to construct BCL-x_L inhibitors by grafting hot-spot residues from its ligands, e.g. BAD, HRK and BID (Figure 4-1), and further improve or modulate the selectivity. To do this, both rational design and computational modelling were employed; alongside biophysical characterisation will be performed to investigate the structure-activity relationship (SAR) and validate the coiled coil design.

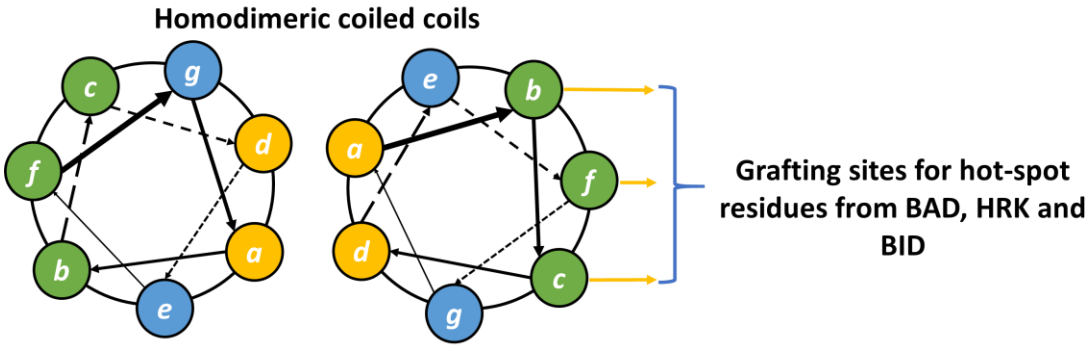

Figure 4-1 A diagram for grafting strategy to construct homodimeric coiled coils as BCL-x_L inhibitors.

4.2 ISAMBARD Modelling and Peptide Design

The *de novo* designed dimer, CC-Di (PDB: 4DZM), was selected as a template for grafting hot-spots due to its well-defined structure and success in designing MCL-1 inhibitors.[197] The Woolfson group developed an open-source

computational tool, ISAMBARD, for parametric modelling and design of biomolecules.[259] This tool allows scientists to generate models without experimentally determined structures. Based on CC-Di, I performed an *in silico* systemic evaluation of variations using ISAMBARD, [259] in order to clarify the influence on replacement of each residue in the sequence to other native amino acids. Each residue was replaced by the other 19 native amino acids individually in each variation. The structures were repacked by SCWRL4.[260] The total energy and steric contribution of each sequence variation were obtained using the BUDE[261] empirical free energy forcefield in ISAMBARD (for python scripts see appendix).

Our modelling provided a heatmap for grafting residues onto the template (Figure 4-2). For example, replacement of most residues with proline caused an increase of total energy with a high steric contribution, which is unfavourable. Variation of the 16 residues (Gly1-Glu16) close to the N-terminus didn't change the total energy significantly. However, variation of Ala4*b*, Ala4*c* and Ala5*b* resulted in dramatic steric clashes, suggesting that these positions are not suitable for grafting other amino acids although they are located at positions *b* or *c* which faced away from the coiled coil dimerisation interface and are usually considered as ideal grafting points.

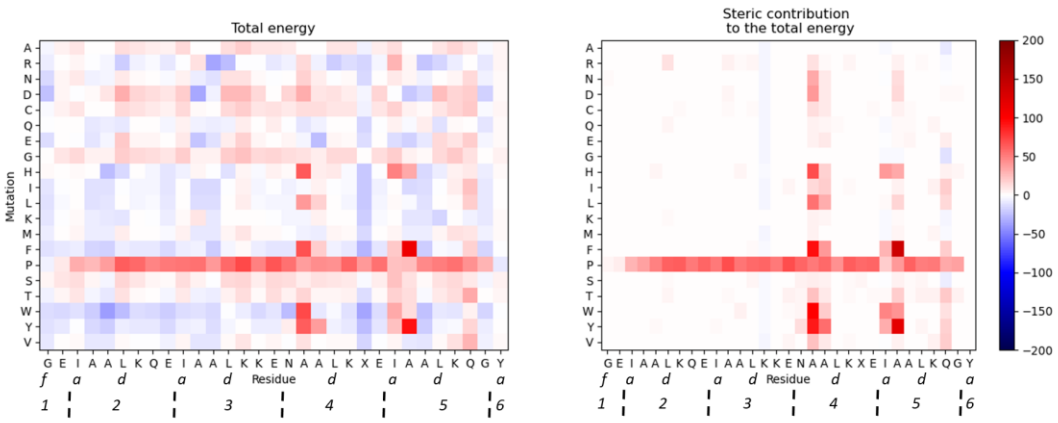

Figure 4-2 Normalised BUDE scores with total energy (BUDE points, left) and extracted steric component (right) in ISAMBARD for saturation variation based on CC-Di.

Thereafter, based on the virtual alanine scan results for the HRK/BCL-x_L (homology model) and BAD/BCL-x_L (PDB ID:1G5J) interactions (see section 3.3.1, chapter 3), I designed 5 peptides by grafting hot-spot residues from both sequences. CC-Di-BAD was designed by inserting hot-spot residues from the BAD/BCL-x_L interaction. All hot-spot residues, including Leu103, Tyr110, Leu114, Arg115, Phe121 and Phe125, were grafted at 2*f*, 3*e*, 4*b*, 4*c*, 5*b* and 5*f*. However, in terms of the ISAMBARD modelling results, substitutions of Ala4*b* with Leu and Ala5*b* with Phe were expected to cause an increase of total energy and steric clashes. In the BID BH3 domain, the position is occupied by a Met residue, which is more tolerable in the variation. Therefore, this Met residues was introduced for further coiled coil design. A number of hot-spot residues from the sequences of BAD, HRK and BID, were introduced onto the grafted positions in the previously reported coiled coil, CC-Di-S, generating CC-Di-HRK1 (Table 4-1). In CC-Di-HRK1, Leu3*b* and Arg3*c* were retained as these residues were also identified as hot-spot residues for the BAD/BCL-x_L interaction. Ile3*e* was replaced by Leu, which was identified as a hot-spot residue for the HRK/BCL-x_L interaction. More binding features from CC-Di-E2 were introduced into CC-Di-HRK2, in order to generate a binder that could bind to both BCL-x_L and MCL-1. One or two additional hot-spot residues of BAD were introduced based on CC-Di-HRK1, leading to CC-Di-HRK3 (Q4*f*F) and CC-Di-HRK4 (K2*e*Y and Q4*f*F), respectively.

Table 4-1 Coiled coil design by grafting hot-spot residues

Peptide	Sequence[a]
	1 2 3 4 5 6
	f gabcdef gabcdef gabcdef gabcdef gab
$BAD_{103-127}$	NL WAAQRYG RELRRMS DEFVDSF KK
HRK_{28-50}	SAAQLTA ARLKALG DELHQRT MW
BID_{80-102}	E DIIRNIA RHLAQVG DSMDRSI W
NOXA-B_{18-44}	P ADLKDEC AQLRRIG DKVNLRQ KLLNM
CC-Di	G EIAALKQ EIAALKK ENAALKQ EIAALKQ GYG
CC-Di-S	G EIAALKQ EILRLIG DNVALKQ EIAALKQ GYG
CC-Di-E1	G EILALKQ EILRLIG DNVALKQ EILNLKQ GYG
CC-Di-E2	G KILALEQ EILRLIG DNVNLKQ EILNLKQ GYG
CC-Di-BAD	G EIAALKL EIAALYK ENLRLKQ EIFALKF GYG
CC-Di-HRK1	G EIAALKQ EILRLLG DNMALKQ EIAALKQ GYG
CC-Di-HRK2	G KILALEQ EILRLLG DNMNLKQ EILNLKQ GYG
CC-Di-HRK3	G EIAALKQ EILRLLG DNMALKF EIAALKQ GYG
CC-Di-HRK4	G EIAALYQ EILRLLG DNMALKF EIAALKQ GYG

[a]Hot-spot residues are coloured: blue for BAD, red for HRK, purple for BID and green for NOXA; positions *a* and *d* are underlined in coiled coils; three alanine residues, (Ala4*b*, Ala4*c* and Ala5*b*, which were sensitive to variation in ISAMBARD modelling) are shown in italic.

I packed all the designed peptides onto the template, CC-Di, using ISAMBARD.[259] Each sequence was modelled onto the dimeric backbone and the side chains were repacked with SCWRL4.[262] The acquired models were scored by the BUDE empirical free energy forcefield for calculation of total energy and steric clashes.[231] Meanwhile, I chose three coiled coils targeting MCL-1 as controls, including CC-Di-S, CC-Di-E1 and CC-Di-E2. As a result, CC-Di-BAD showed positively high total energy due to the replacement of Ala19 and Ala25, indicating an unfavourable structural stability for the coiled coil assembly. The other peptides, CC-Di-HRK1-4, showed negative total energy and positively low steric contribution in ISAMBARD modelling, indicating a better potential for acting as coiled-coil inhibitors targeting BCL-x_L.

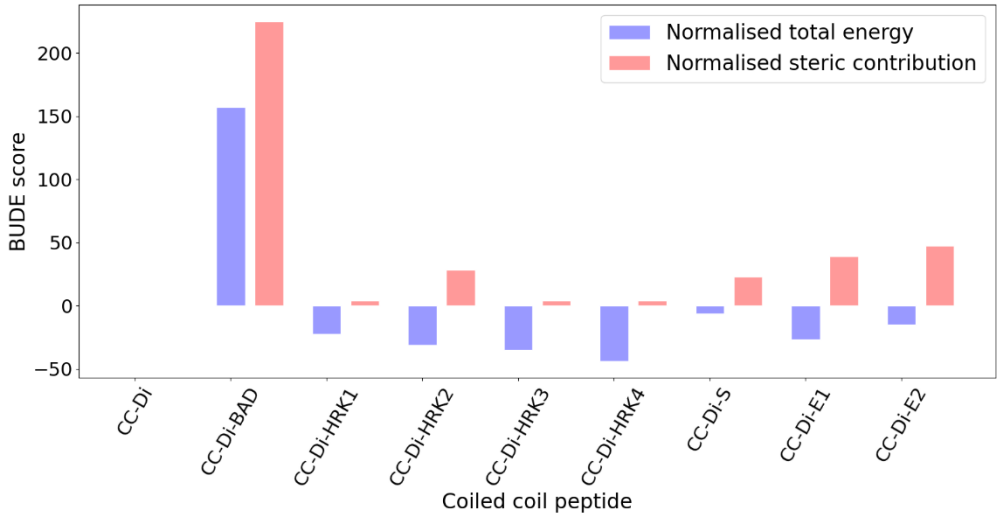

Figure 4-3 Normalised BUDE scores with total energy (BUDE points, left) and extracted steric component (right) in ISAMBARD for the designed coiled coils (for python scripts and detailed values see appendix).

4.3 FA competition assays

All coiled coil peptides were synthesised using standard Fmoc-based solid-phase peptide synthesis and purified by prep-HPLC for further study (purity>90%). All designed peptides were tested in the established competition assay using FAM-Ahx-HRK and with BCL-x_L. Several peptides showed micromolar IC_{50}s and the Q4*f*F variation was observed to improve potency (see appendix); however, the results were not well-reproducible due to the high affinity of the tracer (FAM-Ahx-SAAQLTAARLKALGDELHQRTMW, K_d= 38 ± 6 nM, see chapter 3, section 3.3.2). Therefore, I tested all peptides except CC-Di-HRK3 (as this peptide ran out temporarily) in FA competition assays using a weaker tracer, FAM-Ahx-BAD tracer (FAM-Ahx-QRYGRELRRMSDEFVDSFKK, K_d= 119 ± 23 nM, see Chapter 2, section 2.4.1). I used BID-wt as a positive control in both FA competition assays for inhibition of BID/MCL-1 or BAD/BCL-x_L (Figure 4-4, Figure 4-12). Several peptides were observed to displace the BAD tracer; however, the deviations of most peptides were high, suggesting that optimising the assay is necessary. The wild-type BID was observed to have an IC_{50} of 137.7 ± 31.8 nM for inhibition of BAD/BCL-x_L (Figure 4-4), whilst it was shown to have an IC_{50} of 6.4 ± 1.1 μM for BID/MCL-1 (Figure 4-12). CC-Di-BAD was observed to have an IC_{50} of 15.9 μM although it doesn't contain the conserved Asp residue. CC-Di-HRK1 gave an IC_{50} of 16.1 μM. However, both peptides showed high deviations, diminishing the data quality. CC-Di-HRK2 gave a similar IC_{50} for BCL-x_L with

high standard deviation for fitting (5.1 ± 6.2 μM), whilst it showed some inhibiting potency in the BID/MCL-1 assay. Considering the difference of the BID-wt peptide in both assays, CC-Di-HRK2 could be deduced to have considerable binding to both BCL-x_L and MCL-1. However, the hook effect at high concentration for CC-Di-HRK2 indicated a tendency towards aggregation at high concentration. Another peptide, CC-Di-HRK4, gave a similar IC_{50} (15.7 ± 6.6 μM), with a reasonable fitting error. These peptides showed micromolar potency but also exhibited tendency to aggregate at high concentration, indicating a significant potential to optimise coiled coils for better properties.

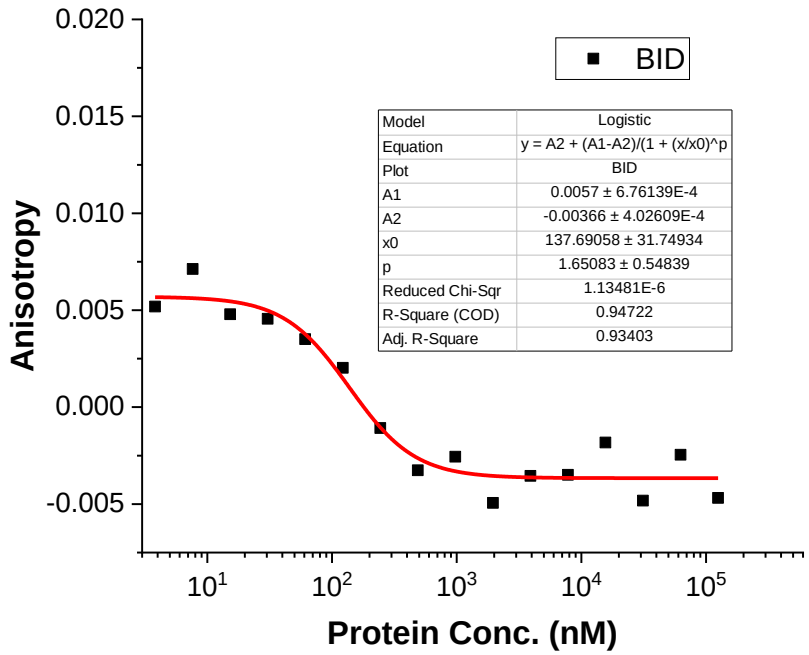

Figure 4-4 Competition FA results of BID-wt for inhibition of BAD/BCL-x_L (20 mM Tris, 150 mM NaCl, pH 7.6, 150 nM BCL-x_L, 25 nM FAM-Ahx-BAD, 20 °C, the experiment was performed without repeat and the error is a fitting error)

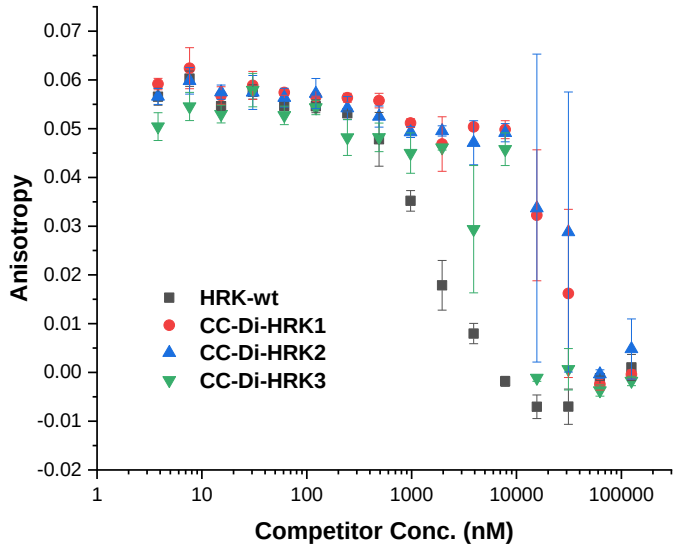

Figure 4-5 Competition FA results of HRK-wt, CC-Di-HRK1, CC-Di-HRK2, and CC-Di-HRK3 (data was not fitted as large deviations; 20 mM Tris, 150 mM NaCl, pH 7.6, 250 nM BCL-x_L, 50 nM FAM-Ahx-HRK, 20 °C, error bars show standard deviations observed in triplicate experiments)

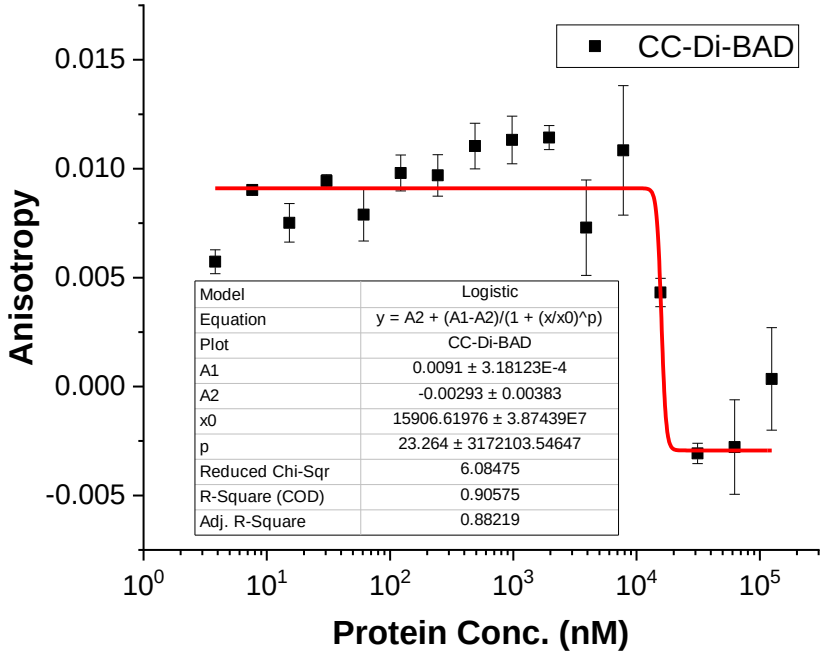

Figure 4-6 Competition FA result for CC-Di-BAD against BAD/BCL-x_L (20 mM Tris, 150 mM NaCl, pH 7.6, 25 nM FAM-Ahx-BAD, 150 nM BCL-x_L, error bars show standard deviations observed in triplicate experiments and errors are standard deviations generated in data fitting)

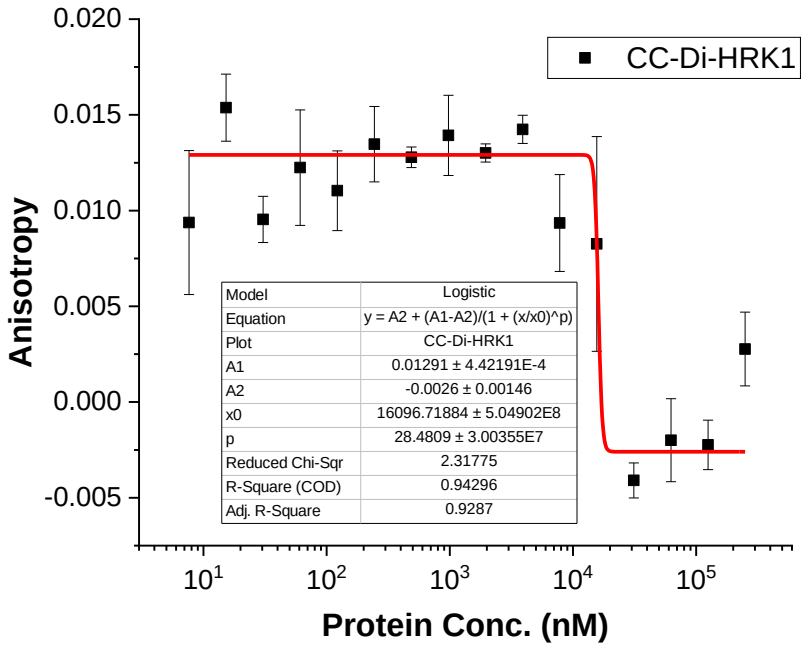

Figure 4-7 Competition FA result for CC-Di-HRK1 against BAD/BCL-x_L (20 mM Tris, 150 mM NaCl, pH 7.6, 25 nM FAM-Ahx-BAD, 150 nM BCL-x_L, error bars show standard deviations observed in triplicate experiments and errors are standard deviations generated in data fitting)

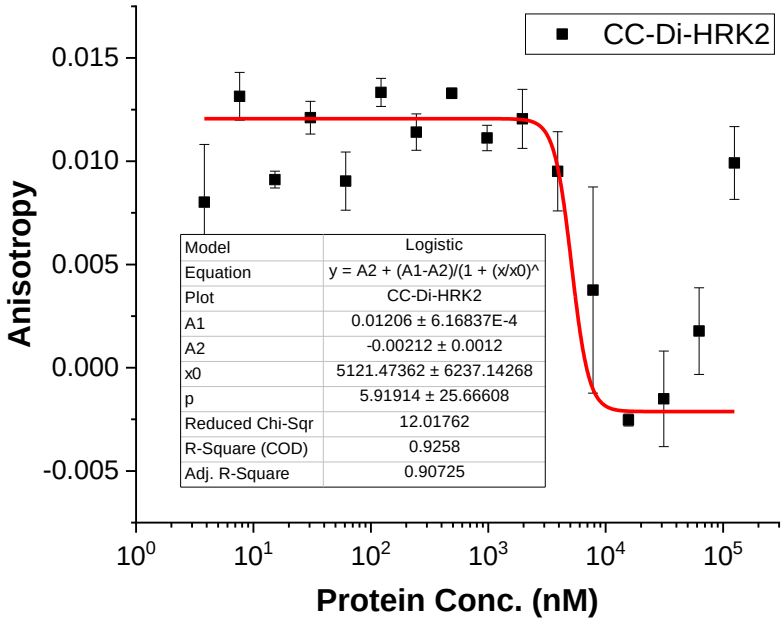

Figure 4-8 Competition FA result for CC-Di-HRK2 against BAD/BCL-x_L (20 mM Tris, 150 mM NaCl, pH 7.6, 25 nM FAM-Ahx-BAD, 150 nM BCL-x_L, error bars show standard deviations observed in triplicate experiments and errors are standard deviations generated in data fitting)

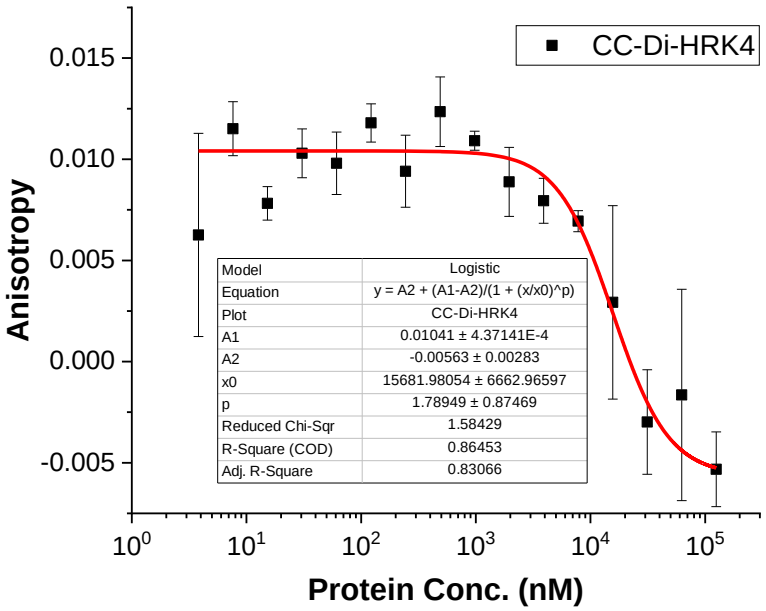

Figure 4-9 Competition FA result for CC-Di-HRK4 against BAD/BCL-x_L (20 mM Tris, 150 mM NaCl, pH 7.6, 25 nM FAM-Ahx-BAD, 150 nM BCL-x_L, error bars show standard deviations observed in triplicate experiments and errors are standard deviations generated in data fitting)

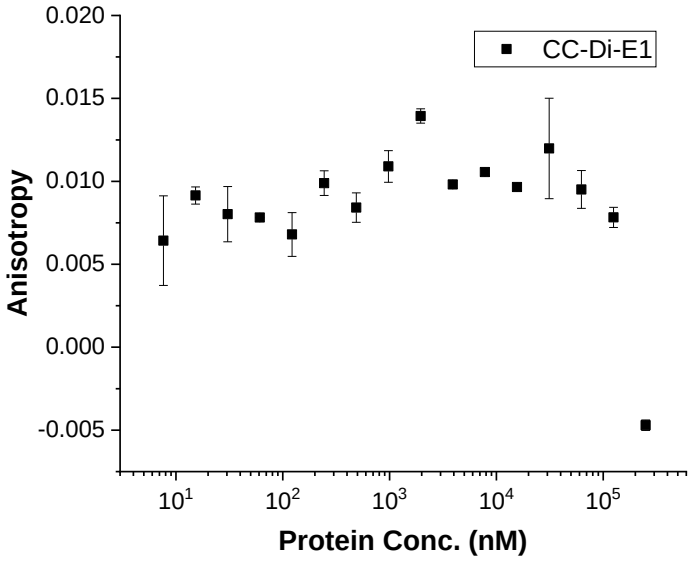

Figure 4-10 Competition FA result for CC-Di-E1 against BAD/BCL-x_L (20 mM Tris, 150 mM NaCl, pH 7.6, 25 nM FAM-Ahx-BAD, 150 nM BCL-x_L, error bars show standard deviations observed in triplicate)

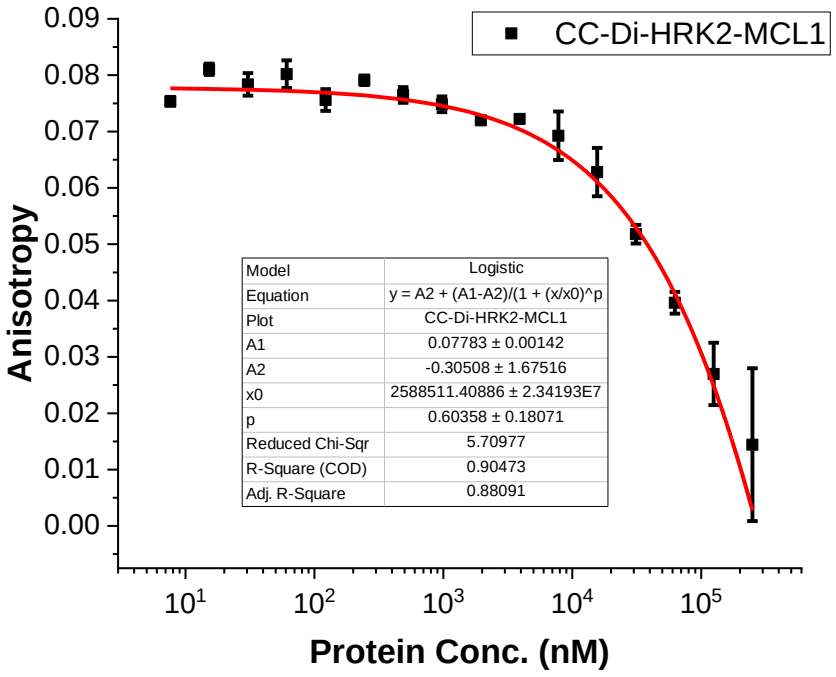

Figure 4-11 Competition FA result for CC-Di-E1 against BID/MCL-1 (20mM Tris, 150 mM NaCl, pH 7.6, 25 nM FAM-Ahx-BID, 150 nM MCL-1, error bars show standard deviations observed in triplicate experiments and errors are standard deviations generated in data fitting).

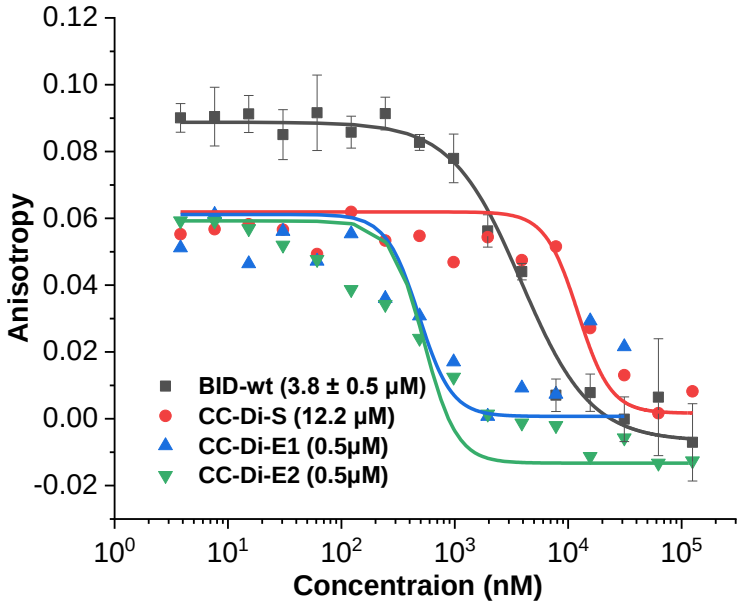

Figure 4-12 Competition FA result for BID-wt, CC-Di-S, CC-Di-E1 and CC-Di-E2 against BID/MCL-1 (20mM Tris, 150 mM NaCl, pH 7.6, 25 nM FAM-Ahx-BID, 150 nM MCL-1, error bars show standard deviations observed in triplicate experiments and errors are standard deviations generated in data fitting).

Table 4-2 FA competition titration results for the coiled coils

Peptide	Sequence[a] f gabcdef gabcdef gabcdef gabcdef gab *h1 h2 h3 h4*	IC_{50} BAD/BCL-x_L[b]	IC_{50} BID/MCL-1[c]
BAD	L WAAQRYG RELRRMS DEFVDSF KK	ND	ND
HRK	SAAQLTA ARLKALG DELHQRT MW	ND	ND
BID	E DIIRNIA RHLAQVG DSMDRSI W	137.7 ± 31.8 nM	3.8 ± 0.5 μM
NOXA-B_{18-44}	P ADLKDEC AQLRRIG DKVNLRQ KLLNM		
CC-Di	G EIAALKQ EIAALKK ENAALKQ EIAALKQ GYG	ND	ND
CC-Di-S	G EIAALKQ EILRLIG DNVALKQ EIAALKQ GYG	ND	12.2 ± 0.5 μM
CC-Di-E1	G EILALKQ EILRLIG DNVALKQ EILNLKQ GYG	No response	0.5 ± 0.05 μM
CC-Di-E2	G KILALEQ EILRLIG DNVNLKQ EILNLKQ GYG	ND	0.5 ± 0.09 μM
CC-Di-BAD	G EIAALKL EIAALYK ENLRLKQ EIFALKF GYG	15.9 μM[d]	ND
CC-Di-HRK1	G EIAALKQ EILRLLG DNMALKQ EIAALKQ GYG	16.1 μM[d]	ND
CC-Di-HRK2	G KILALEQ EILRLLG DNMNLKQ EILNLKQ GYG	5.1 ± 6.2 μM[e]	>50 μM
CC-Di-HRK3	G EIAALKQ EILRLLG DNMALKF EIAALKQ GYG	ND	ND
CC-Di-HRK4	G EIAALYQ EILRLLG DNMALKF EIAALKQ GYG	15.7 ± 6.6 μM	ND

[a]Hot-spot residues are coloured: blue for BAD, red for HRK, purple for BID and green for NOXA; positions *a* and *d* are underlined in coiled coils; Ala4*b*, Ala4*c* and Ala5*b* (sensitive to variation in ISAMBARD modelling) are shown in italic. [b,c]ND: not determined; [d]large deviation of data fitting; [e]hook effect was observed at high concentration.

4.4 Structural study by CD spectroscopy

I investigated the secondary structures of the peptides and the complexes with proteins using CD. I tested CC-Di-BAD and CC-Di-HRK1. Some of the other peptides were not tested singly due to their poor water solubility. Furthermore, their complexes with BCL-x_L, including CC-Di-HRK1/BCL-x_L, CC-Di-HRK2/BCL-x_L, CC-Di-HRK4/BCL-x_L were tested in thermal unfolding CD assays. All samples were prepared with a concentration of 15 μM (concentration of each component), which was similar to their IC_{50}s.As a result, CC-Di-HRK1 showed a classical helical CD spectrum and high helicity, with 78%, whilst CC-Di-BAD showed only 38% helicity (Figure 4-13), indicating a good correlation with the ISAMBARD modelling results which indicated that CC-Di-BAD doesn't have optimal BUDE scores to form a coiled coil (Figure 4-3). In addition, the complex of CC-Di-HRK1 with BCL-x_L showed similar spectrum and helicity to the average results (Figure 4-14), suggesting that CC-Di-HRK1 doesn't affect the helicity of the protein significantly at these concentrations. Several other peptides were not tested due to poor solubility.

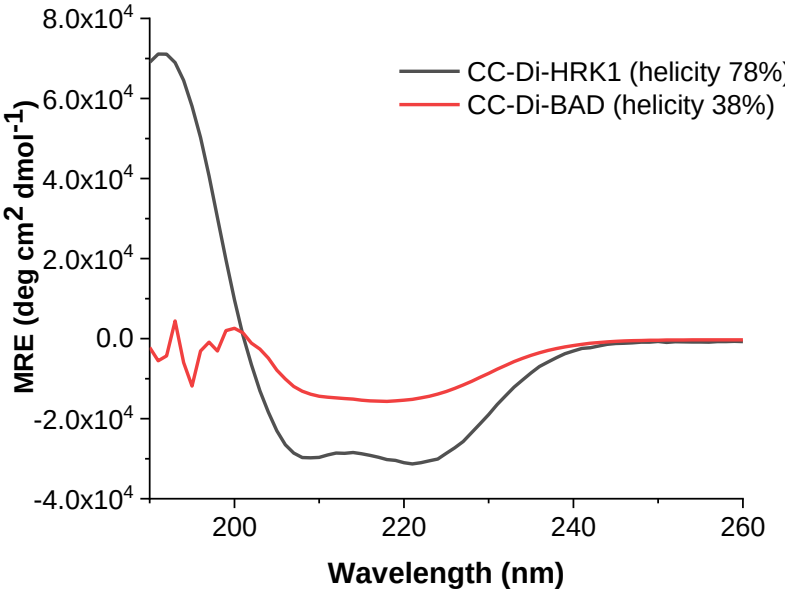

Figure 4-13 CD spectra for CC-Di-HRK1 and CC-Di-BAD (20 mM phosphate, pH7.4, peptide concentration: 15 μM).

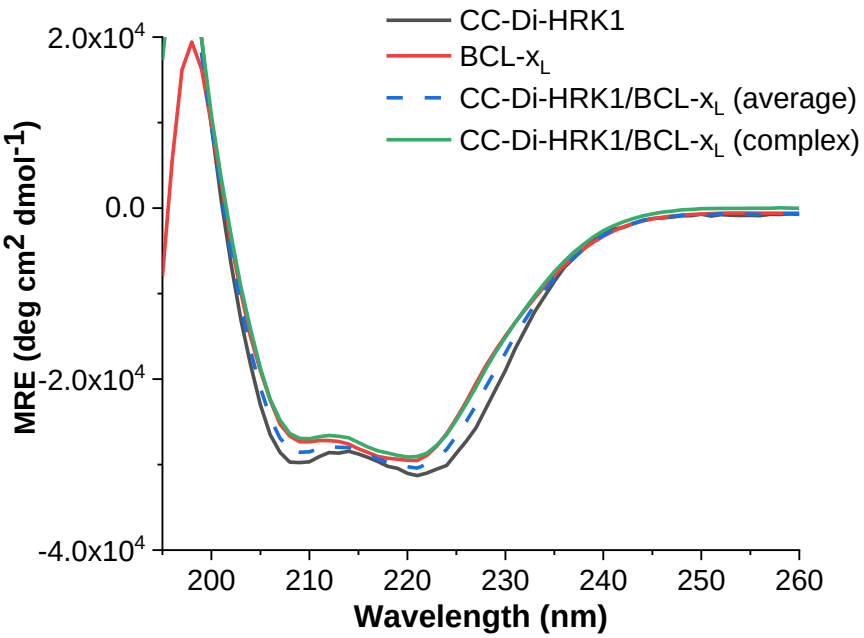

Figure 4-14 CD spectra for CC-Di-HRK1, BCL-x_L, and CC-Di-HRK1/BCL-x_L (20 mM phosphate, pH7.4, peptide concentration: 15 µM).

Next, I investigated the structural stability of CC-Di-BAD and CC-Di-HRK1 in thermal unfolding CD assays; several other peptides were too hydrophobic to be tested. A number of complexes, including CC-Di-BAD/BCL-x_L and CC-Di-HRK1/BCL-x_L, CC-Di-HRK2/BCL-x_L, CC-Di-HRK4/BCL-x_L and CC-Di-HRK2/MCL-1, were also tested using thermal unfolding CD spectroscopy. CC-Di-BAD was observed to have a low T_m, with 33 °C, whilst CC-Di-HRK1 gave a much higher T_m, with 66 °C (Figure 4-15); however, it did not give a typical thermal transition for coiled coils, indicating that it might not form a stable coiled coil; this experiment would be repeated in the future to confirm the results. The CC-Di-HRK1/BCL-x_L complex was observed to have a T_m of 58 °C whilst *apo*-BCL-x_L gave a T_m of 59 °C (Figure 4-16, Table 4-3), indicating a minimal influence on the thermostability from the peptide (32aa-peptide vs 142aa-protein). Similar curves were observed for CC-Di-HRK2/BCL-x_L and CC-Di-HRK4/BCL-x_L, with Tm of 57 °C and 61 °C, respectively.

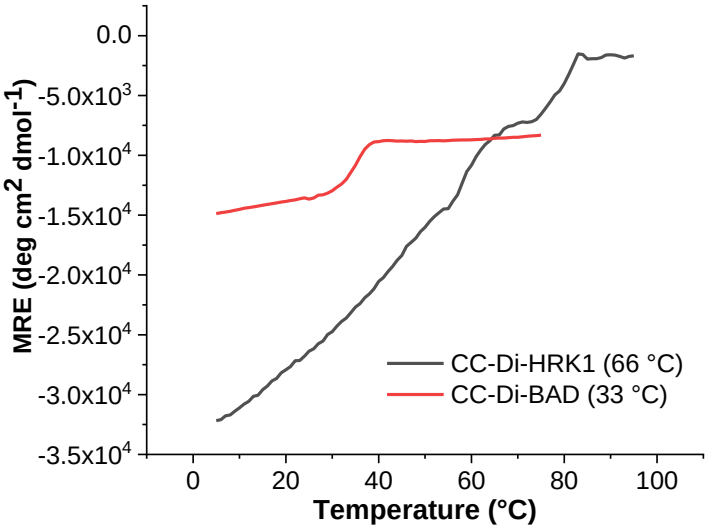

Figure 4-15 Thermal unfolding curves for CC-Di-BAD and CC-Di-HRK1 (20 mM phosphate, pH7.4, peptide concentration: 15 µM; 5-95 °C).

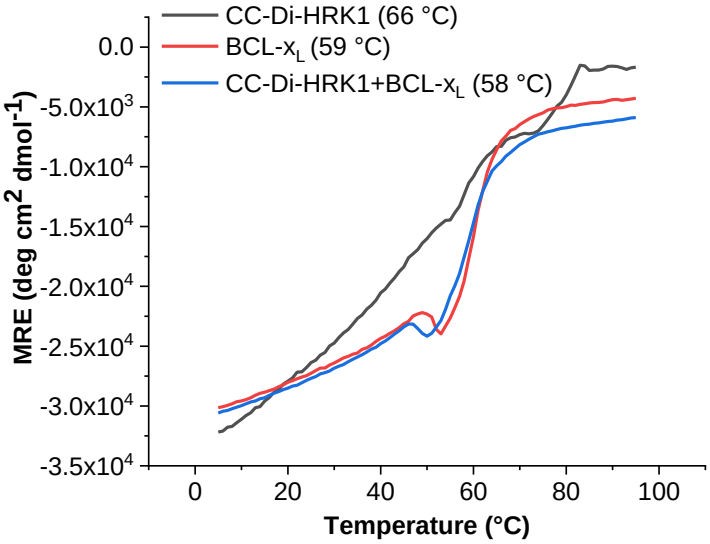

Figure 4-16 Thermal unfolding curves for CC-Di-HRK1, BCL-x_L, and CC-Di-HRK1/BCL-x_L (20 mM phosphate, pH7.4, peptide concentration: 15 µM; 5-95 °C).

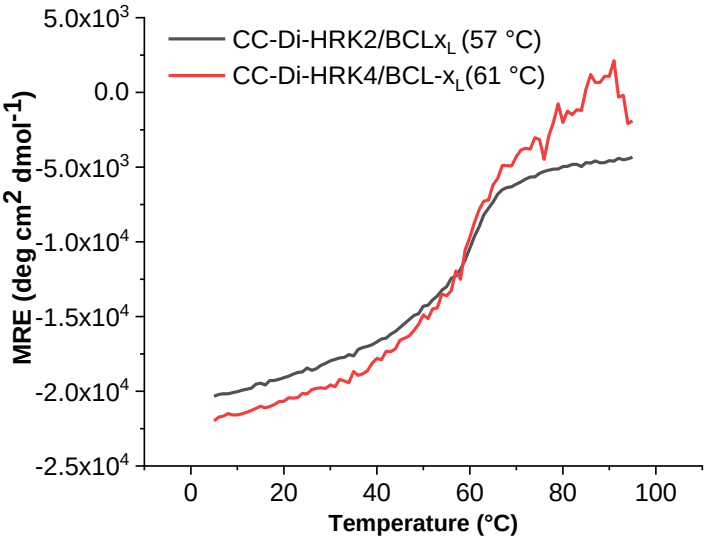

Figure 4-17 Thermal unfolding curves for CC-Di-HRK2/BCL-x_L and CC-Di-HRK4/BCL-x_L complexes (5% DMSO for CC-Di-HRK4, 20 mM phosphate, pH7.4, peptide concentration: 15 μM; 5-95 °C).

Table 4-3 Helicity and melting temperature of the peptides and complexes

Peptide	Sequence[a]	Helicity/ Tm (peptide)	Helicity/Tm (complex with BCL-x_L)
	f gabcdef gabcdef gabcdef gabcdef gab		
CC-Di-BAD	G EIAALKL EIAALYK ENLRLKQ EIFALKF GYG	38%	ND
CC-Di-HRK1	G EIAALKQ EILRLLG DNMALKQ EIAALKQ GYG	78%/66°C	74%/58°C
CC-Di-HRK2	G KILALEQ EILRLLG DNMNLKQ EILNLKQ GYG	ND	51%/57°C
CC-Di-HRK3	G EIAALKQ EILRLLG DNMALKF EIAALKQ GYG	ND	ND
CC-Di-HRK4	G EIAALYQ EILRLLG DNMALKF EIAALKQ GYG	ND	56%/61°C

[a]Hot-spot residues are coloured: blue for BAD, red for HRK, purple for BID and green for NOXA; positions *a* and *d* are underlined in coiled coils.

4.5 Conclusions

In this chapter, I have combined multiple computational tools to inform the design of coiled coils as BCL-x_L inhibitors. First of all, I applied ISAMBARD to investigate the saturation variation of a well-defined coiled coil. Together with virtual alanine scanning results, hot-spot residues from BAD, BID and HRK were grafted onto the template sequence, CC-Di, at suitable sites. Surprisingly, several peptides showed weak potency in the FA competition assays using BAD/BCL-x_L, although optimisation of the assays was needed. Several peptides failed to be tested in CD experiments due to poor solubility; whilst for other peptides, the correlation between BUDE scores and helicities demonstrate the importance of computational modelling. In thermal unfolding assays, a number of peptides did not show typical thermal unfolding curves for a coiled coil and their peptide/protein complexes gave similar results to the *apo*-protein, indicating that these peptides had little impact on the overall helicity and melting temperature for the complexes; the formation of complexes and the oligomeric states of coiled coils would be confirmed by further experiments, e.g. analytical ultracentrifugation (AUC). These results show good starting points for designing new coiled coils targeting BCL-x_L with high potency and selectivity, and also indicate the importance of combining computational tools, e.g. virtual alanine scan and structural modelling, i.e. ISAMBARD in this chapter, and rational design to lead to bioactive and structurally stable coiled coils.

4.6 Future work

4.6.1 FA assay optimisation

Although several peptides were observed to have inhibiting potency against the BCL-x_L, the deviations of data were high. To optimise this, different buffer conditions could be used, e.g. phosphate or tris buffer at different pH; and add different types of detergents, e.g. Triton-X or BSA.

4.6.2 CD assay optimisation

Several CD samples could not be tested due to poor solubility. Further experiments will be focusing on using DMSO-free conditions and also design new peptides with improved solubility. In addition, all assays were performed with a peptide/protein ratio= 1:1 and IC_{50}s were calculated based on the concentrations of monomers; in the future a ratio of 2:1 will be tested as the peptides are supposed to interact with the protein as homodimers.

4.6.3 Investigation of selectivity

A number of peptides in this chapter showed binding to the BCL-x_L. The other peptides will be tested in the FA competition assays using MCL-1 and a tracer which has comparable K_d to the BAD tracer for comparison.

4.6.4 Generation of covalently crosslinked homodimers and heterodimers

Although several peptides did show binding in the FA competition assays, it was difficult to confirm whether they bound to the protein as coiled coils or monomeric peptides. To confirm this, analytical ultracentrifugation (AUC) can be employed to determine the oligomeric states of the peptides in absence of the protein and the formation of complexes between peptides and the protein. In addition, covalently crosslinked dimeric coiled coils will be generated using either disulphide bonds or amide bonds.[216,219] Covalently tethered coiled coils could be more advantageous, e.g. enhanced structural stability and proteolytical stability.[9,217] Once the covalently crosslinked homodimers show binding in the assays, heterodimers will also be designed to functionalise the other face which doesn't participate in the interaction between a coiled coil and the protein, e.g. incorporating cell-penetrating motifs.

Chapter 5 Overall conclusions and future work

The overall aim of the project was to design and develop potent and selective BCL-x_L inhibitors using peptidomimetic approaches. Two main approaches were employed, including constrained peptides and coiled coils. Various computational tools were used to assist rational peptide design in this work. Successful hits could act as useful probes for further structural studies and starting points to develop therapeutics for treatment of BCL-x_L-dependent cancers.

In Chapter 2, the BAD BH3 sequence was chosen for design of BCL-x_L inhibitors. In direct FA titration assays, the BAD tracer showed good affinity and selectivity towards BCL-x_L. Using a combination of virtual alanine scanning and a maleimide-staple scan, I identified suitable sites for incorporation of a maleimide constraint in the wild-type peptide, BAD-s. However, several constrained peptides showed loss of potency although their bis-cysteine precursors did not. CD spectroscopy was used to investigate the secondary structures. The observed helicity from CD did not show strong correlation to the potency. This unusual observation motivated me to use MD simulations to further investigate the *apo*-peptides and also the bound peptides in the complexes with BCL-x_L. These MD simulations suggest that differences in bound-state-helicity between the active and inactive constrained peptides likely influence inhibitory potency; and a constraint at inappropriate positions may disrupt orientation of the key side chains so that optimal interaction with BCL-x_L cannot be achieved. These data highlight the importance of a staple scan alongside computational and structural analyses and the complex outcomes from introducing a constraint.

In Chapter 3, based on the HRK BH3 domain, I constructed the first HRK constrained peptides. Using a combination of homology modelling and virtual alanine scanning, I successfully identified the potential hot-spot residues involved in the HRK/BCL-x_L interaction. A dibromomaleimide staple scan led to an optimal constrained peptide, HRKS4, which gave improved potency, and enhanced helicity in comparison to the unconstrained precursor, alongside increased proteolytic stability. I further compared the maleimide constraint with other types, e.g. hydrocarbon and xylyl. I showed that the maleimide constraint acts as an alternative option to construct constrained peptides with optimal potency in inhibition of HRK/BCL-x_L. I sought to design a second series of peptides with improved selectivity as the first series of HRK-peptides, including the wild-type and the constrained, were observed to inhibit MCL-1 with similar

potency to BCL-x_L. To better inform peptide design for improving selectivity, additional virtual alanine scanning and homology modelling was carried out, resulting in a new series of truncated peptides with retained potency and significantly improved selectivity. Although the maleimide constrained peptide, HRKS4H, did not fully maintained potency, it was observed to have better selectivity. To best of my knowledge, this is the first example of constrained peptides based on the HRK BH3 domain. I have shown that the maleimide constraint can be applied to the HRK sequences and the selectivity can be modulated by truncation and transposition of key residues. These findings will help other scientists who are interested in BCL-2 family PPIs study and develop selective and potent inhibitors.

In Chapter 4, a well-defined homodimeric coiled coil template, CC-Di, was chose for grafting hot-spot residues from BH3 ligands which bind to BCL-x_L. Applying ISAMBARD for a saturation variation scan, I identified suitable grafting sites in the template. Several alanine residues at *b* or *c* positions, which are usually considered ideal for grafting other residues, were found to be sensitive to replacement. A peptide, CC-Di-BAD, designed by grafting hot-spot residues from the BAD BH3 sequence onto CC-Di, showed a nonideal BUDE score in ISAMBARD as well as lower helical structure and low melting temperature in CD experiments. This observation indicated correlation between the acquired energy in ISAMBARD and real structural stability, and has motivated me to optimise the design. Several hot-spot residues from HRK, BAD and BID were transposed into CC-Di at more optimal positions in terms of the saturation variation scanning results. In competition FA assays, a number of peptides showed weak potency against BAD/BCL-x_L. Further studies will focus on optimisation of assays and investigation on selectivity.

In summary, I have applied constrained peptides and coiled coils mainly based on the BAD and HRK BH3 sequences for discovery of BCL-x_L peptidomimetic inhibitors. I have demonstrated that a combination of computational tools, e.g. virtual alanine scanning and homology modelling, with dibromomaleimide staple scanning can rapidly identify suitable sites for peptide constraining and inform design of selective BCL-x_L inhibitors. Furthermore, I have grafted hot-spot residues from the BH3 ligands onto a well-defined coiled coil template assisted by *in silico* methods. Several peptides showed potential as starting points for further optimisation.

In the future, further studies will focus on revealing the corresponding crystal structures and applying the peptides in cell-based assays. In chapter 2 and 3, I

described constrained peptides derived from the BAD and HRK BH3 domains as BCL-x_L inhibitors. Although several structures for complexes between a BH3 peptide and BCL-x_L have been reported, a structure of a constrained peptide derived from these two BH3 domains with BCL-x_L has not been revealed. Solving these structures will help scientists understand the recognition mode and mechanism of selectivity, and design optimal peptidomimetic inhibitors. In addition, structures of complexes between HRK and pro-survival BCL-2 family proteins are less studied. HRK was observed to bind to BCL-x_L and MCL-1 in this study. Prior studies described that HRK could bind to BCL-2.[241] However, none of these structures have been reported. In the future, HRK/BCL-x_L and HRK/MCL-1 are expected to be crystallised and the structures are expected be solved, which will be beneficial for design of new probes targeting these proteins.

In addition to structural studies, cell-based studies will also be carried out. HRK can induce apoptosis in glioblastoma (GBM) cells,[263] therefore the HRK peptides in this work are expected to show ability to induce apoptosis in GBM cells. However, due to the reversibility of maleimide constraint, the constrained peptides are supposed to be partially or fully unconstrained in reducing cytosolic environment and lose benefits from the constraint. Therefore, irreversible constraining methods will be developed based on maleimide linkers. To do this, other approaches, e.g. self-hydrolysing maleimide linkers[145] or monosubstituted maleimides, will be employed. Furthermore, bicyclic peptides will be generated by combining a pair of cysteines and a methionine for constraining. The generated bicyclic peptides are expected have high proteolytic stability, good cell-permeability, and less off-target effect and can be used in cellular studies.

Finally, several coiled coils in chapter 4 showed potential for further optimisation. In the future, more hot-spot residues will be introduced to design new peptides with improved potency, good selectivity and retained structural stability. Coiled coils with different oligomeric states, e.g. heterodimer, homotrimer and heterotrimer, will be designed and generated for event-driven studies, i.e. making proteolysis-targeting chimeras (PROTACs) because PROTACs showed their efficacy in treatment of BCL-x_L over-expressed cancers and reduced side-effects in platelets.[71] Covalent linkers will be used to crosslink the coiled coils, in order to make highly stable molecules.

Chapter 6 Experimental

6.1 Peptide synthesis and purification

6.1.1 General considerations

Rink amide resin, ethyl cyanohydroxyiminoacetate (Oxyma), *N*,*N*-diisopropylethylamine (DIPEA), hydroxybenzotriazole (HOBt), *N*,*N*'-diisopropylcarbodiimide (DIC), piperidine, trifluoroacetic acid (TFA), *O*-(1H-6-Chlorobenzotriazole-1-yl)-1,1,3,3-tetramethyluronium hexafluorophosphate (HCTU), triisopropyl silane (TIPS), 3,6-dioxa-1,8-octanedithiol (DODT) and Fmoc-L-amino acids were purchased from Fluorochem (UK) or Merck (Germany). Dimethylformamide (DMF) was purchased from Sigma-Aldrich (UK). The designed peptides were synthesised using standard Fmoc-based solid-phase methods on a LibertyBlue microwave-assisted automated peptide synthesiser (CEM; Mathews, NC, USA) or a MultiPep2 parallel synthesiser (CEM; Mathews, NC, USA). Peptide purifications were carried out on a 1260 Infinity II prep-HPLC system (Agilent; Santa Clara, CA, USA). The identities of peptides were confirmed by LCMS (Bruker Amazon Speed) or HRMS (Bruker MaXis Impact).

6.1.2 Manual methods for peptide synthesis

Method A: Manual deprotection of N-Fmoc groups

Fmoc-protecting groups were removed using 20% piperidine in DMF (2 mL × 5 min, then 2 mL × 25 min), followed by washing with DMF. Successful deprotection was confirmed by a positive colour change using *Method C*. For initial deprotection, the resin was swelled by addition of DMF (5 mL) and agitated for 15 min before deprotection.

Method B: Manual coupling of amino acids

The desired amino acid (4.5 equiv.) DIPEA (6 equiv.) and HCTU (4.5 equiv.) were dissolved in DMF (5 mL) and added to the resin, followed by agitation for 45 min at room temperature. Upon completion of coupling, the resin was washed with DMF (2 × 3 mL × 2 min) and tested by *Method C*. If a positive colour change was observed, then the coupling step was repeated.

Method C: Kaiser Test

The Kaiser Test was carried out to determine a successful coupling or deprotection reaction. To do this, a small number of resin beads were rinsed by diethyl ether and transferred into a glass vial, followed by the addition of one drops of each of the three solutions in the following order: 1) Ninhydrin (5% w/v) in ethanol; 2) Phenol (80% w/v) in ethanol; 3) 1 mM potassium cyanide (KCN) (aq.) in pyridine (2% v/v). The solution was then heated to 110 °C for 1 min. A successful coupling gave no change in the colour of the beads, whilst dark blue beads illustrate a successful deprotection.

Method D: N-terminal Acetylation

After final deprotection, acetic anhydride (10 equiv.) and DIPEA (10 equiv.) were dissolved in DMF (3 mL) and added to the resin. After 45 min, the resin was drained, washed with DMF (3 × 2 mL × 2 min) and successful capping determined by a negative colour test (*Method C*).

Method E: N-terminal FAM labelling

To make fluorescent labelled tracers, N-terminally free peptides were coupled with Fmoc-Ahx-OH, followed by deprotection using 20 % piperidine in DMF and final coupling with 5(6)-carboxylic fluorescein (4.5 equiv) using HOBt (4.5 equiv.) and DIC (6 equiv.) at room temperature overnight.

Method F: Peptide Cleavage

All peptides were cleaved by TFA/H_2O/TIPS/DODT (92.5 : 2.5 : 2.5 : 2.5) for 3 hours at room temperature. Cleavage cocktail solutions were concentrated under nitrogen flow and crude peptides were precipitated with treatment of cold diethyl ether (diethyl ether: cleavage cocktail=10:1). Crude peptides were dissolved in acetonitrile/H_2O (1:1) and subjected to prep-HPLC directly.

Method G: Dibromomaleimide constraining

Each purified linear peptide was dissolved in ACN/phosphate buffer (ratio=3:7; peptide concentration: 4 mg/mL; phosphate buffer: 20 mM phosphate, 150 mM NaCl, pH = 7.8) and transferred into a 15 mL

centrifuge tube. TCEP (1mg/mL solution in water, 2 equiv.) was added and the peptide was agitated for 30 mins to reduce any disulfide bonds. Thereafter, dibromomaleimide (1mg/mL solution in ACN, 2 equiv.) was added and the peptide was agitated for 2 h. A colour change to yellow was observed during the reaction. The reaction was monitored by LC-MS. Upon completion of the reaction, peptide solutions were injected directly into prep-HPLC to isolate final maleimide-constrained products.

Method H: m-Xylene constraining

After being dissolved and transferred as mentioned above (*method G*), each peptide was treated with TCEP (solution in phosphate buffer, 2equiv.) for 30 mins to reduce disulfide bonds, followed by addition of dibromomethylbenzene (1mg/mL solution in DMF, 2 equiv.) and DIPEA (4 equiv.). The reacting solution was agitated for 2 h and monitored by LC-MS. Upon completion of the reaction, reaction mixtures were purified using prep-HPLC.

Method I: Hydrocarbon stapling

After peptide assembly, the on-resin peptide was acetylated (*Method D*) and transferred to a round bottom flask. Grubbs 1st generation catalyst (0.10 equiv.) was added, followed by addition of anhydrous dichloroethane (DCE, 5 mL). The reaction was stirred in the dark for 4 h under nitrogen flow and repeated by addition of fresh catalyst (0.1 equiv.). The resin bound peptide was washed with DCE (5 mL × 3), cleaved and then crude peptide purified using prep-HPLC.

6.1.3 Cycles for automated peptide synthesis

Table 6-1 Cycles used on the CEM LibertyBlue synthesiser

Step	Parameters
Standard Deprotection	4.5 mL 20% piperidine in DMF, 90 °C, 1 min 30 s
Wash	4 mL DMF, 5s
Wash	4 mL DMF, 5s

Standard Coupling	2.5 mL amino acid (0.5 M in DMF), 1 mL DIC (0.5 M in DMF), 0.5 mL Oxyma (1 M in DMF), 90°C, 5min
Standard Coupling	This step is for double coupling, parameters are as shown above
Wash	4 mL DMF, 5s
Wash	4 mL DMF, 5s
Wash	4 mL DMF, 5s
Wash	4 mL DMF, 5s

Table 6-2 Cycles used on the CEM MultiPep parallel synthesiser

Cycle	Steps
Prepare	RinseNeedle 2 mL DMF × 3, PrimeManifold 5 mL DMF, WashResin 6 mL DMF
1-10	Deprotection 1.5 mL 20% piperidine in DMF × 2, Rinse Needle 2 mL, WashResin 9 mL DMF × 5, Extract 30 s, Double Coupling 0.5 mL amino acid (0.5 M in DMF) + 0.25 mL DIPEA (2 M in NMP) + 0.05 mL NMP +0.52 mL HCTU (0.5 M in DMF), WashResin 9 mL DMF × 5, Extract 30 s
11-end	Deprotection 1.8 mL 20% piperidine in DMF × 2, Rinse Needle 2 mL DMF, WashResin 10 mL DMF × 5, Extract 30 s, Double Coupling 0.6 mL amino acid (0.5 M in DMF) + 0.3 mL DIPEA (2 M in NMP) + 0.05 mL NMP +0.63 mL HCTU (0.5 M in DMF), WashResin 10 mL DMF, Capping 1.8 mL 10% acetic anhydride in DMF, RinseNeedle 2mL DMF, Extract 30 s, WashResin 10 mL DMF × 4, Extract 30 s
Final	Deprotection 1.8 mL 20% piperidine in DMF× 2, Rinse Needle 2 mL NMP, WashResin 10 mL DMF × 5, Extract 30 s

6.2 Modelling section

6.2.1 Virtual alanine scanning using BAlaS

All structures which were used to carry out BAlaS modelling were uploaded on the Bude Alanine Scanning server (https://pragmaticproteindesign.bio.ed.ac.uk/balas/),[232] which is based on the Bristol University Docking Engine (BUDE).[231] Contributions of >4.2 kJ mol-1 were considered as significant.

6.2.2 Generation of homology models using ROSETTA

The ligand peptides were extracted from the original structures in PyMol. The extracted ligands were aligned into the binding sites of the corresponding receptors in PyMol and the originally bound ligands were removed from the complexes. Thereafter, the generated structures were repacked in Rosetta to remove small clashes.

Repack script that was used:

```
<ROSETTASCRIPTS>
        <SCOREFXNS>
        </SCOREFXNS>
        <TASKOPERATIONS>
                <InitializeFromCommandline name="ifcl" />
                <RestrictToRepacking name="rtr" />
        </TASKOPERATIONS>
        <FILTERS>
        </FILTERS>
        <MOVERS>
                <PackRotamersMover name="repack" scorefxn="talaris2014"
task_operations="ifcl,rtr" />
                <MinMover name="minimize_sc" scorefxn="talaris2014" chi="1"
bb="0" jump="0" type="dfpmin_armijo_nonmonotone" tolerance="0.0001" />
        </MOVERS>
```

```
        <APPLY_TO_POSE>
        </APPLY_TO_POSE>
        <PROTOCOLS>
            <Add mover="repack" />
            <Add mover="minimize_sc" />
        </PROTOCOLS>
</ROSETTASCRIPTS>
```

Options file that was used:

```
-in:file:fullatom
-out:file:fullatom
-linmem_ig 10
-ex1
-ex2
-use_input_sc
-score:weights talaris2014.wts
-corrections:restore_talaris_behavior true
-out:file:scorefile repack_1.fasc
```

6.2.3 Molecular dynamics simulations

All peptide/protein complexes were subjected to MD simulations using YASARA structure.[237] Maleimide constraints were modelled in YASARA by swapping the pertinent amino acids for cysteines and connecting to maleimide fragments. Minimised structures were generated using the energy minimisation function with default settings. The modelled complexes were subjected to MD simulations using YASARA structure macro for fast MD run (www.yasara.org/md_runfast.mcr).[264] Briefly, the AMBER14 forcefield was used and the temperature was set as 298.0 K with the timestep set as 2*2.50 fs. Each structure was run for >160ns. Ligand helicity was calculated by averaging per-residue helicity from 50 to 160 ns. Peptide/protein interactions were analysed using Discovery Studio Visualizer and figures were created in PyMol.

6.3 Synthesis of Fmoc-mS5-OH

6.3.1 General considerations

Solvents and reagents were purchased from major suppliers, including Sigma-Aldrich, Fisher, Alfa Aesar, Fluorochem and Merck, and utilised as received without further purification. Anhydrous tetrahydrofuran was obtained from the in-house solvent purification system from Innovative Technology Inc. PureSolv®. Anhydrous dimethyl formamide was obtained from major chemical suppliers equipped with a SureSeal™ (or equivalent). Water used in preparation of solutions and reaction quenching was deionised.

Thin layer chromatography (TLC) was carried out on Merck Kieselgel 60 F254 0.25 mm precoated aluminium plates with visualisation via ultraviolet light (λmax = 254 nm), ninhydrin reagent and/or potassium permanganate. Flash column chromatography was performed using Merck Kieselgel 60 (230-400 mesh) with assistance of a head pump.

NMR spectra were recorded on Bruker AV4 NEO 11.75 T (500 MHz 1H) or Bruker AV3HD 9.4 T (400 MHz 1H) NMR spectrometers. The NMR chemical shifts (δ) are quoted in ppm TMS peak, and with coupling constants (J) quoted to the nearest 0.1 Hz. The identities of small molecules were confirmed by LCMS (Bruker Amazon Speed) or HRMS (Bruker MaXis Impact).

6.3.2 Procedures and data for Fmoc-mS5-OH synthesis

(*S*)-*N*-benzylproline ***3***

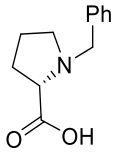

L-Proline (25.01 g, 217.2 mmol, 1 equiv.) was added to a flask, followed by addition of 136 mL methanol. MeONa (81 mL, 30% wt, in methanol solution, 434.3 mmol, 2 equiv.) was added slowly under stirring at room temperature and then the mixture was heated up to 50 °C. After the solution became transparent, Bn-Cl (25 mL, 220 mmol, 1 equiv.) was added and the reaction mixture was stirred at the same temperature overnight. The mixture was neutralised with concentrated HCl (approx. 22 mL) until pH reached ~7 using pH test paper. Then chloroform (100 mL) was added and the mixture was kept stirring for 1 h. The precipitate was filtered and washed with chloroform. The filtrate was concentrated in vacuo and the residue was treated with acetone (30 mL). The

precipitate of crude product was filtered and washed with acetone and then dried thoroughly to give (*S*)-*N*-benzylproline as yellowish solid (43.7 g, 85%), which was used in synthesis of ligand **3** without further purification. δ_H (500 MHz; $CDCl_3$) 1.88-2.05 (2H, m, γ-CH_2), 2.18-2.37 (2H, m, β-CH_2), 2.85 (1H, d, J= 9.9 Hz, δ-CH_2), 3.63 (1H, ddd, J=10.9 Hz, 7.4 Hz, 3.3 Hz, δ-CH_2), 3.76 (1H, dd, J=8.8 Hz, 6.1 Hz, α-C*H*), 4.17 (1H, d, 13.0 Hz, N-CH_2), 4.31 (1H, d, J=13.0 Hz, N-CH_2), 7.33-7.48 (5H, m, Ar-C*H*). δ_C (125 MHz, $CDCl_3$): 23.1, 28.9, 57.7, 66.7, 77.0, 115.9, 116.1, 125.0, 132.0, 133.28, 162.4. ESI-HRMS found m/z 206.1178; $[C12H15NO_2+H]^+$ requires 206.1181. These data agree with that measured in the literature.[101]

(*S*)-2-[*N*-(*N*'-benzylprolyl)amino]-benzophenone (BPB) ***4***

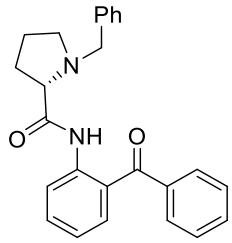

(*S*)-*N*-benzylproline ***3*** (43.7 g, 213.18 mmol, 1 equiv.), *N*-methylimidazole (37.2 mL, 468.67 mmol, 2.2 equiv.) and CH_2Cl_2 (200mL) were added to a flask. MsCl (16.5 mL, 213.35 mmol, 1 equiv.) was added dropwise at 0 °C. After removing the ice bath, 2-aminobenzophenone (37.8 g, 191.68 mmol, 0.9 equiv.) was added and the reaction mixture was stirred at 50 °C overnight. Then, saturated aqueous NH_4Cl (150 mL) was added to the reaction mixture and the organic phase was separated. The aqueous phase was extracted with CH_2Cl_2 (100 mL×3) and the combined organic layers were dried over $MgSO_4$. Solvents were removed *in vacuo* to afford crude ligand ***4*** as a yellow oil which was purified as follows: to the flask containing crude ligand ***4***, acetone (200 mL) was added to dilute the oil, followed by the addition of concentrated HCl (36.35 mL, 2 equiv.). After filtration, the precipitate was washed with acetone twice and then 2/3 of acetone was removed in vacuo. The residue was left at -20 °C overnight, followed by filtration to afford (*S*)-2-[*N*-(*N*'-benzylprolyl)amino]-benzophenone (BPB) ***4*** (23.43 g, 30 %) as colourless solid. δ_H (500 MHz; $CDCl_3$) δ1.71-1.89 (2H, m, γ-CH_2), 1.96 (1H, ddd, *J*=16.9, 8.1, 4.2 Hz,δ-CH_2), 2.19-2.32 (1H, m, δ-CH_2), 2.41 (1H, td, *J*=9.5, 6.9 Hz, β-CH_2), 3.22 (1H, ddd,J=9.0, 6.4, 2.7 Hz, β-CH_2), 3.32 (1H, dd, *J*=10.1, 4.8 Hz, α-C*H*), 3.59 (1H, d, *J*=12.9 Hz, N-CH_2), 3.92 (1H, d, *J*=12.9 Hz, N-CH_2), 7.04-7.20 (4H, m, Ar-C*H*), 7.38 (2H, dt, J=7.4, 3.6

Hz, Ar-C*H*), 7.43-7.58 (4H, m, Ar-C*H*), 7.58-7.66 (1H, m, Ar-CH), 7.78 (2H, dd, *J*=5.2 Hz, 3.3 Hz, Ar-C*H*), 8.57 (1H, d, *J*=8.3 Hz, Ar-C*H*), 11.50 (1H, s, N*H*). δ_C (125 MHz, CDCl3): 21.9, 28.4, 53.4, 64.0, 77.0, 122.4, 123.7, 124.3, 125.1, 126.5, 128.4, 129.1, 129.7, 130.1, 130.7, 131.3, 132.6, 133.4, 133.8, 134.1, 135.8, 137.3, 137.6, 166.3, 197.6. ESI-LCMS found *m*/*z* 385.45 $[M+H]^+$; $C_{25}H_{25}N_2O_2$ requires 385.19. These data agree with that measured in the literature. [101]

(*S*)-({2-[1-(benzyl)benzyl)pyrrolidine-2-carboxamide]phenyl}phenylmethylene)-glycinato-*N*,*N*',*N*'',*O*}nickel (II) (Ni-Gly-2-BPB) ***5***

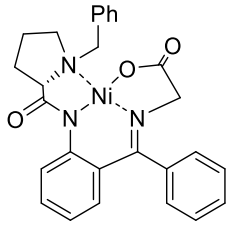

(*S*)-2-[*N*-(*N*'-benzylprolyl)amino]-benzophenone (BPB) ***4*** (5.5 g, 13.05 mmol, 1 equiv.), nickel (II) nitrate hexahydrate (4.54 g, 15.65 mmol, 1.2 equiv.) and glycine (1.95 g, 26.1 mmol, 2 equiv.) were dissolved in methanol (50 mL) at 55°C, followed by addition of NaOMe (30% w/w in methanol solution, 31.3 mL, 26.08 mL, 95.40 mmol, 7.2 equiv.). Additional methanol (120 mL) was added to dilute the mixture. After stirring for 1h, the mixture was cooled down to r.t. and glacial acetic acid (8.5 mL, 148.63 mmol, 10 equiv.) was added, followed by dilution with water (400 mL). The mixture was extracted with $CHCl_3$ (3×100 mL) and dried over Na_2SO_4, then concentrated *in vacuo* followed by a flash column chromatography ($CHCl_3$: Acetone=5:1), to give nickel complex (4) (2.57 g, 38 %) as a glassy scarlet solid. δ_H (400 MHz; $CDCl_3$) δ2.02-2.22 (2H, m, γ-C*H*$_2$), 2.45 (1H, m β-C*H*$_2$), 2.57 (1H, m, β-C*H*$_2$), 3.37 (1H, m, δ-C*H*$_2$), 3.50 (1H, dd, *J*=11.4 Hz, 5.4 Hz, α-C*H*), 3.69 (1H, d, *J*=12.5 Hz, N-C*H*$_2$), 3.71 (1H, d, *J*=20.2 Hz, C*H*$_2$), 3.72 (1H, m, δ-C*H*$_2$), 3.81 (1H, d, *J*=20.2 Hz, C*H*$_2$), 4.52 (1H, d, *J*=12.6 Hz, N-C*H*$_2$), 6.73 (1H, m, Ar-C*H*), 6.82 (1H, dd, *J*=8.2 Hz, 1.6 Hz, Ar-C*H*), 7.00 (1H, m, Ar-C*H*), 7.12 (1H, d, *J*=8.2 Hz, Ar-C*H*), 7.24 (1H, m, Ar-C*H*), 7.34 (1H, m, Ar-C*H*), 7.46 (2H, m, Ar-C*H*), 7.54 (3H, m, Ar-C*H*), 8.09 (2H, m, Ar-C*H*), 8.32 (1H, dd, *J*=8.2, 1.6 Hz, Ar-C*H*). δ_C (100 MHz, CDCl3): 23.7, 30.6, 55.8, 57.3, 61.4, 65.9, 70.0, 116.3, 120.4, 124.3, 124.6, 125.3, 125.7, 126.3, 128.9, 129.3, 129.6, 129.8, 129.9, 131.4, 132.2, 133.3, 134.2, 134.6, 142.5, 171.7, 177.3, 181.0; ESI-HRMS found *m*/*z* 520.1141 $[M+Na]^+$; $C_{27}H_{25}N_3NaNiO_3$ requires 520.1147. These data agree with that measured in the literature. [101]

(*S*)-({2-[1-benzyl)benzyl)pyrrolidine-2-carboxamide]phenyl}phenylmethylene)-(S)- pentenylglycinato}*N*,*N*',*N*'',*O*}nickel (II) (Ni-α-pent-4-enylgly-2-BPB) ***6***

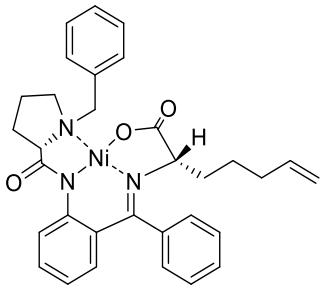

To a flask containing freshly powered NaOH (0.28 g, 6.88 mmol, 4 equiv.) and Ni-Gly complex ***5*** (1 g, 1.72 mmol, 1 equiv.), dry DMF (9 mL) was added and the mixture was stirred at 0 °C under an atmosphere of N_2 for 2 min. The ice bath was removed after 2 min, 5-iodopent-1-ene (1.2g, 5.16 mmol, 3 equiv.) was added to the mixture. The solution was stirred for 15 min at r.t. and then quenched with H_2O (10 mL). The mixture was concentrated and taken up in water (10 mL) and extracted with DCM (3×16 mL). The combined organic layers were dried over $MgSO_4$ and concentrated in vacuo. The crude product was purified using flash chromatography ($CHCl_3$: Acetone=8:1). δ_H (400 MHz; $CDCl_3$) 1.56-1.75 (2H, m, alkyl), 1.82-2.31 (7H, m, alkyl, β-CH_2, γ-CH_2), 2.41-2.59 (m, 1H, β-CH_2), 2.70-2.82 (1H, m, δ-CH_2), 3.40-3.63 (4H, m, N-CH_2, α-CH_2, δ-CH_2, β-(Gly)-CH_2), 3.91 (1H, dd, *J* = 8.1, 3.4 Hz, α-CH_2), 4.45 (1H, d, *J*=13.0 Hz, N-CH_2), 4.92-5.02 (m, 2H, CH=CH_2), 5.73 (ddt, *J* = 16.9, 10.2, 6.7 Hz, 1H, C*H*=CH_2), 6.56-6.70 (m, 2H, Ar-CH), 6.92 (d, *J* = 7.2 Hz, 1H, Ar-C*H*),7.09-7.22 (m, 2H, Ar-C*H*), 7.24-7.27 (m, 1H, Ar-C*H*), 7.35 (t, *J* = 7.6 Hz, 2H, Ar-C*H*), 7.42-7.56 (m, 3H, Ar-C*H*), 8.05 (d, *J* = 7.1 Hz, 2H, Ar-C*H*), 8.13 (d, *J* = 8.7 Hz, 1H, Ar-C*H*). δ_C (100 MHz, $CDCl_3$): 23.7, 24.6, 29.3 30.7, 33.3, 35.4 53.9, 57.0, 63.1, 70.2, 115.3, 116.2, 120.8, 123.8, 126.6, 127.2, 127.1, 127.6, 129.0, 129.7, 131.3, 132.1, 133.2, 133.8, 134.1, 137.8, 142.2, 142.8, 170.5, 179.0, 180.2. ESI-HRMS found *m*/*z* 588.1767 $[M+Na]^+$; $C_{32}H_{33}N_3NaNiO_3$ requires 588.1773. These data agree with that measured in the literature .[101]

(*S*)-2-aminohept-6-enoic acid ***7***

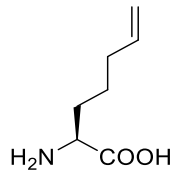

The alkylated Ni complex ***6*** (0.49 g, 0.87 mmol, 1.0 equiv.) was dissolved in methanol (25 mL) and added dropwise to a solution of hydrochloric acid (3 M, 7 mL). The mixture was heated to 70 °C until a colour change from scarlet to yellow/green was observed (after 15 min), then cooled to rt and the solvent was evaporated *in vacuo*. The resulting yellow/white residue was taken up with water (20 mL) extracted with chloroform (3 x 25 mL) to remove the BPB ligand ***4*** for re-use. The aqueous fraction was loaded on an activated Dowex 50X2 100 H+ column (prewashed with H_2O to pH 7), which was then rinsed with methanol (50 mL) and water (50 mL) to remove residual nickel. The amino acid ***7*** was then eluted with 20% ammonium hydroxide:ethanol 1:1, and fractions containing ***7*** were identified by ninhydrin staining. Concentration of the fractions *in vacuo* afforded (*S*)-2-amino-hept-6-enoic acid (6) (118 mg, 62%) as a white, amorphous solid.

δ_H (400 MHz; D_2O) δ1.32-1.56 (2H, m, $CH_2CH_2CH_2$), 1.70-1.87 (2H, m, $CHCH_2CH_2$), 2.04 (2H, q, J=7.2 Hz, $CH_2CH{=}CH_2$), 3.65 (1H, t, *J*=5.9 Hz, β-CH_2), 4.95 (1H, d, *J*=10.3 Hz, CH=CH_2 *cis*), 5.01 (1H, d, *J*=17.3 Hz, CH=CH_2 *trans*), 5.80 (1H, ddt, *J*=17.0, 10.3, 6.6 Hz, $CH{=}CH_2$). δ_C (100 MHz, CDCl3): 23.4, 29.4, 32.4, 53.7, 115.1, 138.4, 174.9 ESI-HRMS found *m*/*z* 144.1018 $[M+H]^+$; $C_7H_{14}NO_2$ requires 144.1025. These data agree with that measured in the literature.[101]

(*S*)-2-((((9H-fluoren-9-yl)methoxy)carbonyl)amino)hept-6-enoic acid ***8***

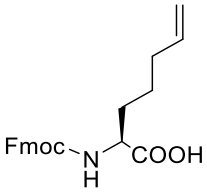

(*S*)-2-amino-hept-6-eneoic acid ***7*** (186 mg, 1.30 mmol, 1 equiv.) and DIPEA (452 µL, 2.59 mmol, 2 equiv.) were dissolved in water (4 mL) and cooled to 4 °C. 9-fluorenylmethyl succinimidyl carbonate (657 mg, 1.95 mmol, 1.5 equiv.) was dissolved in ACN (8 mL) at 4 °C and added dropwise to the amino acid aqueous solution. After 1 h, the reaction was warmed to rt and allowed to

continue for a further 23 h. The reaction suspension was concentrated *in vacuo* and then taken up with water (15 mL) and extracted with ethyl acetate (2 × 25 mL). The organic layers were back-extracted with saturated sodium hydrogen carbonate solution (20 mL). The combined aqueous fractions were acidified to pH 1 with 3M hydrochloric acid and extracted with ethyl acetate (3 × 35 mL). The combined organic fractions were dried (Na_2SO_4) and concentrated *in vacuo* to afford a yellow oil. Purification by flash chromatography (Dichloromethane:methanol:acetic acid 95:4:1) afforded (*S*)-2-((((9H-fluoren-9yl)methoxy)carbonyl)amino)hept-6-enoic acid ***8*** as a viscous, straw coloured oil (260 mg, 53%). δ_H (400 MHz; DMSO-d_6) 1.46 (2H, m, NHCHC*H*$_2$CH$_2$CH$_2$CH=CH$_2$), 1.56-1.85 (2H, m, NHCHCH$_2$C*H*$_2$CH$_2$CH=CH$_2$), 1.96-2.18 (2H, m, NHCHCH$_2$CH$_2$C*H*$_2$CH=CH$_2$), 3.91-4.02 (1H, m, NHC*H*COOH), 4.26 (1H, m, CO$_2$CH$_2$C*H*), 4.29-4.36 (2H, m, NHCO$_2$C*H*$_2$), 5.02 (2H, m, CH=C*H*$_2$), 5.82 (1H, m, C*H*=CH$_2$), 7.29-7.98 (8H, H_{Fmoc}), 12.57 (1H, s, N*H*). δ_C (100 MHz, DMSO-$_{d6}$): 28.3, 33.6, 35.3, 57.2, 68.2, 113.8, 121.0, 123.5, 128.0, 128.8, 135.1, 139.0, 142.3, 144.4, 155.0, 177.1; ESI-HRMS found *m*/*z* 366.1702 $[M+H]^+$, $C_{22}H_{24}NO_4$ requires 366.1705. These data agree with that measured in the literature . [101]

(*S*)-1-(2-Fluorobenzyl)pyrrolidine-2-carboxylic acid ***9***

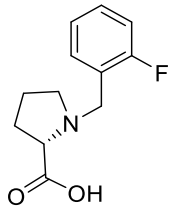

To a flask containing potassium hydroxide (14.6 g, 260.7 mmol, 3 equiv.), iPrOH (100 mL) was added and the mixture was heated to 40 °C, followed by addition of $_L$-Proline (10.0 g, 86.9 mmol, 1 equiv.) and dropwise addition of 2-Fluorobenzyl bromide (10.5 mL, 86.9 mmol, 1 equiv.) White and yellow precipitate was observed and the mixture was stirred at 40 °C for 24 h. The reaction was monitored by TLC. Then aqueous HCl (16 mL) was added to the mixture until the solution reached pH 6 (as determined using pH paper). The resulting suspension was cooled down in ice bath and filtered. The filtrate was dried in vacuo to give (*S*)-1-(2-Fluorobenzyl)pyrrolidine-2-carboxylic acid ***9*** (18.0 g, 92 %) as a yellow solid (Rf=0.45, MeOH:DCM=1:4). δ_H (400 MHz; $CDCl_3$) δ1.87-2.08 (2H, m, γ-C*H*$_2$), 2.15-2.46 (2H, m, β-C*H*$_2$), 2.90-3.10 (1H, m, δ-C*H*$_2$), 3.64-3.78 (1H, m, δ-C*H*$_2$), 3.89 (1H, dd, *J*=9.2, 6.3 Hz, α-C*H*), 4.39 (1H, d, *J*=13.2, N-C*H*$_2$), 4.48 (1H, d, *J*=13.2 Hz, N-C*H*$_2$), 7.11 (1H, dt, *J*=13.0, 7.5

Hz, Ar-C*H*), 7.14-7.21 (1H, m, Ar-C*H*), 7.32-7.43 (1H, m, Ar-C*H*), 7.62 (td, *J*=7.5, 1.5Hz, Ar-C*H*). δ_C (100 MHz; $CDCl_3$): 23.1, 28.9, 50.9, 53.5, 66.7, 115.9, 116.1 119.4, 125.0, 131.9, 133.8, 160.5; ESI-LCMS found *m*/*z* 223.93 $[M+H]^+$, $C_{12}H_{15}FNO_2$ requires 224.11. These data agree with that measured in the literature.[265]

(*S*)-*N*-(2-Benzoylphenyl)-1-(2-fluorobenzyl)pyrrolidine-2-carboxamide ((2*S*)-FBPB) ***10***

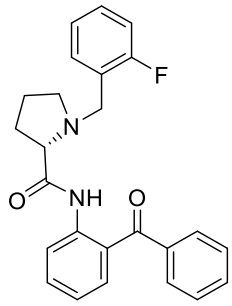

To a flask containing (*S*)-1-(2-Fluorobenzyl)pyrrolidine-2-carboxylic acid (8) (18 g, 80.4 mmol, 1 equiv.), DCM (200 mL) was added, followed by addition of *N*-methylimidazole (14.0 mL, 177.6 mmol, 2.2 equiv.). Then MsCl (6.0 mL, 80.4 mmol, 1 equiv.) was added dropwise at 0°C. After 5 min, 2-aminobenzophenone (14.4 g, 72.6 mmol, 0.9 equiv.) was added and the ice-bath was removed. The reaction mixture was heated to 50 °C and stirred for 16 h. Then the mixture was cooled down and saturated $NaHCO_3$ solution (200mL) was added. The organic phase was separated, and the aqueous phase was extracted with CH_2Cl_2 (3×100mL). The combined organic layers were dried over Na_2SO_4, concentrated *in vacuo* and purified by flash column chromatography (Hexane:EtOAc=4:1) to afford yellow oil (7.75 g, 24%). δ_H (400 MHz; $CDCl_3$) δ 1.71-1.86 (2H, m, γ-CH_2), 1.95 (1H, m, β-CH_2), 2.24 (1H, m, β-CH_2), 2.46 (1H, m, δ-CH_2), 3.23 (1H, m, δ-CH_2)3.35 (1H, dd, *J*=10.2, 4.6 Hz, α-C*H*), 3.73 (1H, d, *J*=13.2 Hz, N-CH_2), 3.89 (1H, d, *J*=13.2 Hz, N-CH_2), 6.78 (1H, dd, J=9.7, 8.6 Hz, Ar-C*H*), 6.92 (1H, td, *J*=7.5, 1.0 Hz, Ar-C*H*), 7.03-7.15 (2H, m, Ar-C*H*), 7.41-7.56 (5H, m, Ar-C*H*), 7.56-7.64 (1H, m, Ar-C*H*), 7.75 (2H, dd, *J*=5.2, 3.2 Hz, Ar-C*H*), 8.54 (1H, d, *J*=8.3 Hz, Ar-C*H*), 11.40 (1H, s, N*H*). δ_C (100 MHz; $CDCl_3$): 24.2, 31.0, 52.0, 53.7, 67.9, 115.0, 115.3, 121.5, 122.3, 123.9, 124.2, 124.8, 125.0, 125.6, 128.3, 128.9, 129.3, 130.1, 131.7, 132.5, 133.3, 138.6, 139.0, 174.5, 197.9. ESI-LCMS found *m*/*z* 403.34 $[M+H]^+$, $C_{25}H_{24}FN_2O_2$ requires 403.18. These data agree with that measured in the literature.[265]

(*S*)-({2-[1-(2-Fluorobenzyl)benzyl)pyrrolidine-2-carboxamide]phenyl}phenylmethylene)-glycinato-*N*,*N*',*N*'',*O*}nickel (II) (Ni-Gly-2-FBPB) ***11***

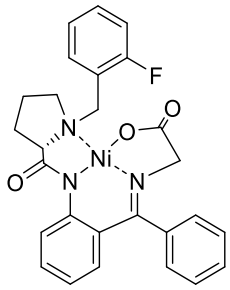

To a flask containing a solution of (2*S*)-FBPB ***10*** (4.0g, 9.96 mmol, 1 equiv.), $Ni(NO_3)_2 \cdot 6H_2O$ (5.9 g, 20 mmol, 2 equiv.), glycine (1.6 g, 20 mmol, 2 equiv.) in methanol (100 mL) and freshly powdered KOH (4 g, 70 mmol, 7 equiv.) was added. The mixture was heated to 70 °C and stirred for 1 h. The mixture was then cooled down and concentrated in vacuo. The resulting residue was taken up in water (100 mL) and extracted with EtOAc (3×100 mL). The combined organic layers were washed with saturated brine solution (3×200 mL), dried over $MgSO_4$ and concentrated in vacuo to afford ***11*** as a scarlet solid (4.0 g, 78 %). δ_H NMR (400 MHz; $CDCl_3$) 2.02-2.21 (2H, m, γ-CH_2), 2.47 (1H, m, β-CH_2), 2.66 (1H, m, β-CH_2), 3.27-3.40 (1H, m, δ-CH_2), 3.66 (1H, dd, *J*=17.8, 10.6 Hz, α-CH_2), 3.72-3.82 (1H, m, δ-CH_2), 3.93 (1H, d, *J*=13.0 Hz, N-CH_2), 4.48 (1H, d, J=13.0 Hz, N-CH_2), 6.72 (1H, ddd, *J*=8.2, 7.0, 1.1 Hz, Ar-C*H*), 6.82 (1H, dd, *J*=8.2, 1.6 Hz, Ar-C*H*), 6.93-7.04 (1H, m, Ar-C*H*), 7.11 (1H, td, *J*=8.4, 1.5 Hz, Ar-C*H*), 7.18-7.25 (2H, m, Ar-C*H*), 7.29-7.39 (2H, m, Ar-C*H*), 7.42-7.59 (3H, m, Ar-C*H*), 8.22-8.39 (2H, m, Ar-C*H*). δ_C NMR (100 MHz; $CDCl_3$): 23.7, 30.7, 55.8, 57.3, 61.4, 70.1, 116.1, 116.3, 120.4, 121.0, 124.6, 125.3, 125.7, 126.3, 129.4, 129.7, 129.8, 131.4, 131.5, 132.3, 133.3, 134.2, 134.6, 142.5, 171.7, 177.3, 181.0. ESI-HRMS found *m*/*z* 516.1155 $C_{27}H_{24}N_3O_3FNi$ [M+H]+ requires 516.1241. These data agree with that measured in the literature.[265]

(*S*)-({2-[1-(2-Fluorobenzyl)benzyl)pyrrolidine-2-carboxamide]phenyl}phenylmethylene)-(*S*)- pentenylglycinato-*N*,*N*',*N*'',*O*}nickel (II) (Ni-α-pent-4-enylgly-2-FBPB) ***12***

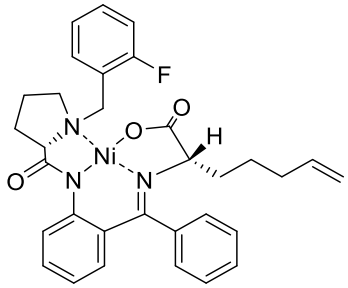

To a flask containing freshly powered NaOH (0.28 g, 6.88 mmol, 4 equiv.) and Ni-Gly complex (10) (1 g, 1.72 mmol, 1 equiv.), dry DMF (9 mL) was added and the mixture was stirred at 0 °C under an atmosphere of N_2 for 2 min. The ice bath was removed after 2 min, 5-iodopent-1-ene (1.2g, 5.16 mmol, 3 equiv.) was added to the mixture. The solution was stirred for 15 min at r.t. and then quenched with H_2O (10 mL). The mixture was concentrated and taken up in water (10 mL) and extracted with DCM (3×16 mL). The combined organic layers were dried over $MgSO_4$ and concentrated in vacuo. The crude product was purified using flash chromatography ($CHCl_3$: Acetone=8:1), to give a red oil (0.8 g, 70%). δ_H (400 MHz; $CDCl_3$) 1.57-1.76 (2H, m, alkyl), 1.85-2.35(6H, m, alkyl, γ-C*H*$_2$), 2.48-2.63 (1H, m, β-C*H*$_2$), 2.83 (1H, dd, *J*=9.2, 5.7 Hz, β-C*H*$_2$), 3.36-3.67 (3H, m, α-C*H*$_2$, δ-C*H*$_2$, C*H*$CH_2CH_2CH_2CH=CH_2$), 3.84 (1H, d, *J*=13.0 Hz, N-C*H*$_2$), 3.90 (1H, dd, *J*=8.0, 3.5 Hz, α-C*H*$_2$), 4.44 (1H, d, *J*=13.0 Hz, N-C*H*$_2$), 4.97 (2H, m, CH=C*H*$_2$), 5.72 (1H, ddt, *J*=17.0, 10.2, 6.7 Hz, C*H*=CH_2), 6.61-6.71 (2H, m, Ar-C*H*), 6.92 (1H, d, *J*=7.5 Hz, Ar-C*H*), 7.04 (1H, dd, *J*=10.9, 6.6 Hz, Ar-C*H*), 7.16 (2H, ddd, *J*=8.3,4.8, 2.3 Hz, Ar-C*H*), 7.19-7.25 (2H, m, Ar-C*H*), 7.37-7.56 (3H, m, Ar-C*H*), 8.16 (1H, d, *J*=8.5 Hz, Ar-C*H*), 8.31 (1H, td, *J*=7.4, 1.6 Hz, Ar-C*H*). δ_C (100 MHz, $CDCl_3$): 23.6, 24.7, 30.3 30.7, 33.3, 34.9 56.5, 57.0, 63.1, 70.2, 115.3, 120.8, 123.7, 126.5, 127.2, 127.6, 128.9, 129.1, 129.7, 131.6, 132.1, 133.2, 133.6, 133.8, 134.1, 137.8, 142.2, 142.8, 170.9, 179.4, 180.4. ESI-HRMS found *m*/*z* 584.1808 $C_{32}H_{33}N_3O_3FNi$ [M+H]+ requires 584.1789. These data agree with that measured in the literature.[265]

The alkylated Ni complex ***12*** (0.49 g, 0.87 mmol, 1.0 equiv.) was dissolved in methanol (25 mL) and added dropwise to a solution of hydrochloric acid (3 M, 7 mL). The mixture was heated to 70 °C until a colour change from scarlet to yellow/green was observed (after 15 min), then cooled to rt and the solvent was evaporated *in vacuo*. The resulting yellow/white residue was taken up with water (20 mL) extracted with chloroform (3 x 25 mL) to remove the FBPB ligand ***10*** for re-use. The aqueous fraction was loaded on an activated Dowex 50X2 100 H+ column (prewashed with H_2O to pH 7), which was then rinsed with methanol (50 mL) and water (50 mL) to remove residual nickel. The amino acid ***7*** was then eluted with 20% ammonium hydroxide:ethanol 1:1, and fractions

containing ***7*** were identified by ninhydrin staining. Concentration of the fractions *in vacuo* afforded (*S*)-2-amino-hept-6-enoic acid ***7*** (118 mg, 62%) as a white, amorphous solid. See characterisation above.

tert-butyl-2-(((1*R*,2*R*,5*R*,*E*)-2-hydroxy-2,6,6-trimethylbicyclo[3.1.1]heptan-3-ylidene)amino)acetate ***13***

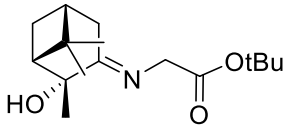

To a flask containing glycine *tert*-butylester hydrochloride (1.5 g, 9 mmol, 1.5 equiv.), toluene (50 mL) was added followed by addition of triethylamine (1.85 mL, 9 mmol, 1.5 equiv.), then the suspension was stirred for 1.5 h. After removal of triethylammonium chloride by filtration, (1*R*, 2*R*, 5*R*)-2-hydroxy-3-pinanone (1 g, 5.98 mmol, 1 equiv.) was added to the free amine solution. After addition of boron trifluoride diethyl ether (0.1 mL) the mixture was heated to 130 °C. Water that formed during the reaction was removed with a Dean–Stark trap. The reaction was monitored using TLC (hexane:EtOAc=7:3, Rf (product)=0.34). Flash chromatography (Hexane:EtOAc=7:3 containing 1% TEA) gave the title compound as a yellowish oil (0.80 g, 48%). δ_H (400 MHz; $CDCl_3$) δ0.80 (3H, s, C$H_{3bridge}$), 1.26 (3H, s, C$H_{3bridge}$), 1.42 (9H, s, C(CH_3)$_3$), 1.45 (3H, s, C(OH)CH_3), 1.84-2.05 (3H, m, CH_2CHC(OH)), 2.21-2.33 (1H, m, CHCH$_2$CN), 2.34-2.49 (2H, m, CH$_2$CN), 4.01 (2H, d, *J*=1.1 Hz, CNCH_2). ESI-LCMS found *m*/*z* 282.28 $[M+H]^+$, $C_{16}H_{28}NO_3$ requires 282.21. These data agree with that measured in the literature.[265]

tert-butyl (*S*)-2-(((1*R*,2*R*,5*R*,*E*)-2-hydroxy-2,6,6-trimethylbicyclo[3.1.1]heptan-3-ylidene)amino)hept-6-enoate ***14***

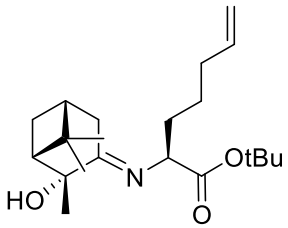

To a solution of diisopropylamine (1mL, 7.13 mmol, 2.5 equiv.) in dry THF (18 mL), the solution of n-butyllithium (4.3 mL of 1.6M in hexane, 7.13 mmol, 2.5 equiv.) was added dropwise at -78 °C (dry ice/acetone). Then the solution of compound ***13*** (0.80 g, 2.85 mmol, 1 equiv.) in dry THF (4 mL) was added to the

cold mixture. After 30 min, 5-bromo-pent-1-ene (0.6 mL, 5.13 mmol, 1.8 equiv.) was added at -78°C. The low temperature was kept for 6 h by addition of fresh dry ice and then the reaction mixture was left stirring overnight. The reaction was quenched by a saturated NH_4Cl solution (30 mL) and then TLC was used to monitor the reaction (Hexane: EtOAc=9:4, Rf (product)=0.71). The solvents were concentrated under 140 Torr at 40°C and then the aqueous layer was extracted with EtOAc (3×50 mL). The organic layer was dried over Mg_2SO_4. After concentration, the crude product was purified by flash chromatography on silica (hexane: EtOAc=4:1 containing 1% TEA), to afford a colourless oil (0.48 g, 48%). δ_H (400 MHz; $CDCl_3$) 0.82 (3H, s, C$H_{3bridge}$), 1.32 (2H, m, CH_2CHCH_2), 1.33 (3H, s, C$H_{3bridge}$), 1.42 (9H, s, C(CH_3)$_3$), 1.46 (3H, s, C(OH)CH_3), 1.78-1.97 (2H, m, CH_2=CHCH_2CH_2CH_2), 1.99-2.13 (4H, m, C(OH)CHCH_2 and CH_2=CHCH_2), 2.26-2.38 (1H, m, C(OH)C*H*), 2.45-2.64 (2H, m, NCCH_2), 4.06 (1H, dd, *J*=8.5, 4.8 Hz, NC*H*CO_2tBu), 4.98 (2H, m, CH_2=CH), 5.79 (1H, ddt, *J*=16.9, 10.2, 6.6 Hz, CH_2=C*H*). ESI-LCMS found *m*/*z* 350.52 $[M+H]^+$, $C_{21}H_{36}NO_3$ requires 350.27. The values agree with the values in the reference.[266]

tert-butyl (*S*)-2-((((9H-fluoren-9-yl)methoxy)carbonyl)amino)hept-6-enoate ***15***

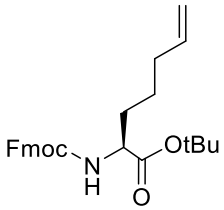

Precursor ***14*** (0.48 g, 1.37 mmol, 1 equiv.) was dissolved in THF (3 mL) followed by addition of a solution of citric acid (15 % in water, 8.2 mL). The mixture was stirred at r.t. for 4 days monitored by LCMS. After removing THF in vacuo (140 Torr at 40°C), the aqueous layer was extracted with diethyl ether (3×15 mL) to remove the ketone. Then, the pH was increased to 8-9 with K_2CO_3 anhydrous (2.5 g). The free amine was then extracted with EtOAc (20 mL × 3 times). The organic layer was concentrated at 30 ° C under 100 Torr. Then the oil was dissolved in EtOAc (6.5 mL) and Fmoc-OSu (0.60 g, 1.78 mmol, 1.3 equiv.) and DIPEA (478 µL, 2.74 mmol, 2 equiv.) were added. The mixture was stirred overnight. Solvents were removed in vacuo followed by flash chromatography of the residue (Hexane:EtOAc=4:1) to give Fmoc-protected amino acid precursor ***15*** as a colorless oil (0.30 g, 0.69 mmol, 52 % two steps). δ_H NMR (400 MHz; $CDCl_3$) δ 1.48 (9H, s, OC(CH_3)$_3$), 1.59-1.92 (2H, m, CH_2=CHCH_2CH_2CH_2), 1.95-2.17 (2H, m, CH2=CHCH_2CH_2CH_2), 4.25 (2H, m,

$CO_2CH_2CH_{(Fmoc)}$ and NHC*H*), 4.39 (2H, d, J=6.9 Hz, $CO_2CH_{2\ Fmoc}$), 4.87-5.09 (2H, m, CH_2=CH), 5.66-5.86 (1H, m, CH_2=C*H*), 7.29-7.85 (8H, H_{Fmoc}). ESI-HRMS found *m*/*z* 444.2147 $[M+Na]^+$, $C_{26}H_{31}NNaO_4$ requires 444.2151.The values agree with the values in the reference. [266]

Compound ***15*** (300 mg, 0.71 mmol, 1 equiv.) was dissolved in DCM (3 mL), followed by addition of TFA (3 mL) and the reaction mixture was stirred for 1 h. The reaction was monitored by TLC. The mixture was then concentrated *in vacuo* and loaded on a silica gel column after being dissolved in the following mobile phase (3mL). After a flash chromatography (EtOAc: toluene: Acetic acid=2:17:1), the product was dried *in vacuo* and then freeze dried ($MeOH/H_2O$, 2 mL/2 mL) to give ***8*** as a white solid (180 mg, 70.4 %). See characterisation above.

6.4 Protein expression

The pET28a HIS-SUMO BCL-x_L (1-198, missing 26-81) was over-expressed in the E. coli strain BL21 (DE3) and the pET28a HIS-SUMO MCL-1 (172-327) was over-expressed in the E. coli strain Rosetta 2. 10 ml of overnight culture was used to inoculate 1 L LB media containing 100 µg mL^{-1} Ampicillin. Cultures were being shaken at 37 °C until OD600 ~ 0.6 – 0.8, thereafter the protein expression was induced by the addition of 0.1 mM IPTG and the induced cultures were grown at 18 °C overnight. After harvesting by centrifugation, cells were resuspended in 25 mM Tris, 500 mM NaCl, pH 8.0 solution and lysed using sonication. The lysate was spun down and the supernatant was filtered before applied to a 5mL HisTrap column. The HisTrap was then washed with 10 CV of 25 mM Tris, 500 mM NaCl, 15 mM imidazole, pH 8.0 solution followed by elution with 25 mM Tris, 500 mM NaCl, 300 mM imidazole, pH 8.0 solution. The His-SUMO tag was cleaved in overnight dialysis (25 mM Tris, 250 mM NaCl, pH 8.0) at 4 °C with presence of Smt3 protease, Ulp1. Uncleaved materials and residual HIS-SUMO tag were removed by reapplication to a HisTrap and the flow-through was collected and further purified using a Superdex 75 SEC system (GE healthcare; Chicago, IL, USA).

6.5 Circular dichroism spectroscopy

The peptides were dissolved in phosphate buffer (peptide concentration: 15-50 μM, 20 mM phosphate, 100 mM NaCl, pH 7.4) to a final concentration of 50 μM. The CD spectra were obtained on a Chirascan circular dichroism spectrometer (Applied Photophysics, UK), at 20 °C, using a 1 mm quartz cuvette. The parameters were set as follows: wavelength 195-260 nm, scan speed 5 nm· min^{-1}, step resolution 1 nm. The spectra were averaged over triplicates after subtracting buffer baselines. The percentages of helicity were calculated based on the mean residue ellipticity at 222 nm using the following equation:

$$f = \frac{[\theta]_{222} - [\theta]_0}{[\theta]_{max} - [\theta]_0} \quad (1)$$

Where $[\theta]_{222}$ is the observed residue ellipticity at 222 nm and calculated using: $[\theta]_{222}=1/n\cdot[\theta]_{obs}/(10\cdot l\cdot C)$, where n = number of residues; $[\theta]_{obs}$ = measured value in mdeg; C = sample concentration (mol/L); l = path length of the cuvette in cm. $[\theta]_0$ is the mean residue ellipticity of a random coiled peptide and calculated by (2220-53T). $[\theta]_{max}$ is the theoretically maximum mean residue ellipticity of a n-mer helical peptide and equals to $[\theta]_\infty \cdot (n-3)/n$, where $[\theta]_\infty$ equals to (-44000 + 250T) (T is the temperature of peptide solutions in Celsius; 20 °C was used in the calculations in this study).

6.6 Fluorescence anisotropy assays

Fluorescence anisotropy assays were performed using 384-well plates (Greiner Bio-one, UK). Each assay was performed in triplicates and fluorescence anisotropy was measured using an EnVisionTM 2103 MultiLabel plate reader (Perkin Elmer; Waltham, MA, USA). Excitation wavelength of 480 nm (30 nm bandwidth) and emission wavelength of 535 nm (30 nm bandwidth) were used for the FAM labelled peptides. All assays were performed in 20mM Tris, 150 mM NaCl, pH 7.6 solutions. Fluorescence anisotropy data were processed and analysed as previously described.[239] Briefly, the measured data of the P (perpendicular intensity) and S (parallel intensity) channels were subtracted by the corresponding control wells, and used to calculate the intensity and anisotropy using the following equations:

$$I = (2PG) + S \quad (2)$$

$$r = (S - PG) \quad (3)$$

$$L_b = \frac{r - r_{min}}{\lambda(r_{max} - r) + r - r_{min}} \quad (4)$$

$$y = \frac{(k + x + [FL]) - \sqrt{(k + x + [FL]^2 - 4 \times x \times [FL])}}{2} \quad (5)$$

$$y = r_{max} + \frac{r_{min} - r_{max}}{1 + (x/x_0)^p} \quad (6)$$

Where I = total intensity; P = perpendicular intensity; S = parallel intensity; G = instrument factor which was set to 1.1 for all assays; r = anisotropy; L_b = ligand bound fraction; λ = 1, [FL] = fluorescent ligand concentration; k = K_d; y = L_b × Flu-trimer and x = added protein concentration. For analysis of direct titration FA assays, equations (3), (4) and (5) were used to calculate K_d values. For competition FA assays, the average anisotropy and the average standard deviation of the values derived from equation (2) were calculated and fit to a sigmoidal logistic model (equation (6)) using Origin 2021.

6.7 Proteolysis

Each peptide was dissolved in Tris buffer (20 mM Tris, 150 mM NaCl, pH 7.5) to a final concentration of 150 μM. α-chymotrypsin or trypsin was prepared as a stock solution of 600 nM and added to the peptide solutions (n/n=1/25000). Then the mixtures were incubated at 37 °C, with aliquots removed after 0, 5, 15, 30, 60, and 90 min. Test samples were quenched in the same volume of acetonitrile containing 2% TFA. All assays were repeated three times. The HPLC analysis was performed on an Agilent 1290 Infinity II HPLC analytical system (20 μL injection, 0.5 mL min-1 flow rate, 5-95% acetonitrile:water gradient, 10 min run time). The HPLC time points were converted into a percentage of the original substrate (S), and plotted as a natural logarithm (lnS) against time (t) in minutes. Half-lives ($t_{1/2}$) were calculated by dividing –ln(2) by the slope of the graph, plotted in Origin 2021.

6.8 MS data for all peptides

Table 6-3 Peptide characterisation data

Peptide	Sequence[a]	$Mass_{exp}$	$[M+4H]4^{+}_{Exp}$	$[M+4H]^{4+}_{Obs}$[b]
BAD-25mer	Ac-N**L**WAAQR**Y**GRE**LR**RMSDE**F**VDS**F**KK-NH_2	3142.5883	786.6470	786.9078
BAD-19mer	Ac-R**Y**GRE**LR**RMSDE**F**VDS**F**KK-NH_2	2459.2492	820.7497	821.0944
FAM-Ahx-BAD	FAM-Ahx-R**Y**GRE**LR**RMSDE**F**VDS**F**KK-NH_2	2888.6772	963.8924	964.1346
BADL1	Ac-**C**Y**C**GR**C****LR**RMSDE**F**VDS**F**KK-NH_2	2380.1239	596.0310	595.7872
BADS1	Ac-***C***Y**C**GR***C*****LR**RMSDE**F**VDS**F**KK-NH_2	2473.1649	619.2912	619.5359
BADL2	Ac-R**Y****C**RE**L****C**RMSDE**F**VDS**F**KK-NH_2	2452.1450	614.0363	614.2955
BADS2	Ac-R**Y*****C***RE**L*****C***RMSDE**F**VDS**F**KK-NH_2	2545.1860	637.2965	637.5424
BADL3	Ac-R**Y**G**C**E**LR****C**MSDE**F**VDS**F**KK-NH_2	2353.0653	589.2663	589.5262
BADS3	Ac-R**Y**G***C***E**LR*****C***MSDE**F**VDS**F**KK-NH_2	2446.1063	612.5266	612.7714
BADL4	Ac-R**Y**GRE**L****C**RMS**C**E**F**VDS**F**KK-NH_2	2394.1395	599.5349	599.7952
BADS4	Ac-R**Y**GRE**L*****C***RMS***C***E**F**VDS**F**KK-NH_2	2487.1805	622.7951	623.0417
BADL5	Ac-R**Y**GRE**LR****C**MSD**C****F**VDS**F**KK-NH_2	2380.1239	596.0310	596.2914
BADS5	Ac-R**Y**GRE**LR*****C***MSD***C*****F**VDS**F**KK-NH_2	2473.1649	619.2912	619.5357

BADL6	Ac-R**Y**GRE**LR**RM**C**DE**F**C**D**S**F**KK-NH_2	2479.1671	620.7918	621.0528
BADS6	Ac-R**Y**GRE**LR**RM***C***DE**F*****C**DS**F**KK-NH_2	2572.2081	644.0520	644.2964
BADL7	Ac-R**Y**GRE**LR**RMS**C**E**F**V**C**S**F**KK-NH_2	2435.2137	609.8034	610.0643
BADS7	Ac-R**Y**GRE**LR**RMS***C***E**F**V***C***S**F**KK-NH_2	2528.2547	633.0637	633.7970
BADL8	Ac-R**Y**GRE**LR**RMSD**C**F**V**D**C**F**KK-NH_2	2449.1929	613.2982	613.5583
BADS8	Ac-R**Y**GRE**LR**RMSD***C***F**V**D***C***F**KK-NH_2	2542.2339	636.5585	636.8055
HRK-wt	Ac-SAAQLTAAR**LK**A**L**GDE**L**HQRTMW-NH_2	2607.3704	652.8499	652.8517
FAM-Ahx-HRK	FAM-Ahx-SAAQLTAAR**LK**A**L**GDE**L**HQRTMW-NH_2	3036.4916	760.1302	760.1298
HRKC1	Ac-S**C**AQL**C**AAR**LK**A**L**GDE**L**HQRTMW-NH_2	2641.3040	661.3333	661.3392
HRKS1	Ac-S***C***AQL***C***AAR**LK**A**L**GDE**L**HQRTMW-NH_2	2734.2890	684.5795	684.5794
HRKC2	Ac-SA**C**QLT**C**AR**LK**A**L**GDE**L**HQRTMW-NH_2	2671.3145	668.8359	668.8351
HRKS2	Ac-SA***C***QLT***C***AR**LK**A**L**GDE**L**HQRTMW-NH_2	2764.2996	692.0822	692.0828
HRKC3	Ac-SAA**C**LTA**C**R**LK**A**L**GDE**L**HQRTMW-NH_2	2614.2931	654.5805	654.5808
HRKS3	Ac-SAA***C***LTA***C***R**LK**A**L**GDE**L**HQRTMW-NH_2	2707.2781	677.8268	677.8312
HRKC4	Ac-SAAQLTA**C**R**LK****C****L**GDE**L**HQRTMW-NH_2	2671.3145	668.8359	668.8340
HRKS4	Ac-SAAQLTA***C***R**LK*****C*****L**GDE**L**HQRTMW-NH_2	2764.2996	692.0822	692.0828
HRKC5	Ac-SAAQLTAAR**LK****C****L**GD**C****L**HQRTMW-NH_2	2613.3090	654.3345	654.3304

HRKS5	Ac-SAAQLTAARLK*C*LGD*C*LHQRTMW-NH_2	2706.2941	677.5808	677.5816
HRKC6	Ac-SAAQLTAARLKALCDELCQRTMW-NH_2	2619.3084	655.8344	NO
HRKS6	Ac-SAAQLTAARLKAL*C*DEL*C*QRTMW-NH_2	2712.2935	679.0806	679.0731
HRKC7	Ac-SAAQLTAARLKALGCELHCRTMW-NH_2	2570.3032	643.5831	643.5839
HRKS7	Ac-SAAQLTAARLKALG*C*ELH*C*RTMW-NH_2	2663.2883	666.8294	666.8301
HRKC8	Ac-SAAQLTAARLKALGDCLHQCTMW-NH_2	2528.2450	633.0685	NO
HRKS8	Ac-SAAQLTAARLKALGD*C*LHQ*C*TMW-NH_2	2621.2301	656.3148	656.2970
HRKC9	Ac-SAAQLTAARLKALGDELCQRTCW-NH_2	2545.2894	637.3296	637.3299
HRKS9	Ac-SAAQLTAARLKALGDEL*C*QRT*C*W-NH_2	2638.2744	660.5759	660.5749
HRKC10	Ac-SAAQLTAARLCALGCELHQRTMW-NH_2	2570.2668	643.5740	643.5721
HRKS10	Ac-SAAQLTAARL*C*ALG*C*ELHQRTMW-NH_2	2663.2519	666.8203	NO
HRKC4-DCys	Ac-SAAQLTAcRLKcLGDELHQRTMW-NH_2	2671.3145	668.8359	668.8338
HRKS4-DCys	Ac-SAAQLTA*c*RLK*c*LGDELHQRTMW-NH_2	2764.2996	692.0822	692.0839
HRKC4-hCys	Ac-SAAQLTAhCRLKhCLGDELHQRTMW-NH_2	2699.3458	675.8437	675.8429
HRKS4-hCys	Ac-SAAQLTA*hC*RLK*hC*LGDELHQRTMW-NH_2	2792.3309	699.0900	699.0923
HRKC4-ChC	Ac-SAAQLTACRLKhCLGDELHQRTMW-NH_2	2792.3309	672.3398	672.3414
HRKS4-ChC	Ac-SAAQLTA*C*RLK*hC*LGDELHQRTMW-NH_2	2778.3153	695.5861	695.5810

HRKS4-xylene	Ac-SAAQLTA*C*R**LK***C***L**GDE**L**HQRTMW-NH_2	2773.3615	694.3476	694.3483
HRKL4-hydrocarbon	Ac-SAAQLTAmS5R**LK**mS5**L**GDE**L**HQRTMW-NH_2	2715.4643	679.8733	679.8750
HRKS4-hydrocarbon	Ac-SAAQLTA***mS5***R**LK*****mS5*****L**GDE**L**HQRTMW-NH_2	2687.4330	672.8655	672.8670
HRK-S	Ac-SAAQLTAAR**LK**A**L**GDE**L**HQ-NH_2	2033.1018	509.2827	NO
HRK-1	Ac-SAAQL**Y**AAR**LK**A**L**GDE**L**HQ-NH_2	2095.1174	524.7866	524.7868
HRK-2	Ac-SAAQL**Y**AAR**LK**A**L**GDE**F**HQ-NH_2	2129.1018	533.2827	NO
HRK-3	Ac-SAAQL**Y**AAR**LK**AZGDE**F**HQ-NH_2	2129.1018	533.2827	NO
HRK-4	Ac-SAAQL**L**AAR**LK**A**L**GDE**L**HQ-NH_2	2045.1382	512.2918	NO
HRK-5	Ac-SAAQL**L**AAR**LK**A**F**GDE**F**HQ-NH_2	2113.1069	529.2840	NO
HRK-hybrid	Ac-SAAQL**Y**AAR**LK**A**F**GDE**F**HQ-NH_2	2163.0861	541.7788	NO
HRKC4H	Ac-SAAQL**Y**A**C**R**LK****C****F**GDE**F**HQ-NH_2	2227.0303	557.7648	NO
HRKS4H	Ac-SAAQL**Y**A***C***R**LK*****C*****F**GDE**F**HQ-NH_2	2320.0154	581.0111	NO
Beclin-1-wt	Ac-T**M**EN**L**SRR**LK**VTGDL**F**DIMS-NH_2	2366.2086	592.5594	NO
FAM-Ahx-Beclin-1	FAM-Ahx-T**M**EN**L**SRR**LK**VTGDL**F**DIMS-NH_2	2795.3299	699.8397	699.8413

FAM-Ahx-MULE	FAM-Ahx-MTQEVGQLLQDMGDDVYQQYRSL-NH_2	3219.7018	805.9335	805.8530
MULE-wt	Ac-MTQEVGQLLQDMGDDVYQQYRSL-NH_2	2757.2738	690.3262	690.5753
CC-Di-S	Ac-GE**I**AA**L**KQE**I**LR**L**IGD**N***V*A**L**KQE**I***A*A**L**KQG**Y**G-NH_2	3462.9561	866.7468	866.9976
CC-Di-E1	Ac-GE**I**LA**L**KQE**I**LR**L**IGD**N***V*A**L**KQE**I***LN***L**KQG**Y**G-NH_2	3590.0558	898.5217	898.7734
CC-Di-E2	Ac-G**K****I**LA**L****E**QE**I**LR**L**IGD**N***VN***L**KQE**I***LN***L**KQG**Y**G-NH_2	3633.0616	909.2732	909.7782
CC-Di-BAD	Ac-GE**I**AA**L**K**L**E**I**AA**L****Y**KE**N***LR***L**KQE**I***F*A**L**K**F**G**Y**G-NH_2	3650.0598	913.5227	914.0301
CC-Di-HRK1	Ac-GE**I**AA**L**KQE**I**LR**L****L**GD**N***M*A**L**KQE**I***A*A**L**KQG**Y**G-NH_2	3494.9282	874.7398	874.9915
CC-Di-HRK2	Ac-G**K****I**LA**L****E**QE**I**LR**L****L**GD**N***M****N***L**KQE**I***LN***L**KQG**Y**G-NH_2	3665.0337	917.2662	917.7699
CC-Di-HRK3	Ac-GE**I**AA**L**KQE**I**LR**L****L**GD**N***M*A**L**K**F**E**I***A*A**L**KQG**Y**G-NH_2	3513.9380	879.4923	879.9995
CC-Di-HRK4	Ac-GE**I**AA**L****Y**QE**I**LR**L****L**GD**N***M*A**L**K**F**E**I***A*A**L**KQG**Y**G-NH_2	3548.9064	888.2344	888.7358

[a]Hot-spot residues involving relevant PPIs are shown in bold; constraining sites in constrained peptides are italic and the two positions for the sensitive alanine residues in ISAMBARD modelling are italic; all colors and other formats are consistent with the ones in relevant chapters; [b]NO: not observed; HRKC6: $[M+3H]^{3+}_{Exp}$ 874.1101, $[M+3H]^{3+}_{Obs}$ 874.1106; HRKC8: $[M+3H]^{3+}_{Exp}$ 843.7556, $[M+3H]^{3+}_{Obs}$ 843.7556; HRKS10: $[M+3H]^{3+}_{Exp}$ 888.7579, $[M+3H]^{3+}_{Obs}$ 888.7593; HRK-s: $[M+2H]^{2+}_{Exp}$=1017.5582, $[M+2H]^{2+}_{obs}$=1017.5571; HRK-2: $[M+3H]^{3+}_{Exp}$ 710.7079, $[M+3H]^{3+}_{Obs}$ 710.7089; HRK-3: $[M+3H]^{3+}_{Exp}$ 710.7079, $[M+3H]^{3+}_{Obs}$ 710.7096; HRK-4: $[M+3H]^{3+}_{Exp}$ 682.7200, $[M+3H]^{3+}_{Obs}$ 682.7208; HRK-5: $[M+3H]^{3+}_{Exp}$ 705.3762, $[M+3H]^{3+}_{Obs}$ 705/3773; HRK-hybrid: $[M+3H]^{3+}_{Exp}$ 722.0360, $[M+3H]^{3+}_{Obs}$ 722.0364; HRKC4H: $[M+3H]^{3+}_{Exp}$ 743.3507, $[M+3H]^{3+}_{Obs}$ 743.3511; HRKS4H: $[M+3H]^{3+}_{Exp}$ 774.3457, $[M+3H]^{3+}_{Obs}$ 774.3463; Beclin-1-wt: $[M+3H]^{3+}_{Exp}$ 789.7435, $[M+3H]^{3+}_{Obs}$ 789.7452.

Chapter 7 Appendices

7.1 Additional modelling data for coiled coils

The following table shows the ISAMBARD modelling results, which supports section 4.2 in Chapter 4.

Table 7-1 A summary of ISAMBARD modelling results

Peptide	Total energy	Normalised total energy	Steric contribution	Normalised steric contribution
CC-Di	-769.7	0	20.8	0
CC-Di-BAD	-612.62	157.1	245.7	224.8
CC-Di-HRK1	-791.9	-22.3	25.1	4.3
CC-Di-HRK2	-800.7	-31.0	49.5	28.6
CC-Di-HRK3	-804.8	-35.1	25.1	4.3
CC-Di-HRK4	-813.3	-43.6	25.1	4.3
CC-Di-S	-775.9	-6.2	44.0	23.1
CC-Di-E1	-796.4	-26.7	60.0	39.1
CC-Di-E2	-784.7	-15.1	68.3	47.4

7.2 Additional biophysical data for coiled coils

The Woolfson Group computationally designed several coiled coil peptides targeting BCL-x_L or MCL-1, using AlphaFold or ISAMBARD. I synthesised and tested those peptides in FA competition assays (Table 7-2).

Table 7-2 A summary of FA results for the newly designed coiled coils for BCL-x_L

Peptide	Sequence	IC_{50}
iBCL-x_L-RPS	GIAALDQEIEALKLEIGILKQENAQLKQEG	ND
iBCL-x_L-HS	GQEIRALKQEIYALKLENLSLKQEIAYLKG	No response
iBCL-x_L-LD	GQEIRALKQEIAALKLENMSLKFEIAYLKG	No response
iBCL-x_L-OB	GALKQEIYALKLEIISLKLENAYLKQEIAG	No response
aBCL-x_L-RPS	GLKQEIAALRLRIASLKFENAYLKQEIAAG	ND
aBCL-x_L-HS	GQEIRALKQEIYALKLKNASLKQEIYALKG	No response
aBCL-x_L-LD	GEIAALKQEILKLKSDNFALYQEIAALKQG	No response
aBCL-x_L-OB	GQEIAALRLEIAALYQENLKLKSEIAALKG	ND

Table 7-3 A summary of FA results for the newly designed coiled coils for MCL-1

Peptide	Sequence	IC_{50}
iMCL-1-RPS	GIAALDQEIEALKLEIIGLKQENAQLKQEG	No response
iMCL-1-HS	GKQEIEALKLEIIGLKQENAQLKQNIAALG	No response
iMCL-1-LD	GAALKQEILALEQEILALIGENVALKQEIG	ND
iMCL-1-OB	GKQEIAALKLEIAGLKVENRQLKQEIAALG	No response
aMCL-1-RPS	GEIAALKLEIAGLKQENRQLKQNIAALKQG	No response
aMCL-1-HS	GEIAALKLRIAGLKVENAQLKQNIAALKQG	ND
aMCL-1-LD	GIAALKLEIEALKLRIAGLKQENAQLKQEG	ND
aMCL-1-OB	GQEIAALQLEIAGLKQENRALKLEIAALKG	ND

7.3 Python scripts for saturation scanning of coiled coil using ISAMBARD and visualisation of modelling results

```
import isambard
import ampal
import isambard.specifications as specifications
import isambard.modelling as modelling
import pathlib

FILESPATH = pathlib.Path(__file__).parent / 'PDB'

CC_Di = ampal.load_pdb(str(FILESPATH / '4dzm.pdb'))

sequence = CC_Di.sequences
print(sequence)
print(CC_Di)
print(sequence[0])
Sequence_monomer = sequence[0]
Aminoacid = ('ARNDCQEGHILKMFPSTWYV')
Sequence_dimer = [Sequence_monomer, Sequence_monomer]
CC_Di_model = modelling.pack_side_chains_scwrl(CC_Di, Sequence_dimer)
import budeff
import numpy as np
Scores_scan_total_energy = np.zeros((20,31))
Scores_scan_steric = np.zeros((20,31))
Normalised_scan_total_energy = np.zeros((20,31))
Normalised_scan_steric = np.zeros((20,31))
score = budeff.get_internal_energy(CC_Di_model)
for i in range(len(Aminoacid)):
    Sequence_scan = Sequence_monomer
```

```
    for j in range(len(Sequence_monomer)):
        l = list(Sequence_monomer)
        l[j]=Aminoacid[i]
        Sequence_scan = "".join(l)
        print(Sequence_scan)
        Sequence_scan_dimer = [Sequence_scan,Sequence_scan]
        CC_Di_scan = modelling.pack_side_chains_scwrl(CC_Di,
Sequence_scan_dimer)
        score_scan = budeff.get_internal_energy(CC_Di_scan)
        Scores_scan_total_energy[i][j]=score_scan.total_energy
        Scores_scan_steric[i][j] = score_scan.steric
print(Scores_scan_total_energy)
print(Scores_scan_steric)
for i in range(20):
    for j in range(31):
        Normalised_scan_total_energy[i][j] = Scores_scan_total_energy[i][j]-
score.total_energy
        Normalised_scan_steric[i][j] = Scores_scan_steric[i][j]-score.steric
print(Normalised_scan_total_energy)
print(Normalised_scan_steric)


import matplotlib.pyplot as plt


plt.figure()
plt.subplot(1,2,1)
plt.imshow(Normalised_scan_total_energy, cmap='seismic', vmin=-200,
vmax=200, aspect='auto')
plt.title('Total energy')
x_pos = np.arange(len(Sequence_monomer))
plt.xticks(x_pos, Sequence_monomer, rotation = 0)
```

```
plt.xlabel('Residue')
plt.ylabel('Mutation')
y_pos = np.arange(len(Aminoacid))
plt.yticks(y_pos, Aminoacid)
plt.subplot(1,2,2)
plt.imshow(Normalised_scan_steric, cmap='seismic', vmin=-200, vmax=200, aspect='auto')
plt.title('Steric contribution \n to the total energy')
plt.xlabel('Residue')
x_pos = np.arange(len(Sequence_monomer))
plt.xticks(x_pos, Sequence_monomer, rotation = 0)
y_pos = np.arange(len(Aminoacid))
plt.yticks(y_pos, Aminoacid)
plt.colorbar()
plt.show()
```

7.4 HRMS data and sequencing result for BCL-x_L

These data support section 6.4 in Chapter 6

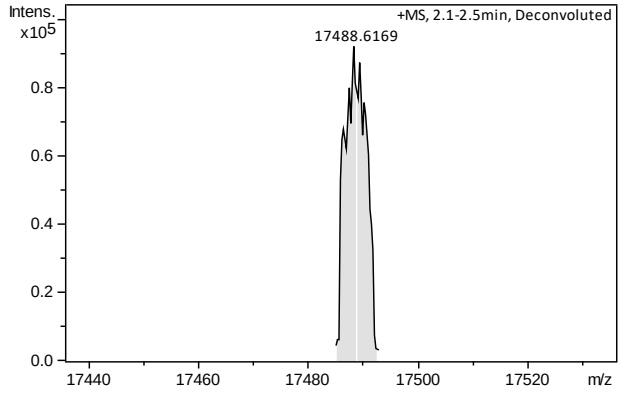

Sequencing result (agrees with that measured in the literature[63]):

NNNNGGAAATTCCCCTCTAGAATAATTTTGTTTAACTTTAAGAAGGAGATATACCATGGGCAGCAGC

CATCATCATCATCATCACAGCAGCGGCCTGGTGCCGCGCGGCAGCCATATGTCGGACTCAGAAGT

CAATCAAGAAGCTAAGCCAGAGGTCAAGCCAGAAGTCAAGCCTGAGACTCACATCAATTTAAAGGT

GTCCGATGGATCTTCAGAGATCTTCTTCAAGATCAAAAAGACCACTCCTTTAAGAAGGCTGATGGAA

GCGTTCGCTAAAAGACAGGGTAAGGAAATGGACTCCTTAAGATTCTTGTACGACGGTATTAGAATT

CAAGCTGATCAGACCCCTGAAGATTTGGACATGGAGGATAACGATATTATTGAGGCTCACAGAGAA

CAGATTGGTGGAATGTCTCAGTCTAACCGTGAACTGGTTGTTGACTTCCTGTCTTACAAACTGTCTC

AGAAAGGTTACTCTTGGTCTCAGATGGCTGCTGTTAAACAGGCTCTGCGTGAAGCTGGTGACGAAT

TTGAACTGCGTTACCGTCGTGCTTTCTCTGACCTGACCTCTCAGCTGCACATCACCCCGGGTACCG

CTTACCAGTCTTTCGAACAGGTTGTTAACGAACTGTTCCGTGACGGTGTTAACTGGGGTCGTATCG

TTGCTTTCTTCTCTTTCGGTGGTGCTCTGTGCGTTGAATCTGTTGACAAAGAAATGCAGGTTCTGGT

TTCTCGTATCGCTGCTTGGATGGCTACCTACCTGAACGACCACCTGGAACCGTGGATTCAGGAAAA

CGGTGGTTGGGACACCTTCGTTGAACTGTACGGTAACAACGCTGCTGCGGAATCTCGTAAAGGTC

AGGAACGTTAGGATCCGGCTGCTAACAAAGCCCGAAAGGAAGCTGAGTTGGCTGCTGCCACCGCT

GAGCATTAACTAGCATAACCCCTTGGGGCNTCTAAACGGGTCTTGAGGGGTTTTTTGCTGAAACGG

AGGAACTATATCNNGGATTGTCGAAAGGGACGCGCCCTGTAGCCGGCCCATTAAGCGCGTCCGGG

TGAGGTGGTTACGCGCAGCCGTGACCGCTTCCCATGCCAGCCGCCTNAGGCGCCTGTATCCTTTC

AGTTTCTTACCTTTCTTTTCCCGACCAGATTACCCGGTTTTGCCCGCCANNTTTTCTAATNNNGGGG

TTCCTTTTAGGGTCCCAATTNGTTTTTTCACGCACCCCTANNTCAAAAAAACTGGTCAACAAGAAAA

GNCTNCCCNNANGGGGGGCACACCCCCCCCGATGAAAGTGTTTTTTCTCTTTTTGCNNNTTTGTAC

7.5 HRMS data and HPLC traces for peptides

BAD-wt ($BAD_{103-127}$)

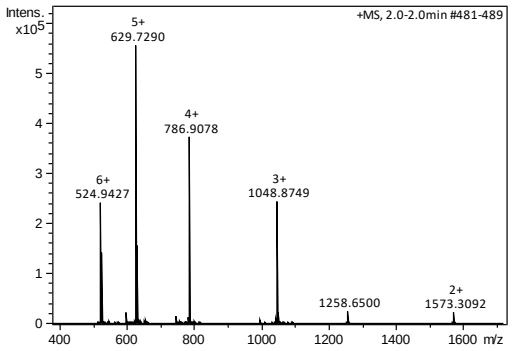

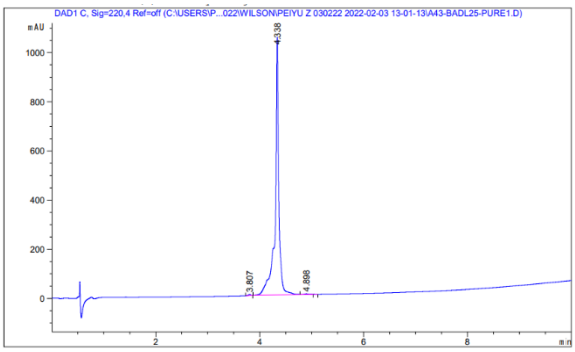

BAD-s ($BAD_{109-127}$)

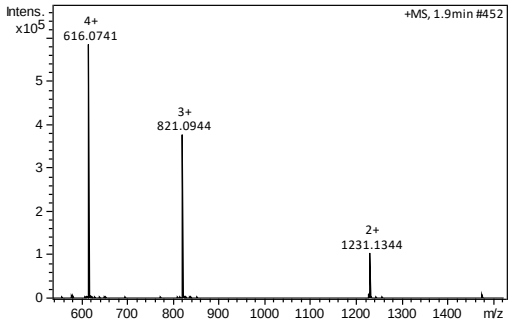

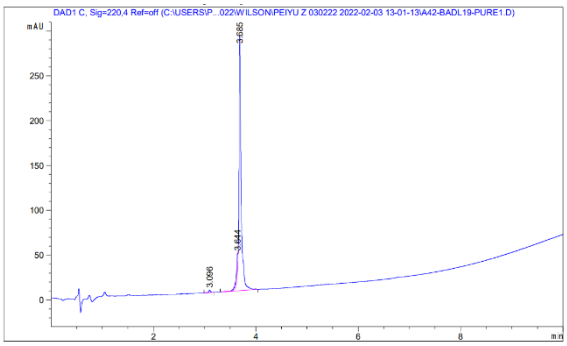

FAM-Ahx-BAD ($BAD_{109-127}$)

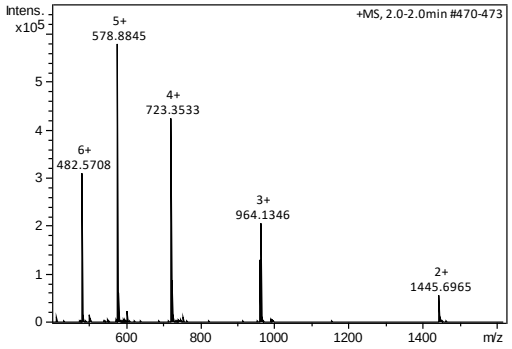

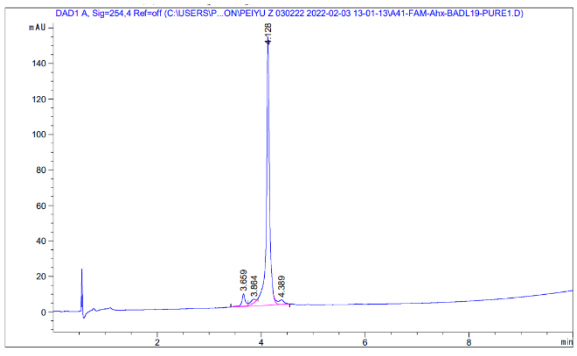

BADL1

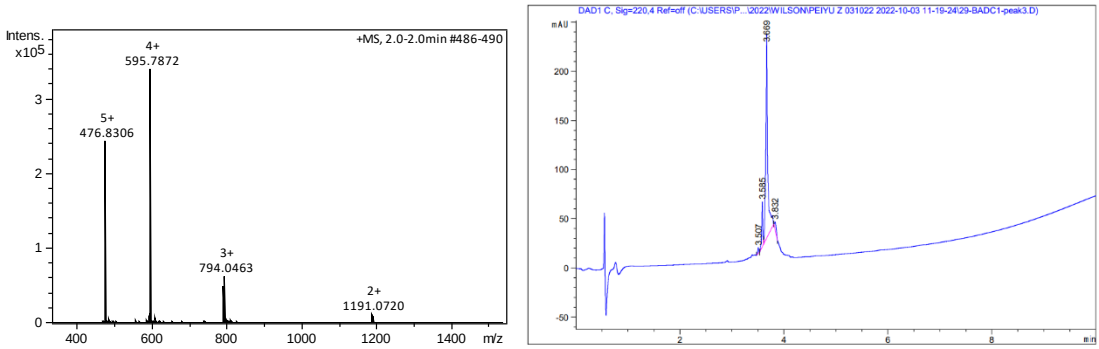

BADS1

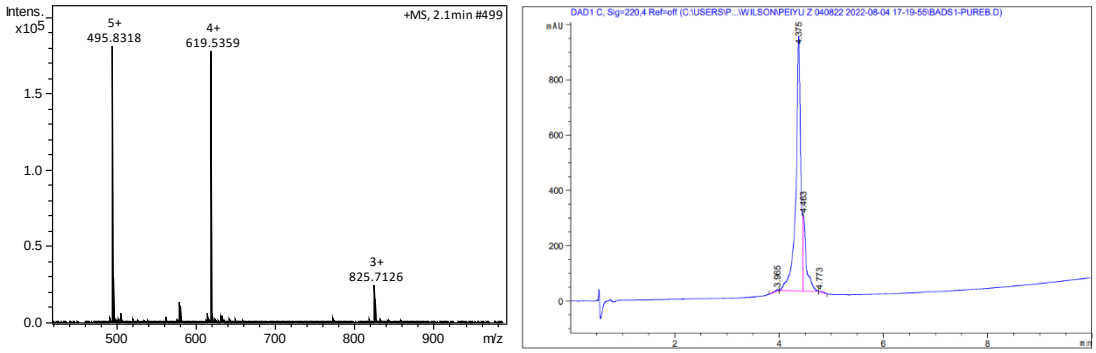

BADL2

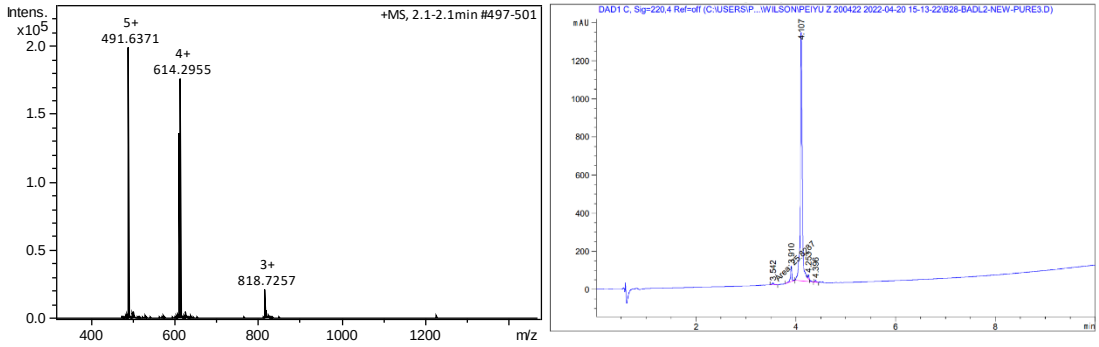

BADS2

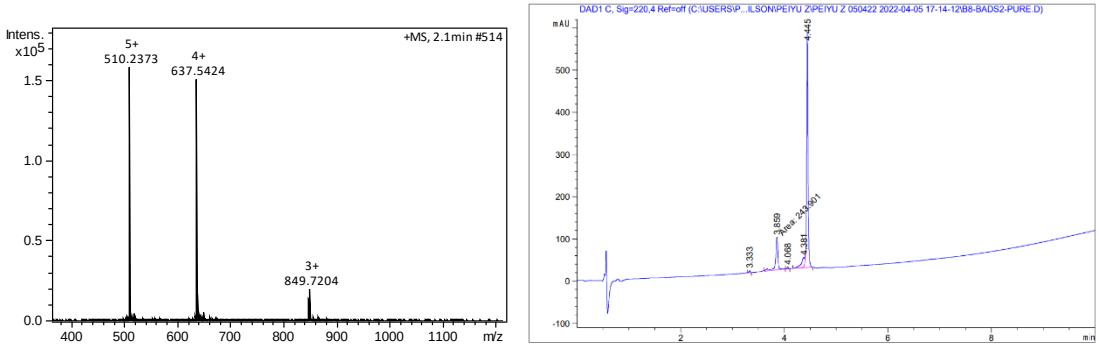

BADL3

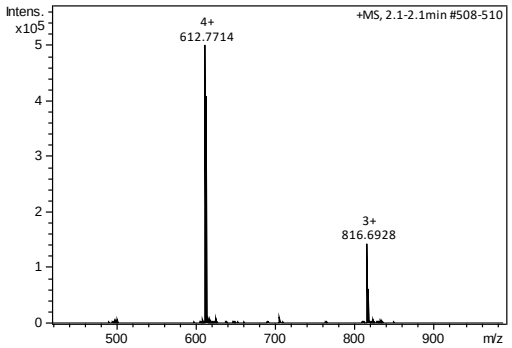

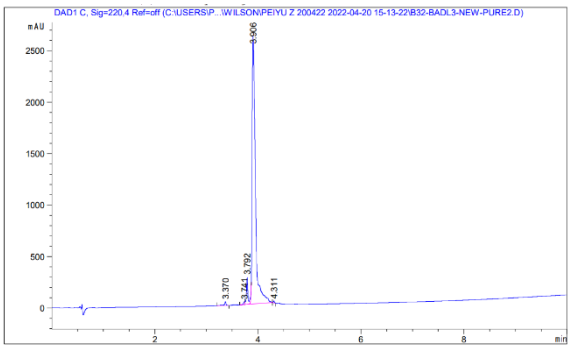

BADS3

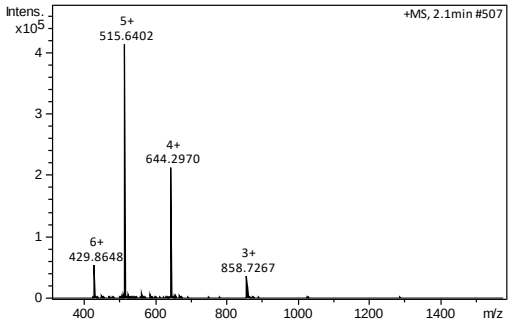

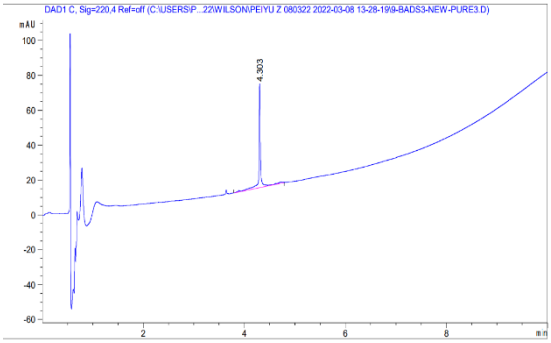

BADL4

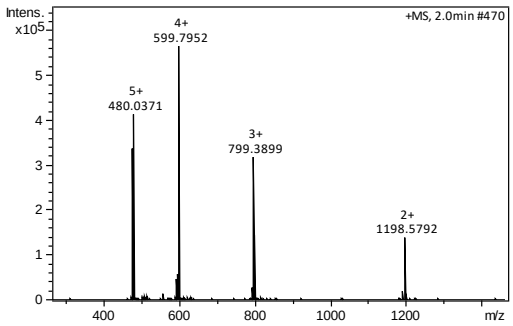

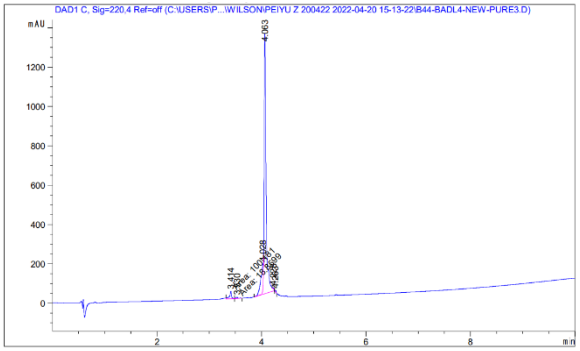

BADS4

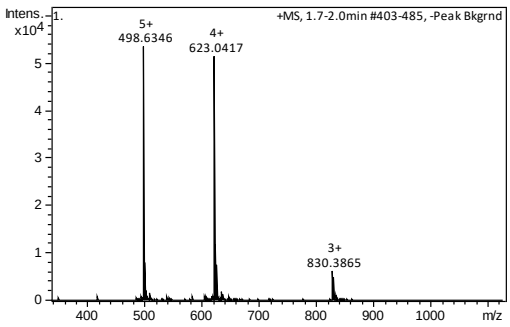

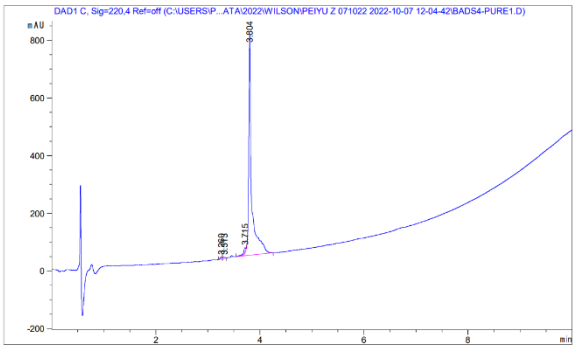

BADL5

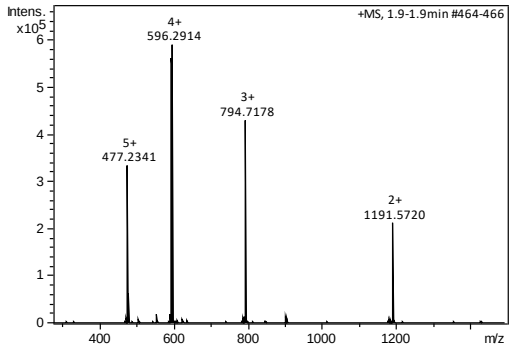

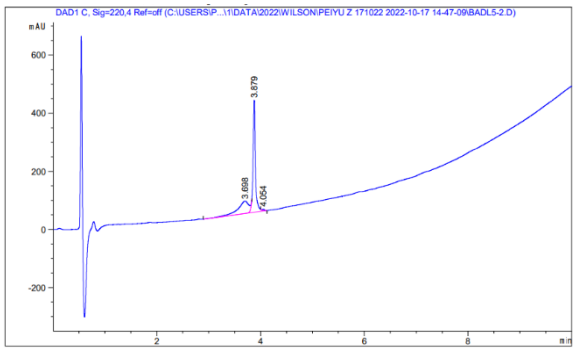

BADS5

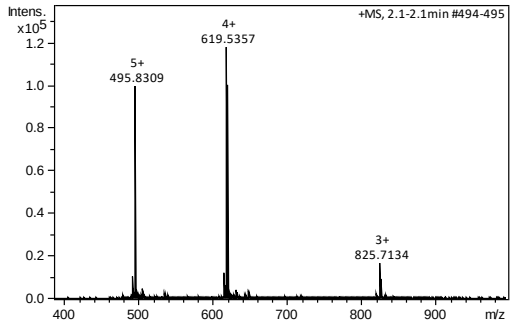

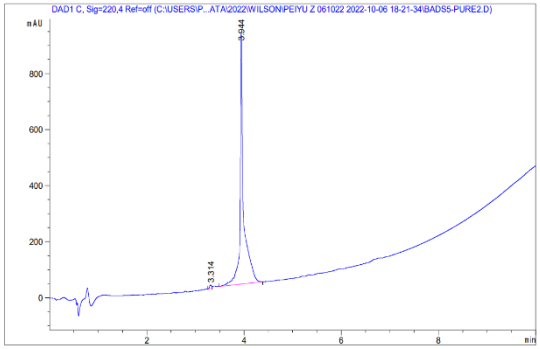

BADL6

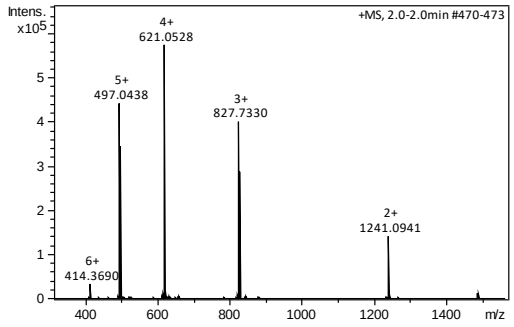

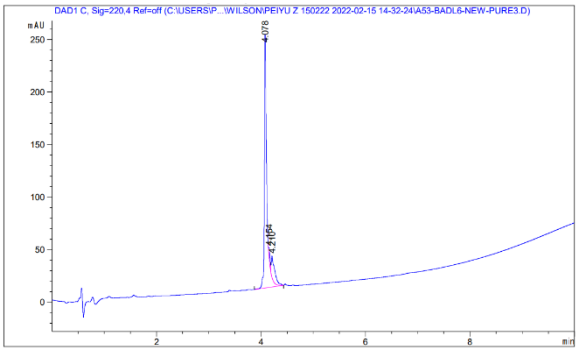

BADS6

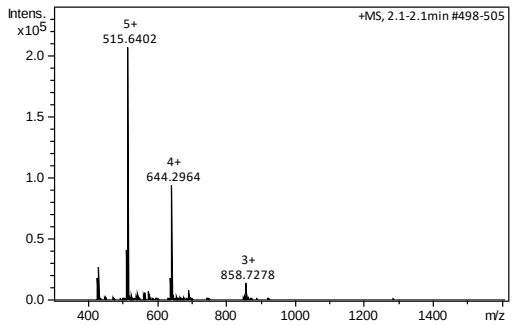

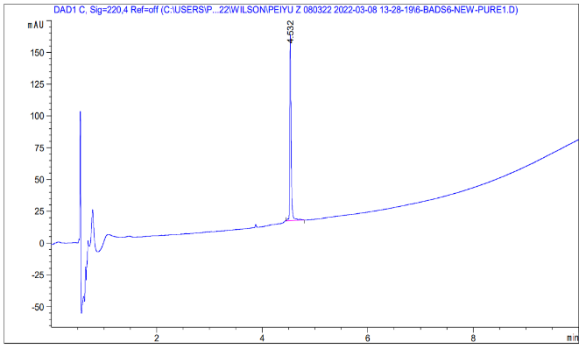

BADL7

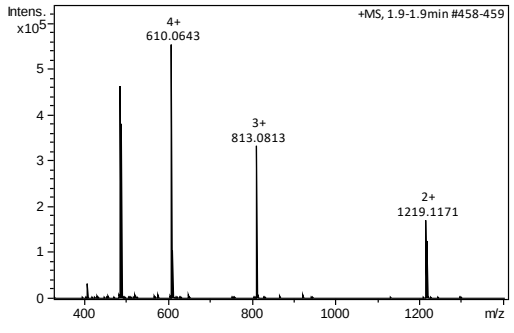

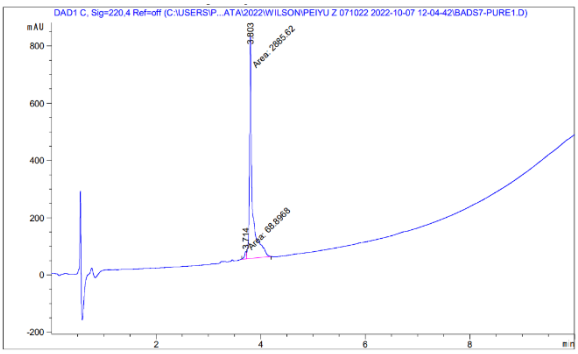

BADS7

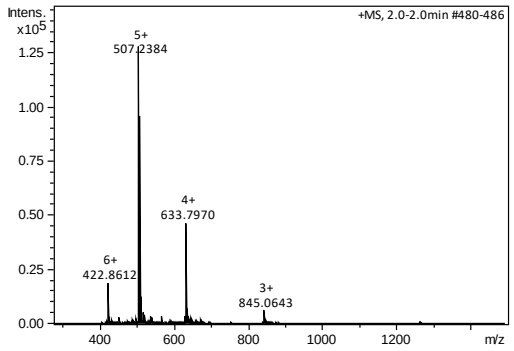

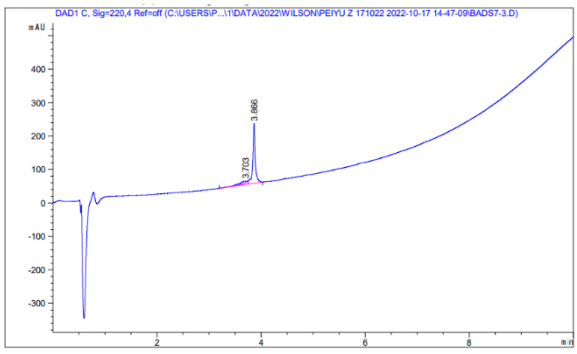

BADL8

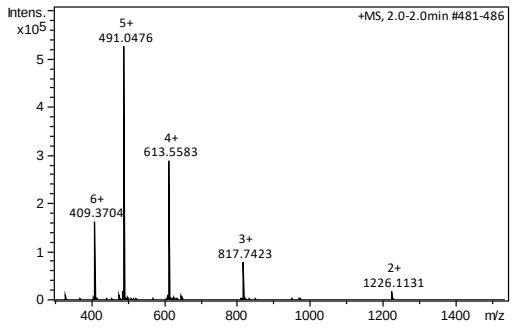

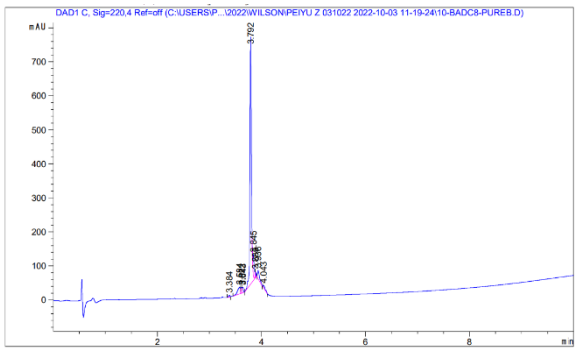

BADS8

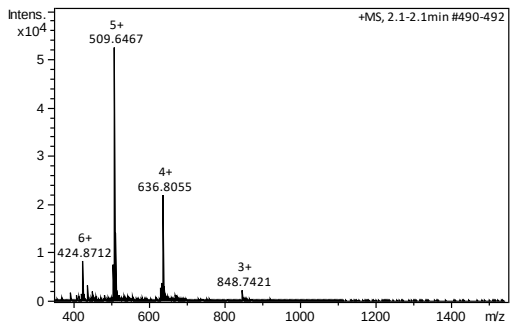

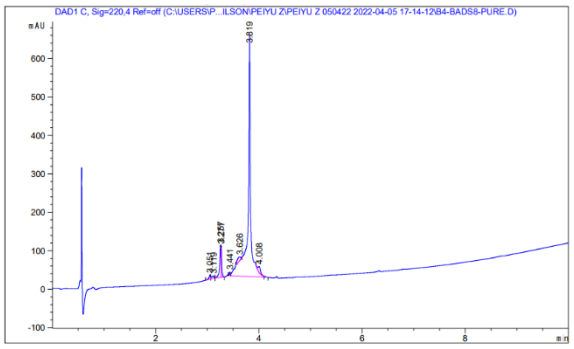

HRK-wt

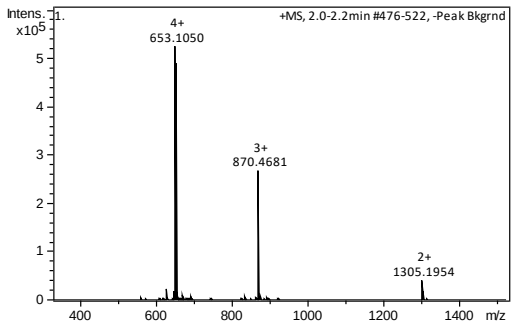

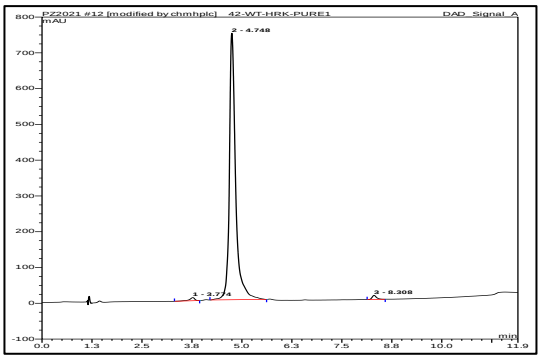

FAM-Ahx-HRK

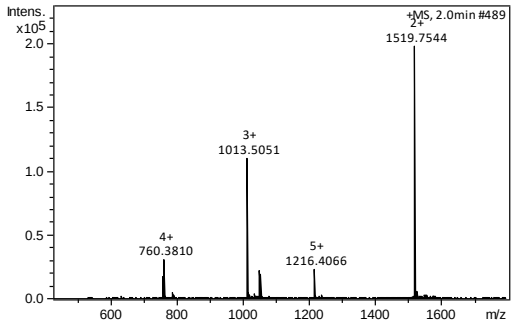

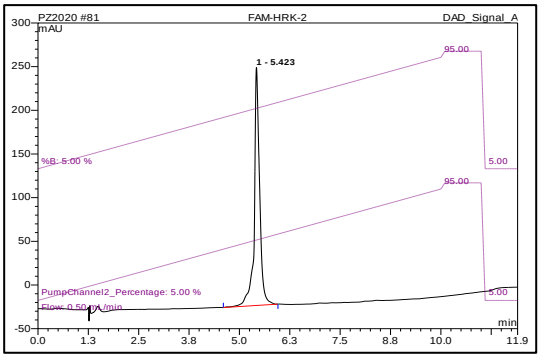

HRKC1

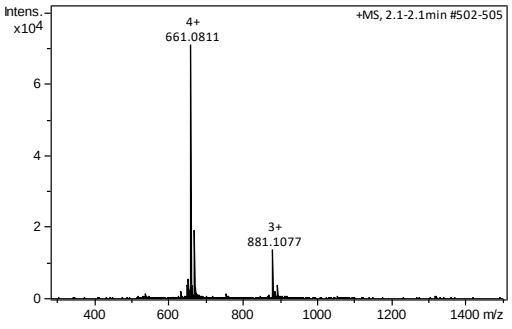

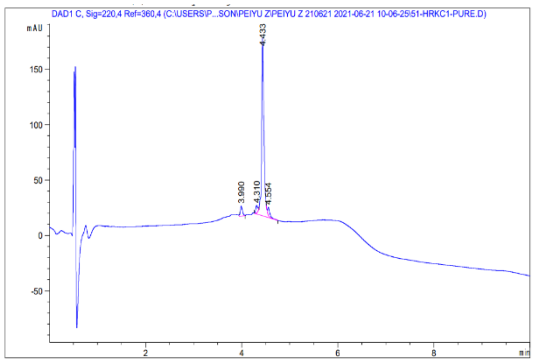

HRKS1

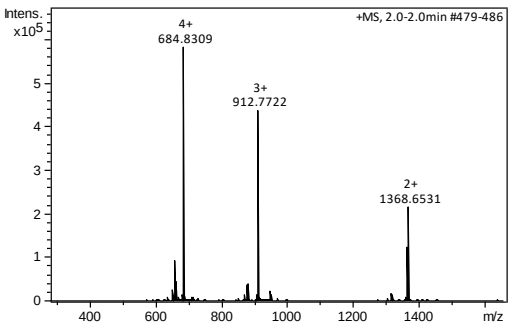

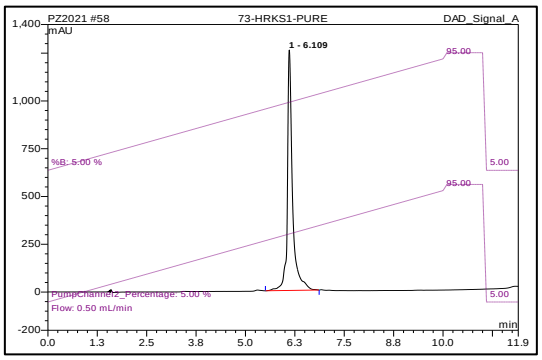

HRKC2

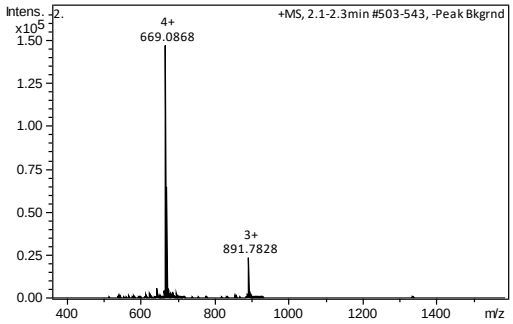

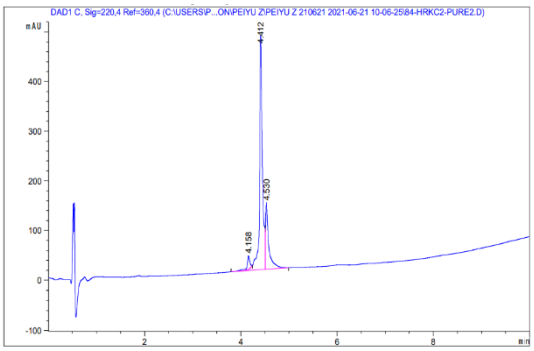

HRKS2

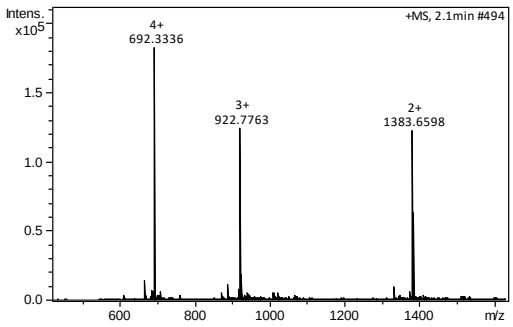

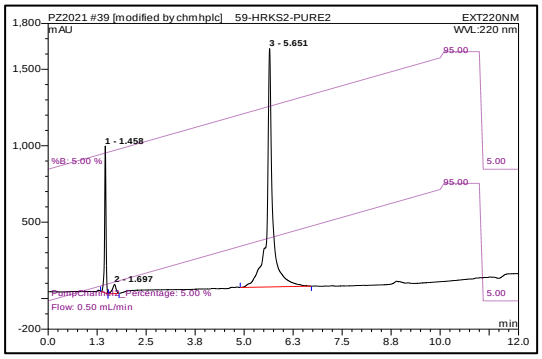

HRKC3

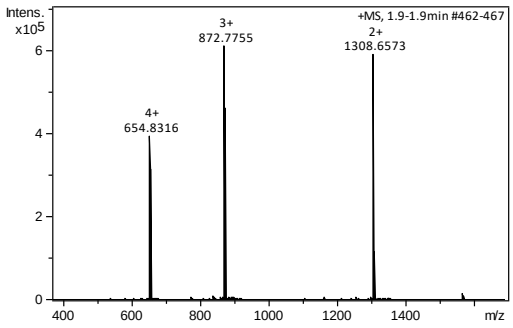

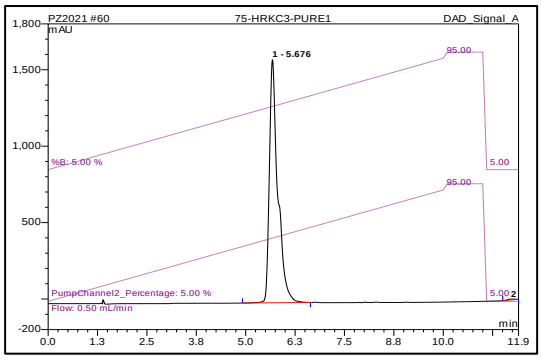

HRKS3

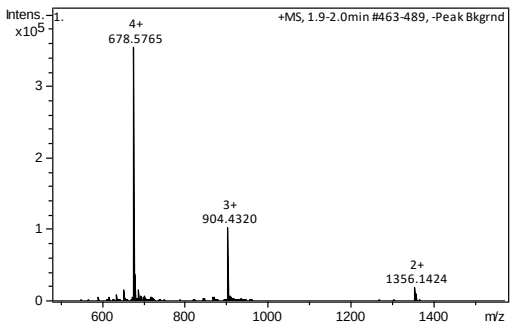

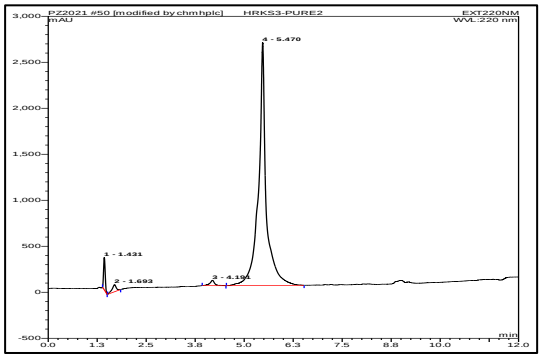

HRKC4

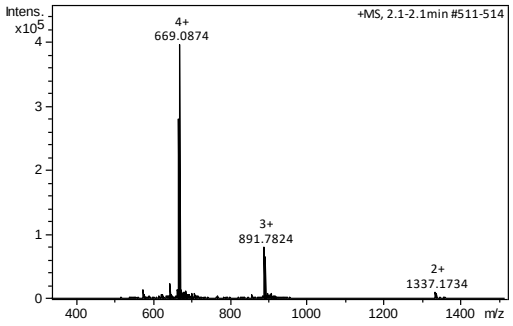

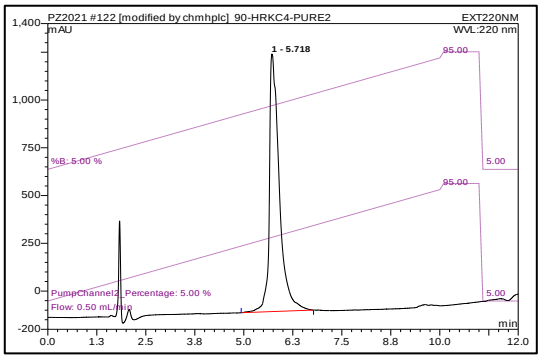

HRKS4

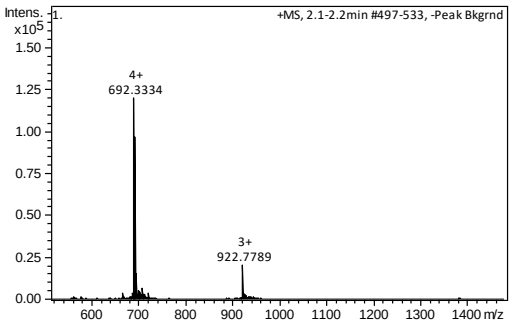

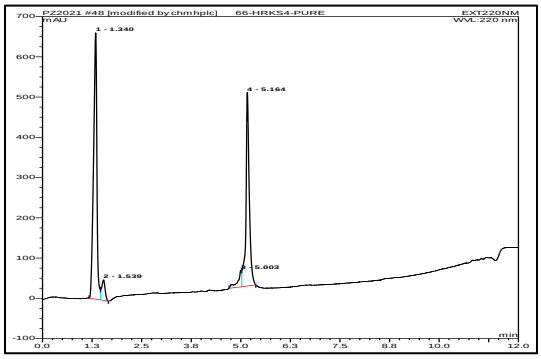

HRKC5

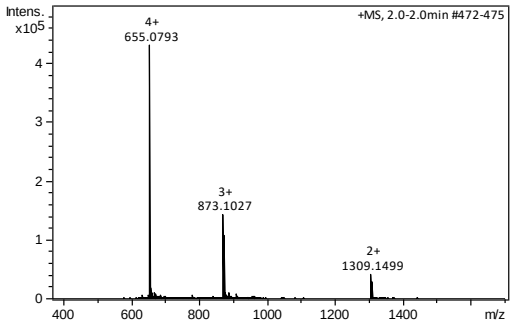

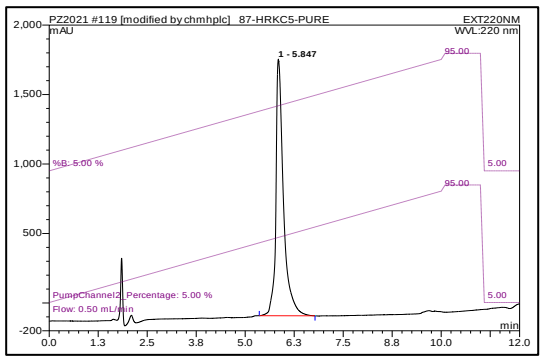

HRKS5

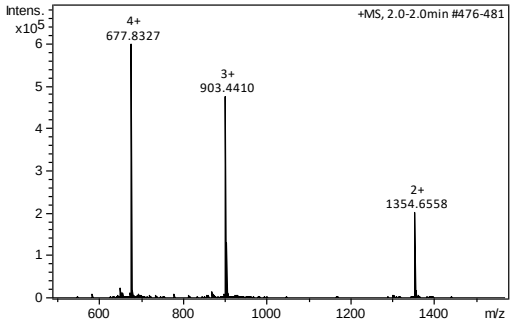

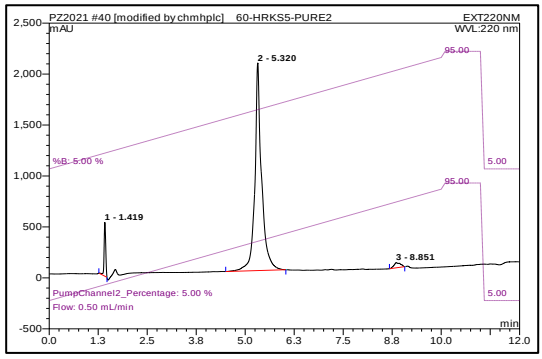

HRKC6

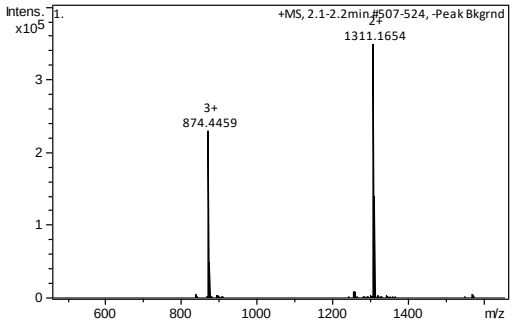

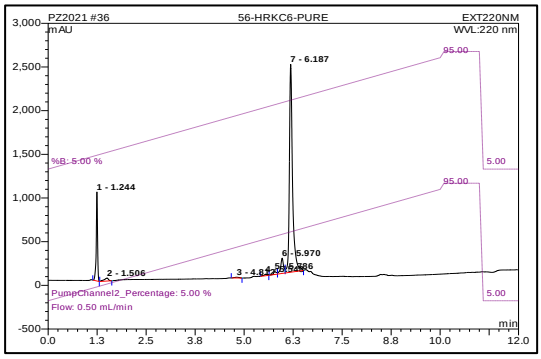

HRKS6

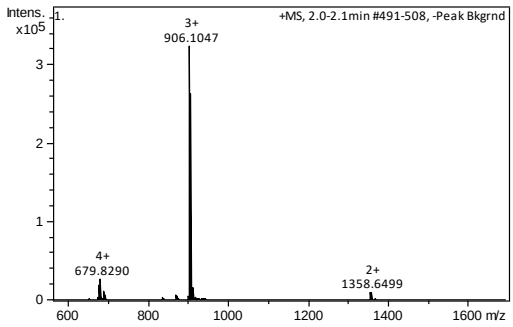

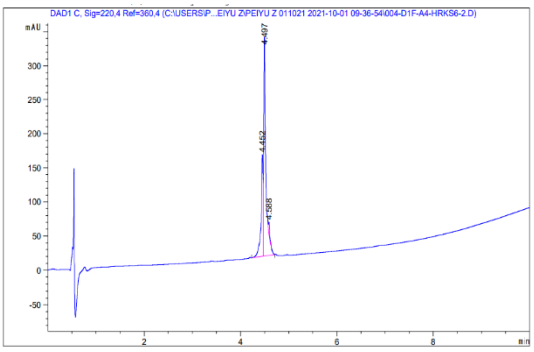

HRKC7

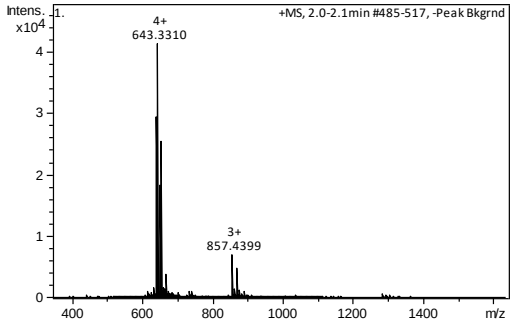

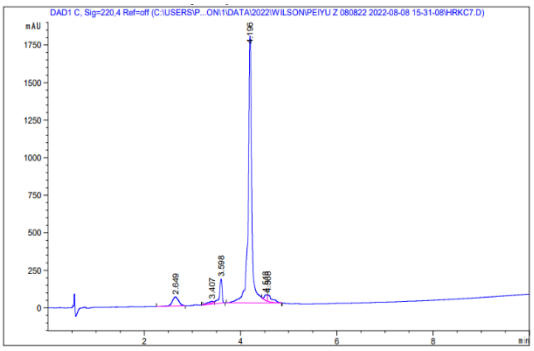

HRKS7

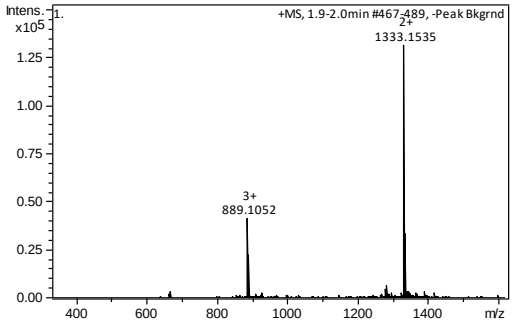

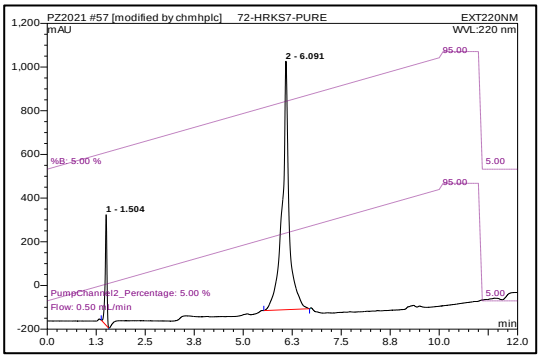

HRKC8

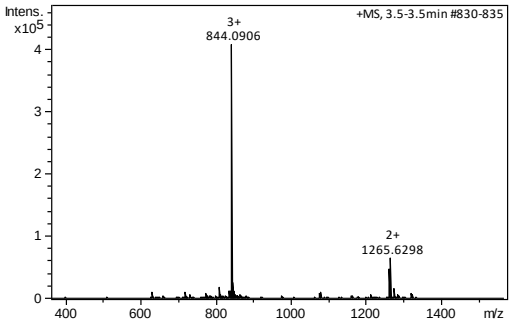

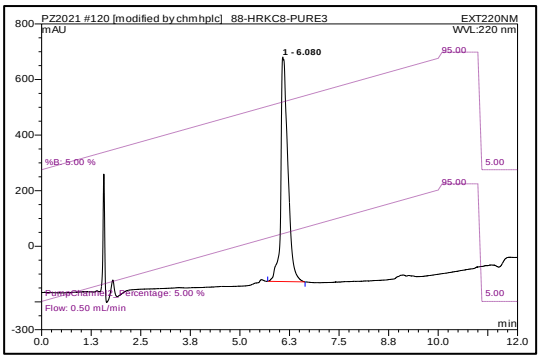

HRKS8

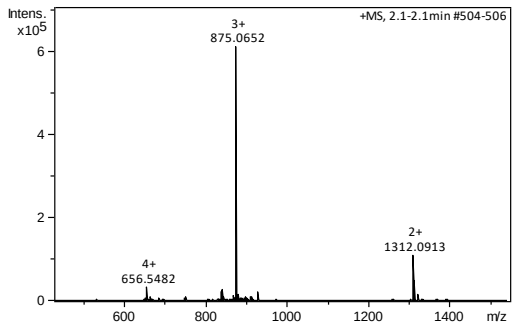

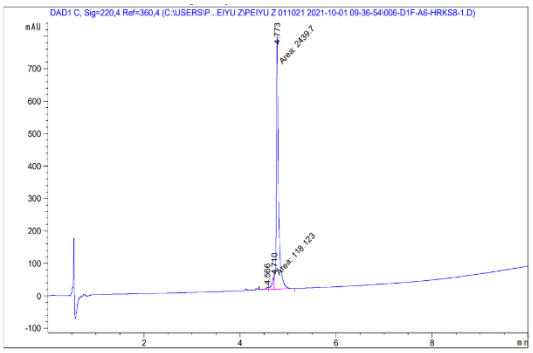

HRKC9

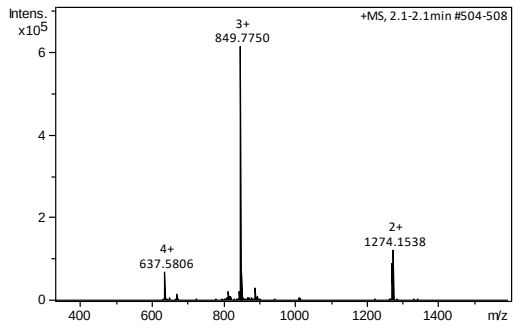

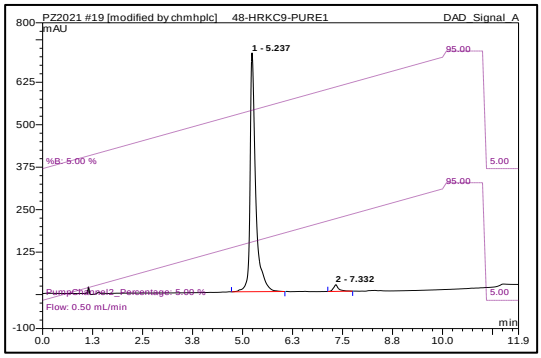

HRKS9

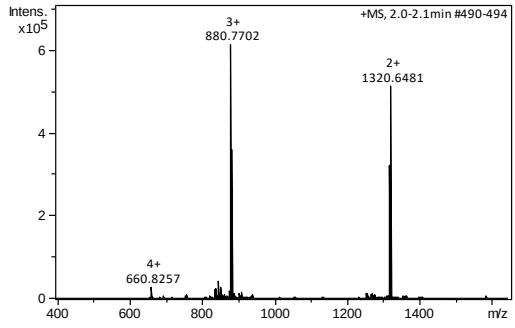

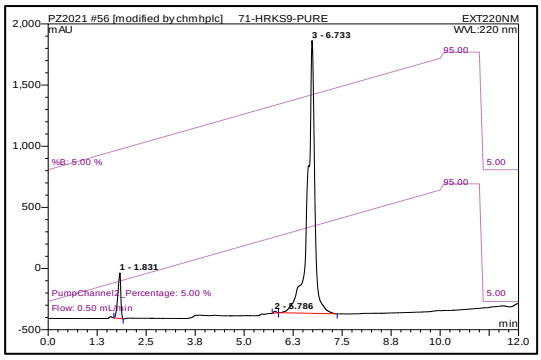

HRKC10

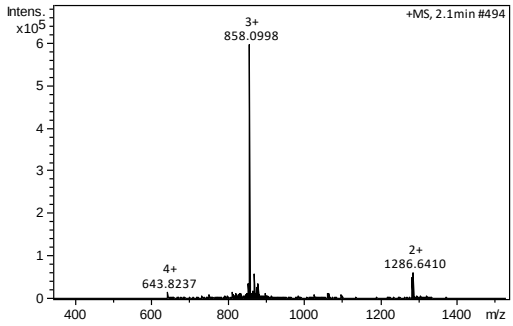

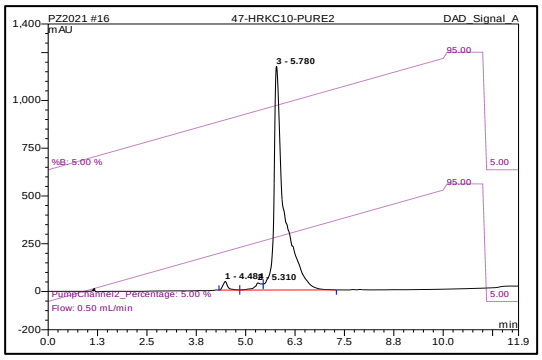

HRKS10

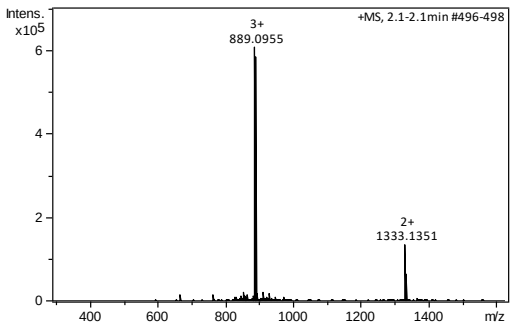

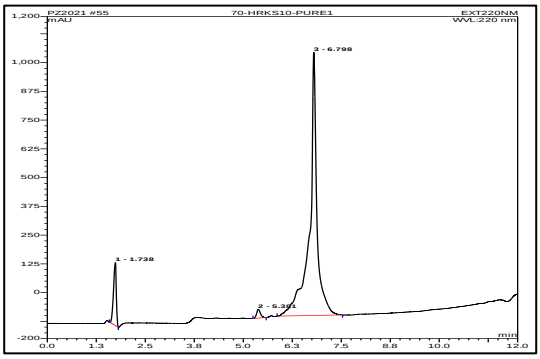

HRKC4-DCys

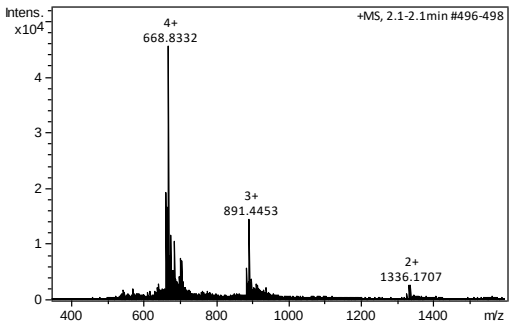

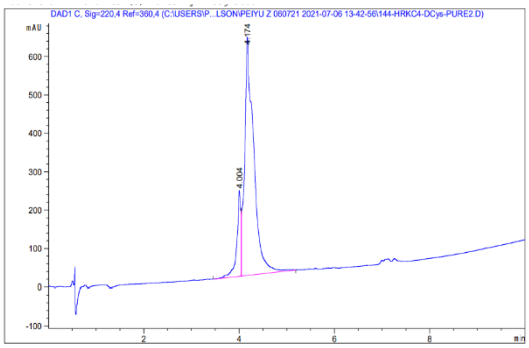

HRKS4-DCys

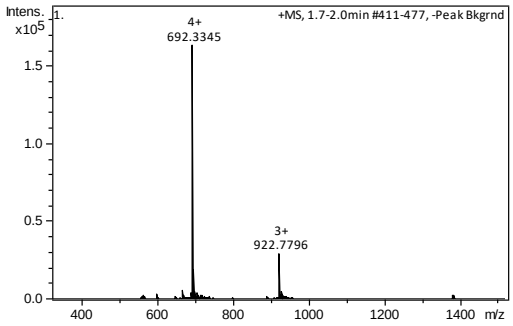

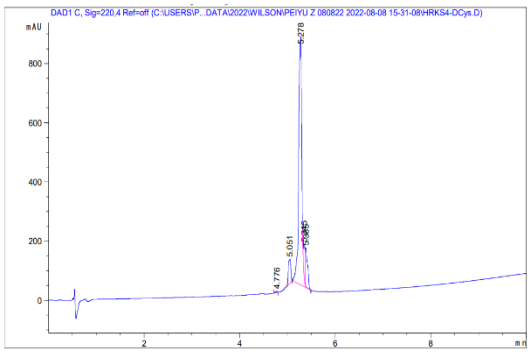

HRKC4-hCys

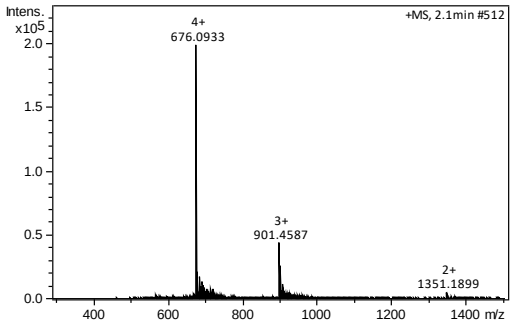

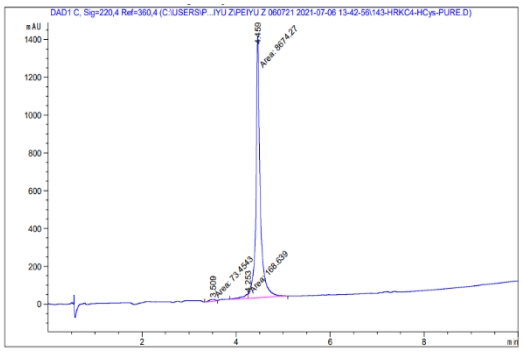

HRKS4-hCys

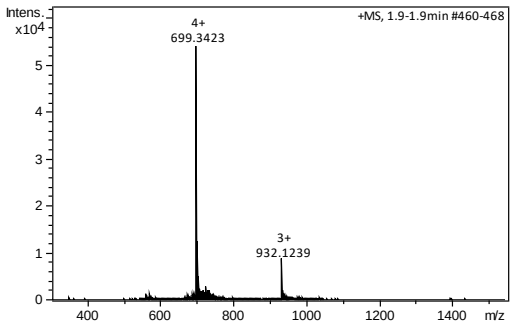

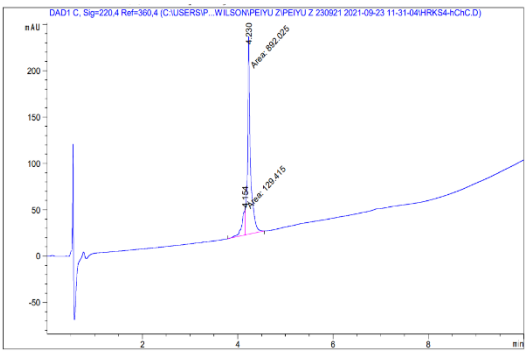

HRKC4-ChC

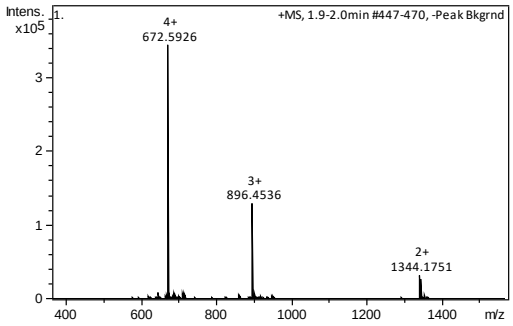

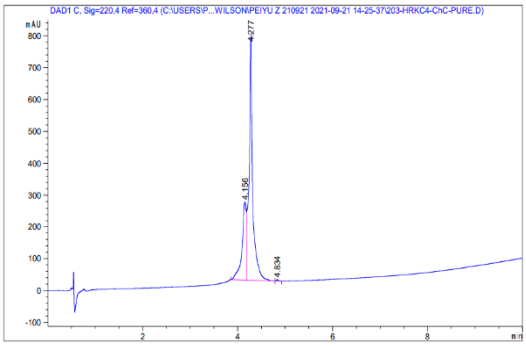

HRKS4-ChC

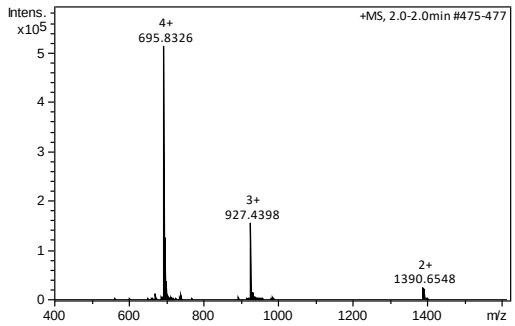

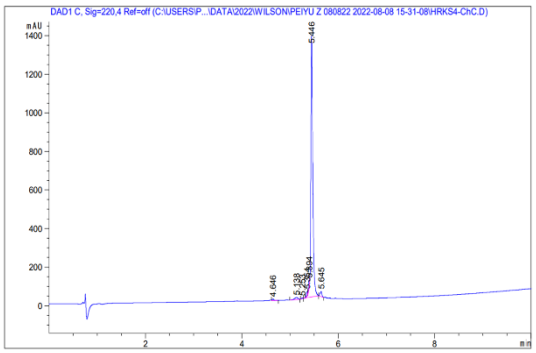

HRKS4-Xylene

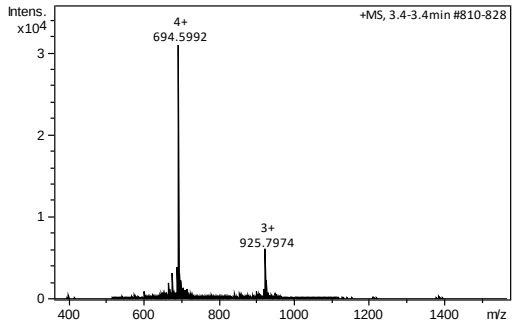

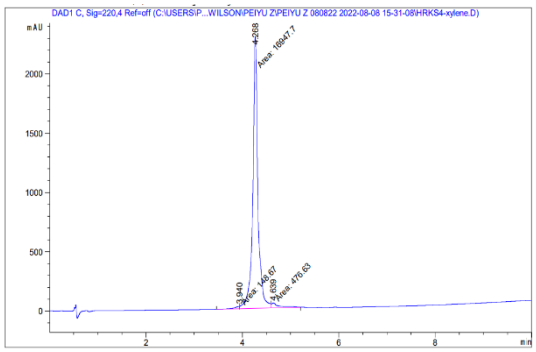

HRKL4-hydrocarbon

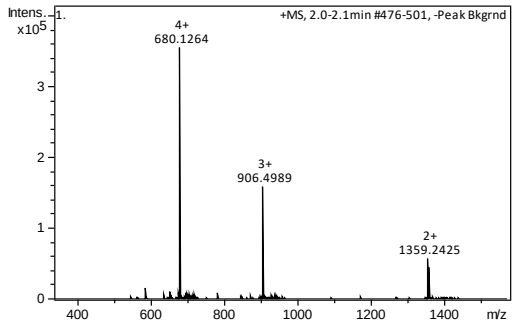

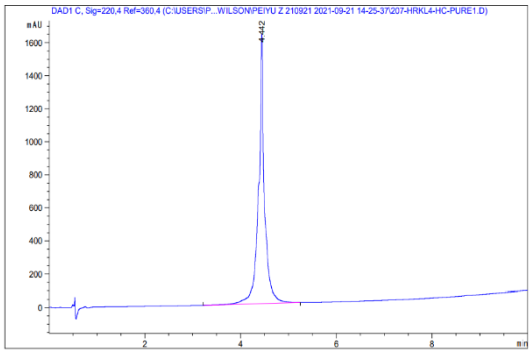

HRKS4-hydrocarbon

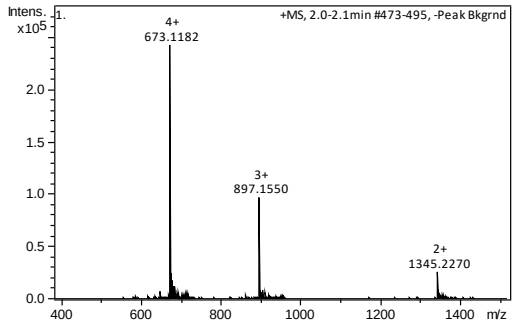

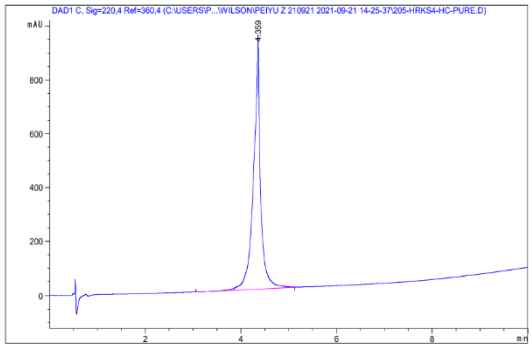

HRK-S

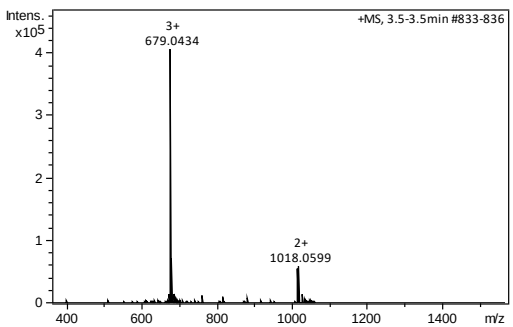

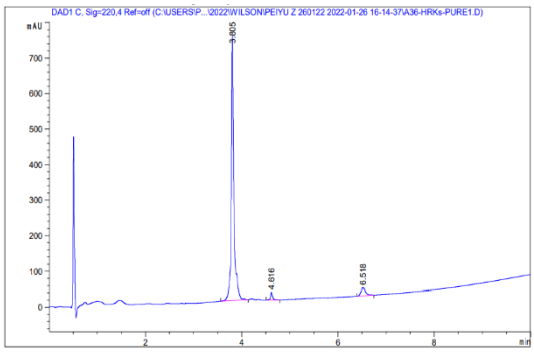

HRK-1

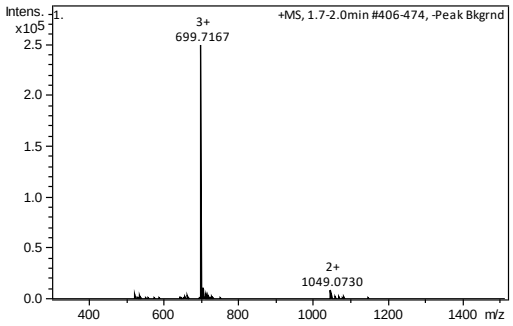

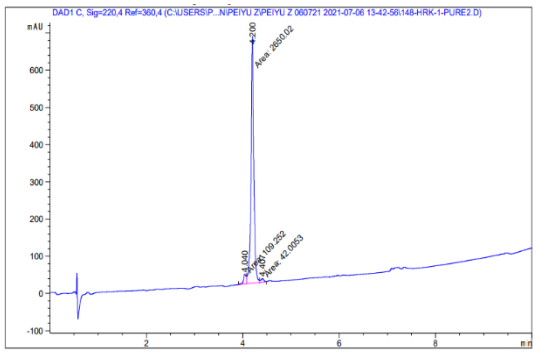

HRK-2

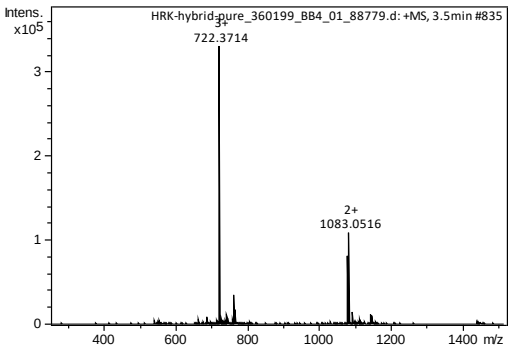

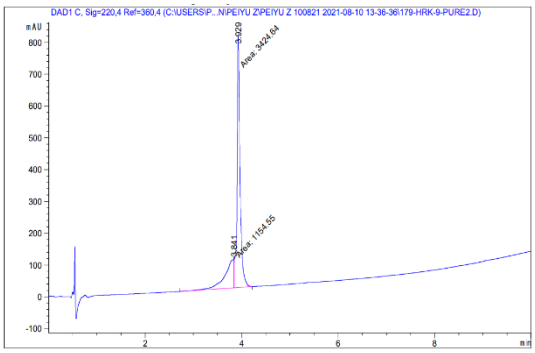

HRK-3

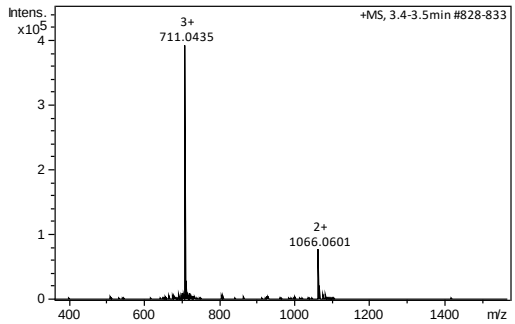

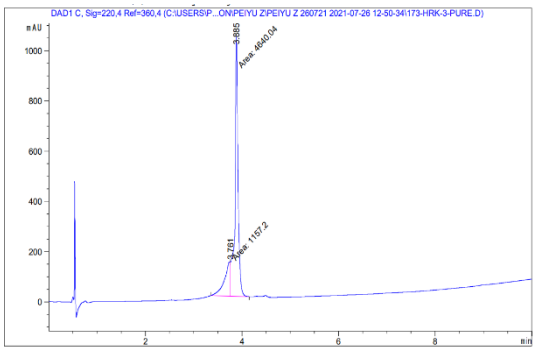

HRK-4

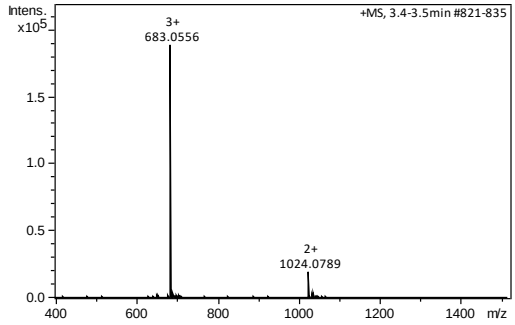

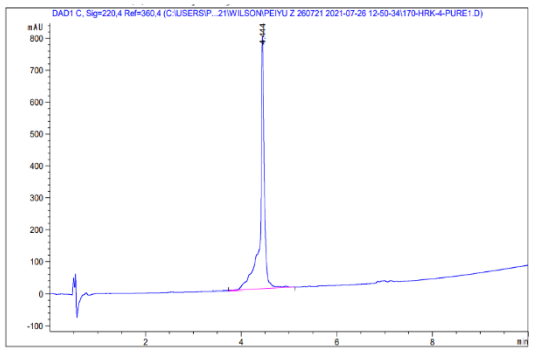

HRK-5

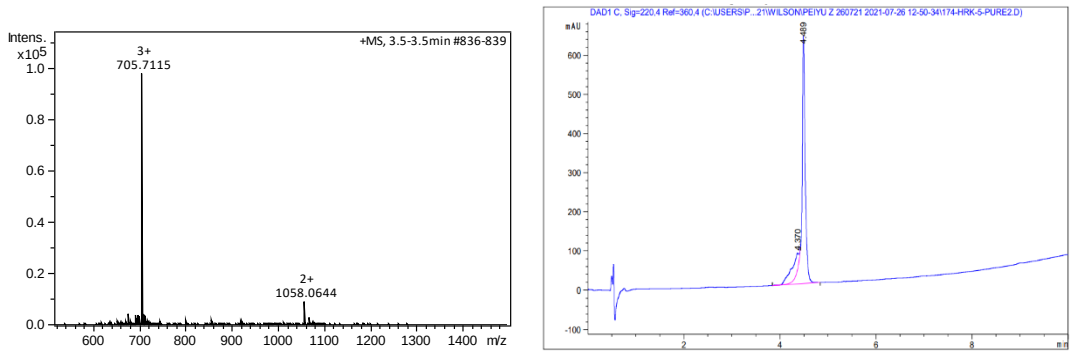

HRK-hybrid

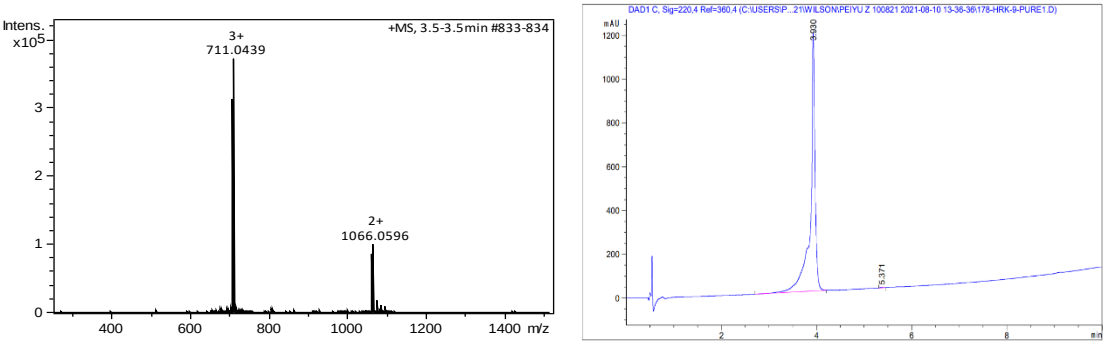

HRKC4H

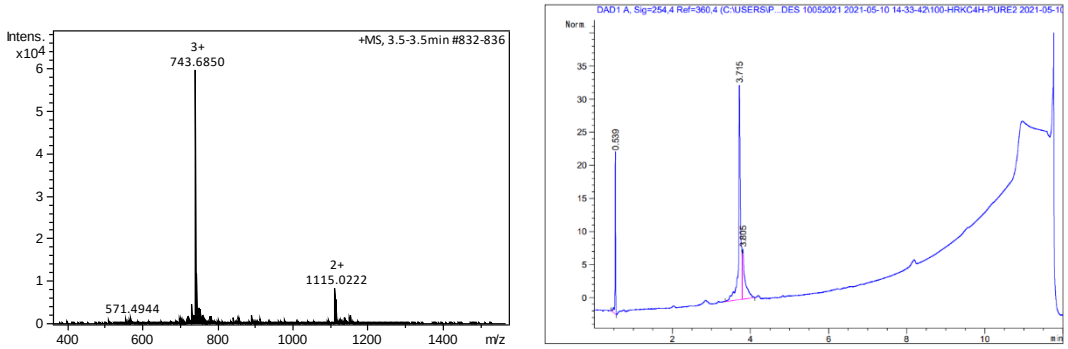

HRKS4H

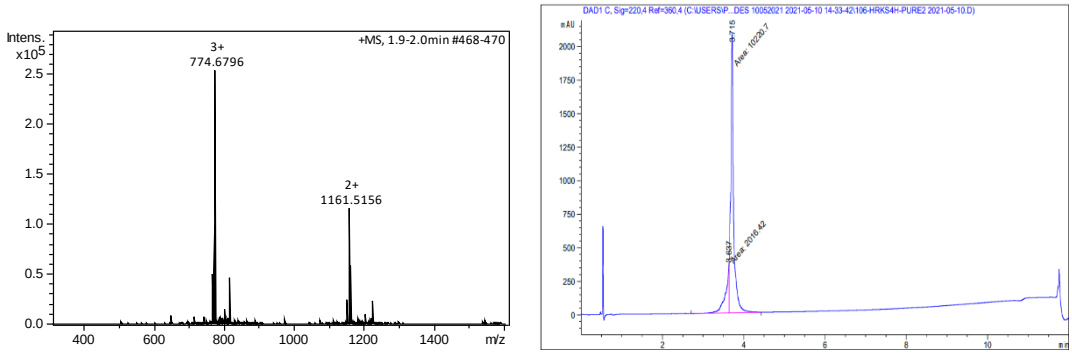

Beclin-1-wt

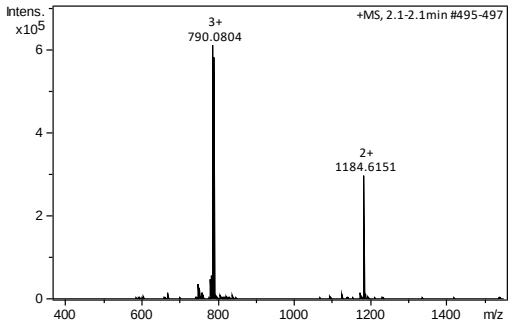

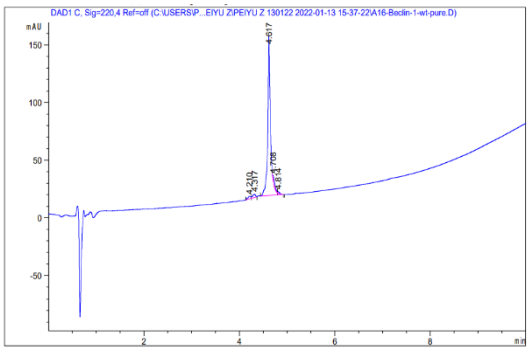

FAM-Ahx-Beclin-1

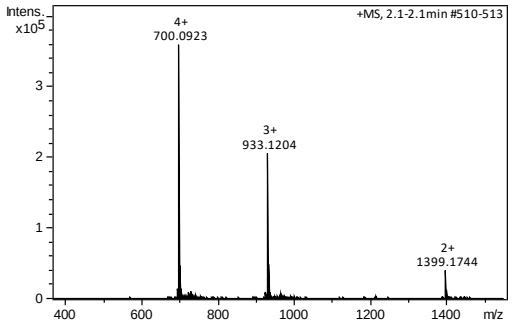

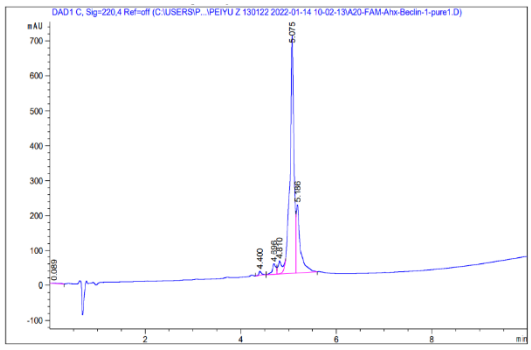

FAM-Ahx-MULE

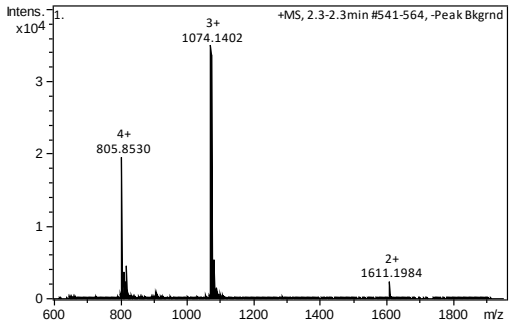

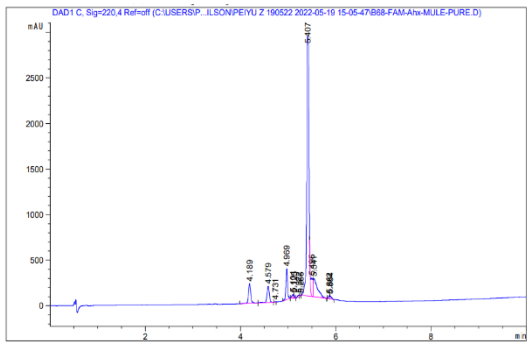

MULE-wt

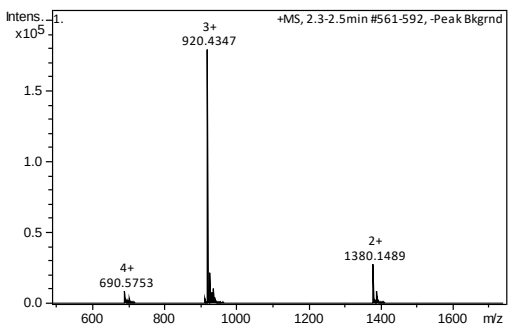

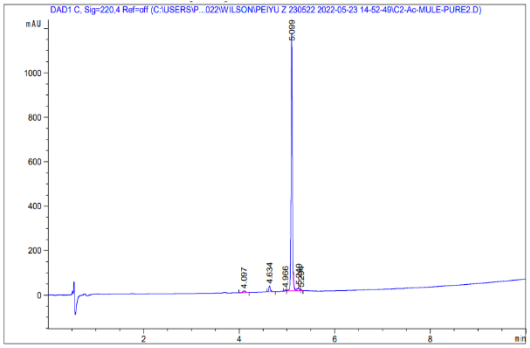

CC-Di-S

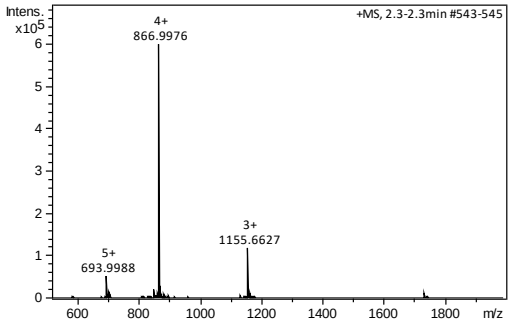

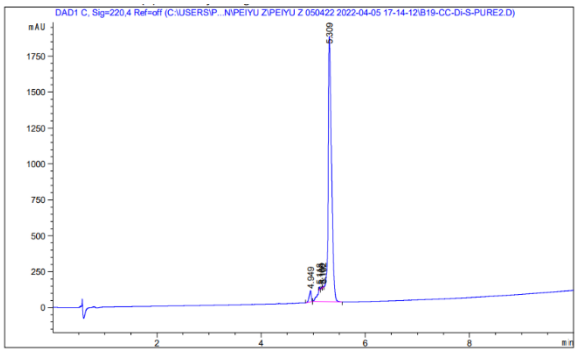

CC-Di-E1

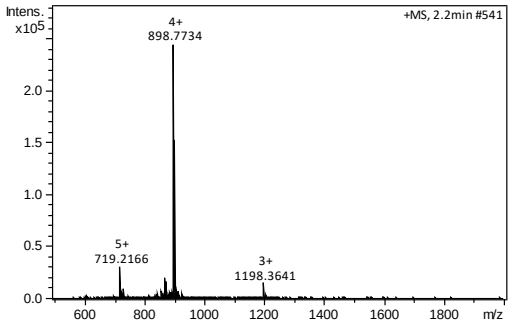

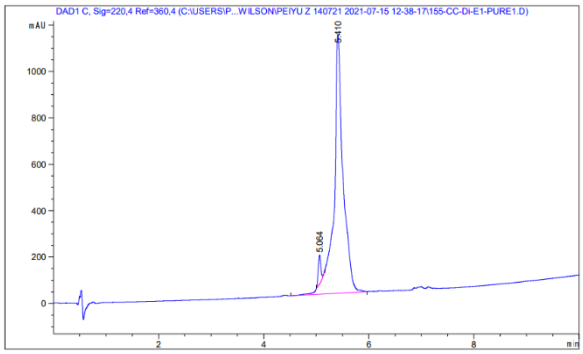

CC-Di-E2

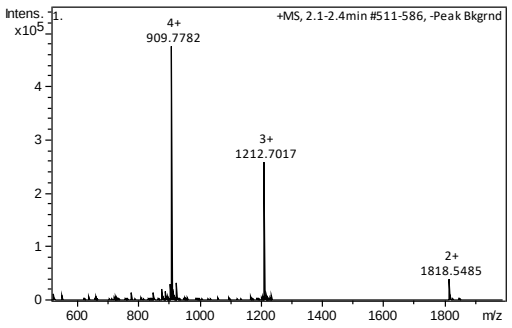

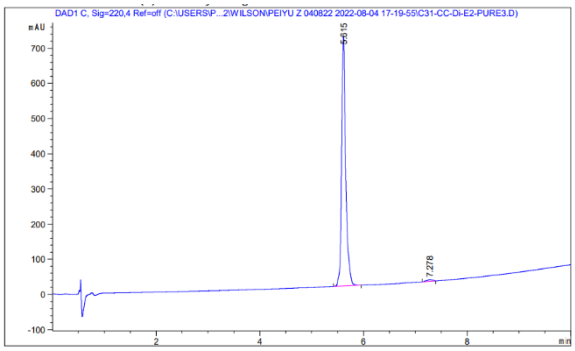

CC-Di-HRK1

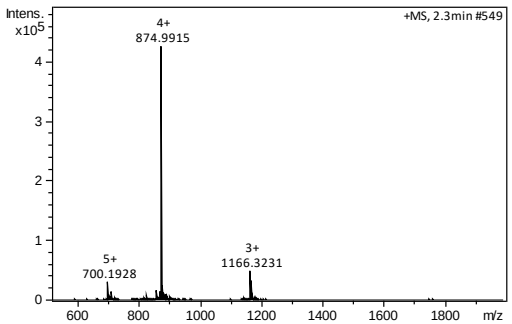

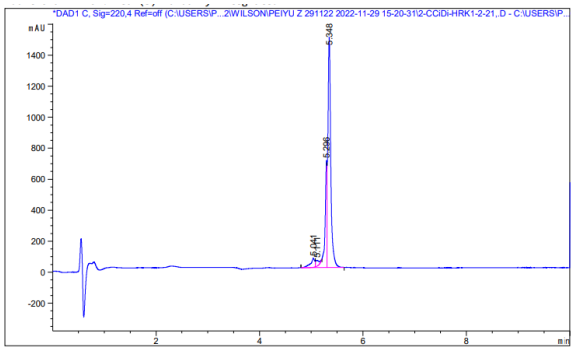

CC-Di-HRK2

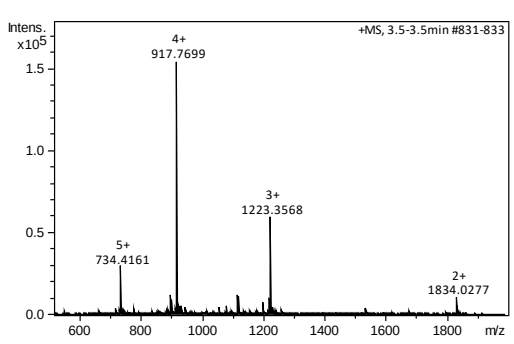

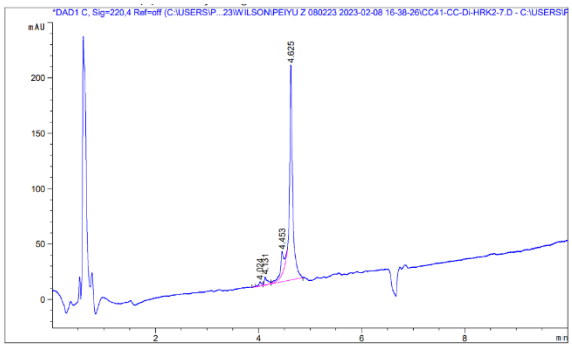

CC-Di-HRK3

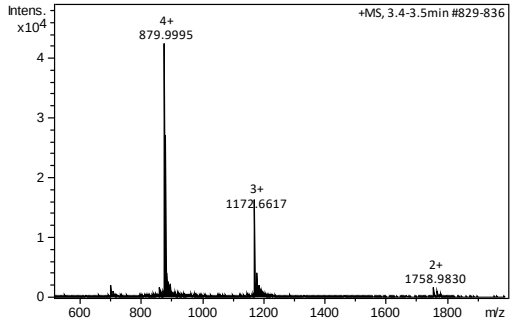

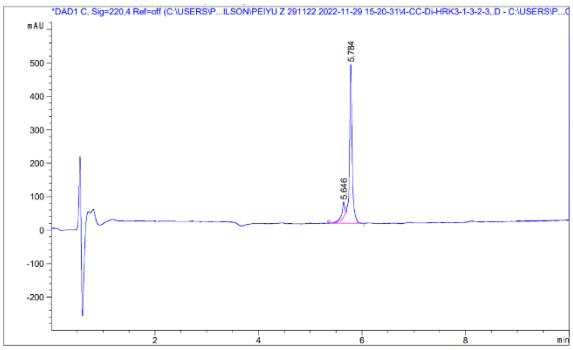

CC-Di-HRK4

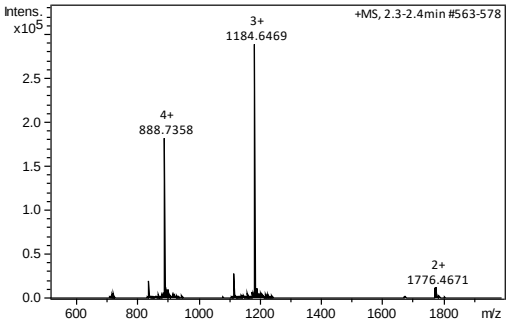

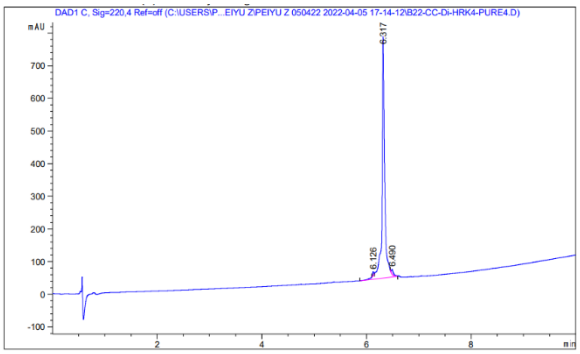

Reference

(1) Petta, I.; Lievens, S.; Libert, C.; Tavernier, J.; De Bosscher, K. Modulation of Protein–Protein Interactions for the Development of Novel Therapeutics. *Mol. Ther.* **2016**, *24* (4), 707–718.

(2) Stumpf, M. P. H.; Thorne, T.; De Silva, E.; Stewart, R.; An, H. J.; Lappe, M.; Wiuf, C. Estimating the Size of the Human Interactome. *Proc. Natl. Acad. Sci.* **2008**, *105* (19), 6959–6964.

(3) Ryan, D. P.; Matthews, J. M. Protein–Protein Interactions in Human Disease. *Curr. Opin. Struct. Biol.* **2005**, *15* (4), 441–446.

(4) Pelay-Gimeno, M.; Glas, A.; Koch, O.; Grossmann, T. N. Structure-Based Design of Inhibitors of Protein–Protein Interactions: Mimicking Peptide Binding Epitopes. *Angew. Chemie Int. Ed.* **2015**, *54* (31), 8896–8927. https://doi.org/10.1002/ANIE.201412070.

(5) Wilson, A. J. Inhibition of Protein–Protein Interactions Using Designed Molecules. *Chem. Soc. Rev.* **2009**, *38* (12), 3289–3300. https://doi.org/10.1039/b807197g.

(6) Moreira, I. S.; Fernandes, P. A.; Ramos, M. J. Hot Spots - A Review of the Protein-Protein Interface Determinant Amino-Acid Residues. *Proteins: Structure, Function and Genetics*. John Wiley & Sons, Ltd September 1, 2007, pp 803–812. https://doi.org/10.1002/prot.21396.

(7) Clackson, T.; Wells, J. A. A Hot Spot of Binding Energy in a Hormone-Receptor Interface. *Science (80-.).* **1995**, *267* (5196), 383–386. https://doi.org/10.1126/science.7529940.

(8) Rosário-Ferreira, N.; Bonvin, A. M. J. J.; Moreira, I. S. Using Machine-Learning-Driven Approaches to Boost Hot-Spot's Knowledge. *WIREs Comput. Mol. Sci.* **2022**, *12* (5), e1602. https://doi.org/https://doi.org/10.1002/wcms.1602.

(9) Kenneth Morrow, J.; Zhang, S. Computational Prediction of Protein Hot Spot Residues. *Curr. Drug Metab.* **2012**, *18* (9), 1255–1265. https://doi.org/10.2174/138920012799362909.

(10) Qiu, Y.; Li, X.; He, X.; Pu, J.; Zhang, J.; Lu, S. Computational Methods-Guided Design of Modulators Targeting Protein-Protein Interactions (PPIs). *Eur. J. Med. Chem.* **2020**, *207*, 112764.

(11) Azzarito, V.; Long, K.; Murphy, N. S.; Wilson, A. J. Inhibition of α-Helix-Mediated Protein-Protein Interactions Using Designed Molecules. *Nat. Chem.* **2013**, *5* (3), 161–173. https://doi.org/10.1038/nchem.1568.

(12) Kussie, P. H.; Gorina, S.; Marechal, V.; Elenbaas, B.; Moreau, J.; Levine, A. J.; Pavletich, N. P. Structure of the MDM2 Oncoprotein Bound to the P53 Tumor Suppressor Transactivation Domain. *Science (80-.).* **1996**, *274* (5289), 948–953. https://doi.org/10.1126/science.274.5289.948.

(13) Petros, A. M.; Olejniczak, E. T.; Fesik, S. W. Structural Biology of the Bcl-2 Family of Proteins. *Biochimica et Biophysica Acta - Molecular Cell*

Research. Elsevier March 1, 2004, pp 83–94. https://doi.org/10.1016/j.bbamcr.2003.08.012.

(14) Chan, D. C.; Fass, D.; Berger, J. M.; Kim, P. S. Core Structure of Gp41 from the HIV Envelope Glycoprotein. *Cell* **1997**, *89* (2), 263–273. https://doi.org/10.1016/S0092-8674(00)80205-6.

(15) Rezaei Araghi, R.; Keating, A. E. Designing Helical Peptide Inhibitors of Protein-Protein Interactions. *Curr. Opin. Struct. Biol.* **2016**, *39*, 27–38. https://doi.org/10.1016/j.sbi.2016.04.001.

(16) Bromley, E. H. C.; Channon, K.; Moutevelis, E.; Woolfson, D. N. Peptide and Protein Building Blocks for Synthetic Biology: From Programming Biomolecules to Self-Organized Biomolecular Systems. *ACS Chem. Biol.* **2008**, *3* (1), 38–50. https://doi.org/10.1021/cb700249v.

(17) Walshaw, J.; Woolfson, D. N. Extended Knobs-into-Holes Packing in Classical and Complex Coiled-Coil Assemblies. *J. Struct. Biol.* **2003**, *144* (3), 349–361. https://doi.org/10.1016/j.jsb.2003.10.014.

(18) Meng, G.; Pu, J.; Li, Y.; Han, A.; Tian, Y.; Xu, W.; Zhang, T.; Li, X.; Lu, L.; Wang, C.; Jiang, S.; Liu, K. Design and Biological Evaluation of M-Xylene Thioether-Stapled Short Helical Peptides Targeting the HIV-1 Gp41 Hexameric Coiled-Coil Fusion Complex. *J. Med. Chem.* **2019**, *62* (19), 8773–8783. https://doi.org/10.1021/acs.jmedchem.9b00882.

(19) Mullard, A. Proteing-Protein Interaction Inhibitors Get into the Groove. *Nat. Rev. Drug Discov.* **2012**, *11* (3), 173–175. https://doi.org/10.1038/nrd3680.

(20) Lu, M.; Stoller, M. O.; Wang, S.; Liu, J.; Fagan, M. B.; Nunberg, J. H. Structural and Functional Analysis of Interhelical Interactions in the Human Immunodeficiency Virus Type 1 Gp41 Envelope Glycoprotein by Alanine-Scanning Mutagenesis. *J. Virol.* **2001**, *75* (22), 11146–11156.

(21) Lu, L.; Liu, Q.; Zhu, Y.; Chan, K.-H.; Qin, L.; Li, Y.; Wang, Q.; Chan, J. F.-W.; Du, L.; Yu, F. Structure-Based Discovery of Middle East Respiratory Syndrome Coronavirus Fusion Inhibitor. *Nat. Commun.* **2014**, *5* (1), 3067.

(22) Malashkevich, V. N.; Schneider, B. J.; McNally, M. L.; Milhollen, M. A.; Pang, J. X.; Kim, P. S. Core Structure of the Envelope Glycoprotein GP2 from Ebola Virus at 1.9-Å Resolution. *Proc. Natl. Acad. Sci.* **1999**, *96* (6), 2662–2667.

(23) Pelay-Gimeno, M.; Glas, A.; Koch, O.; Grossmann, T. N. Structure-Based Design of Inhibitors of Protein-Protein Interactions: Mimicking Peptide Binding Epitopes. *Angew. Chemie - Int. Ed.* **2015**, *54* (31), 8896–8927. https://doi.org/10.1002/anie.201412070.

(24) Jones, S.; Thornton, J. M. Review Principles of Protein-Protein Interactions. **1996**, *93* (January), 13–20.

(25) London, N.; Raveh, B.; Schueler-Furman, O. Druggable Protein-Protein Interactions - from Hot Spots to Hot Segments. *Curr. Opin. Chem. Biol.* **2013**, *17* (6), 952–959. https://doi.org/10.1016/j.cbpa.2013.10.011.

(26) Chang, Y. S.; Graves, B.; Guerlavais, V.; Tovar, C.; Packman, K.; To, K. H.; Olson, K. A.; Kesavan, K.; Gangurde, P.; Mukherjee, A.; Baker, T.; Darlak, K.; Elkin, C.; Filipovic, Z.; Qureshi, F. Z.; Cai, H.; Berry, P.; Feyfant, E.; Shi, X. E.; Horstick, J.; Annis, D. A.; Manning, A. M.; Fotouhi, N.; Nash, H.; Vassilev, L. T.; Sawyer, T. K. Stapled α-Helical Peptide Drug Development: A Potent Dual Inhibitor of MDM2 and MDMX for P53-Dependent Cancer Therapy. *Proc. Natl. Acad. Sci. U. S. A.* **2013**, *110* (36), E3445–E3454. https://doi.org/10.1073/pnas.1303002110.

(27) Kussie, P. H.; Gorina, S.; Marechal, V.; Elenbaas, B.; Moreau, J.; Levine, A. J.; Pavletich, N. P. Structure of the MDM2 Oncoprotein Bound to the P53 Tumor Suppressor Transactivation Domain. *Science (80-.).* **1996**, *274* (5289), 948–953. https://doi.org/10.1126/science.274.5289.948.

(28) Rajan, S.; Choi, M.; Baek, K.; Yoon, H. S. Bh3 Induced Conformational Changes in Bcl-Xl Revealed by Crystal Structure and Comparative Analysis. *Proteins Struct. Funct. Bioinforma.* **2015**, *83* (7), 1262–1272. https://doi.org/10.1002/prot.24816.

(29) Singh, R.; Letai, A.; Sarosiek, K. Regulation of Apoptosis in Health and Disease: The Balancing Act of BCL-2 Family Proteins. *Nature Reviews Molecular Cell Biology*. Nature Publishing Group March 1, 2019, pp 175–193. https://doi.org/10.1038/s41580-018-0089-8.

(30) Peña-Blanco, A.; García-Sáez, A. J. Bax, Bak and beyond — Mitochondrial Performance in Apoptosis. *FEBS Journal*. Blackwell Publishing Ltd February 1, 2018, pp 416–431. https://doi.org/10.1111/febs.14186.

(31) Chipuk, J. E.; Moldoveanu, T.; Llambi, F.; Parsons, M. J.; Green, D. R. The BCL-2 Family Reunion. *Molecular Cell*. Cell Press February 12, 2010, pp 299–310. https://doi.org/10.1016/j.molcel.2010.01.025.

(32) Luna-Vargas, M. P. A.; Chipuk, J. E. Physiological and Pharmacological Control of BAK, BAX, and Beyond. *Trends in Cell Biology*. Elsevier Ltd December 1, 2016, pp 906–917. https://doi.org/10.1016/j.tcb.2016.07.002.

(33) Luna-Vargas, M. P. A.; Chipuk, J. E. Physiological and Pharmacological Control of BAK, BAX, and Beyond. *Trends Cell Biol.* **2016**, *26* (12), 906–917. https://doi.org/10.1016/j.tcb.2016.07.002.

(34) Singh, R.; Letai, A.; Sarosiek, K. Regulation of Apoptosis in Health and Disease: The Balancing Act of BCL-2 Family Proteins. *Nat. Rev. Mol. Cell Biol.* **2019**, *20* (3), 175–193. https://doi.org/10.1038/s41580-018-0089-8.

(35) Kong, W.; Zhou, M.; Li, Q.; Fan, W.; Lin, H.; Wang, R. Experimental Characterization of the Binding Affinities between Proapoptotic BH3 Peptides and Antiapoptotic Bcl-2 Proteins. *ChemMedChem* **2018**, *13* (17), 1763–1770. https://doi.org/10.1002/cmdc.201800321.

(36) Gutschner, T.; Diederichs, S. The Hallmarks of Cancer: A Long Non-Coding RNA Point of View. *RNA Biology*. Taylor and Francis Inc. 2012,

pp 703–719. https://doi.org/10.4161/rna.20481.

(37) Tse, C.; Shoemaker, A. R.; Adickes, J.; Anderson, M. G.; Chen, J.; Jin, S.; Johnson, E. F.; Marsh, K. C.; Mitten, M. J.; Nimmer, P. ABT-263: A Potent and Orally Bioavailable Bcl-2 Family Inhibitor. *Cancer Res.* **2008**, *68* (9), 3421–3428.

(38) Walensky, L. D.; Kung, A. L.; Escher, I.; Malia, T. J.; Barbuto, S.; Wright, R. D.; Wagner, G.; Verdine, G. L.; Korsmeyer, S. J. Activation of Apoptosis in Vivo by a Hydrocarbon-Stapled BH3 Helix. *Science (80-.).* **2004**, *305* (5689), 1466–1470. https://doi.org/10.1126/science.1099191.

(39) Schenk, R. L.; Strasser, A.; Dewson, G. BCL-2: Long and Winding Path from Discovery to Therapeutic Target. *Biochemical and Biophysical Research Communications*. Elsevier B.V. January 15, 2017, pp 459–469. https://doi.org/10.1016/j.bbrc.2016.10.100.

(40) Letai, A. S63845, an MCL-1 Selective BH3 Mimetic: Another Arrow in Our Quiver. *Cancer Cell*. Cell Press December 12, 2016, pp 834–835. https://doi.org/10.1016/j.ccell.2016.11.016.

(41) Kale, J.; Osterlund, E. J.; Andrews, D. W. BCL-2 Family Proteins: Changing Partners in the Dance towards Death. *Cell Death Differ.* **2018**, *25* (1), 65–80. https://doi.org/10.1038/cdd.2017.186.

(42) Tsujimoto, Y.; Croce, C. M. Analysis of the Structure, Transcripts, and Protein Products of Bcl-2, the Gene Involved in Human Follicular Lymphoma. *Proc. Natl. Acad. Sci.* **1986**, *83* (14), 5214–5218.

(43) Cleary, M. L.; Smith, S. D.; Sklar, J. Cloning and Structural Analysis of CDNAs for Bcl-2 and a Hybrid Bcl-2/Immunoglobulin Transcript Resulting from the t (14; 18) Translocation. *Cell* **1986**, *47* (1), 19–28.

(44) Tsujimoto, Y.; Finger, L. R.; Yunis, J.; Nowell, P. C.; Croce, C. M. Cloning of the Chromosome Breakpoint of Neoplastic B Cells with the t (14; 18) Chromosome Translocation. *Science (80-.).* **1984**, *226* (4678), 1097–1099.

(45) Tsujimoto, Y.; Jaffe, E.; Cossman, J.; Gorham, J.; Nowell, P. C.; Croce, C. M. Clustering of Breakpoints on Chromosome 11 in Human B-Cell Neoplasms with the t (11; 14) Chromosome Translocation. *Nature* **1985**, *315*, 340–343.

(46) Pattingre, S.; Tassa, A.; Qu, X.; Garuti, R.; Liang, X. H.; Mizushima, N.; Packer, M.; Schneider, M. D.; Levine, B. Bcl-2 Antiapoptotic Proteins Inhibit Beclin 1-Dependent Autophagy. *Cell* **2005**, *122* (6), 927–939.

(47) Caroline, H. Y.; Pan, H.; Seebacher, J.; Jang, I.-H.; Hyberts, S. G.; Heffron, G. J.; Vander Heiden, M. G.; Yang, R.; Li, F.; Locasale, J. W. Metabolic Regulation of Protein N-Alpha-Acetylation by Bcl-XL Promotes Cell Survival. *Cell* **2011**, *146* (4), 607–620.

(48) Berman, S. B.; Chen, Y.; Qi, B.; McCaffery, J. M.; Rucker III, E. B.; Goebbels, S.; Nave, K.-A.; Arnold, B. A.; Jonas, E. A.; Pineda, F. J. Bcl-XL Increases Mitochondrial Fission, Fusion, and Biomass in Neurons. *J. Cell Biol.* **2009**, *184* (5), 707–719.

(49) Gross, A.; Katz, S. G. Non-Apoptotic Functions of BCL-2 Family Proteins. *Cell Death Differ.* **2017**, *24* (8), 1348–1358.

(50) Rinkenberger, J. L.; Horning, S.; Klocke, B.; Roth, K.; Korsmeyer, S. J. Mcl-1 Deficiency Results in Peri-Implantation Embryonic Lethality. *Genes Dev.* **2000**, *14* (1), 23–27.

(51) Motoyama, N.; Wang, F.; Roth, K. A.; Sawa, H.; Nakayama, K.; Nakayama, K.; Negishi, I.; Senju, S.; Zhang, Q.; Fujii, S. Massive Cell Death of Immature Hematopoietic Cells and Neurons in Bcl-x-Deficient Mice. *Science (80-.).* **1995**, *267* (5203), 1506–1510.

(52) Chen, H.-C.; Kanai, M.; Inoue-Yamauchi, A.; Tu, H.-C.; Huang, Y.; Ren, D.; Kim, H.; Takeda, S.; Reyna, D. E.; Chan, P. M. An Interconnected Hierarchical Model of Cell Death Regulation by the BCL-2 Family. *Nat. Cell Biol.* **2015**, *17* (10), 1270–1281.

(53) Veis, D. J.; Sorenson, C. M.; Shutter, J. R.; Korsmeyer, S. J. Bcl-2-Deficient Mice Demonstrate Fulminant Lymphoid Apoptosis, Polycystic Kidneys, and Hypopigmented Hair. *Cell* **1993**, *75* (2), 229–240.

(54) Nakayama, K.; Nakayama, K.; Negishi, I.; Kuida, K.; Shinkai, Y.; Louie, M. C.; Fields, L. E.; Lucas, P. J.; Stewart, V.; Alt, F. W. Disappearance of the Lymphoid System in Bcl-2 Homozygous Mutant Chimeric Mice. *Science (80-.).* **1993**, *261* (5128), 1584–1588.

(55) Qi, B.; Hardwick, J. M. A Bcl-XL Timer Sets Platelet Life Span. *Cell* **2007**, *128* (6), 1035–1036.

(56) Mason, K. D.; Carpinelli, M. R.; Fletcher, J. I.; Collinge, J. E.; Hilton, A. A.; Ellis, S.; Kelly, P. N.; Ekert, P. G.; Metcalf, D.; Roberts, A. W. Programmed Anuclear Cell Death Delimits Platelet Life Span. *Cell* **2007**, *128* (6), 1173–1186.

(57) Muchmore, S. W.; Sattler, M.; Liang, H.; Meadows, R. P.; Harlan, J. E.; Yoon, H. S.; Nettesheim, D.; Chang, B. S.; Thompson, C. B.; Wong, S.-L. X-Ray and NMR Structure of Human Bcl-XL, an Inhibitor of Programmed Cell Death. *Nature* **1996**, *381* (6580), 335–341.

(58) Maiuri, M. C.; Le Toumelin, G.; Criollo, A.; Rain, J. C.; Gautier, F.; Juin, P.; Tasdemir, E.; Pierron, G.; Troulinaki, K.; Tavernarakis, N.; Hickman, J. A.; Geneste, O.; Kroemer, G. Functional and Physical Interaction between Bcl-XL and a BH3-like Domain in Beclin-1. *EMBO J.* **2007**, *26* (10), 2527–2539. https://doi.org/10.1038/sj.emboj.7601689.

(59) Ambrosi, E.; Capaldi, S.; Bovi, M.; Saccomani, G.; Perduca, M.; Monaco, H. L. Structural Changes in the BH3 Domain of SOUL Protein upon Interaction with the Anti-Apoptotic Protein Bcl-XL. *Biochem. J.* **2011**, *438* (2), 291–301.

(60) Sattler, M.; Liang, H.; Nettesheim, D.; Meadows, R. P.; Harlan, J. E.; Eberstadt, M.; Yoon, H. S.; Shuker, S. B.; Chang, B. S.; Minn, A. J.; Thompson, C. B.; Fesik, S. W. Structure of Bcl-XL-Bak Peptide Complex: Recognition Between Regulators of Apoptosis. *Science (80-.).* **1997**, *275* (5302), 983–986. https://doi.org/10.1126/SCIENCE.275.5302.983.

(61) Feng, W.; Huang, S.; Wu, H.; Zhang, M. Molecular Basis of Bcl-XL's Target Recognition Versatility Revealed by the Structure of Bcl-XL in Complex with the BH3 Domain of Beclin-1. *J. Mol. Biol.* **2007**, *372* (1), 223–235.

(62) Thébault, S.; Agez, M.; Chi, X.; Stojko, J.; Cura, V.; Telerman, S. B.; Maillet, L.; Gautier, F.; Billas-Massobrio, I.; Birck, C. TCTP Contains a BH3-like Domain, Which Instead of Inhibiting, Activates Bcl-XL. *Sci. Rep.* **2016**, *6* (1), 19725.

(63) Miles, J. A.; Yeo, D. J.; Rowell, P.; Rodriguez-Marin, S.; Pask, C. M.; Warriner, S. L.; Edwards, T. A.; Wilson, A. J. Hydrocarbon Constrained Peptides-Understanding Preorganisation and Binding Affinity. *Chem. Sci.* **2016**, *7* (6), 3694–3702. https://doi.org/10.1039/c5sc04048e.

(64) Yoon, M.-K.; Kim, B.-Y.; Lee, J.-Y.; Ha, J.-H.; Kim, S. A.; Lee, D.-H.; Lee, M.-S.; Lee, M.-K.; Choi, J. S.; Cho, J. H. Cytoplasmic Pro-Apoptotic Function of the Tumor Suppressor P73 Is Mediated through a Modified Mode of Recognition of the Anti-Apoptotic Regulator Bcl-XL. *J. Biol. Chem.* **2018**, *293* (51), 19546–19558.

(65) Wilson, W. H.; O'Connor, O. A.; Czuczman, M. S.; LaCasce, A. S.; Gerecitano, J. F.; Leonard, J. P.; Tulpule, A.; Dunleavy, K.; Xiong, H.; Chiu, Y.-L. Navitoclax, a Targeted High-Affinity Inhibitor of BCL-2, in Lymphoid Malignancies: A Phase 1 Dose-Escalation Study of Safety, Pharmacokinetics, Pharmacodynamics, and Antitumour Activity. *Lancet Oncol.* **2010**, *11* (12), 1149–1159.

(66) Roberts, A. W.; Seymour, J. F.; Brown, J. R.; Wierda, W. G.; Kipps, T. J.; Khaw, S. L.; Carney, D. A.; He, S. Z.; Huang, D. C. S.; Xiong, H. Substantial Susceptibility of Chronic Lymphocytic Leukemia to BCL2 Inhibition: Results of a Phase I Study of Navitoclax in Patients with Relapsed or Refractory Disease. *J. Clin. Oncol.* **2012**, *30* (5), 488.

(67) Rudin, C. M.; Hann, C. L.; Garon, E. B.; Ribeiro de Oliveira, M.; Bonomi, P. D.; Camidge, D. R.; Chu, Q.; Giaccone, G.; Khaira, D.; Ramalingam, S. S. Phase II Study of Single-Agent Navitoclax (ABT-263) and Biomarker Correlates in Patients with Relapsed Small Cell Lung CancerNavitoclax for Recurrent Small Cell Lung Cancer. *Clin. Cancer Res.* **2012**, *18* (11), 3163–3169.

(68) Deeks, E. D. Venetoclax: First Global Approval. *Drugs* **2016**, *76*, 979–987.

(69) Souers, A. J.; Leverson, J. D.; Boghaert, E. R.; Ackler, S. L.; Catron, N. D.; Chen, J.; Dayton, B. D.; Ding, H.; Enschede, S. H.; Fairbrother, W. J. ABT-199, a Potent and Selective BCL-2 Inhibitor, Achieves Antitumor Activity While Sparing Platelets. *Nat. Med.* **2013**, *19* (2), 202–208.

(70) Tao, Z.-F.; Hasvold, L.; Wang, L.; Wang, X.; Petros, A. M.; Park, C. H.; Boghaert, E. R.; Catron, N. D.; Chen, J.; Colman, P. M. Discovery of a Potent and Selective BCL-XL Inhibitor with in Vivo Activity. *ACS Med. Chem. Lett.* **2014**, *5* (10), 1088–1093.

(71) Khan, S.; Zhang, X.; Lv, D.; Zhang, Q.; He, Y.; Zhang, P.; Liu, X.; Thummuri, D.; Yuan, Y.; Wiegand, J. S. A Selective BCL-XL PROTAC

Degrader Achieves Safe and Potent Antitumor Activity. *Nat. Med.* **2019**, *25* (12), 1938–1947.

(72) Follis, A. V.; Chipuk, J. E.; Fisher, J. C.; Yun, M.-K.; Grace, C. R.; Nourse, A.; Baran, K.; Ou, L.; Min, L.; White, S. W. PUMA Binding Induces Partial Unfolding within BCL-XL to Disrupt P53 Binding and Promote Apoptosis. *Nat. Chem. Biol.* **2013**, *9* (3), 163–168.

(73) Chung, C. W.; Dai, H.; Fernandez, E.; Tinworth, C. P.; Churcher, I.; Cryan, J.; Denyer, J.; Harling, J. D.; Konopacka, A.; Queisser, M. A.; Tame, C. J.; Watt, G.; Jiang, F.; Qian, D.; Benowitz, A. B. Structural Insights into PROTAC-Mediated Degradation of Bcl-XL. *ACS Chem. Biol.* **2020**, *15* (9), 2316–2323. https://doi.org/10.1021/acschembio.0c00266.

(74) Follis, A. V.; Llambi, F.; Ou, L.; Baran, K.; Green, D. R.; Kriwacki, R. W. The DNA-Binding Domain Mediates Both Nuclear and Cytosolic Functions of P53. *Nat. Struct. Mol. Biol.* **2014**, *21* (6), 535–543.

(75) Tan, Y. S.; Lane, D. P.; Verma, C. S. Stapled Peptide Design: Principles and Roles of Computation. *Drug Discov. Today* **2016**, *21* (10), 1642–1653.

(76) Vlieghe, P.; Lisowski, V.; Martinez, J.; Khrestchatisky, M. Synthetic Therapeutic Peptides: Science and Market. *Drug Discov. Today* **2010**, *15* (1–2), 40–56. https://doi.org/10.1016/j.drudis.2009.10.009.

(77) Walensky, L. D.; Bird, G. H. Hydrocarbon-Stapled Peptides: Principles, Practice, and Progress. *J. Med. Chem* **2014**, *57*, 6275–6288.

(78) Scott, D. E.; Bayly, A. R.; Abell, C.; Skidmore, J. Small Molecules, Big Targets: Drug Discovery Faces the Protein-Protein Interaction Challenge. *Nat. Rev. Drug Discov.* **2016**, *15* (8), 533–550. https://doi.org/10.1038/nrd.2016.29.

(79) Muttenthaler, M.; King, G. F.; Adams, D. J.; Alewood, P. F. Trends in Peptide Drug Discovery. *Nat. Rev. Drug Discov.* **2021**, *20* (4), 309–325. https://doi.org/10.1038/s41573-020-00135-8.

(80) Zhang, H.; Chen, S. Cyclic Peptide Drugs Approved in the Last Two Decades (2001–2021). *RSC Chem. Biol.* **2022**, *3* (1), 18–31. https://doi.org/10.1039/d1cb00154j.

(81) Li, X.; Chen, S.; Zhang, W. D.; Hu, H. G. Stapled Helical Peptides Bearing Different Anchoring Residues. *Chem. Rev.* **2020**, *120* (18), 10079–10144. https://doi.org/10.1021/ACS.CHEMREV.0C00532/ASSET/IMAGES/MEDIUM/CR0C00532_0064.GIF.

(82) Walensky, L. D.; Bird, G. H. Hydrocarbon-Stapled Peptides: Principles, Practice, and Progress. *Journal of Medicinal Chemistry*. American Chemical Society August 14, 2014, pp 6275–6288. https://doi.org/10.1021/jm4011675.

(83) Li, X.; Chen, S.; Zhang, W. D.; Hu, H. G. Stapled Helical Peptides Bearing Different Anchoring Residues. *Chem. Rev.* **2020**, *120* (18), 10079–10144. https://doi.org/10.1021/acs.chemrev.0c00532.

(84) Klein, M. Stabilized Helical Peptides: Overview of the Technologies and Its Impact on Drug Discovery. *Expert Opin. Drug Discov.* **2017**, *12* (11), 1117–1125. https://doi.org/10.1080/17460441.2017.1372745.

(85) Lau, J. L.; Dunn, M. K. Therapeutic Peptides: Historical Perspectives, Current Development Trends, and Future Directions. *Bioorganic Med. Chem.* **2018**, *26* (10), 2700–2707. https://doi.org/10.1016/j.bmc.2017.06.052.

(86) Lau, Y. H.; De Andrade, P.; Wu, Y.; Spring, D. R. Peptide Stapling Techniques Based on Different Macrocyclisation Chemistries. *Chem. Soc. Rev.* **2015**, *44* (1), 91–102. https://doi.org/10.1039/c4cs00246f.

(87) Schafmeister, C. E.; Po, J.; Verdine, G. L. An All-Hydrocarbon Cross-Linking System for Enhancing the Helicity and Metabolic Stability of Peptides [8]. *Journal of the American Chemical Society*. American Chemical Society June 21, 2000, pp 5891–5892. https://doi.org/10.1021/ja000563a.

(88) Kawamoto, S. A.; Coleska, A.; Ran, X.; Yi, H.; Yang, C. Y.; Wang, S. Design of Triazole-Stapled BCL9 α-Helical Peptides to Target the β-Catenin/B-Cell CLL/Lymphoma 9 (BCL9) Protein-Protein Interaction. *J. Med. Chem.* **2012**, *55* (3), 1137–1146. https://doi.org/10.1021/jm201125d.

(89) Brunel, F. M.; Dawson, P. E. Synthesis of Constrained Helical Peptides by Thioether Ligation: Application to Analogs of Gp41. *Chem. Commun.* **2005**, No. 20, 2552–2554. https://doi.org/10.1039/b419015g.

(90) Blackwell, H. E.; Grubbs, R. H. Highly Efficient Synthesis of Covalently Cross-linked Peptide Helices by Ring-closing Metathesis. *Angew. Chemie Int. Ed.* **1998**, *37* (23), 3281–3284.

(91) Walensky, L. D.; Kung, A. L.; Escher, I.; Malia, T. J.; Barbuto, S.; Wright, R. D.; Wagner, G.; Verdine, G. L.; Korsmeyer, S. J. Activation of Apoptosis in Vivo by a Hydrocarbon-Stapled BH3 Helix. *Science (80-.).* **2004**, *305* (5689), 1466–1470. https://doi.org/10.1126/science.1099191.

(92) Cromm, P. M.; Spiegel, J.; Grossmann, T. N. Hydrocarbon Stapled Peptides as Modulators of Biological Function. *ACS Chem. Biol.* **2015**, *10* (6), 1362–1375. https://doi.org/10.1021/cb501020r.

(93) Kim, Y. W.; Verdine, G. L. Stereochemical Effects of All-Hydrocarbon Tethers in i,I+4 Stapled Peptides. *Bioorganic Med. Chem. Lett.* **2009**, *19* (9), 2533–2536. https://doi.org/10.1016/j.bmcl.2009.03.022.

(94) Shim, S. Y.; Kim, Y. W.; Verdine, G. L. A New i, i + 3 Peptide Stapling System for α-Helix Stabilization. *Chem. Biol. Drug Des.* **2013**, *82* (6), 635–642. https://doi.org/10.1111/cbdd.12231.

(95) Kim, Y. W.; Grossmann, T. N.; Verdine, G. L. Synthesis of All-Hydrocarbon Stapled ±-Helical Peptides by Ring-Closing Olefin Metathesis. *Nat. Protoc.* **2011**, *6* (6), 761–771. https://doi.org/10.1038/nprot.2011.324.

(96) Kim, Y. W.; Kutchukian, P. S.; Verdine, G. L. Introduction of All-Hydrocarbon i,i + 3 Staples into α-Helices via Ring-Closing Olefin

Metathesis. *Org. Lett.* **2010**, *12* (13), 3046–3049. https://doi.org/10.1021/ol1010449.

(97) Kannan, S.; Aronica, P. G. A.; Ng, S.; Lian, D. T. G.; Frosi, Y.; Chee, S.; Shimin, J.; Yuen, T. Y.; Sadruddin, A.; Kaan, H. Y. K. Macrocyclization of an All-d Linear α-Helical Peptide Imparts Cellular Permeability. *Chem. Sci.* **2020**, *11* (21), 5577–5591.

(98) Bird, G. H.; Madani, N.; Perry, A. F.; Princiotto, A. M.; Supko, J. G.; He, X.; Gavathiotis, E.; Sodroski, J. G.; Walensky, L. D. Hydrocarbon Double-Stapling Remedies the Proteolytic Instability of a Lengthy Peptide Therapeutic. *Proc. Natl. Acad. Sci.* **2010**, *107* (32), 14093–14098.

(99) Hilinski, G. J.; Kim, Y. W.; Hong, J.; Kutchukian, P. S.; Crenshaw, C. M.; Berkovitch, S. S.; Chang, A.; Ham, S.; Verdine, G. L. Stitched α-Helical Peptides via Bis Ring-Closing Metathesis. *J. Am. Chem. Soc.* **2014**, *136* (35), 12314–12322. https://doi.org/10.1021/ja505141j.

(100) Kim, Y. W.; Grossmann, T. N.; Verdine, G. L. Synthesis of All-Hydrocarbon Stapled ±-Helical Peptides by Ring-Closing Olefin Metathesis. *Nat. Protoc.* **2011**, *6* (6), 761–771. https://doi.org/10.1038/nprot.2011.324.

(101) Yeo, D. J.; Warriner, S. L.; Wilson, A. J. Monosubstituted Alkenyl Amino Acids for Peptide “Stapling.” *Chem. Commun.* **2013**, *49* (80), 9131–9133. https://doi.org/10.1039/C3CC45231J.

(102) Tan, Y. S.; Lane, D. P.; Verma, C. S. Stapled Peptide Design: Principles and Roles of Computation. *Drug Discov. Today* **2016**, *21* (10), 1642–1653. https://doi.org/10.1016/j.drudis.2016.06.012.

(103) Speltz, T. E.; Fanning, S. W.; Mayne, C. G.; Fowler, C.; Tajkhorshid, E.; Greene, G. L.; Moore, T. W. Stapled Peptides with γ-Methylated Hydrocarbon Chains for the Estrogen Receptor/Coactivator Interaction. *Angew. Chemie - Int. Ed.* **2016**, *55* (13), 4252–4255. https://doi.org/10.1002/anie.201510557.

(104) Wu, Y.; Li, Y.-H.; Li, X.; Zou, Y.; Liao, H.-L.; Liu, L.; Chen, Y.-G.; Bierer, D.; Hu, H.-G. A Novel Peptide Stapling Strategy Enables the Retention of Ring-Closing Amino Acid Side Chains for the Wnt/β-Catenin Signalling Pathway. *Chem. Sci.* **2017**, *8* (11), 7368–7373.

(105) Devaraj, N. K.; Finn, M. G. Introduction: Click Chemistry. *Chemical Reviews*. ACS Publications 2021, pp 6697–6698.

(106) Tang, W.; Becker, M. L. “click” Reactions: A Versatile Toolbox for the Synthesis of Peptide-Conjugates. *Chem. Soc. Rev.* **2014**, *43* (20), 7013–7039. https://doi.org/10.1039/c4cs00139g.

(107) Empting, M.; Avrutina, O.; Meusinger, R.; Fabritz, S.; Reinwarth, M.; Biesalski, M.; Voigt, S.; Buntkowsky, G.; Kolmar, H. “Triazole Bridge”: Disulfide-Bond Replacement by Ruthenium-Catalyzed Formation of 1,5-Disubstituted 1,2,3-Triazoles. *Angew. Chemie - Int. Ed.* **2011**, *50* (22), 5207–5211. https://doi.org/10.1002/anie.201008142.

(108) Li, X. Click to Join Peptides/Proteins Together. *Chem. - An Asian J.*

2011, *6* (10), 2606–2616. https://doi.org/10.1002/asia.201100329.

(109) Tala, S. R.; Singh, A.; Lensing, C. J.; Schnell, S. M.; Freeman, K. T.; Rocca, J. R.; Haskell-Luevano, C. 1, 2, 3-Triazole Rings as a Disulfide Bond Mimetic in Chimeric AGRP-Melanocortin Peptides: Design, Synthesis, and Functional Characterization. *ACS Chem. Neurosci.* **2017**, *9* (5), 1001–1013.

(110) Torres, O.; Yüksel, D.; Bernardina, M.; Kumar, K.; Bong, D. Peptide Tertiary Structure Nucleation by Side-Chain Crosslinking with Metal Complexation and Double “Click” Cycloaddition. *ChemBioChem* **2008**, *9* (11), 1701–1705. https://doi.org/10.1002/cbic.200800040.

(111) Lau, Y. H.; De Andrade, P.; Quah, S. T.; Rossmann, M.; Laraia, L.; Sköld, N.; Sum, T. J.; Rowling, P. J. E.; Joseph, T. L.; Verma, C.; Hyvönen, M.; Itzhaki, L. S.; Venkitaraman, A. R.; Brown, C. J.; Lane, D. P.; Spring, D. R. Functionalised Staple Linkages for Modulating the Cellular Activity of Stapled Peptides. *Chem. Sci.* **2014**, *5* (5), 1804–1809. https://doi.org/10.1039/c4sc00045e.

(112) Iegre, J.; Ahmed, N. S.; Gaynord, J. S.; Wu, Y.; Herlihy, K. M.; Tan, Y. S.; Lopes-Pires, M. E.; Jha, R.; Lau, Y. H.; Sore, H. F. Stapled Peptides as a New Technology to Investigate Protein–Protein Interactions in Human Platelets. *Chem. Sci.* **2018**, *9* (20), 4638–4643.

(113) Wiedmann, M. M.; Tan, Y. S.; Wu, Y.; Aibara, S.; Xu, W.; Sore, H. F.; Verma, C. S.; Itzhaki, L.; Stewart, M.; Brenton, J. D. Development of Cell-Permeable, Non-Helical Constrained Peptides to Target a Key Protein–Protein Interaction in Ovarian Cancer. *Angew. Chemie Int. Ed.* **2017**, *56* (2), 524–529.

(114) Sharma, K.; Strizhak, A. V.; Fowler, E.; Wang, X.; Xu, W.; Hatt Jensen, C.; Wu, Y.; Sore, H. F.; Lau, Y. H.; Hyvönen, M.; Itzhaki, L. S.; Spring, D. R. Water-Soluble, Stable and Azide-Reactive Strained Dialkynes for Biocompatible Double Strain-Promoted Click Chemistry. *Org. Biomol. Chem.* **2019**, *17* (34), 8014–8018. https://doi.org/10.1039/c9ob01745c.

(115) Agard, N. J.; Prescher, J. A.; Bertozzi, C. R. A Strain-Promoted [3 + 2] Azide-Alkyne Cycloaddition for Covalent Modification of Biomolecules in Living Systems. *J. Am. Chem. Soc.* **2004**, *126* (46), 15046–15047. https://doi.org/10.1021/ja044996f.

(116) Lau, Y. H.; Wu, Y.; Rossmann, M.; Tan, B. X.; De Andrade, P.; Tan, Y. S.; Verma, C.; McKenzie, G. J.; Venkitaraman, A. R.; Hyvönen, M.; Spring, D. R. Double Strain-Promoted Macrocyclization for the Rapid Selection of Cell-Active Stapled Peptides. *Angew. Chemie - Int. Ed.* **2015**, *54* (51), 15410–15413. https://doi.org/10.1002/anie.201508416.

(117) Sharma, K.; Strizhak, A. V; Fowler, E.; Xu, W.; Chappell, B.; Sore, H. F.; Galloway, W. R. J. D.; Grayson, M. N.; Lau, Y. H.; Itzhaki, L. S. Functionalized Double Strain-Promoted Stapled Peptides for Inhibiting the P53-MDM2 Interaction. *ACS omega* **2020**, *5* (2), 1157–1169.

(118) Zhang, Y.; Zhang, Q.; Wong, C. T. T.; Li, X. Chemoselective Peptide Cyclization and Bicyclization Directly on Unprotected Peptides. *J. Am. Chem. Soc.* **2019**, *141* (31), 12274–12279.

https://doi.org/10.1021/jacs.9b03623.

(119) Todorovic, M.; Schwab, K. D.; Zeisler, J.; Zhang, C.; Bénard, F.; Perrin, D. M. Fluorescent Isoindole Crosslink (FlICk) Chemistry: A Rapid, User-friendly Stapling Reaction. *Angew. Chemie* **2019**, *131* (40), 14258–14262. https://doi.org/10.1002/ange.201906514.

(120) Chalker, J. M.; Gunnoo, S. B.; Boutureira, O.; Gerstberger, S. C.; Fernández-González, M.; Bernardes, G. J. L.; Griffin, L.; Hailu, H.; Schofield, C. J.; Davis, B. G. Methods for Converting Cysteine to Dehydroalanine on Peptides and Proteins. *Chem. Sci.* **2011**, *2* (9), 1666–1676. https://doi.org/10.1039/c1sc00185j.

(121) Charoenpattarapreeda, J.; Tan, Y. S.; Iegre, J.; Walsh, S. J.; Fowler, E.; Eapen, R. S.; Wu, Y.; Sore, H. F.; Verma, C. S.; Itzhaki, L. Targeted Covalent Inhibitors of MDM2 Using Electrophile-Bearing Stapled Peptides. *Chem. Commun.* **2019**, *55* (55), 7914–7917.

(122) Tian, Y.; Li, J.; Zhao, H.; Zeng, X.; Wang, D.; Liu, Q.; Niu, X.; Huang, X.; Xu, N.; Li, Z. Stapling of Unprotected Helical Peptides via Photo-Induced Intramolecular Thiol–Yne Hydrothiolation. *Chem. Sci.* **2016**, *7* (5), 3325–3330.

(123) Wang, D.; Yu, M.; Liu, N.; Lian, C.; Hou, Z.; Wang, R.; Zhao, R.; Li, W.; Jiang, Y.; Shi, X. A Sulfonium Tethered Peptide Ligand Rapidly and Selectively Modifies Protein Cysteine in Vicinity. *Chem. Sci.* **2019**, *10* (19), 4966–4972.

(124) Fairlie, D. P.; Dantas de Araujo, A. Stapling Peptides Using Cysteine Crosslinking. *Pept. Sci.* **2016**, *106* (6), 843–852.

(125) Kumita, J. R.; Smart, O. S.; Woolley, G. A. Photo-Control of Helix Content in a Short Peptide. *Proc. Natl. Acad. Sci.* **2000**, *97* (8), 3803–3808.

(126) Muppidi, A.; Doi, K.; Edwardraja, S.; Drake, E. J.; Gulick, A. M.; Wang, H. G.; Lin, Q. Rational Design of Proteolytically Stable, Cell-Permeable Peptide-Based Selective Mcl-1 Inhibitors. *J. Am. Chem. Soc.* **2012**, *134* (36), 14734–14737. https://doi.org/10.1021/ja306864v.

(127) Muppidi, A.; Wang, Z.; Li, X.; Chen, J.; Lin, Q. Achieving Cell Penetration with Distance-Matching Cysteine Cross-Linkers: A Facile Route to Cell-Permeable Peptide Dual Inhibitors of Mdm2/Mdmx. *Chem. Commun.* **2011**, *47* (33), 9396–9398. https://doi.org/10.1039/c1cc13320a.

(128) Jo, H.; Meinhardt, N.; Wu, Y.; Kulkarni, S.; Hu, X.; Low, K. E.; Davies, P. L.; Degrado, W. F.; Greenbaum, D. C. Development of α-Helical Calpain Probes by Mimicking a Natural Protein-Protein Interaction. *J. Am. Chem. Soc.* **2012**, *134* (42), 17704–17713. https://doi.org/10.1021/ja307599z.

(129) Spokoyny, A. M.; Zou, Y.; Ling, J. J.; Yu, H.; Lin, Y. S.; Pentelute, B. L. A Perfluoroaryl-Cysteine SNAr Chemistry Approach to Unprotected Peptide Stapling. *J. Am. Chem. Soc.* **2013**, *135* (16), 5946–5949. https://doi.org/10.1021/ja400119t.

(130) Louis, L. E. S.; Rodriguez, T. M.; Waters, M. L. A Study of 2-Component i, I+ 3 Peptide Stapling Using Thioethers. *Bioorg. Med. Chem.* **2018**, *26* (6), 1203–1205.

(131) Luo, Q.; Tao, Y.; Sheng, W.; Lu, J.; Wang, H. Dinitroimidazoles as Bifunctional Bioconjugation Reagents for Protein Functionalization and Peptide Macrocyclization. *Nat. Commun.* **2019**, *10* (1), 142.

(132) Peraro, L.; Zou, Z.; Makwana, K. M.; Cummings, A. E.; Ball, H. L.; Yu, H.; Lin, Y. S.; Levine, B.; Kritzer, J. A. Diversity-Oriented Stapling Yields Intrinsically Cell-Penetrant Inducers of Autophagy. *J. Am. Chem. Soc.* **2017**, *139* (23), 7792–7802. https://doi.org/10.1021/jacs.7b01698.

(133) Brown, S. P.; Smith III, A. B. Peptide/Protein Stapling and Unstapling: Introduction of s-Tetrazine, Photochemical Release, and Regeneration of the Peptide/Protein. *J. Am. Chem. Soc.* **2015**, *137* (12), 4034–4037.

(134) Grison, C. M.; Burslem, G. M.; Miles, J. A.; Pilsl, L. K. A.; Yeo, D. J.; Imani, Z.; Warriner, S. L.; Webb, M. E.; Wilson, A. J. Double Quick, Double Click Reversible Peptide “Stapling.” *Chem. Sci.* **2017**, *8* (7), 5166–5171. https://doi.org/10.1039/c7sc01342f.

(135) Assem, N.; Ferreira, D. J.; Wolan, D. W.; Dawson, P. E. Acetone-Linked Peptides: A Convergent Approach for Peptide Macrocyclization and Labeling. *Angew. Chemie - Int. Ed.* **2015**, *54* (30), 8665–8668. https://doi.org/10.1002/anie.201502607.

(136) Grison, C. M.; Burslem, G. M.; Miles, J. A.; Pilsl, L. K. A.; Yeo, D. J.; Imani, Z.; Warriner, S. L.; Webb, M. E.; Wilson, A. J. Double Quick, Double Click Reversible Peptide “Stapling.” *Chem. Sci.* **2017**, *8* (7), 5166–5171.

(137) Haney, C. M.; Loch, M. T.; Horne, W. S. Promoting Peptide α-Helix Formation with Dynamic Covalent Oxime Side-Chain Cross-Links. *Chem. Commun.* **2011**, *47* (39), 10915–10917. https://doi.org/10.1039/c1cc12010g.

(138) Haney, C. M.; Horne, W. S. Receptor-Templated Stapling of Intrinsically Disordered Peptide Ligands. *Org. Biomol. Chem.* **2015**, *13* (14), 4183–4189. https://doi.org/10.1039/C5OB00269A.

(139) Mendive-Tapia, L.; Preciado, S.; García, J.; Ramón, R.; Kielland, N.; Albericio, F.; Lavilla, R. New Peptide Architectures through C–H Activation Stapling between Tryptophan–Phenylalanine/Tyrosine Residues. *Nat. Commun.* **2015**, *6* (1), 7160. https://doi.org/10.1038/ncomms8160.

(140) Noisier, A. F. M.; García, J.; Ionuţ, I. A.; Albericio, F. Stapled Peptides by Late-Stage C(Sp 3)−H Activation . *Angew. Chemie* **2017**, *129* (1), 320–324. https://doi.org/10.1002/ange.201608648.

(141) Montgomery, J. E.; Donnelly, J. A.; Fanning, S. W.; Speltz, T. E.; Shangguan, X.; Coukos, J. S.; Greene, G. L.; Moellering, R. E. Versatile Peptide Macrocyclization with Diels-Alder Cycloadditions. *J. Am. Chem. Soc.* **2019**, *141* (41), 16374–16381. https://doi.org/10.1021/jacs.9b07578.

(142) Smith, M. E. B.; Schumacher, F. F.; Ryan, C. P.; Tedaldi, L. M.; Papaioannou, D.; Waksman, G.; Caddick, S.; Baker, J. R. Protein Modification, Bioconjugation, and Disulfide Bridging Using Bromomaleimides. *J. Am. Chem. Soc.* **2010**, *132* (6), 1960–1965.

(143) Schumacher, F. F.; Nobles, M.; Ryan, C. P.; Smith, M. E. B.; Tinker, A.; Caddick, S.; Baker, J. R. In Situ Maleimide Bridging of Disulfides and a New Approach to Protein PEGylation. *Bioconjug. Chem.* **2011**, *22* (2), 132–136.

(144) Du, J. Z.; Li, H. J.; Wang, J. Tumor-Acidity-Cleavable Maleic Acid Amide (TACMAA): A Powerful Tool for Designing Smart Nanoparticles to Overcome Delivery Barriers in Cancer Nanomedicine. *Acc. Chem. Res.* **2018**, *51* (11), 2848–2856. https://doi.org/10.1021/acs.accounts.8b00195.

(145) Schumacher, F. F.; Nunes, J. P. M.; Maruani, A.; Chudasama, V.; Smith, M. E. B.; Chester, K. A.; Baker, J. R.; Caddick, S. Next Generation Maleimides Enable the Controlled Assembly of Antibody–Drug Conjugates via Native Disulfide Bond Bridging. *Org. Biomol. Chem.* **2014**, *12* (37), 7261–7269.

(146) Richards, D. A.; Fletcher, S. A.; Nobles, M.; Kossen, H.; Tedaldi, L.; Chudasama, V.; Tinker, A.; Baker, J. R. Photochemically Re-Bridging Disulfide Bonds and the Discovery of a Thiomaleimide Mediated Photodecarboxylation of C-Terminal Cysteines. *Org. Biomol. Chem.* **2015**, *14* (2), 455–459.

(147) Wang, H.; Dawber, R. S.; Zhang, P.; Walko, M.; Wilson, A. J.; Wang, X. Peptide-Based Inhibitors of Protein–Protein Interactions: Biophysical, Structural and Cellular Consequences of Introducing a Constraint. *Chem. Sci.* **2021**, *12* (17), 5977–5993. https://doi.org/10.1039/D1SC00165E.

(148) Vogt, A. D.; Pozzi, N.; Chen, Z.; Di Cera, E. Essential Role of Conformational Selection in Ligand Binding. *Biophys. Chem.* **2014**, *186*, 13–21.

(149) Vogt, A. D.; Di Cera, E. Conformational Selection or Induced Fit? A Critical Appraisal of the Kinetic Mechanism. *Biochemistry* **2012**, *51* (30), 5894–5902.

(150) Williams, D. H.; Stephens, E.; O'Brien, D. P.; Zhou, M. Understanding Noncovalent Interactions: Ligand Binding Energy and Catalytic Efficiency from Ligand-induced Reductions in Motion within Receptors and Enzymes. *Angew. Chemie Int. Ed.* **2004**, *43* (48), 6596–6616.

(151) Sauer, P. V.; Timm, J.; Liu, D.; Sitbon, D.; Boeri-Erba, E.; Velours, C.; Mücke, N.; Langowski, J.; Ochsenbein, F.; Almouzni, G. Insights into the Molecular Architecture and Histone H3-H4 Deposition Mechanism of Yeast Chromatin Assembly Factor 1. *Elife* **2017**, *6*, e23474.

(152) Bakail, M.; Rodriguez-Marin, S.; Hegedüs, Z.; Perrin, M. E.; Ochsenbein, F.; Wilson, A. J. Recognition of ASF1 by Using Hydrocarbon-constrained Peptides. *ChemBioChem* **2019**, *20* (7), 891–895.

(153) Lama, D.; Quah, S. T.; Verma, C. S.; Lakshminarayanan, R.; Beuerman, R. W.; Lane, D. P.; Brown, C. J. Rational Optimization of Conformational Effects Induced By Hydrocarbon Staples in Peptides and Their Binding Interfaces. *Sci. Rep.* **2013**, *3* (1), 3451. https://doi.org/10.1038/srep03451.

(154) Zhang, Y.; Guo, J.; Cheng, J.; Zhang, Z.; Wu, X.; Chu, Q. High-Throughput Screening of Stapled Helical Peptides in Drug Discovery. **2022**. https://doi.org/10.1021/acs.jmedchem.2c01541.

(155) Yeo, D. J.; Warriner, S. L.; Wilson, A. J. Monosubstituted Alkenyl Amino Acids for Peptide "Stapling." *Chem. Commun.* **2013**, *49* (80), 9131–9133. https://doi.org/10.1039/c3cc45231j.

(156) Moldoveanu, T.; Grace, C. R.; Llambi, F.; Nourse, A.; Fitzgerald, P.; Gehring, K.; Kriwacki, R. W.; Green, D. R. BID-Induced Structural Changes in BAK Promote Apoptosis. *Nat. Struct. Mol. Biol.* **2013**, *20* (5), 589–597.

(157) Peña-Blanco, A.; García-Sáez, A. J. Bax, Bak and beyond — Mitochondrial Performance in Apoptosis. *FEBS J.* **2018**, *285* (3), 416–431. https://doi.org/10.1111/febs.14186.

(158) Gavathiotis, E.; Suzuki, M.; Davis, M. L.; Pitter, K.; Bird, G. H.; Katz, S. G.; Tu, H.-C.; Kim, H.; Cheng, E. H.-Y.; Tjandra, N. BAX Activation Is Initiated at a Novel Interaction Site. *Nature* **2008**, *455* (7216), 1076–1081.

(159) LaBelle, J. L.; Katz, S. G.; Bird, G. H.; Gavathiotis, E.; Stewart, M. L.; Lawrence, C.; Fisher, J. K.; Godes, M.; Pitter, K.; Kung, A. L. A Stapled BIM Peptide Overcomes Apoptotic Resistance in Hematologic Cancers. *J. Clin. Invest.* **2012**, *122* (6), 2018–2031.

(160) Rautureau, G. J. P.; Yabal, M.; Yang, H.; Huang, D. C. S.; Kvansakul, M.; Hinds, M. G. The Restricted Binding Repertoire of Bcl-B Leaves Bim as the Universal BH3-Only Prosurvival Bcl-2 Protein Antagonist. *Cell Death Dis.* **2012**, *3* (12), e443–e443.

(161) Fire, E.; Gullá, S. V; Grant, R. A.; Keating, A. E. Mcl-1–Bim Complexes Accommodate Surprising Point Mutations via Minor Structural Changes. *Protein Sci.* **2010**, *19* (3), 507–519.

(162) Okamoto, T.; Zobel, K.; Fedorova, A.; Quan, C.; Yang, H.; Fairbrother, W. J.; Huang, D. C. S.; Smith, B. J.; Deshayes, K.; Czabotar, P. E. Stabilizing the Pro-Apoptotic BimBH3 Helix (BimSAHB) Does Not Necessarily Enhance Affinity or Biological Activity. *ACS Chem. Biol.* **2013**, *8* (2), 297–302. https://doi.org/10.1021/cb3005403.

(163) Bird, G. H.; Gavathiotis, E.; Labelle, J. L.; Katz, S. G.; Walensky, L. D. Distinct BimBH3 (BimSAHB) Stapled Peptides for Structural and Cellular Studies. *ACS Chem. Biol.* **2014**, *9* (3), 831–837. https://doi.org/10.1021/cb4003305.

(164) Edwards, A. L.; Wachter, F.; Lammert, M.; Huhn, A. J.; Luccarelli, J.; Bird, G. H.; Walensky, L. D. Cellular Uptake and Ultrastructural Localization Underlie the Pro-Apoptotic Activity of a Hydrocarbon-

Stapled BIM BH3 Peptide. *ACS Chem. Biol.* **2015**, *10* (9), 2149–2157. https://doi.org/10.1021/acschembio.5b00214.

(165) Reynolds, C.; Roderick, J. E.; LaBelle, J. L.; Bird, G.; Mathieu, R.; Bodaar, K.; Colon, D.; Pyati, U.; Stevenson, K. E.; Qi, J.; Harris, M.; Silverman, L. B.; Sallan, S. E.; Bradner, J. E.; Neuberg, D. S.; Look, A. T.; Walensky, L. D.; Kelliher, M. A.; Gutierrez, A. Repression of BIM Mediates Survival Signaling by MYC and AKT in High-Risk T-Cell Acute Lymphoblastic Leukemia. *Leukemia* **2014**, *28* (9), 1819–1827. https://doi.org/10.1038/leu.2014.78.

(166) Rezaei Araghi, R.; Ryan, J. A.; Letai, A.; Keating, A. E. Rapid Optimization of Mcl-1 Inhibitors Using Stapled Peptide Libraries Including Non-Natural Side Chains. *ACS Chem. Biol.* **2016**, *11* (5), 1238–1244. https://doi.org/10.1021/acschembio.5b01002.

(167) Rezaei Araghi, R.; Bird, G. H.; Ryan, J. A.; Jenson, J. M.; Godes, M.; Pritz, J. R.; Grant, R. A.; Letai, A.; Walensky, L. D.; Keating, A. E. Iterative Optimization Yields Mcl-1–Targeting Stapled Peptides with Selective Cytotoxicity to Mcl-1–Dependent Cancer Cells. *Proc. Natl. Acad. Sci.* **2018**, *115* (5), E886–E895.

(168) Iegre, J.; Ahmed, N. S.; Gaynord, J. S.; Wu, Y.; Herlihy, K. M.; Tan, Y. S.; Lopes-Pires, M. E.; Jha, R.; Lau, Y. H.; Sore, H. F.; Verma, C.; O'Donovan, D. H.; Pugh, N.; Spring, D. R. Stapled Peptides as a New Technology to Investigate Protein-Protein Interactions in Human Platelets. *Chem. Sci.* **2018**, *9* (20), 4638–4643. https://doi.org/10.1039/c8sc00284c.

(169) Kang, M. H.; Reynolds, C. P. Bcl-2 Inhibitors: Targeting Mitochondrial Apoptotic Pathways in Cancer Therapy. *Clin. cancer Res.* **2009**, *15* (4), 1126–1132.

(170) Juin, P.; Geneste, O.; Gautier, F.; Depil, S.; Campone, M. Decoding and Unlocking the BCL-2 Dependency of Cancer Cells. *Nature Reviews Cancer*. Nature Publishing Group July 20, 2013, pp 455–465. https://doi.org/10.1038/nrc3538.

(171) Stewart, M. L.; Fire, E.; Keating, A. E.; Walensky, L. D. The MCL-1 BH3 Helix Is an Exclusive MCL-1 Inhibitor and Apoptosis Sensitizer. *Nat. Chem. Biol.* **2010**, *6* (8), 595–601. https://doi.org/10.1038/nchembio.391.

(172) Joseph, T. L.; Lane, D. P.; Verma, C. S. Stapled BH3 Peptides against MCL-1: Mechanism and Design Using Atomistic Simulations. *PLoS One* **2012**, *7* (8), e43985.

(173) Kelekar, A.; Chang, B. S.; Harlan, J. E.; Fesik, S. W.; Thompson, C. B. Bad Is a BH3 Domain-Containing Protein That Forms an Inactivating Dimer with Bcl-XL. *Mol. Cell. Biol.* **1997**, *17* (12), 7040–7046. https://doi.org/10.1128/MCB.17.12.7040.

(174) Danial, N. N.; Walensky, L. D.; Zhang, C.-Y.; Choi, C. S.; Fisher, J. K.; Molina, A. J. A.; Datta, S. R.; Pitter, K. L.; Bird, G. H.; Wikstrom, J. D.; Deeney, J. T.; Robertson, K.; Morash, J.; Kulkarni, A.; Neschen, S.; Kim, S.; Greenberg, M. E.; Corkey, B. E.; Shirihai, O. S.; Shulman, G. I.;

Lowell, B. B.; Korsmeyer, S. J. Dual Role of Proapoptotic BAD in Insulin Secretion and Beta Cell Survival. *Nat. Med.* **2008**, *14* (2), 144–153. https://doi.org/10.1038/nm1717.

(175) Szlyk, B.; Braun, C. R.; Ljubicic, S.; Patton, E.; Bird, G. H.; Osundiji, M. A.; Matschinsky, F. M.; Walensky, L. D.; Danial, N. N. A Phospho-BAD BH3 Helix Activates Glucokinase by a Mechanism Distinct from That of Allosteric Activators. *Nat. Struct. Mol. Biol.* **2014**, *21* (1), 36–42. https://doi.org/10.1038/nsmb.2717.

(176) Shepherd, N. E.; Harrison, R. S.; Ruiz-Gomez, G.; Abbenante, G.; Mason, J. M.; Fairlie, D. P. Downsizing the BAD BH3 Peptide to Small Constrained α-Helices with Improved Ligand Efficiency. *Org. Biomol. Chem.* **2016**, *14* (46), 10939–10945. https://doi.org/10.1039/c6ob02185a.

(177) Muppidi, A.; Doi, K.; Ramil, C. P.; Wang, H. G.; Lin, Q. Synthesis of Cell-Permeable Stapled BH3 Peptide-Based Mcl-1 Inhibitors Containing Simple Aryl and Vinylaryl Cross-Linkers. *Tetrahedron* **2014**, *70* (42), 7740–7745. https://doi.org/10.1016/j.tet.2014.05.104.

(178) Huhn, A. J.; Guerra, R. M.; Harvey, E. P.; Bird, G. H.; Walensky, L. D. Selective Covalent Targeting of Anti-Apoptotic BFL-1 by Cysteine-Reactive Stapled Peptide Inhibitors. *Cell Chem. Biol.* **2016**, *23* (9), 1123–1134.

(179) Harvey, E. P.; Seo, H.-S.; Guerra, R. M.; Bird, G. H.; Dhe-Paganon, S.; Walensky, L. D. Crystal Structures of Anti-Apoptotic BFL-1 and Its Complex with a Covalent Stapled Peptide Inhibitor. *Structure* **2018**, *26* (1), 153-160.e4. https://doi.org/https://doi.org/10.1016/j.str.2017.11.016.

(180) Liu, J.; Rost, B. Comparing Function and Structure between Entire Proteomes. *Protein Sci.* **2001**, *10* (10), 1970–1979. https://doi.org/https://doi.org/10.1110/ps.10101.

(181) Wolf, E.; Kim, P. S.; Berger, B. MultiCoil: A Program for Predicting Two- and Three-Stranded Coiled Coils. *Protein Sci.* **1997**, *6* (6), 1179–1189. https://doi.org/https://doi.org/10.1002/pro.5560060606.

(182) Crick, F. The Packing of [Alpha]-Helices: Simple Coiled-Coils. *Acta Crystallogr.* **1953**, *6* (8–9), 689–697.

(183) Lapenta, F.; Aupič, J.; Strmšek, Ž.; Jerala, R. Coiled Coil Protein Origami: From Modular Design Principles towards Biotechnological Applications. *Chem. Soc. Rev.* **2018**, *47* (10), 3530–3542. https://doi.org/10.1039/C7CS00822H.

(184) Ljubetič, A.; Lapenta, F.; Gradišar, H.; Drobnak, I.; Aupič, J.; Strmšek, Ž.; Lainšček, D.; Hafner-Bratkovič, I.; Majerle, A.; Krivec, N.; Benčina, M.; Pisanski, T.; Veličković, T. Ć.; Round, A.; Carazo, J. M.; Melero, R.; Jerala, R. Design of Coiled-Coil Protein-Origami Cages That Self-Assemble in Vitro and in Vivo. *Nat. Biotechnol.* **2017**, *35*. https://doi.org/10.1038/nbt.3994.

(185) Thomas, F.; Burgess, N. C.; Thomson, A. R.; Woolfson, D. N. Controlling the Assembly of Coiled–Coil Peptide Nanotubes. *Angew.*

Chemie Int. Ed. **2016**, *55* (3), 987–991. https://doi.org/https://doi.org/10.1002/anie.201509304.

(186) Thomson, A. R.; Wood, C. W.; Burton, A. J.; Bartlett, G. J.; Sessions, R. B.; Brady, R. L.; Woolfson, D. N. Computational Design of Water-Soluble α-Helical Barrels. *Science (80-.).* **2014**, *346* (6208), 485–488. https://doi.org/10.1126/science.1257452.

(187) Naik, R. R.; Kirkpatrick, S. M.; Stone, M. O. The Thermostability of an α-Helical Coiled-Coil Protein and Its Potential Use in Sensor Applications. In *Biosensors and Bioelectronics*; Elsevier, 2001; Vol. 16, pp 1051–1057. https://doi.org/10.1016/S0956-5663(01)00226-3.

(188) Reja, R. M.; Khan, M.; Singh, S. K.; Misra, R.; Shiras, A.; Gopi, H. N. PH Sensitive Coiled Coils: A Strategy for Enhanced Liposomal Drug Delivery. *Nanoscale* **2016**, *8* (9), 5139–5145. https://doi.org/10.1039/C5NR07734F.

(189) Fujiwara, Y.; Takeshita, K.; Nakagawa, A.; Okamura, Y. Structural Characteristics of the Redox-Sensing Coiled Coil in the Voltage-Gated H^+ Channel *. *J. Biol. Chem.* **2013**, *288* (25), 17968–17975. https://doi.org/10.1074/jbc.M113.459024.

(190) Lebar, T.; Lainšček, D.; Merljak, E.; Aupič, J.; Jerala, R. A Tunable Orthogonal Coiled-Coil Interaction Toolbox for Engineering Mammalian Cells. *Nat. Chem. Biol.* **2020**. https://doi.org/10.1038/s41589-019-0443-y.

(191) Negron, C.; Keating, A. E. A Set of Computationally Designed Orthogonal Antiparallel Homodimers That Expands the Synthetic Coiled-Coil Toolkit. *J. Am. Chem. Soc.* **2014**, *136* (47), 16544–16556. https://doi.org/10.1021/ja507847t.

(192) Grigoryan, G.; Keating, A. E. Structural Specificity in Coiled-Coil Interactions. *Curr. Opin. Struct. Biol.* **2008**, *18* (4), 477–483. https://doi.org/10.1016/j.sbi.2008.04.008.

(193) Mason, J. M.; Arndt, K. M. Coiled Coil Domains: Stability, Specificity, and Biological Implications. *ChemBioChem* **2004**, *5* (2), 170–176. https://doi.org/10.1002/cbic.200300781.

(194) Steinmetz, M. O.; Jelesarov, I.; Matousek, W. M.; Honnappa, S.; Jahnke, W.; Missimer, J. H.; Frank, S.; Alexandrescu, A. T.; Kammerer, R. A. Molecular Basis of Coiled-Coil Formation. **2007**, *104* (17).

(195) Kreitler, D. F.; Yao, Z.; Steinkruger, J. D.; Mortenson, D. E.; Huang, L.; Mittal, R.; Travis, B. R.; Forest, K. T.; Gellman, S. H. A Hendecad Motif Is Preferred for Heterochiral Coiled-Coil Formation. *J. Am. Chem. Soc.* **2019**, *141* (4), 1583–1592. https://doi.org/10.1021/jacs.8b11246.

(196) Drobnak, I.; Gradišar, H.; Ljubetič, A.; Merljak, E.; Jerala, R. Modulation of Coiled-Coil Dimer Stability through Surface Residues While Preserving Pairing Specificity. *J. Am. Chem. Soc.* **2017**, *139* (24), 8229–8236. https://doi.org/10.1021/jacs.7b01690.

(197) Fletcher, J. M.; Horner, K. A.; Bartlett, G. J.; Rhys, G. G.; Wilson, A. J.; Woolfson, D. N. De Novo Coiled-Coil Peptides as Scaffolds for

Disrupting Protein-Protein Interactions. *Chem. Sci.* **2018**, *9* (39), 7656–7665. https://doi.org/10.1039/c8sc02643b.

(198) O'Shea, E. K.; Klemm, J. D.; Kim, P. S.; Alber, T. X-Ray Structure of the GCN4 Leucine Zipper, a Two-Stranded, Parallel Coiled Coil. *Science (80-.).* **1991**, *254* (5031), 539–544. https://doi.org/10.1126/science.1948029.

(199) Harbury, P. B.; Zhang, T.; Kim, P. S.; Alber, T. A Switch between Two-, Three-, and Four-Stranded Coiled Coils in GCN4 Leucine Zipper Mutants. *Science (80-.).* **1993**, *262* (5138), 1401–1407. https://doi.org/10.1126/science.8248779.

(200) Fletcher, J. M.; Boyle, A. L.; Bruning, M.; Bartlett, Sg. J.; Vincent, T. L.; Zaccai, N. R.; Armstrong, C. T.; Bromley, E. H. C.; Booth, P. J.; Brady, R. L.; Thomson, A. R.; Woolfson, D. N. A Basis Set of de Novo Coiled-Coil Peptide Oligomers for Rational Protein Design and Synthetic Biology. *ACS Synth. Biol.* **2012**, *1* (6), 240–250. https://doi.org/10.1021/sb300028q.

(201) Fletcher, J. M.; Bartlett, G. J.; Boyle, A. L.; Danon, J. J.; Rush, L. E.; Lupas, A. N.; Woolfson, D. N. N@ a and N@ d: Oligomer and Partner Specification by Asparagine in Coiled-Coil Interfaces. *ACS Chem. Biol.* **2017**, *12* (2), 528–538. https://doi.org/10.1021/acschembio.6b00935.

(202) O'Shea, E. K.; Lumb, K. J.; Kim, P. S. Peptide "Velcro": Design of a Heterodimeric Coiled Coil. *Curr. Biol.* **1993**, *3* (10), 658–667. https://doi.org/10.1016/0960-9822(93)90063-T.

(203) Graddis, T. J.; Myszka, D. G.; Chaiken, I. M. Controlled Formation of Model Homo- and Heterodimer Coiled Coil Polypeptides. *Biochemistry* **1993**, *32* (47), 12664–12671. https://doi.org/10.1021/bi00210a015.

(204) Monera, O. D.; Kay, C. M.; Hodges, R. S. Electrostatic Interactions Control the Parallel and Antiparallel Orientation of .Alpha.-Helical Chains in Two-Stranded .Alpha.-Helical Coiled-Coils. *Biochemistry* **1994**, *33* (13), 3862–3871. https://doi.org/10.1021/bi00179a010.

(205) Nautiyal, S.; Woolfson, D. N.; King, D. S.; Alber, T. A Designed Heterotrimeric Coiled Coil. *Biochemistry* **1995**, *34* (37), 11645–11651. https://doi.org/10.1021/bi00037a001.

(206) Suzuki, K.; Hiroaki, H.; Kohda, D.; Tanaka, T. An Isoleucine Zipper Peptide Forms a Native-like Triple Stranded Coiled Coil in Solution. *Protein Eng. Des. Sel.* **1998**, *11* (11), 1051–1055. https://doi.org/10.1093/protein/11.11.1051.

(207) Kiyokawa, T.; Kanaori, K.; Tajima, K.; Kawaguchi, M.; Mizuno, T.; Oku, J. I.; Tanaka, T. Selective Formation of AAB- and ABC-Type Heterotrimeric α-Helical Coiled Coils. *Chem. - A Eur. J.* **2004**, *10* (14), 3548–3554. https://doi.org/10.1002/chem.200305729.

(208) Rhys, G. G.; Wood, C. W.; Lang, E. J. M.; Mulholland, A. J.; Brady, R. L.; Thomson, A. R.; Woolfson, D. N. Maintaining and Breaking Symmetry in Homomeric Coiled-Coil Assemblies. *Nat. Commun.* **2018**, *9* (1), 4132. https://doi.org/10.1038/s41467-018-06391-y.

(209) Dahiyat, B. I.; Benjamin Gordon, D.; Mayo, S. L. Automated Design of the Surface Positions of Protein Helices. *Protein Sci.* **1997**, *6* (6), 1333–1337. https://doi.org/https://doi.org/10.1002/pro.5560060622.

(210) Kaplan, J. B.; Reinke, A. W.; Keating, A. E. Increasing the Affinity of Selective BZIP-Binding Peptides through Surface Residue Redesign. *Protein Sci.* **2014**, *23* (7), 940–953. https://doi.org/https://doi.org/10.1002/pro.2477.

(211) Li, Y.; Kaur, H.; Oakley, M. G. Probing the Recognition Properties of the Antiparallel Coiled Coil Motif from PKN by Protein Grafting. *Biochemistry* **2008**, *47* (51), 13564–13572. https://doi.org/10.1021/bi8017448.

(212) Maesaki, R.; Ihara, K.; Shimizu, T.; Kuroda, S.; Kaibuchi, K.; Hakoshima, T. The Structural Basis of Rho Effector Recognition Revealed by the Crystal Structure of Human RhoA Complexed with the Effector Domain of PKN/PRK1. *Mol. Cell* **1999**, *4* (5), 793–803. https://doi.org/https://doi.org/10.1016/S1097-2765(00)80389-5.

(213) Lee, J.-H.; Kang, E.; Lee, J.; Kim, J.; Lee, K. H.; Han, J.; Kang, H. Y.; Ahn, S.; Oh, Y.; Shin, D.; Hur, K.; Chae, S. Y.; Song, P. H.; Kim, Y.-I.; Park, J. C.; Lee, J. Il. Protein Grafting of P53TAD onto a Leucine Zipper Scaffold Generates a Potent HDM Dual Inhibitor. *Nat. Commun.* **2014**, *5* (1), 3814. https://doi.org/10.1038/ncomms4814.

(214) Eron, J. J.; Gulick, R. M.; Bartlett, J. A.; Merigan, T.; Arduino, R.; Kilby, J. M.; Yangco, B.; Diers, A.; Drobnes, C.; DeMasi, R.; Greenberg, M.; Melby, T.; Raskino, C.; Rusnak, P.; Zhang, Y.; Spence, R.; Miralles, G. D. Short-Term Safety and Antiretroviral Activity of T-1249, a Second-Generation Fusion Inhibitor of HIV. *J. Infect. Dis.* **2004**, *189* (6), 1075–1083. https://doi.org/10.1086/381707.

(215) Cai, L.; Jiang, S. Development of Peptide and Small-Molecule HIV-1 Fusion Inhibitors That Target Gp41. *ChemMedChem* **2010**, *5* (11), 1813–1824. https://doi.org/https://doi.org/10.1002/cmdc.201000289.

(216) Bianchi, E.; Finotto, M.; Ingallinella, P.; Hrin, R.; Carella, A. V; Hou, X. S.; Schleif, W. A.; Miller, M. D.; Geleziunas, R.; Pessi, A. Covalent Stabilization of Coiled Coils of the HIV Gp41 N Region Yields Extremely Potent and Broad Inhibitors of Viral Infection. *Proc. Natl. Acad. Sci.* **2005**, *102* (36), 12903–12908. https://doi.org/10.1073/pnas.0502449102.

(217) Wuo, M. G.; Mahon, A. B.; Arora, P. S. An Effective Strategy for Stabilizing Minimal Coiled Coil Mimetics. *J. Am. Chem. Soc.* **2015**, *137* (36), 11618–11621. https://doi.org/10.1021/jacs.5b05525.

(218) Wang, C.; Lai, W.; Yu, F.; Zhang, T.; Lu, L.; Jiang, X.; Zhang, Z.; Xu, X.; Bai, Y.; Jiang, S.; Liu, K. De Novo Design of Isopeptide Bond-Tethered Triple-Stranded Coiled Coils with Exceptional Resistance to Unfolding and Proteolysis: Implication for Developing Antiviral Therapeutics. *Chem. Sci.* **2015**, *6* (11), 6505–6509. https://doi.org/10.1039/C5SC02220G.

(219) Lai, W.; Wang, C.; Yu, F.; Lu, L.; Wang, Q.; Jiang, X.; Xu, X.; Zhang, T.;

Wu, S.; Zheng, X.; Zhang, Z.; Dong, F.; Jiang, S.; Liu, K. An Effective Strategy for Recapitulating N-Terminal Heptad Repeat Trimers in Enveloped Virus Surface Glycoproteins for Therapeutic Applications. *Chem. Sci.* **2016**, *7* (3), 2145–2150. https://doi.org/10.1039/C5SC04046A.

(220) Chipuk, J. E.; Moldoveanu, T.; Llambi, F.; Parsons, M. J.; Green, D. R. The BCL-2 Family Reunion. *Mol. Cell* **2010**, *37* (3), 299–310.

(221) Bouillet, P.; Metcalf, D.; Huang, D. C. S.; Tarlinton, D. M.; Kay, T. W. H.; Kontgen, F.; Adams, J. M.; Strasser, A. Proapoptotic Bcl-2 Relative Bim Required for Certain Apoptotic Responses, Leukocyte Homeostasis, and to Preclude Autoimmunity. *Science (80-.).* **1999**, *286* (5445), 1735–1738.

(222) Coultas, L.; Bouillet, P.; Loveland, K. L.; Meachem, S.; Perlman, H.; Adams, J. M.; Strasser, A. Concomitant Loss of Proapoptotic BH3-only Bcl-2 Antagonists Bik and Bim Arrests Spermatogenesis. *EMBO J.* **2005**, *24* (22), 3963–3973.

(223) Ranger, A. M.; Zha, J.; Harada, H.; Datta, S. R.; Danial, N. N.; Gilmore, A. P.; Kutok, J. L.; Le Beau, M. M.; Greenberg, M. E.; Korsmeyer, S. J. Bad-Deficient Mice Develop Diffuse Large B Cell Lymphoma. *Proc. Natl. Acad. Sci.* **2003**, *100* (16), 9324–9329.

(224) Villunger, A.; Michalak, E. M.; Coultas, L.; Mullauer, F.; Bock, G.; Ausserlechner, M. J.; Adams, J. M.; Strasser, A. P53-and Drug-Induced Apoptotic Responses Mediated by BH3-Only Proteins Puma and Noxa. *Science (80-.).* **2003**, *302* (5647), 1036–1038.

(225) Datta, S. R.; Katsov, A.; Hu, L.; Petros, A.; Fesik, S. W.; Yaffe, M. B.; Greenberg, M. E. 14-3-3 Proteins and Survival Kinases Cooperate to Inactivate BAD by BH3 Domain Phosphorylation. *Mol. Cell* **2000**, *6* (1), 41–51.

(226) Zha, J.; Harada, H.; Yang, E.; Jockel, J.; Korsmeyer, S. J. Serine Phosphorylation of Death Agonist BAD in Response to Survival Factor Results in Binding to 14-3-3 Not BCL-X(L). *Cell* **1996**, *87* (4), 619–628. https://doi.org/10.1016/S0092-8674(00)81382-3.

(227) Danial, N. N.; Gramm, C. F.; Scorrano, L.; Zhang, C.-Y.; Krauss, S.; Ranger, A. M.; Robert Datta, S.; Greenberg, M. E.; Licklider, L. J.; Lowell, B. B. BAD and Glucokinase Reside in a Mitochondrial Complex That Integrates Glycolysis and Apoptosis. *Nature* **2003**, *424* (6951), 952–956.

(228) Clackson, T.; Wells, J. A. A Hot Spot of Binding Energy in a Hormone-Receptor Interface. *Science (80-.).* **1995**, *267* (5196), 383–386. https://doi.org/10.1126/SCIENCE.7529940.

(229) London, N.; Raveh, B.; Schueler-Furman, O. Druggable Protein–Protein Interactions – from Hot Spots to Hot Segments. *Curr. Opin. Chem. Biol.* **2013**, *17* (6), 952–959. https://doi.org/10.1016/J.CBPA.2013.10.011.

(230) Suraweera, C. D.; Caria, S.; Järvå, M.; Hinds, M. G.; Kvansakul, M. A Structural Investigation of NRZ Mediated Apoptosis Regulation in

Zebrafish. *Cell Death Dis.* **2018**, *9* (10), 967.

(231) McIntosh-Smith, S.; Price, J.; Sessions, R. B.; Ibarra, A. A. High Performance in Silico Virtual Drug Screening on Many-Core Processors. *Int. J. High Perform. Comput. Appl.* **2015**, *29* (2), 119–134. https://doi.org/10.1177/1094342014528252.

(232) Wood, C. W.; Ibarra, A. A.; Bartlett, G. J.; Wilson, A. J.; Wilson, A. J.; Woolfson, D. N.; Woolfson, D. N.; Woolfson, D. N.; Sessions, R. B.; Sessions, R. B. BAlaS: Fast, Interactive and Accessible Computational Alanine-Scanning Using BudeAlaScan. *Bioinformatics* **2020**, *36* (9), 2917–2919. https://doi.org/10.1093/BIOINFORMATICS/BTAA026.

(233) Ibarra, A. A.; Bartlett, G. J.; Hegedüs, Z.; Dutt, S.; Hobor, F.; Horner, K. A.; Hetherington, K.; Spence, K.; Nelson, A.; Edwards, T. A.; Woolfson, D. N.; Sessions, R. B.; Wilson, A. J. Predicting and Experimentally Validating Hot-Spot Residues at Protein-Protein Interfaces. *ACS Chem. Biol.* **2019**, *14* (10), 2252–2263. https://doi.org/10.1021/acschembio.9b00560.

(234) Certo, M.; Moore, V. D. G.; Nishino, M.; Wei, G.; Korsmeyer, S.; Armstrong, S. A.; Letai, A. Mitochondria Primed by Death Signals Determine Cellular Addiction to Antiapoptotic BCL-2 Family Members. *Cancer Cell* **2006**, *9* (5), 351–365. https://doi.org/10.1016/J.CCR.2006.03.027.

(235) Rogers, J. M.; Oleinikovas, V.; Shammas, S. L.; Wong, C. T.; De Sancho, D.; Baker, C. M.; Clarke, J. Interplay between Partner and Ligand Facilitates the Folding and Binding of an Intrinsically Disordered Protein. *Proc. Natl. Acad. Sci.* **2014**, *111* (43), 15420–15425.

(236) Rogers, J. M.; Wong, C. T.; Clarke, J. Coupled Folding and Binding of the Disordered Protein PUMA Does Not Require Particular Residual Structure. *J. Am. Chem. Soc.* **2014**, *136* (14), 5197–5200.

(237) Krieger, E.; Vriend, G. YASARA View—Molecular Graphics for All Devices—from Smartphones to Workstations. *Bioinformatics* **2014**, *30* (20), 2981–2982.

(238) Miles, J. A.; Yeo, D. J.; Rowell, P.; Rodriguez-Marin, S.; Pask, C. M.; Warriner, S. L.; Edwards, T. A.; Wilson, A. J. Hydrocarbon Constrained Peptides – Understanding Preorganisation and Binding Affinity. *Chem. Sci.* **2016**, *7* (6), 3694–3702. https://doi.org/10.1039/C5SC04048E.

(239) Hetherington, K.; Hegedus, Z.; Edwards, T. A.; Sessions, R. B.; Nelson, A.; Wilson, A. J. Stapled Peptides as HIF-1α/P300 Inhibitors: Helicity Enhancement in the Bound State Increases Inhibitory Potency. *Chem. – A Eur. J.* **2020**, *26* (34), 7638–7646. https://doi.org/10.1002/CHEM.202000417.

(240) Wang, H.; Dawber, R. S.; Zhang, P.; Walko, M.; Wilson, A. J.; Wang, X. Peptide-Based Inhibitors of Protein–Protein Interactions: Biophysical, Structural and Cellular Consequences of Introducing a Constraint. *Chem. Sci.* **2021**, *12* (17), 5977–5993. https://doi.org/10.1039/D1SC00165E.

(241) Inohara, N.; Ding, L.; Chen, S.; Núñez, G. Harakiri, a Novel Regulator of Cell Death, Encodes a Protein That Activates Apoptosis and Interacts Selectively with Survival-Promoting Proteins Bcl-2 and Bcl-X(L). *EMBO J.* **1997**, *16* (7), 1686–1694. https://doi.org/10.1093/emboj/16.7.1686.

(242) Imaizumi, K.; Benito, A.; Kiryu-Seo, S.; Gonzalez, V.; Inohara, N.; Leiberman, A. P.; Kiyama, H.; Nuñez, G. Critical Role for DP5/Harakiri, a Bcl-2 Homology Domain 3-Only Bcl-2 Family Member, in Axotomy-Induced Neuronal Cell Death. *J. Neurosci.* **2004**, *24* (15), 3721–3725.

(243) Oppenheim, R. W.; Flavell, R. A.; Vinsant, S.; Prevette, D.; Kuan, C.-Y.; Rakic, P. Programmed Cell Death of Developing Mammalian Neurons after Genetic Deletion of Caspases. *J. Neurosci.* **2001**, *21* (13), 4752–4760.

(244) Gurzov, E. N.; Ortis, F.; Cunha, D. A.; Gosset, G.; Li, M.; Cardozo, A. K.; Eizirik, D. L. Signaling by IL-1β+ IFN-γ and ER Stress Converge on DP5/Hrk Activation: A Novel Mechanism for Pancreatic β-Cell Apoptosis. *Cell Death Differ.* **2009**, *16* (11), 1539–1550.

(245) Coultas, L.; Terzano, S.; Thomas, T.; Voss, A.; Reid, K.; Stanley, E. G.; Scott, C. L.; Bouillet, P.; Bartlett, P.; Ham, J. Hrk/DP5 Contributes to the Apoptosis of Select Neuronal Populations but Is Dispensable for Haematopoietic Cell Apoptosis. *J. Cell Sci.* **2007**, *120* (12), 2044–2052.

(246) Hadji, A.; Schmitt, G. K.; Schnorenberg, M. R.; Roach, L.; Hickey, C. M.; Leak, L. B.; Tirrell, M. V.; LaBelle, J. L. Preferential Targeting of MCL-1 by a Hydrocarbon-Stapled BIM BH3 Peptide. *Oncotarget* **2019**, *10* (58), 6219–6233. https://doi.org/10.18632/oncotarget.27262.

(247) Suraweera, C. D.; Burton, D. R.; Hinds, M. G.; Kvansakul, M. Crystal Structures of the Sheeppox Virus Encoded Inhibitor of Apoptosis SPPV14 Bound to the Proapoptotic BH3 Peptides Hrk and Bax. *FEBS Lett.* **2020**, *594* (12), 2016–2026. https://doi.org/10.1002/1873-3468.13807.

(248) Okamoto, T.; Campbell, S.; Mehta, N.; Thibault, J.; Colman, P. M.; Barry, M.; Huang, D. C. S.; Kvansakul, M. Sheeppox Virus SPPV14 Encodes a Bcl-2-like Cell Death Inhibitor That Counters a Distinct Set of Mammalian Proapoptotic Proteins. *J. Virol.* **2012**, *86* (21), 11501–11511.

(249) Kong, W.; Zhou, M.; Li, Q.; Fan, W.; Lin, H.; Wang, R. Experimental Characterization of the Binding Affinities between Proapoptotic BH3 Peptides and Antiapoptotic Bcl-2 Proteins. *ChemMedChem* **2018**, *13* (17), 1763–1770. https://doi.org/10.1002/cmdc.201800321.

(250) Walensky, L. D.; Bird, G. H. Hydrocarbon-Stapled Peptides: Principles, Practice, and Progress. *J. Med. Chem.* **2014**, *57* (15), 6275–6288. https://doi.org/10.1021/JM4011675/ASSET/IMAGES/LARGE/JM-2013-011675_0011.JPEG.

(251) Mendive-Tapia, L.; Wang, J.; Vendrell, M.; Mcallister, T. E.; Coleman, O. D.; Roper, G.; Kawamura, A.; Howl, J.; Jones, S.; Bluntzer, M. T. J.; O'connell, J.; Baker, T. S.; Michel, J.; Hulme, A. N.; Baibek, A.; Üçüncü, M.; Blackburn, E. A.; Bradley, M.; Lilienkampf, A.; Huwaitat, R.; Coulter,

S. M.; Porter, S. L.; Pentlavalli, S.; Laverty, G.; Foster, A. D.; Chung, C.-W.; Hann, M. M.; Simpson, G. L.; Tavassoli, A.; Knuhtsen, A.; Whiting, R.; Mcwhinnie, F. S.; Whitmore, C.; Smith, B. O.; Green, A. C.; Timperley, C. M.; Kinnear, K. I.; Jamieson, A. G. Structural Optimization of Reversible Dibromomaleimide Peptide Stapling. *Pept. Sci.* **2021**, *113* (1), e24157. https://doi.org/10.1002/PEP2.24157.

(252) Akgul, C. Mcl-1 Is a Potential Therapeutic Target in Multiple Types of Cancer. *Cell. Mol. life Sci.* **2009**, *66* (8), 1326–1336.

(253) Shore, G. C.; Warr, M. R. Unique Biology of Mcl-1: Therapeutic Opportunities in Cancer. *Curr. Mol. Med.* **2008**, *8* (2), 138–147.

(254) Kong, W.; Zhou, M.; Li, Q.; Fan, W.; Lin, H.; Wang, R. Experimental Characterization of the Binding Affinities between Proapoptotic BH3 Peptides and Antiapoptotic Bcl-2 Proteins. *ChemMedChem* **2018**, *13* (17), 1763–1770. https://doi.org/10.1002/CMDC.201800321.

(255) Dutta, S.; Ryan, J.; Chen, T. S.; Kougentakis, C.; Letai, A.; Keating, A. E. Potent and Specific Peptide Inhibitors of Human Pro-Survival Protein Bcl-Xl. *J. Mol. Biol.* **2015**, *427* (6), 1241–1253. https://doi.org/10.1016/j.jmb.2014.09.030.

(256) Hegedüs, Z.; Hóbor, F.; Shoemark, D. K.; Celis, S.; Lian, L. Y.; Trinh, C. H.; Sessions, R. B.; Edwards, T. A.; Wilson, A. J. Identification of β-Strand Mediated Protein-Protein Interaction Inhibitors Using Ligand-Directed Fragment Ligation. *Chem. Sci.* **2021**, *12* (6), 2286–2293. https://doi.org/10.1039/d0sc05694d.

(257) Kannan, S.; Aronica, P. G. A.; Ng, S.; Gek Lian, D. T.; Frosi, Y.; Chee, S.; Shimin, J.; Yuen, T. Y.; Sadruddin, A.; Kaan, H. Y. K.; Chandramohan, A.; Wong, J. H.; Tan, Y. S.; Chang, Z. W.; Ferrer-Gago, F. J.; Arumugam, P.; Han, Y.; Chen, S.; Rénia, L.; Brown, C. J.; Johannes, C. W.; Henry, B.; Lane, D. P.; Sawyer, T. K.; Verma, C. S.; Partridge, A. W. Macrocyclization of an All-Dlinear α-Helical Peptide Imparts Cellular Permeability. *Chem. Sci.* **2020**, *11* (21), 5577–5591. https://doi.org/10.1039/c9sc06383h.

(258) Dongyuan Wang‡, a, Mengying Yu‡, a, Na Liua, Chenshan Liana, Zhanfeng Houa, Rui Wangb, Rongtong Zhaoa, Wenjun Lia, Yixiang Jianga, Xiaodong Shia, Shuiming Li*, c, Feng Yin*, a, Zigang Li*, A. A Sulfonium Tethered Peptide Ligand Rapidly and Selectively Modifies Protein Cysteine in Vicinity. *Chem. Sci.* **2019**. https://doi.org/10.1039/C9SC00034H.

(259) Wood, C. W.; Heal, J. W.; Thomson, A. R.; Bartlett, G. J.; Ibarra, A.; Brady, R. L.; Sessions, R. B.; Woolfson, D. N. ISAMBARD: An Open-Source Computational Environment for Biomolecular Analysis, Modelling and Design. *Bioinformatics* **2017**, *33* (19), 3043–3050. https://doi.org/10.1093/bioinformatics/btx352.

(260) Krivov, G. G.; Shapovalov, M. V.; Dunbrack, R. L. Improved Prediction of Protein Side-Chain Conformations with SCWRL4. *Proteins Struct. Funct. Bioinforma.* **2009**, *77* (4), 778–795. https://doi.org/10.1002/prot.22488.

(261) McIntosh-Smith, S.; Price, J.; Sessions, R. B.; Ibarra, A. A. High Performance in Silico Virtual Drug Screening on Many-Core Processors. *Int. J. High Perform. Comput. Appl.* **2015**, *29* (2), 119–134. https://doi.org/10.1177/1094342014528252.

(262) Krivov, G. G.; Shapovalov, M. V.; Dunbrack, R. L. Improved Prediction of Protein Side-Chain Conformations with SCWRL4. *Proteins Struct. Funct. Bioinforma.* **2009**, *77* (4), 778–795. https://doi.org/10.1002/prot.22488.

(263) Kaya-Aksoy, E.; Cingoz, A.; Senbabaoglu, F.; Seker, F.; Sur-Erdem, I.; Kayabolen, A.; Lokumcu, T.; Sahin, G. N.; Karahuseyinoglu, S.; Bagci-Onder, T. The Pro-Apoptotic Bcl-2 Family Member Harakiri (HRK) Induces Cell Death in Glioblastoma Multiforme. *Cell Death Discov.* **2019**, *5* (1). https://doi.org/10.1038/s41420-019-0144-z.

(264) Krieger, E.; Vriend, G. New Ways to Boost Molecular Dynamics Simulations. *J. Comput. Chem.* **2015**, *36* (13), 996–1007.

(265) Boris Aillard, a Naomi S. Robertson, a Adam R. Baldwin, a S. R. and A. G. J. Robust Asymmetric Synthesis of Unnatural Alkenyl Amino Acids for Conformationally Constrained α-Helix Peptides. *Org. Biomol. Chem.* **2014**. https://doi.org/10.1039/b000000x.

(266) Fanelli, R.; Jeanne, L.; Adeline, J.; Martinez, J.; Cavelier, F. Stereoselective Synthesis of Unsaturated α - Amino Acids. *Amino Acids* **2015**, 1107–1115. https://doi.org/10.1007/s00726-015-1934-0.